Characterisation of the Haemodynamic Response Function (HRF) in the neonatal brain using functional MRI

Dr Tomoki Arichi

A thesis submitted for the Degree of Doctor of Philosophy

Imperial College London, University of London; 2012

Neonatal Medicine & Cognitive Neuroimaging groups

MRC Clinical Sciences Centre

Institute of Clinical Science, Imperial College London

ABSTRACT

Background: Preterm birth is associated with a marked increase in the risk of later neurodevelopmental impairment. With the incidence rising, novel tools are needed to provide an improved understanding of the underlying pathology and better prognostic information. Functional Magnetic Resonance Imaging (fMRI) with Blood Oxygen Level Dependent (BOLD) contrast has the potential to add greatly to the knowledge gained through traditional MRI techniques. However, it has been rarely used with neonatal subjects due to difficulties in application and inconsistent results. Central to this is uncertainity regarding the effects of early brain development on the Haemodynamic Response Function (HRF), knowledge of which is fundamental to fMRI methodology and analysis.

Hypotheses: (1) Well localised and positive BOLD functional responses can be identified in the neonatal brain. (2) The morphology of the neonatal HRF differs significantly during early human development. (3) The application of an age-appropriate HRF will improve the identification of functional responses in neonatal fMRI studies.

Methods: To test these hypotheses, a systematic fMRI study of neonatal subjects was carried out using a custom made somatosensory stimulus, and an adapted study design and analysis pipeline. The neonatal HRF was then characterised using an event related study design. The potential future application of the findings was then tested in a series of small experiments.

Results: Well localised and positive BOLD functional responses were identified in neonatal subjects, with a maturational tendency towards an increasingly complex pattern of activation. A positive amplitude HRF was identified in neonatal subjects, with a maturational trend of a decreasing time-

to-peak and increasing positive peak amplitude. Application of the empirical HRF significantly improved the precision of analysis in further fMRI studies.

Conclusions: fMRI can be used to study functional activity in the neonatal brain, and may provide vital new information about both development and pathology.

This thesis is protected by copyright and other intellectual property rights. Copyright in the material it contains belongs to the author unless stated otherwise. No information or quotation from the thesis may be published or re-used without proper acknowledgment.

"*the one knowledge worth having is to know one's own mind*"

F.H. Bradley 1930

"*In many ways there are greater differences between the brain of a 28 week infant and that of a 36 week infant than there are between the brain of the three-month old baby and an adult*"

Pape and Wigglesworth 1979

For my family, Judy, Hanako and Gen-chan

I thank my supervisors, Professor David Edwards and Professor Christian Beckmann for their unfailing vision, guidance, support, vast knowledge, and above all enthusiasm for this work.

I also thank my colleagues, Etienne, Alejandro and Alessandro in the Human Robotics group, Imperial College London for their hard work and considerable skill. This work would not have been possible without the development of the subject interface tools designed and made by them, and through the continuing efforts of Alessandro.

I am eternally grateful to my colleagues in the Imaging Physics group for tolerating my ignorance about the fundamentals of MR science, and for help in the sequence development, processing, and analysis. A particular thank you must be extended to Gianlorenzo Fagiolo for taking the time to answer any and all of my “stupid questions”. I also thank my fellow students and colleagues in the Imaging Sciences and Neonatal Medicine groups: Valentina, Michela, Miriam, Naaz, Nora, Libuse, Francesco, Kathryn, Andrew, Hilary, Joanna, Amy, Matt, Tracey and Serena not only for their considerable efforts in the collection of the data reported in this thesis, but also for their discussion and friendship.

I particularly thank the families and patients who kindly agreed to participate in this work, and the staff of the Queen Charlotte and Chelsea Neonatal Unit and the Children’s ambulatory Unit, Hammersmith Hospital, without whom this work would not have been possible.

Lastly, I thank my family for their unquestioning love, support, and of course putting up with my pretensions of being a “scientist” over the last 3 years.

Declaration of Originality

I declare that all of the work described in and the contents of this thesis are my own work, and that all else is appropriately referenced.

Statement of Publications

The work described in this thesis has been published in:

Arichi T, Moraux A, Melendez A, Doria V, Groppo M, Merchant N, Combs S, Burdet E, Larkman DJ, Counsell SJ, Beckmann CF, Edwards AD, 2010. Somatosensory cortical activation identified by functional MRI in preterm and term infants. Neuroimage; 49(3): 2063-71.

Arichi T, Doria V, Edwards AD, 2011. What are newborn babies thinking? Clues from MRI. Imaging in Medicine; 3(2): 137-40.

Arichi T, 2012. Functional MRI of the developing neonatal brain: potential and challenges for the future. Developmental Medicine and Child Neurology; 54(8): 680.

Arichi T, Fagiolo G, Varela M, Melendez-Calderon A, Allievi A, Merchant N, Tusor N, Counsell SJ, Burdet E, Beckmann CF, Edwards AD, 2012. Development of BOLD signal Hemodynamic Responses in the Human brain. Neuroimage; 63(2): 663-73.

Conference abstracts and Presentations

The work described in this thesis has been presented at the following meetings:

Arichi T, Moraux A, Melendex A, Doria V, Burdet E, Larkman DJ, Beckmann CF, Edwards AD. Somatosensory cortical activation in the preterm brain identified with functional MRI and a programmable hand interface (abstract and presentation). *Neonatal Society Meeting, London UK; November 2008.*

Arichi T, Moraux A, Melendex A, Doria V, Burdet E, Larkman DJ, Beckmann CF, Edwards AD. Somatosensory cortical activation in the premature brain identified with functional MRI and a programmable hand interface (abstract and e-poster presentation). *ISMRM annual scientific meeting, Honolulu, Hawaii, USA; April 2009.*

Arichi T, Moraux A, Melendex A, Doria V, Burdet E, Larkman DJ, Beckmann CF, Edwards AD. Somatosensory cortical activation in the preterm brain identified with functional MRI and a programmable hand interface (abstract and poster presentation). *Pediatric Academic Society annual meeting, Baltimore, USA; May 2009.*

Arichi T, Counsell SJ, Tusor N, Merchant N, Cowan FM, Rutherford MA, Beckmann CF, Burdet E, Edwards AD. Characterization of early somatosensory functional and structural cerebral organization following neonatal haemorrhagic parenchymal infarction with functional magnetic resonance imaging and probabilistic tractography. *British Paediatric Neurology Association annual meeting, Edinburgh, UK; January 2011.*

Arichi T, Fagiolo G, Melendez A, Tusor N, Merchant N, Counsell SJ, Burdet E, Beckmann CF, Edwards AD. Characterisation of the BOLD signal Hemodynamic Response Function (HRF) in the neonatal somatosensory cortex. *ISMRM annual scientific meeting, Montreal, Canada; May 2011.*

Allievi A, **Arichi T**, Melendez-Calderon A, Edwards AD, Burdet E. A novel robot for fMRI investigation of the developing motor system in preterm infants. *Pediatric Academic Meeting, Boston, USA; May 2012.*

Arichi T, Counsell SJ, Chew AM, Allievi A, Melendez-Calderon A, Merchant N, Tusor N, Burdet E, Beckmann CF, Cowan FM, Edwards AD. Characterization of structural and functional connectivity in the developing somatosensory system following focal neonatal brain injury. *Pediatric Academic Meeting, Boston, USA; May 2012.*

Gordon-Williams RM, Allievi A, Hayat T, **Arichi T**, Burdet E, Groves AM, Edwards AD. A computer-controlled stimulator for fMRI of the neonatal olfactory system. *Pediatric Academic Meeting, Boston, USA; May 2012.*

THESIS CONTENTS

List of figures 15

List of tables 18

List of equations 19

List of abbreviations 20

1. Imaging the developing human brain 23

1.1. A need for accurate biomarkers of early brain pathology 24

1.2. Human brain development 28

1.2.1 Neuralation and development of the prosencephalon 29

1.2.2. Cell proliferation, neuronal migration and differentiation 31

1.2.3. Maturation and folding of the cerebral cortex 33

1.2.4. Glial cells and myelination 35

1.2.5. Neurotransmitter receptor expression and activity 36

1.2.6. Intracranial vascular development 39

1.3. MRI of the developing human brain 40

1.3.1. MRI of normal brain development in the third trimester 43

1.3.2. MRI of normal postnatal brain development 47

1.4. Brain injury and Preterm Birth 49

1.4.1. Intraventricular haemorrhage 50

1.4.2. Periventricular Leukomalacia and White matter injury 51

1.4.2.1. MRI appearances of white matter injury 54

1.4.2.2. Detailed MRI studies of white matter microstructure 55

1.4.3. Brain growth and volume 57

1.4.3.1. Cortical volume and development 58

1.4.3.2. Thalamo-cortical connectivity 60

1.4.3.3. Cerebellar growth and development 61

1.5. Summary 62

2. Functional Magnetic Resonance Imaging 63

2.1. Basic principles of MRI 66

2.1.1. Nuclear Magnetic Resonance 66

2.1.2. Basics of Image contrast 69

2.1.3. Image formation 72

2.2. fMRI 73

2.2.1. T2* effects and BOLD contrast 74

2.2.2. Neurovascular coupling 76

2.2.3. Linking electrical activity to fMRI BOLD contrast 79

2.2.4. Modelling the response to stimulation 80

2.2.4.1. The Haemodynamic Response Function (HRF) 80

2.2.4.2. Biophysical models of the BOLD haemodynamic response 84

2.2.4.3. Induced changes in the BOLD response 86

2.3. fMRI methodology 89

2.3.1. Image acquisition 90

2.3.2. Data pre-processing 93

2.3.2.1. Slice acquisition time correction 94

2.3.2.2. Motion correction 94

2.3.2.3. Distortion correction 97

2.3.2.4. Intensity normalisation 98

2.3.2.5. Spatial filtering 98

2.3.2.6. Temporal filtering 99

2.3.3. Study design 99

2.3.4. Principles of data analysis 102

2.3.4.1. The General Linear Model (GLM) 103

2.3.4.2. Higher level group analysis 105

2.3.4.3. Independent Component Analysis (ICA) 107

2.4. Summary 108

3. fMRI studies of the newborn 109

3.1. Reported studies in the literature 110

3.1.1. Visual Stimulation 118

3.1.2. Sensori-motor stimulation 122

3.1.3. Auditory stimulation 123

3.1.4. Resting state connectivity 124

3.2. Potential but major challenges 126

3.2.1. Practical considerations 127

3.2.2. Study population 128

3.2.3. Choice of image acquisition parameters 128

3.2.4. Stimulation paradigms 130

3.2.5. Data analysis 131

3.3. Summary 133

4. Thesis Aims and Hypotheses 134

4.1. Thesis study plan 134

4.2. Thesis Aims 135

4.3. Thesis Hypotheses 136

5. Characterising functional responses to hand movement with fMRI in neonatal subjects 137

5.1. Somatosensory system development in early human life 138

5.1.1. Studies of somatosensory function in neonates 141

5.2. Study aims and hypotheses 143

5.3. Methods and materials 144

5.3.1. Study population 144

5.3.2. Image acquisition 147

5.3.3. Somatosensory stimulus 149

5.3.3.1. Stimulus design and architecture 150

5.3.3.2. Stimulus control 152

5.3.3.3. Experimental design 153

5.3.4. fMRI data analysis 156

5.3.4.1. Individual subject analysis 156

5.3.4.2. Linear Basis sets 157

5.3.4.3. Standard template registration 159

5.3.4.4. Higher level analysis 161

5.3.5. Probabilistic tractography 161

5.4. Results 162

5.4.1. Preterm group 163

5.4.2. Term Control group 165

5.4.3. Ex-preterm at term equivalent PMA group 166

5.4.4. Probabilistic tractography 170

5.5. Discussion 172

5.5.1. Development of somatosensory activation 172

5.5.2. Explaining negative BOLD 173

5.5.3. Study limitations and implications 176

5.6. Study conclusions 178

6. Characterisation of the HRF in the preterm and neonatal period 179

6.1. The effect of intersubject HRF variability on fMRI analysis 180

6.1.1. Maturational changes in the HRF in childhood and old age 182

6.1.2. HRF development in early life 183

6.2. Study aims and hypothesis 185

6.3. Materials and methods 186

6.3.1. fMRI Study population 186

6.3.2. fMRI image acquisition 188

6.3.3. fMRI experimental design 190

6.3.4. fMRI data analysis and HRF model fitting 191

6.3.5. Global CBF estimation 195

6.3.6. Application of empirical HRFs to experimental data 198

6.4. Results 199

6.4.1. HRF characterisation 201

6.4.1.1. Adult group 203

6.4.1.2. Term equivalent PMA infant group 204

6.4.1.3. Preterm infant group 205

5.4.1.4. Characterising HRF development 206

6.4.2. Global CBF estimation 210

6.4.3. Application of empirical HRFs to experimental data 211

6.5. Discussion 215

6.5.1. Developmental changes in neurovascular coupling 215

6.5.2. Trends in cerebral haemodynamics in early life 216

6.5.2. Possible effects of sedative medication 219

6.5.3. Study design, limitations and implications 220

6.6. Study conclusions 222

7. Further work and applications 224

7.1. Further investigation of the neonatal HRF 224

7.1.1. Characterising the neonatal HRF to auditory stimulation 225

7.1.2. Exploring the linearity of the neonatal HRF 227

7.1.2.1. The effect of varying the Interstimulus-interval 227

7.1.2.2. HRF summation in block paradigms 230

7.2. Novel applications for fMRI studies of the newborn brain 233

7.2.1. Further characterisation of the immature motor system 233

7.2.2. The olfactory system 236

7.3. fMRI in the study of perinatal brain injury 239

7.4. Summary 242

8. Thesis Conclusions 243

References 250

Appendix A: Balloon manufacturing process 302

Appendix B: Shell script for creating peristimulus data 306

List of Figures

1.1.	Summary of key timings in early human brain development	29
1.2.	Neuronal migration in corticogenesis	31
1.3.	Cortical surface area and folding	34
1.4.	Neonatal MRI studies by year	42
1.5.	Maturational changes on T2-weighted brain MRI	44
1.6.	Maturational changes on T1-weighted brain MRI	46
1.7.	Progression of white matter myelination	48
1.8.	White matter pathology in preterm infants	54
1.9.	TBSS of white matter integrity at term equivalent age	57
1.10.	Regional volume loss at term equivalent age	59
2.1.	The Basic NMR experiment	69
2.2.	Tissue-specific T1 and T2 constants	70
2.3.	Spatial and temporal resolution of functional brain imaging tools	74
2.4.	The neurovascular coupling cascade	77
2.5.	The canonical HRF waveform	81
2.6.	The modified balloon model	86
2.7.	Effects of agents which alter baseline CBF on the HRF	87
2.8.	Echo-Planar Imaging	91
2.9.	Head motion as a confounder	95
2.10.	fMRI experimental design and efficiency	102
3.1.	Published fMRI studies in early infancy	111
3.2.	“Inverse gamma” HRF of early infancy	121
3.3.	Development of the motor resting state network	125
3.4.	Maturation of tissue-specific T2* values	129
5.1.	The Somatic sensory pathways	140
5.2.	The neonatal MRI scanner	147
5.3.	Schematic of Somatosensory stimulus setup	150
5.4.	Stimulus control box and data acquisition card	151

5.5. Custom made inflatable balloon stimulus 152
5.6. Stimulus investigator interface 153
5.7. Pilot adult data 154
5.8. Block paradigm used for experiment 155
5.9. Linear basis functions for the GLM 159
5.10. Neonatal templates 160
5.11. Preterm individual subject results 164
5.12. Preterm group analysis results 165
5.13. Term control group analysis results 166
5.14. Ex-preterm at term equivalent age group analysis results 168
5.15. Longitudinal imaging of single infants 169
5.16. Probabilistic tractography of somatosensory pathways 171

6.1. HRF variation in healthy adult populations 181
6.2. Development of the HRF in immature rats 185
6.3. Planning of the acquisition sequence 189
6.4. Example head motion traces 192
6.5. Double gamma HRF modelling 195
6.6. Planning of the PCA sequence 196
6.7. Global CBF measurement using PCA 198
6.8. Clusters of somatosensory induced functional activation 199
6.9. Example BOLD signal timeseries from the event related experiment 200
6.10. Comparative peristimulus timeseries from the frontal lobe 201
6.11. Peristimulus data fitting 202
6.12. Adult group sampled HRF 203
6.13. Term equivalent PMA infant group sampled HRF 204
6.14. Preterm infant group sampled HRF 205
6.15. Combined plot of sampled HRF waveforms 206
6.16. Boxplots of group HRF parameters 209
6.17. Plot of time to peak and PMA in neonatal subjects 210
6.18. Application of empirical HRFs to data 213
6.19. Example peristimulus model fitting 214

7.1. Auditory HRF 226
7.2. Effect of varying the interstimulus interval – simulations 229
7.3. Effect of varying the interstimulus interval – pilot data 230
7.4. Effect of varying stimulus frequency in a block design 232
7.5. Wrist stimulation device 234
7.6. Localisation of passive & active motor functional activity 236
7.7. Neonatal olfactometer 238
7.8. fMRI in perinatal localised brain injury 241

List of Tables

3.1. List of previous infant fMRI studies 112

5.1. Somatosensory study population characteristics 146

5.2. Pulse sequence parameters for neonatal MRI examination 148

6.1. HRF characterisation study population characteristics 188

6.2. Summary of HRF parameters 207

6.3. Global CBF estimation 211

List of equations

[2.1] Larmor equation	67
[2.2] T2* decay	75
[2.3] Grubb's Power law	84
[2.4] Signal-to-Noise Ratio (SNR)	90
[2.5] Standard General Linear Model (GLM)	103
[2.6] Extended GLM for 2 or more design matrices	104
[6.7] Percentage signal change calculation in fMRI	194
[6.8] Double Gamma HRF model	194
[6.9] Mean Transit Time (Stewart Hamilton principle)	218

List of abbreviations

α	flip angle (degrees)
3D	3-dimensions
ACh	Acetylcholine
ADC	Apparent Diffusion Coefficient
ADP	Adenosine di-phosphate
AEBR	auditory evoked brainstem responses
ASL	Arterial Spin Labelling
ATP	Adenosine Tri-phosphate
BET	Brain Extraction Tool
BNC	Bayonet Neill-Concelman (connector)
BOLD	Blood Oxygen Level Dependent contrast
Ca^{2+}	calcium ion
CBF	cerebral blood flow
CBV	cerebral blood volume
Cl^-	chloride ion
cm	centimetres
$CMRO_2$	cerebral metabolic rate of oxygen
CNS	central nervous system
CO_2	carbon dioxide
CP	Cerebral Palsy
CSF	cerebro-spinal fluid
CT	Computerised Tomography
DAQ	Data Acquisition Card
DBM	Deformation Based Morphometry
DEHSI	Diffuse Excessive High Signal Intensity
d-Hb	deoxygenated haemoglobin
DMN	Default Mode Network
DNA	Deoxyribonucleic Acid
DTI	Diffusion Tensor Imaging
DWI	Diffusion Weighted Imaging
EEG	electo-encephalography
EPI	Echo Planar Imaging
FA	fractional anisotropy

FDR	false discovery rate
FEAT	FMRI expert analysis tool
FID	free induction decay
FLIRT	FMRIB's linear image registration tool
FLOBS	FMRIB's linear optimal basis sets
fMRI	functional Magnetic Resonance Imaging
FNIRT	FMRIB's non-linear image registration tool
FSL	FMRIB's Software Library
FWE	family wise error
FWHM	full width half maximum
GA	gestational age (weeks)
GABA	gamma Amino-butyric acid
GLM	General Linear Model
GRE	Gradient Recalled Echo
GUI	Graphical User Interface
H^+	Hydrogen ion
H_2O	water
Hb	Haemoglobin
$Hb\text{-}O_2$	oxygenated haemoglobin
Hct	Haematocrit
HPI	Haemorrhagic Parenchymal Infarction
HRF	Haemodynamic Response Function
ICA	Independent Component Analysis
ISI	inter-stimulus interval
IVH	Intra-ventricular haemorrhage
K^+	potassium ion
LFP	Local Field Potentials
MEG	Magneto-encephalography
MELODIC	Model-free fMRI analysis using Probabilistic Independent Component Analysis (PICA)
MNI152	Montreal Neurological Institute 152 brain
MPRAGE	Magnetisation Prepared Rapid Acquisition Gradient Echo
MRI	Magnetic Resonance Imaging
msec	milliseconds

MTT	mean transit time
Na^+	sodium ion
nCPAP	nasal continuous positive airway pressure
NIRS	Near-infrared Spectroscopy
NMR	Nuclear Magnetic Resonance
OEF	oxygen extraction fraction
OFC	Occipito-frontal head circumference (centimetres)
OLS	Ordinary Least Squares
PCA	Phase Contrast Angiography
pCO_2	partial pressure of carbon dioxide
PET	Positron Emission Tomography
PLIC	posterior limb of the internal capsule
PMA	postmenstrual age (weeks)
PVL	Periventricular Leukomalacia
RF	Radiofrequency
SATs	slow activity transients
SD	standard deviation
SE	Spin Echo
SEFs	somatosensory evoked magnetic fields
SEM	standard error of the mean
SSE	sum of squared errors
SSEP	somato-sensory evoked potentials
SNR	Signal to Noise ratio
SPM	Statistical Parametric Mapping
SWI	Susceptibility weighted imaging
T	Tesla
TBSS	Tract Based Spatial Statistics
TE	echo time (usually in milliseconds)
TFCE	Threshold Free Cluster Enhancement
TMS	Transcranial Magnetic Stimulation
TR	repetition time (usually in milliseconds)
TTL	transistor-to-transistor logic (pulse)
US	Ultrasound Scan
VEP	Visual Evoked potentials

Chapter 1

1. Imaging the developing brain

Explaining the workings of the brain, and thereby understanding and attempting to model its associated functions (including the somewhat ambiguous concept of consciousness) has always intrigued and yet evaded humankind. The challenge of such a vast and complex undertaking is emphasised when it is considered that the mature human brain contains an estimated 86 billion neurons (Brenner & Sejnowski 2011). Integral to such a process must be a deeper understanding of the development of the central nervous system (CNS), and moreover the mechanisms which underlie the establishment of the neural structural and functional pathways which ultimately mediate an individual's interaction with the external environment.

During approximately 40 weeks of gestational life, the central nervous system undergoes a rapid and dramatic, but highly structured sequence of programmed maturation and organisation (Rutherford 2002-12, de-Graaf-Peters & Hadders-Algra 2006). At full term, the neonatal brain represents something of a dichotomy; highly complex in configuration and structure with much of the characteristic anatomy seen in adult life recognisable even at this early stage; and yet seemingly immature in terms of function, with only rudimentary primary sensory capabilities and an apparent lack of "conscious" thought processes (Lagercrantz & Changeux 2009). In recent years, dramatic advances seen in the field of neuro-imaging have led to the development of powerful novel techniques which have for the first time, allowed scientists and clinicians to visualise in-vivo, the developing human brain. Wide-spread application of these tools, has not only allowed developmental neuroscientists to begin the process of carefully characterising the brain's early growth and maturation, but has also transformed clinical practice by providing a non-invasive means by which to assess a pathological brain state and gain vital diagnostic and prognostic information. Characteristic patterns of brain injury can now be recognised, many of which are unique to the developing brain. Imaging tools offer the potential to not only accurately characterise these lesions,

but moreover to understanding their immediate and long-term consequences. In recent years, remarkable advances in imaging are now allowing investigators the exciting opportunity to visualise and measure the functional activity of the living brain, which has the potential to dramatically add to our understanding of both normal and pathological brain development.

The focus of this thesis is the optimisation of one of these novel techniques: functional MRI (fMRI), for use in studies of the developing human brain during the preterm and neonatal period. In the first chapter of this thesis, I will review the normal sequence of brain development and specifically how this can be characterised and studied using Magnetic Resonance Imaging (MRI). I will also discuss the compelling need for a deeper understanding of the harmful effects of preterm birth on the developing brain, and highlight how MRI has added immeasurably to this process. In the second chapter of this thesis, I present a brief overview of the fundamentals of MR imaging, with particular emphasis on the underlying principles of fMRI signal generation, methodology, and analysis. In the third chapter, I will summarise the findings of previously reported infant fMRI studies from the literature, and in doing so, attempt to identify possible reasons which may explain why the technique has been rarely applied to infant subjects (despite undoubted potential), and in particular why the field has been plagued by inconsistent results. These identified factors are then used to form the basis of the thesis aims and hypotheses as described in chapter 4. Two major studies were carried out during this thesis to try and achieve the aims of the thesis, which are then set out in chapters 5 and 6. Lastly, I have briefly described the methods and findings of a number of smaller projects in progress, to highlight the applicability of the findings derived from the main studies, and describe further key questions which are yet to be resolved.

1.1. A need for accurate biomarkers of early brain pathology

The neonatal period is particularly distinguished by a significant “structural-functional disconnect” in the state of the CNS, as at no other time in human life are the external manifestations of a particular

brain state as indistinct or subtle (Volpe 2008). Acquired or congenital pathology at this juncture in development are likely to lead to life-long changes in brain structure and function, the detrimental effects of which may not become apparent until later in life when the associated function is noted to have been adversely affected (or a further pathological state has developed). The exemplar of this effect is cerebral palsy, defined as a group of disorders of movement and postural control caused by a non-progressive defect or lesion of the developing brain (Bax 1964, Palmer 2004, Bax et al. 2005). Cerebral palsy represents a descriptive diagnosis of the neurological deficit and its associated disabilities, and in which the underlying aetiology may be known but is not required either for the diagnosis or classification (Palmer 2004, Bax et al. 2005). Frequently the diagnosis is therefore not made in the neonatal period, but more often in the second year of life when the affected child has been assessed by a clinician due to concerns about their neurodevelopment as the neurological and behavioural effects of the causative pathology become apparent (Wood 2006).

In the developed world, the incidence of cerebral palsy has remained relatively unchanged in recent years at approximately 2.5 per 1000 live births in the UK, despite major and continuing advances in obstetric and neonatal clinical care (Blair & Watson 2006). This figure may be partly explained by the increasing incidence of preterm birth (delivery at less than 37 weeks gestation (Tucker et al. 2004)) which now represents 7-13% of all births in the developed world (Larroque et al. 2008, Mangham et al. 2009). Coupled with the increased survival of those born extremely preterm (less than 28 weeks gestation (Tucker et al. 2004)), the increasing numbers of these infants may mitigate somewhat the findings of recent population based studies which have found falling proportionate rates of cerebral palsy in premature infants at follow-up (explained in some part by a significant decrease in the incidence of the major causative pathologies such as cystic Periventricular-Leukomalacia (PVL)) (Hamrick et al. 2004, Platt et al. 2007, Robertson et al. 2007, Surman et al. 2009, van Haastert et al. 2011, Sugiura et al. 2012). Regardless of these findings, the incidence rate of cerebral palsy is markedly increased in comparison to those delivered at term; as evidenced by the EPIPAGE cohort of

infants delivered between 22 and 32 weeks gestation in France, in which 8.2% of the infants at 2 years of age and 9% at 5 years of age were affected by the condition (Ancel et al. 2006, Beaino et al. 2010).

Premature infants in early childhood have also been found to suffer from significantly poorer health outcomes in a number of other systems, including impaired growth and nutritional status, abnormal cardiovascular and respiratory function, and higher rates of respiratory pathologies (in particular chronic obstructive pulmonary diseases) (Doyle 2010, Hayes et al. 2011). In addition, studies in child- and young adulthood have also found that premature birth is an independent risk factor for the later development of perhaps more subtle (but no less significant) adverse neurological outcomes, including lower educational achievement, neurosensory disorders, learning and behavioural disabilities, and psychiatric illness (Hintz et al. 2005b, Allen 2008, Hack 2009, Doyle 2010, Nosarti et al. 2012). A specific pattern of childhood psychiatric disturbances appears to be particularly prominent and has been collectively termed the "preterm behavioural phenotype", encompassing difficulties with inattention/hyperactivity, social, emotional, and internalising behaviour (Johnson et al. 2010, Johnson & Marlow 2011). Increased features of autistic spectrum disorder have been frequently reported in long term follow-up studies of preterm children, although the specificity of screening is likely affected by the increased prevalence of developmental delay and learning disabilities within the population (Johnson & Marlow 2011). A recent study by Nosarti and colleagues (2012) has also reported a marked increase in adult-onset psychiatric hospital admissions, suggesting that these difficulties are not benign in nature. Of importance, these adverse long-term neurological outcomes are seen to occur even in the absence of overt intra-cerebral pathology (Broitman et al. 2007, Allen 2008).

The allocation of medical treatment and long-term supportive care required for the survivors of preterm birth has therefore become one of the major public health concerns for our current

generation (Kruse et al. 2009, Mangham et al. 2009, Ment et al. 2009). For a single child affected with cerebral palsy, the lifetime cost of the required healthcare and social interventions has been approximated at up to €860,000 in Denmark (Kruse et al. 2009); while in the UK the total cost per annum for a child with hemiplegia has been estimated at £13,050, with only 43% of this accounting for expenses directly related to their impairment (Beecham et al. 2001). Similarly, the annual economic costs of preterm birth to the public sector have been estimated to be a staggering £2.946 billion, with an inverse relationship between the gestational age at birth and the average public sector cost per surviving child (Mangham et al. 2009).

There are currently no established preventative strategies for the neurological sequelae of either preterm birth or cerebral palsy. Current treatments are predominately targeted at specific neurological problems (or their associated disabilities) and are initiated later in childhood when these deficits are behaviourally and clinically manifest (Allen 2002, Wood 2006, Ment et al. 2009). Although the implementation of interventional therapies as early as possible to change later outcome would ostensibly seem ideal, the evidence in support of such currently available strategies is not clear: with some studies suggesting a positive (but not sustained) effect on cognitive outcome in early childhood, but no benefit for later motor function (Blauw-Hospers & Hadders-Algra 2005, Orton et al. 2009, KoIdewijn et al 2010, Hadders-Algra 2011, Øberg et al. 2012). While these findings may represent a true limitation in effect; it is also possible that the development of new tools may allow for better targeted strategies which can take advantage of the early brain's increased capacity for neurophysiological plasticity, particularly if they can be initiated before an acquired lesion is fully established (Johnston 2009, Staudt 2010, Hadders-Algra 2011, Øberg et al. 2012). There is therefore a pressing need for the development of novel highly accurate techniques with which both scientists and clinicians can understand more about the early development of the infant brain, the response to perinatal brain injury, and to gain diagnostic and prognostic insight (Ment et al. 2009). One might envisage that the information gained from these techniques could then be used as "biomarkers" to

precisely test and monitor the effects of any novel interventional strategies (including within the framework of a clinical trial), and to identify those patients who may benefit from a specific intervention well before any clinical signs may be apparent.

1.2. Human brain development

The structure and function of the mature human brain is the culmination of a complex and rapid, but highly structured programme of developmental changes in the morphology, organisation, and function of the central nervous system; starting from the first few weeks of in-utero fetal life and continuing through to young adulthood (*summarised in figure 1.1*) (Battin & Rutherford 2002, de Graaf-Peters & Hadders-Algra 2005, Volpe 2008). The importance of the correct timing and completion of these very early stages of brain ontogeny (the in-utero and peri-natal periods) is emphasised by the life-long and often severe consequences of the disruption caused by congenital disorders and other forms of brain pathology acquired within this period (Volpe JJ 2008, 2009b). Although a detailed description of all of the processes involved in the formation and maturation of the human brain is outside the scope of this thesis, a broad overview is presented here and is essential to put the work described later in context.

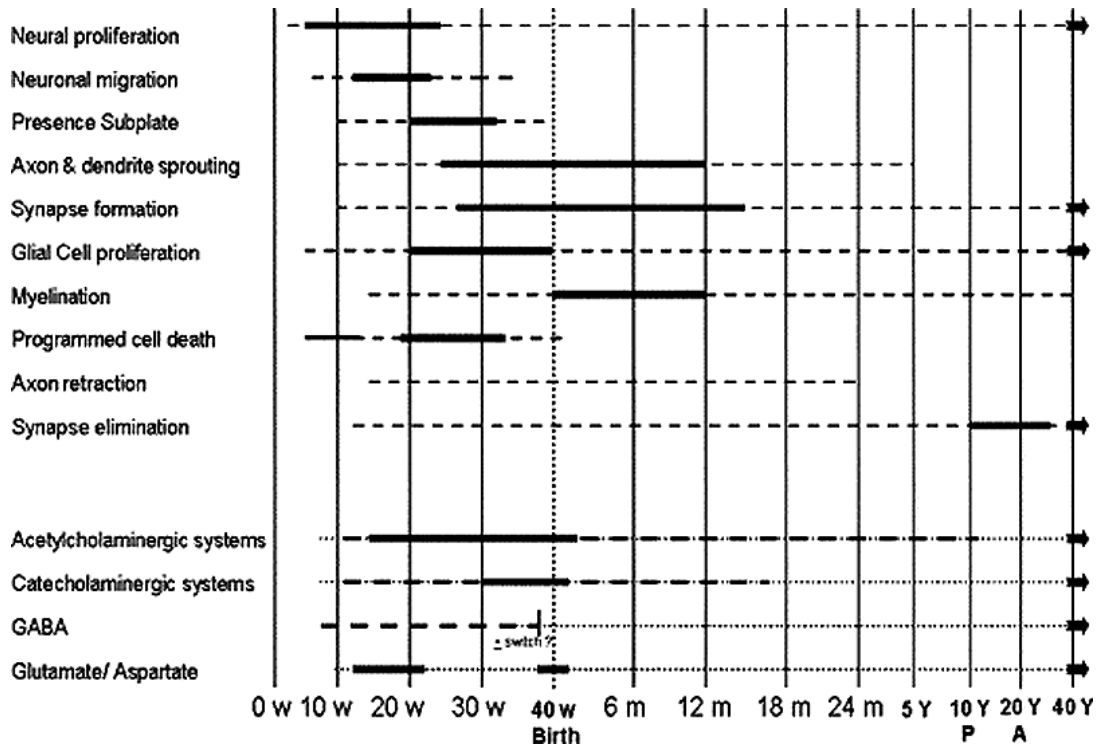

Figure 1.1: ***Summary chart displaying the timing of onset and activity of developmental processes in the human central nervous system.*** Broken lines denote an active process, with the bold lines denoting periods of greatest activity. During these processes, changes are also seen in the major neurotransmitter systems (lower part of figure; continuous bold lines denote periods of transmitter overexpression, thin broken lines denote that the transmitter is present). The GABA system is unique in that the function is known to switch form excitatory (bold broken line) to inhibitory (thin broken line) at approximately 40 weeks post-menstrual age (PMA). *(Figure reproduced from de Graaf-Peters & Hadders-Algra 2005)*

1.2.1 Neurulation and development of the prosencephalon

From the 3rd-4th weeks of human gestation, the dorsal aspect of the embryo undergoes a process of induction collectively known as "neurulation" which ultimately results in the formation of the central nervous system (brain and spinal cord) (Encha-Razavi & Sonigo 2003, Sadler 2005, Volpe 2008). The first key stages of "primary" neurulation occur at 18 days post conception, when the middle of the nascent ectoderm is induced to differentiate into the primitive neural plate; with elevation and then fusion of the lateral borders leading to neural tube formation during days 21 to 30 (Sadler 2005). These primary processes result in the formation of the brain and the majority of the spinal cord, with

secondary neurulation (4-7 weeks gestation) responsible for the remaining caudal sections of the spinal cord through the epithelisation of coalesced mesodermal cells (Sadler 2005, Volpe 2008). Under the influence of gradients of gene expression, the neural tube then differentiates along several axes thus leading to the establishment of the major subdivisions of the central nervous system (Lagercrantz & Ringstedt 2001, de Graaf-Peters & Hadders-Algra 2005, Krispin et al. 2010).

At 5 weeks gestation, the cephalic end of the neural tube gives rise to three primary vesicles which represent the putative hind-brain (rhomboencephalon), mid-brain (mesencephalon), and forebrain (prosencephalon) (Volpe 2008, Volpe P et al. 2009). Processes are mediated through transient signalling centres which code positional information on recipient cells in which combinations of transcription factors are induced leading to the acquisition of specific cellular identities (Rallu et al. 2002, Richards et al. 2004). Development of the prosencephalon proceeds as a sequence of three events: firstly prosencephalic formation itself, followed by prosencephalic cleavage in 3 major planes; (*horizontal*) leading to paired olfactory and optic structures; (*transverse*) resulting in the separation of the diencephalon (which later give rise to posterior forebrain structures such as the thalamus) and the telencephalon (giving rise to the cerebral hemispheres); and (*sagittal*) forming the paired cerebral hemispheres, basal ganglia and lateral ventricles (Volpe 2008). The final stage comprises the development of the midline prosencephalic structures including the corpus callosum (beginning at 9 weeks gestation), the septum pellucidae, the optic chiasm, and the hypothalamus (Richards et al. 2004, Volpe 2008, Volpe P et al. 2009). Disruption to these crucial processes can therefore lead to a spectrum of clinical disorders from the relatively mild, such as partial agenesis of the corpus callosum, to the invariably lethal aprosencephaly (completely absent telencephalon and diencephalon) (Volpe P et al. 2009).

1.2.2. Cell proliferation, neuronal migration and differentiation

Soon after the closure of the neural tube (approximately embryonic day 30), dividing neuroepithelial cells (also known as neural stem cells) form a rapidly proliferating subependymal layer or "ventricular zone" (Dhavan et al. 2001, Bystron et al. 2008). The processes of morphological and molecular differentiation which constitute neurogenesis then initiate in the ventricular zone at approximately embryonic day 33, with multipotent radial glial cells prominently generated at this stage (Bryston et al. 2008, Volpe 2008). In humans, a distinct upper layer of mitotic neurogenic cells is also visualised (termed the subventricular zone), which continues to proliferate through development eventually superseding the ventricular zone as the principal source of cortical neurons by 25 weeks gestation (Bryston et al. 2008). At approximately 7 weeks gestation, the preplate forms above the ventricular zone, which represents a transient community of neurons through which neurons migrate radially eventually leading to the formation the true cortical plate below a cell-sparse subpial marginal zone (Dhavan et al. 2001). The cortex is then formed in an "inside-out" manner (*figure 1.2(i)*), as each subsequent wave of cells migrate along radial glial fibres through the intermediate zone, subplate, and past earlier-born cortical plate neurons to settle below the marginal zone (Dhavan et al. 2001, Gilmore and Herrup 2001, Bryston et al. 2008).

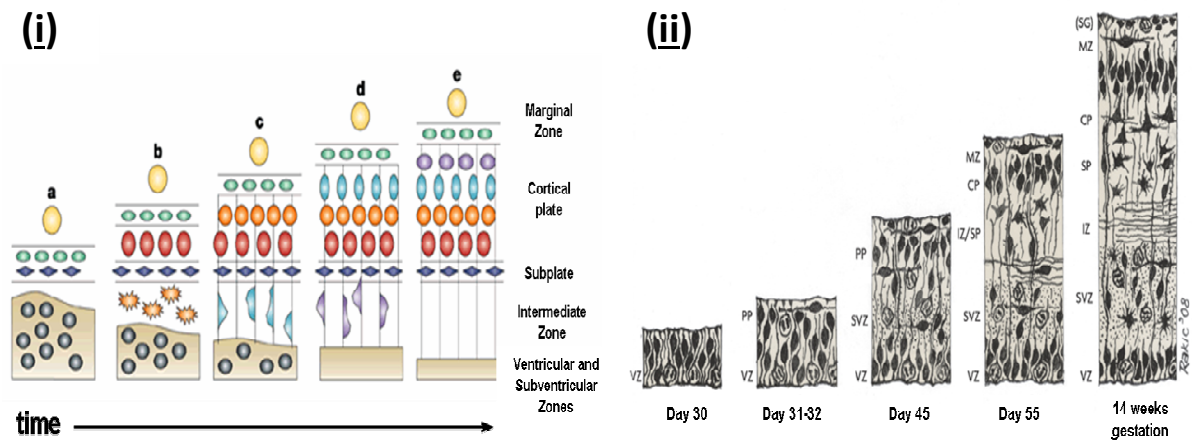

Figure 1.2: (i) ***Schematic diagram of neuronal migration seen during corticogenesis.*** (a): Dividing cells initially occupy the ventricular zone (black circles), with only a thin mantle layer of cortical primordium forming the

preplate above; (b) As waves of neurons migrate out of the ventricular zone (orange) into the preplate, it splits into the cell-sparse marginal zone, the cortical plate (accommodating the newly arrived neurons), and the subplate. (c–e) Further waves of neurons continue to migrate along radial glial fibres, and transit through the subplate and cortical plate. Later-born neurons therefore reside in the more superficial layers of the cortex. (*Figure reproduced and adapted from Dhavan et al. 2001).* **(ii): *The timeline of human cortical layer development.*** On embryonic day 30, the ventricular zone (VZ) is recognised, with subsequent formation of the preplate (PP) seen soon after on day 31-32. On day 45, new cells are visible within the subventricular zone (SVZ), with splitting of the preplate (as described above) into the intermediate (IZ), subplate (SP), cortical plate (CP), and marginal (MZ) (also containing the subpial granular layer (SG)) zones seen by 14 weeks gestation; (*figure(ii) reproduced and adapted from Bystron et al. 2008*).

Connections develop as the immature neurons sprout axons, which are guided to their targets by chemo-attractive and repellent processes (De Graaf-Peters & Hadders-Algra 2005, Kostović & Jovanov-Milošević 2006). Of particular interest at this juncture is a relatively cell-sparse area below the cortical plate termed the subplate, which is thought to act as a transient "waiting room" for afferent sprouting axons (originating from the thalamus, basal forebrain, and brainstem nuclei) before they reach their cortical destination (Kostivić & Rakic 1990, Kostović & Jovanov-Milošević 2006). The subplate is visible from approximately 12 weeks gestation, and is thickest and most easily recognised around 29 weeks gestation as the afferent fibres grow into the cortical plate and form connections (De Graaf-Peters & Hadders-Algra 2005, Kostović & Jovanov-Milošević 2006). The temporary afferents residing in the subplate appear not to be functionally silent, and are thought to have a unique and characteristic electrophysiological signature known as slow activity transients (SATs) (Vanhatalo et al. 2005, Hartley et al. 2012). After approximately the 31st gestational week, the subplate is seen to gradually regress and then disappear completely by full term gestation (De Graaf-Peters & Hadders-Algra 2005, Kostović & Jovanov-Milošević 2006).

A particularly key process during this relatively rapid sequence of maturation is selective cell death (De Graaf-Peters & Hadders-Algra 2005, Volpe 2008). The term “Apoptosis” collectively refers to the programmed series of molecular and cellular events which are fundamental to the establishment of the normal pattern of brain organisation by regulating the growth of neuronal progenitor cells and removing aberrant synapses and axons, thereby maximising the efficiency of brain function and connectivity (Volpe 2008, Johnston 2009, Bullmore & Sporns 2012). Of interest, the apoptotic mechanisms resulting from excito-toxicity and mitochondrial dysfunction have also been found to be crucial during pathological events such as neonatal hypoxic ischaemic brain injury (Thornton et al. 2012).

1.2.3. Maturation and folding of the cerebral cortex

The size of the surface area of the brain is closely related to the number of radial units projecting from the ventricular zone to the cortical plate, with regions characterised by a longer and later period of mitotic progenitor cell division generally developing a larger size (Rakic 1995, White et al. 2010). Early in gestation, the brain is relatively lissencephalic (with a smooth surface), but very early signs of gyrification are present as early as 10 gestational weeks (Chi et al. 1977, White et al. 2010). The development sequence of gyrification has been well characterised and has been found to follow an precise timetable, with the large interhemispheric (10-15 weeks) and sylvian (14-19 weeks) fissures first to form (Chi et al. 1977, Battin & Rutherford 2002, White et al. 2010). The secondary and tertiary gyri (such as the central sulcus) are not seen until approximately 18-20 weeks when neuronal migration has been concluded (Van der Knaap et al. 1996, Volpe 2008, White et al. 2010, Habas et al. 2012). Macroscopically, the sulci are seen to first start as shallow grooves which progressively become deeper with the side walls gradually steepening, approximating and eventually abutting (Van der Knaap et al. 1996, Battin et al. 1998, Habas et al. 2012). As they mature during the later stages of gestation (after approximately 32 weeks), the gyri and sulci develop a far more complex configuration and shape with the development of side branches and the intricate

patterns of folding characteristically seen in the mature adult brain (Battin & Rutherford 2002, Dubois et al. 2008).

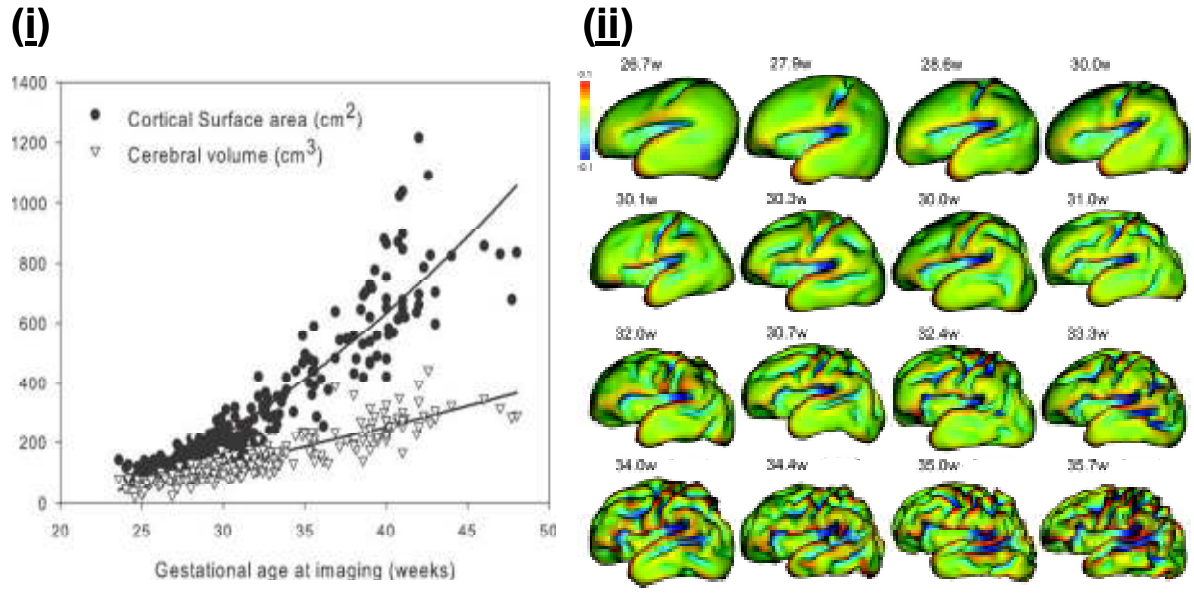

Figure 1.3: (i) ***The surface area of the brain increases more rapidly than brain volume during the third trimester of gestation.*** Human brain growth is seen to obey an allometric scaling law with an exponent of 2/3 explaining the relationship between the rapidly folding cortical surface area and the whole brain volume (*figure reproduced from Kapellou et al. 2006*). **(ii)** ***Development of cortical folding from 26 to 36 weeks post-menstrual age.*** The rapid changes in gyrification and sulcation seen during the third trimester of human development are clearly evident on these inner cortical surface reconstructions derived from MRI data. At 26 weeks, the brain is relatively lissencephalic with the exception of the central sulci and sylvian fissures, in marked contrast to deeper and intricate (but still relatively immature) pattern of folding seen at 36 weeks. (*Figure reproduced and adapted from Dubois et al. 2008*).

This pattern of cortical growth leads to a dramatic increase in the brain's surface area (rather than thickness) in the third trimester of human development (24-36 weeks) with an exponential growth trajectory seen in contrast to a linear increase in whole brain volume (*figure 1.3(i)*) (Kapellou et al. 2006, White et al. 2010). The relationship between the surface area and brain volume obeys an allometric scaling law, with similar scaling laws found to both across mammalian species and in

relation to other tissue types (Zhang and Sejnowski 2000, Kapellou et al. 2006). The mechanistic forces generated by "visoelastic tension" through the developing connections of the cortical fibres have been proposed to underlie the formation of the cortical gyri (Van Essen 1997, White et al. 2010). Under this theory, areas of cortex which are densely connected to each other are "pulled together" by the tension exerted by the fibres, thereby leading to the protrusion of gyri as the brain continues to grow (with the sulci formed if the converse is true) (Van Essen 1997). This process also serves to maximise the efficiency of the brain's framework of intrinsic connectivity by shortening the distance between communicating regions (Bullmore and Sporns 2012).

1.2.4. Glial cells and myelination

Although it is estimated that there are between 75 and 125 billion neurons in the mature human brain; they are far surpassed by the glial cells which can be up to 10 times more abundant (this relationship is highly region specific, with this ratio being largest in the white matter) (Lent et al. 2011). Throughout the brain, neurons are surrounded by and interact with the two major subdivisions of glial cell; the microglia and macroglia, both of which perform a diverse set of functions which are vital for appropriate brain development and function (Parpura et al. 2012). Microglia migrate into and colonise the brain from the haematopoietic system early in development, and are the resident macrophages of the central nervous system (Pont-Lezica et al. 2012). In the fetal brain, microglia have been found to be most concentrated in areas of cell death, angiogenesis, and in the marginal layer; and are closely associated with radial glial cells (Pont-Lezica et al. 2012). Macroglia in contrast, are derived from the same progenitor cells as neurons, with the most prominent forms being astrocytes and oligodendocytes (Miller 2002, Volpe 2008, Parpura et al. 2012). Astrocytes perform an extensive role in development including nutritive and supportive roles for neuronal homeostasis, the removal of excess neurotransmitters, inflammatory responses, and the induction and elimination of synapses (Parpura et al. 2012). In the mature brain, they perform

further vital roles in neuronal plasticity, neurotransmission, and are a key component of the neurovascular unit involved in neuro-vascular coupling (Attwell et al. 2010, Parpura et al. 2012).

Oligodendrocytes are generally thought to be the last cell type to proliferate and differentiate during CNS development. Although the earliest oligodendrocyte precursors are seen to arise in the neural tube itself and later from the ventricular and subventricular zones, they have been found to migrate considerable distances to reach their final destinations predominately in the cerebral and spinal cord white matter (Miller 2002). Immature oligodendrocytes proliferate and surround the developing axons of the white matter, mature through neuronal neuregulin expression, and are then responsible for the formation of the fatty myelin bilayer which insulates the axons and allows rapid and efficient impulse conduction (Vartanian et al. 1994, Miller 2002, Volpe 2008). Although some myelin protein expression is seen in the spinal cord as early as the first trimester, myelination is predominately an ex-utero post-term process which occurs relatively rapidly throughout the first 2 postnatal years, but continues even in adolescence (Kinney et al. 1988, Weidenheim et al. 1996, Battin & Rutherford 2002, Deoni et al. 2011). As with nearly all other aspects of CNS development, myelination is seen to proceed according to a recognised and structured schedule: with the proximal pathways myelinating prior to the distal; the afferent sensory pathways before the motor/efferent; the projection pathways before associative; the central areas before the cerebral poles; and the occipital pole prior to the frontotemporal poles (Kinney et al. 1988, Deoni et al. 2011).

1.2.5. Neurotransmitter receptor expression and actvity

In addition to their clear role in signal transmission across synapses, neurotransmitters are thought to also play an essential role in neural development, and are integral to the processes of proliferation, migration, and differentiation (Verney 2003, Luján et al. 2005, Manent & Repressa 2007, Aronica et al. 2011). An exemplar of these roles can be seen in the transient but highly correlated increases in acetylcholinesterase positive staining within the fibres which accumulate in

both the subplate and the medio-dorsal thalamus in the 2nd and 3rd trimesters of gestation (Kostović & Goldman-Rakic, 1983, Kostović et al. 2002). Positive-staining cells for all of the major neurotransmitter receptors are seen from the first trimester of gestation, with region and time specific changes in their expression seen throughout development (Verney 1999, 2003, de Graaf-Peters & Hadders-Algra 2005, Aronica et al. 2011). A good example of these differences in expression during development is found in the catecholaminergic system which is thought to be present from approximately 8-10 weeks gestation. Whilst some serotonin receptor subtypes appear to acquire mature numbers by full term gestation, the receptors of the dopaminergic system have been found to increase at a much slower rate with mature levels in the pyramidal system not seen until puberty (Verney 1999, 2002, 2003).

The primary excitatory and inhibitory neurotransmitter systems in the mature adult brain are glutamate and γ–aminobutyric acid (GABA) respectively; and receptors of both systems are known to be extensively expressed in the developing human brain (Verney 2003, Luján et al. 2005, Manent and Repressa 2007). Both transmission systems mediate their actions through ionotropic (ligand-gated channels) and metabotropic (G-protein coupled) receptors, with marked differences in the proportion of receptor sub-types and the expression of particular sub-units seen throughout the early human development (Verney 2003, Luján et al. 2005). The principal excitatory neurotransmitter in the fetal and early neonatal brain is paradoxically GABA, acting predominately through ionotropic $GABA_A$ chloride-permeable receptor channels (Ben-Ari et al. 2007, Briggs & Galanopoulou 2011). This effect occurs due to the higher intracellular chloride (Cl^-) environment of immature neurons: with depolarisation occurring as a result of the raised concentration leading to an efflux of Cl^- ions following opening of the GABA receptor channel (Briggs & Galanopoulou 2011).

Functional receptors to both glutamate and GABA are seen during the early proliferative stages of brain development, and blockage has been found to profoundly alter patterns of DNA synthesis (and

resultant cell differentiation) (Luján et al. 2005, Manent and Repressa 2007). Alterations in the expression of receptors to both systems also thought to play a role in neuronal migration and chemotaxis, via the induction of neuronal cell motility, the promotion of cell layer entry, and the prevention of over-migration through modulatory signals (Manent and Repressa 2007). In addition, the complex sequence of processes which lead to synapse formation and maturation are also partially mediated through trends in neurotransmitter receptor expression, with resultant effects on cell–cell adhesion, inter-neuronal signalling, site-specific recruitment of protein complexes, and activity-dependent postsynaptic development (Luján et al. 2005).

Rapid synaptogenesis continues postnatally up to approximately 2 years of age, from which the density and number gradually decrease during adolescence to approximately 60% of the maximum level in infancy (Huttenlocher & Dabholkar 1997). Synapse production is highly region specific during early development, with rapid bursts occurring firstly in the visual and auditory cortices, with the frontal and prefrontal areas the last to peak (Huttenlocher & Dabholkar 1997, Sowell et al. 1999, Johnston 2009). These bursts of synaptogenesis largely correlate with known region-specific milestones of behavioural neuro-development and are intrinsically regulated through a complicated pattern of axonal and target derived factors, and glial cell activity (Bourgeois et al. 1989, Johnston 2009, Eroglu & Barres 2010). Synapse elimination in contrast, is highly activity dependent and can be permanently affected by alterations in the environment as suggested by the landmark visual deprivation experiments of Hubel and Wiesel (*reviewed in Constatine-Paton 2008*). The overproduction of synapses and subsequent selective pruning is thought key to the plasticity which underlies both the normal processes of learning throughout childhood and the greater propensity of the neonatal brain to compensate for localised brain injury (Johnston 2009).

Intracellular calcium (Ca^{2+}) control is critical throughout human brain development; in particular playing a prominent role in neuronal migration, and in the development and organisation of

neuronal systems through the regulation of neurite outgrowth, synapse formation, and selective cell death (Volpe 2008, Michaelsen and Lohman 2010). Developmental plateaus in the expression of particular glutamate and GABA receptor subtypes appear to allow enhanced Ca^{2+} influx; with the relative over-expression of two particular subtypes of the ionotropic glutamate receptor (NMDA and AMPA) seemingly leading to a tendency towards excitability in the neonatal brain, thus rendering the brain overtly susceptible to the excito-toxic effects of hypoxic ischaemic injury (Volpe 2008, Aronica et al. 2011, Thornton et al. 2012). Coupled with the relative underdevelopment of the GABA inhibitory system, the neonatal brain is therefore also relatively predisposed to seizures, which are commonly seen following acute cerebral insults (Ben-Ari et al. 2007, Briggs & Galanopoulou 2011).

1.2.6. Intracranial vascular development

In correspondence with the rapid development and growth of the human brain, the vascular system develops in a predominately adaptive manner so that the metabolic and nutritional requirements of the adjacent neural tissue can be met (Raybaud 2010). In the first 8 gestational weeks, the metabolic and nutritional requirements of the developing CNS are fed firstly via simple diffusion from the surrounding amniotic fluid, and then via a primitive menigeal meshwork within dense connective tissue (meninx primitiva) around the newly closed neural tube (Padget 1948, Raybaud 2010, Kathuria et al. 2011). At approximately 5-7 weeks gestation, the primary vesicles of the brain differentiate (*as described in section 1.2.1*), and the first foundations of the arterial circulation are seen when the meninx primitiva invaginates into the neural tube and deposits a primitive choroid plexus (Padget 1948, Kathuria et al. 2011). As the maturing neural tube grows and thickens, intrinsic capillaries then develop and branch out from the meninx primitiva to penetrate the underlying parenchyma and supply areas with the highest metabolic demand: starting with the ventricular and subventricular zones early in gestation, and later the cortex in the third trimester and onwards (Gilles 2001, Takashima et al. 2009, Raybaud 2010). The first recognisable vessel to form at the base of the developing cerebrum is the internal carotid artery (at approximately 28 days gestation) which feeds

the vesicles of the forebrain, midbrain, and hindbrain, with subsequent branching and further development of the vertebral and basilar arteries leading to a more recognisable adult-like arterial organisation by approximately 35 days gestation (Padget 1948). In this arrangement, approximately 97% of the intracerebral blood supply is provided via flow through the paired internal carotid arteries and basilar artery, with the remaining 3% supplied to the cerebellum via branches of the vertebral artery (Nagasawa et al. 2000).

Angiogenesis proceeds in two discrete forms of germinal matrix; the striatal channels (which support the metabolic requirements of the central grey matter) and the extra-striatal channels (which supply the future white matter and cortex) (Gilles 2001). Muscularisation of the vessel walls are seen firstly in the striatal channels, with the majority of extra-striatal channels lacking a muscularis until the end of normal gestation (Norman & O'Klusky 1986, Kamei et al. 1992, Gilles 2001). Extra-striatal channel development appears to be governed through the rapid increase in cortical surface area over the third trimester of gestation, with rapid branching and penetration into the parenchyma maintaining an approximate interval of 100 micrometers between vessels (Kuban and Gilles 1985, Gilles 2001, Risser et al. 2009). During early human infancy, capillary branching continues to proceed at a significant rate with a two to three-fold increase in vascular volume, exchange surface area, and vessel length seen into adulthood (Risser et al. 2009).

1.3. MR imaging of the developing human brain

Much of the knowledge about human brain development described in the previous passages has been gained through a handful of landmark ex-vivo studies performed on small groups of post-mortem specimens, many of which had been affected by varying degrees of pathology (Padget 1948, Chi et al. 1977, Kuban & Gilles 1985, Kinney et al. 1988, Kostivić and Rakic 1990, Judaš et al. 2011). While some information (particularly on a cellular level) is likely only to ever be gained by this means, a complementary understanding of the living brain is also clearly essential to gain a complete picture

of its overall structure, function and development. Knowledge and visualisation of the in-vivo brain is of particular relevance in the clinical setting, as evidenced by the exponential rise in the use of medical imaging techniques which have become an indispensable component of patient investigation and management. Whilst widely available imaging tools such as projection radiography (X-rays) and ultrasound have long provided invaluable diagnostic information, these techniques suffer from innate limitations which restrict either their use (such as the potential harm to a patient from recurrent exposure to the ionising radiation of X-rays) and their ability to accurately visualise different body tissue types due to limits in the possible contrast and/or resolution.

MR imaging allows the acquisition of high spatial resolution images with excellent tissue contrast, which can be obtained in any plane (including in 3-dimensions), and without the risks of ionising radiation (Westbrook & Roth 2005). The principle of the technique lies in the detection of changes in the magnetic properties of the hydrogen ion nucleus, and in particular within the highly abundant water molecules of biological tissue (Westbrook & Roth 2005, McRobbie et al. 2010). Further major advantages of the technique also lie in the quantifiable nature of the acquired signal and the inherent flexibility, which can allow the detailed visualisation and accurate measurement of diverse aspects of macroscopic tissue structure, integrity, and composition. In addition, specially designed acquisition sequences can be used to investigate in-vivo functional measures of the tissue, such as the chemical composition (MR spectroscopy) and the local cerebral blood flow (Arterial Spin Labelling (ASL)) (McRobbie et al. 2010). These attributes have made MR imaging now commonplace both as a clinical investigation and for use in the research setting; where the objective measures provided can be utilised to accurately characterise specific tissue properties, directly test study hypotheses, and as a biomarker for clinical research (Miller 2004, Ment et al. 2009, Limperopoulos 2010, Thayyil et al. 2010, Matthews et al. 2011). An overview of the principles of MR signal generation and acquisition is provided in Chapter 2, with specific reference to the detection of

localised changes in the oxygen binding state of haemoglobin which are associated with brain activity and underlie the focus of this thesis, functional MRI (fMRI).

The use of MR imaging in studies of the neonatal brain has dramatically increased over the last 30 years, such that a medline search shows an increase in publications (using the search terms "neonate", "MRI", "human" "brain") from just 3 in 1982, to 263 in 2011 (see *figure 1.4*) (http://www.ncbi.nlm.nih.gov/pubmed). MRI techniques are particularly suited for studying the developing brain, as many of the described positive safety and image quality attributes are particularly paramount in research involving human fetuses and infants (Rutherford et al. 2008, Merchant et al 2009, Limperopoulos 2010, Panigrahy et al. 2010). Moreover, the quantitative nature of MRI data is particularly suitable for longitudinal studies of the early brain, as the growth and development can be accurately characterised and modelled (Battin & Rutherford 2002, Kapellou et al. 2006, Rutherford et al. 2008, Aljabar et al. 2011, Kuklisova-Murgasova et al. 2011, Silk & Wood 2011, Serag et al. 2012).

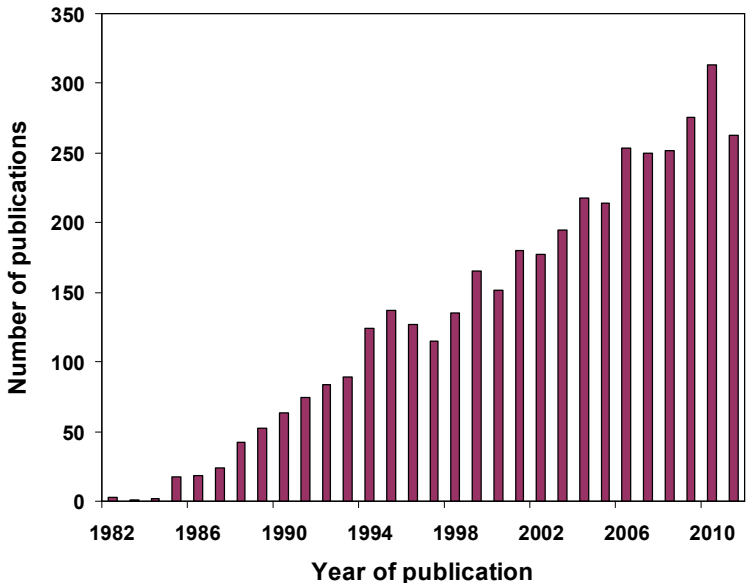

Figure 1.4: ***Since 1982, the number of published articles describing work involving MRI studies of the human neonatal brain has steadily increased.*** (Figure derived from a total number of 4074 publications identified through medline using the search terms "neonate" "MRI" "human" and "brain").

MR imaging therefore provides a means with which to accurately study and characterise early human CNS development, as the previously described developmental processes translate into dramatic macroscopic changes in the growth, composition, and function of the brain. These processes underlie a fundamental challenge of the field, which is to make suitable adaptations to optimise the image acquisition (and later analysis) to appropriately account for their cumulative effects (Rutherford et al. 2004, 2008, Panigrahy et al. 2010, Studholme 2011). These challenges include the purely practical (appropriate monitoring, immobilisation of the subject to minimise motion artefact, maintenance of clinical stability throughout the period of scanning); to making necessary adaptations to the acquisition sequence parameters; to altering computerised software packages for image analysis to take into account the very different contrast characteristics of developing brain tissue (Merchant et al. 2009, Maalouf & Counsell 2002, Xue et al. 2007, Panigrahy et al. 2010).

1.3.1. MRI of normal brain development in the third trimester

The majority of information gained from MRI studies of the developing brain prior to full term, have been gained from premature infants of an equivalent post-menstrual age (PMA) to the third trimester of human gestation (24 weeks to full term). With the development of advanced fetal imaging techniques (and in particular robust motion correction algorithms), complementary information has been gained from in-utero infants from approximately 20 weeks gestation (Jiang et al. 2007, Rutherford et al. 2008, Studholme 2011). As described previously, the fetal brain begins as a relatively lissencephalic structure, with the most of the major gyri and sulci not visible until the third trimester (*as shown in figure 1.5(i), section 1.2.3*) (Van der Knaap 1996, Battin et al. 1998, White et al. 2010). Owing to the mutli-planar nature of the technique, MR imaging is particularly suited to the characterisation of shape and the accurate measurement of volume; and these properties have allowed careful study of the patterns of maturation in both fetal and preterm infant populations (Van der Knaap 1996, Battin et al. 1998, Hűppi et al. 1998, Kapellou et al. 2006, Dubois

et al. 2008, Habas et al. 2012). While brain volume has been measured to steadily increase in the third trimester at a rate of 22ml/wk (resulting in an approximate threefold increase); the increases in cortical grey matter volume are even greater (approximately fourfold) (Hűppi et al. 1998, Kapellou et al. 2006, Xue et al. 2007). The rate of increase in cortical volume is further exceeded by the surface area of the brain (as the increase in volume does not correspond to an increase in cortical thickness), with an allometric scaling law (of approximate exponent 1.3) relating the whole brain volume to surface area (*see figure 1.3(i)*) (Kapellou et al. 2006, Xue at al. 2007).

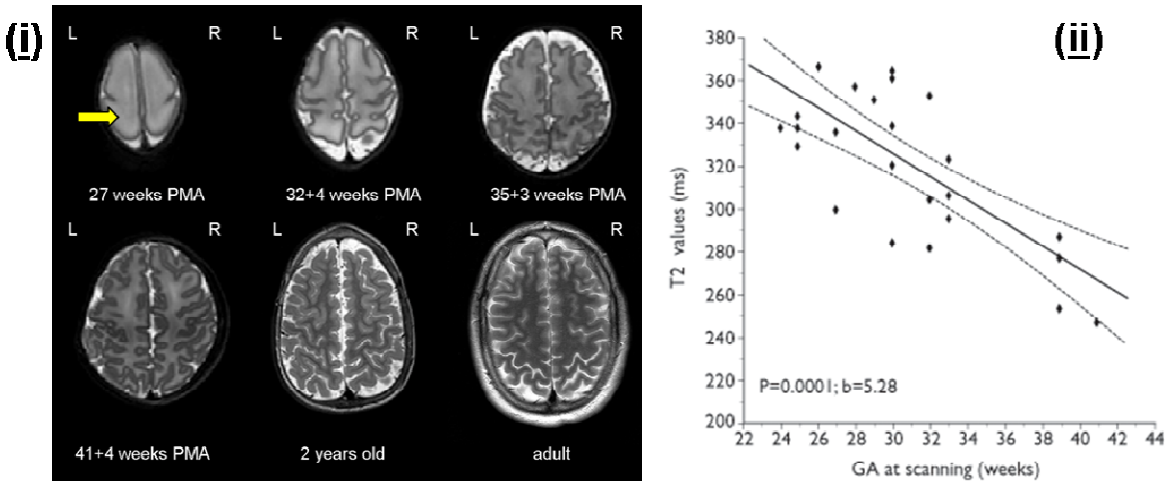

Figure 1.5 (i): ***Marked maturational changes in the appearances of the brain can be seen on T2-weighted MR imaging.*** At 27 weeks PMA, the brain is relatively smooth with only the central sulcus visible bilaterally. The white matter is of high signal, and concentric "bands" representing the laminar structure of the developing cortex are still visible (yellow arrow). Sulcation and gyrification can be seen to progress through the third trimester, with a progressive decrease in the white matter signal. The appearance of the 2 year old brain is far more similar to that of the mature adult brain on T2-weighted MR imaging, with a rich and complex pattern of cortical folding and low signal in the white matter (*Images not to scale*). **(ii):** ***The T2 value of the white matter in the centrum semi-ovale shows a linear decrease with increasing PMA*** (*figure (ii) reproduced from Counsell et al. 2003*).

In addition to the structural growth of the brain, tissue specific changes in contrast are visualised throughout development, largely due to maturational changes in cellular density and an associated decrease in tissue water content (*see figures 1.5(i) and 1.6*) (Battin & Rutherford 2002, Counsell et al. 2003). This process can be quantified by measuring changes in tissue specific MR properties such as the T2 value (the transverse relaxation time); which is higher in free water (where the interactions between protons are weaker) than in a bound state (as in macromolecules such as fat and protein) (Deoni 2010, McRobbie et al. 2010). With increasing PMA, T2 values are therefore seen to linearly decrease in both the deep grey matter (basal ganglia and thalamus) and immature white matter (*Figure 1.5(ii)*) (Counsell et al. 2003).

In the early third trimester, concentric bands of alternating signal intensity are visible within the white matter on both T1 and T2 weighted imaging, and are thought to represent transient features of the laminar structure of the developing cortex (*figure 1.5(i)*) (Battin et al. 1998, Battin & Rutherford 2002, Kostović et al. 2002, 2006, Radoš et al. 2006). At the start of the third trimester (24 gestational weeks), four distinct "bands" are seen at the level of the centrum semi-ovale representing a cortical layer, the subcortical white matter, an intermediate zone of migrating glial cells, and a periventricular zone of developing white matter adjacent to the germinal matrix (Battin et al. 1998). Inferiorly, the bands are present but incomplete and are described as "caps" (adjacent to the anterior horns of the lateral ventricles) and "arrowheads" (adjacent to the posterior horns) (Battin & Rutherford 2002). Through post-mortem MRI and correlated histological staining studies, KostoviĆ and colleagues have suggested that the relatively thick band of low signal on T1 imaging (and high on T2 imaging, *see figure 1.5(i)*) immediately below the cortical plate represents the transient subplate, which is characterised by a large extracellular space, and an abundance of glycosaminoglycans and chondroitin sulphate proteoglycans (Kostović et al. 2002, 2006, Radoš et al. 2006). On MR imaging, the subplate is most prominent at approximately 28-29 gestational weeks (at this stage is approximately 4-5 times thicker than the cortical plate), and is then seen to gradually

regress from approximately 31-32 weeks until it is no longer visible at full term gestation (Kostović et al. 2006, Radoš et al. 2006).

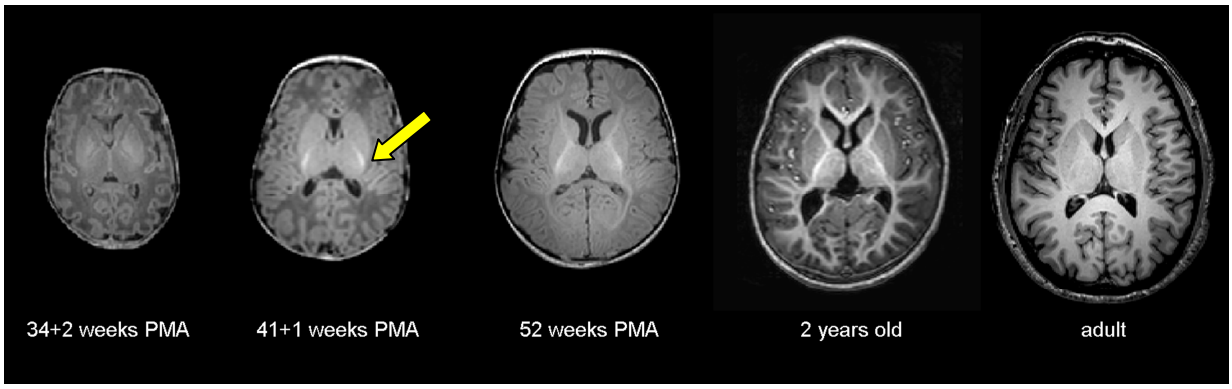

Figure 1.6: ***Progression of axonal myelination as visualised on T1-weighted MR imaging.*** At 34+2 weeks PMA, myelin is not evident and the white matter is uniformly of low signal on T1-weighted imaging. At approximately term equivalent age (41+1 weeks PMA), myelin is first seen in the posterior limb of the internal capsule (PLIC) as a thin band of high signal (arrowed yellow). By 3 months of age (52 weeks PMA), myelin is also now visible in the anterior limb of the internal capsule, and optic radiations. By 2 years of age, myelination is far more extensive and can be seen throughout the periventricular white matter and the external limb of the internal capsule. Therefore, in comparison to the preterm infant, the contrast of the white matter in the mature adult brain is completely reversed and universally of high signal. (*Images are not to scale*).

Although histologically, early evidence of myelin can be identified as early as the 12th gestational week, the majority of intracerebral myelination is known to occur post-term. Myelination is first seen in the posterior limb of the internal capsule (PLIC) at approximately 36 weeks gestation, with a clear band of myelin visible at term equivalent age (*see figure 1.6*) (Van der Knaap & Valk 1990, Rutherford et al. 1998, Battin & Rutherford 2002). In other areas, although myelin is not clearly visible, more sensitive markers of white matter microstructure and function such as those derived from diffusion weighted imaging show maturational changes consistent with an early "pre-myelinating" state, which further correlates with histological increases in axonal calibre, local oligodendrocytes and the levels of microtubule-associated proteins (which together are also

associated with faster axonal conduction velocities) (Wimberger et al. 1995, Hűppi et al. 1998, Neil et al. 1998, Dudink et al. 2008).

1.3.2. MRI of normal postnatal brain development

Despite clear differences in functional capability, the human neocortex at full term gestation surprisingly contains the same number of neurons as a mature adult (Bhadwaj et al. 2006, Nowakowski 2006, Lagercrantz & Changeux 2009). Although the rate of overall brain growth continues to be rapid over the subsequent 2 years of life (as measured through increases in whole brain volume) (Zhang et al. 2005), much of the development during this period has been found to involve tissue specific maturation and activity dependent changes in connectivity (Lagercrantz & Changeux 2009). A prime example of this is that all of the sulci and gyri which can be identified in the mature adult brain are recognisable by full term gestation; although the sulci continue to deepen throughout infancy and the folding becomes more convoluted to accommodate the increasing whole brain size (Armstrong et al. 1995, White et al. 2010).

Changes in the volume and MR signal of the cortex in early childhood appear to correlate with the heterochronous patterns of postnatal synaptogenesis (Huttenlocher & Dabholkar 1997, Sowell et al. 2004, Westlye et al. 2010). Similarly, the thinning of the cortex seen in later childhood is thought to be representative of the selective synaptic pruning occurring at that time (Sowell et al. 2004, Westlye et al. 2010). T1 and T2 values are both seen to decrease in the grey matter and more significantly within the white matter during the first year of postnatal life due to a reduction in free water content (together with increasing compartmentalisation of water by macromolecules such as myelin) and increases in the paramagnetic iron content (Leppert et al. 2009, Deoni et al. 2010, 2011). Subtle changes in signal are also seen in other key structures including the deep grey matter, with increasingly clear demarcation of the distinct nuclei within the basal ganglia and thalamus evident postnatally (Barkovich 1998, Cowan 2002).

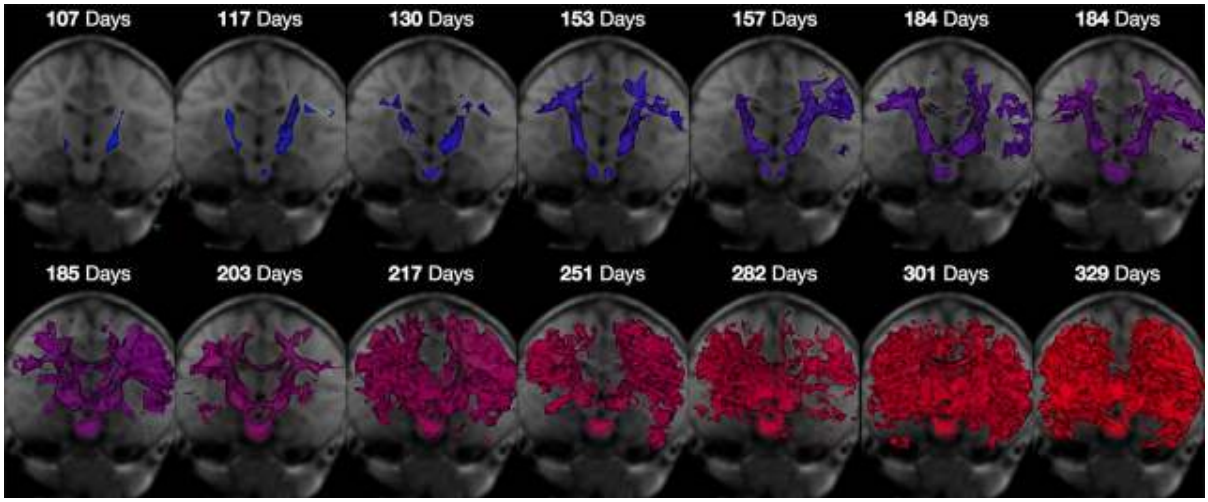

Figure 1.7: ***Myelination of the white matter during the first year of postnatal life as measured through changes in the Myelin Water Fraction.*** As seen in histological studies, quantitative data derived from MR measurements using multi-component relaxometry shows a clear spatiotemporal progression with myelin first seen in the deep white matter (internal capsule), and then later the superficial areas such as the periventricular white matter. (*Figure reproduced from Deoni et al. 2011*)

The major driver of the enormous changes in T1 and T2 values within the developing white matter at this juncture is myelination, which proceeds throughout the central nervous system in a caudal to cephalic manner, with the frontal white matter last to myelinate (Barkovich 1998, Cowan 2002, Deoni et al. 2011). In addition to characterising the schedule of myelination visually with MRI, it is also possible to quantify the developmental changes indirectly using techniques such as diffusion weighted imaging (such as the Apparent Diffusion Coefficient (ADC) and Fractional Anisotropy (FA)), and directly by measuring the myelin water fraction (MWF) using multi-component relaxometry (*see figure 1.7*) (Cowan 2002, Ben Bashat et al. 2005, Zhang et al. 2005, Huang et al. 2006, Deoni et al. 2011, Geng et al. 2012). Furthermore, through constructing a mathematical tensor which can represent the underlying directionality of the restricted water diffusion in axon fibre bundles, it is also possible to delineate and visualise the trajectory and integrity of specific fibre "pathways" (termed diffusion tensor imaging (DTI) tractrography) (Dudink et al. 2008, Geng et al. 2012).

1.4. Brain injury and preterm birth

As survival rates have improved with advances in neonatal care, it has become apparent that preterm birth engenders a very specific pathological phenotype in young adulthood with suboptimal function affecting a number of physiological systems through the complex interplay of multiple gene-environment interactions (Allen 2008, Ment et al. 2009, Hack 2009, Doyle 2010). Neurological difficulties are particularly prevalent; with up to 9% of infants affected by cerebral palsy, and up to 50% of very low birthweight (<1000g) affected by cognitive impairment, behavioural difficulties and a requirement for special educational support (Hintz et al. 2005b, Allen 2008, Larroque et al. 2008, Johnson et al. 2009, Beaino et al. 2010, Johnson et al. 2010). Disabilities are greater in male infants, and those delivered at younger gestational ages (Beaino et al. 2010, Kent et al. 2012). Although the incidence and spectrum of disabilities have been well described, the underlying neuropathalogical correlates remain relatively poorly understood and cover a spectrum of lesions, many of which are unique to prematurity (Ment et al. 2009, Volpe JJ 2009b).

Pioneering research has led to a greater understanding of the physiological processes which comprise early human development, which have importantly then led to marked improvements in the standard and outcomes of neonatal clinical care. These include knowledge of the potential pathogenic effects of inappropriate treatment such as excessive invasive ventilation and oxygen therapy, and the benefits of appropriate temperature control and nutrition (Ambalavanan & Carlo 2006, Eichenwald & Stark 2008, Groenendaal et al. 2010, Civardi et al. 2011). Similarly, these changes in clinical practice have seen gradual improvements in the incidence of previously common severe forms of preterm brain injury, in particular cystic-PVL and Haemorrhagic Parenchymal Infarction (HPI) (Platt et al. 2007, Robertson et al. 2007, Surman et al. 2009, Groenendaal et al. 2010, van Haastert et al. 2011). Of importance, neurodevelopment abnormalities remain common in preterm infants even in the absence of these rarer forms of overt brain injury, suggesting a more

global insult to brain development which Volpe has termed the “Encephalopathy of Prematurity” (Allen et al. 2008, Volpe JJ 2009a,b).

The anatomical appearances of the brain in the neonatal period visualised with both cranial ultrasound and less commonly MRI are often used by clinicians to identify high risk infants and provide families with prognostic information about neurodevelopment. However, existing studies suggest that the qualitative assessment of the images derived from both techniques suffers from wide confidence intervals and cannot be considered to be reliable for predicting later adverse outcome, with the exception of motor impairment (Nongena et al. 2010). By accurately quantifying changes in brain structure and function, the more widespread application of advanced MRI techniques has started to allow researchers to begin to truly understand the underlying pathophysiology and objectively characterise its effects on development. These studies have suggested that preterm birth engenders a specific pathological brain phenotype, and further that specific alterations in neural connectivity may underlie the life-long impairments in neurological function (Ment & Constable 2007, Dudink et al. 2008, Ment et al. 2009, Lubsen et al. 2011, Smyser et al. 2011). In this section, I will briefly summarise the spectrum of brain injury seen in infants born prematurely, and highlight how information derived from MRI techniques has added enormously to the knowledge of the underlying pathophysiology.

1.4.1. Intraventricular Haemorrhage

Intraventricular haemorrhage (IVH) remains a common problem affecting between 20-49% of extremely low birth weight infants (Larroque et al. 2003, Kadri et al. 2006, Volpe 2008). The haemorrhage arises from the highly vascularised and densely cellular subependymal germinal matrix of the developing brain (Volpe 2008). This germinal matrix contains an elaborate capillary bed, with a rich arterial blood supply and a well developed venous drainage system which terminates in the vein of Galen (Kuban & Gilles 1985, Takashima et al. 2009, Raybaud 2010). The haemorrhage most

commonly arises in the fragile endothelial-lined vessels of the capillary bed, with subsequent spread into the adjoining lateral ventricles (Volpe 2008). Pathogenesis is multi-factorial, with specific facets of preterm physiology and clinical management thought to predispose the infants to IVH including: a lack of cerebral autoregulation, frequent and sudden episodes of rapid cerebral blood flow change secondary to ventilatory support, an increased incidence of anaemia, platelet and coagulation disturbances, and immature vascular integrity (Perlman et al. 1983, Amato et al. 1988, Soul et al. 2007, Volpe 2008, Takashima et al. 2009). The consequences of IVH can generally be classified into three categories: destruction of the germinal matrix leading to a loss of glial precursor cells; post-haemorrhagic ventricular dilatation and hydrocephalus; and infarction of the adjacent parenchyma (termed a Haemorrhagic Parenchymal Infarction (HPI)) due to impaired drainage of the medullary veins in the periventricular white matter (de Vries et al. 2001, Volpe 2008).

IVH is typically classified into 4 “grades” based on ultrasound appearances (Levene & de Crispgny 1983). In the EPIPAGE cohort, the incidence of IVH without ventricular dilatation (grades 1 and 2) was 20% amongst all of the infants delivered between 22-32 weeks gestation, although the incidence was markedly higher in the most immature infants (40% of infants delivered at 23-24 weeks gestation) (Larroque et al. 2003). The incidences of IVH with ventricular dilatation (grade 3) and extension into the adjacent parenchyma (grade 4 with HPI) are significantly less affecting 3-5.7% of preterm infants (Larroque et al. 2003, Groenendaal et al. 2010). Both grade 3 and 4 IVH carry a significant risk of developing severe adverse sequelae, with post-haemorrhagic ventricular dilatation requiring surgical intervention in up to 56% of infants, and cerebral palsy in nearly 50% of infants with grade 4 IVH (Brouwer et al. 2008).

1.4.2. Periventricular Leukomalacia and white matter injury

White matter injury is the most common form of neuropathology affecting at least 50% of all preterm infants (Volpe JJ 2008, 2009b). Abnormalities can be both focal (as in HPI) or global, and are

accompanied by varying degrees of neuronal-axonal injury throughout the brain including the cortex, deep grey matter (thalamus and basal ganglia), brain stem, and cerebellum (*figure 1.8*) (Volpe JJ 2009a,b, Ment et al. 2009). With the exception of focal injury secondary to grade 4 IVH (HPI), current theories contend that all other forms of white matter preterm injury result from a common pathophysiological pathway which result in a spectrum of injury which can all be described within a continuum of periventricular leukamalacia (PVL) (Volpe JJ 2009a,b). The primary pathogenic mechanisms of PVL are generally considered to be hypoxia-ischaemia and inflammation which have been initiated through intra-uterine infection and/or postnatal sepsis, although some evidence has also suggested an additional causative role for high grade IVH (Volpe 2008, Kusters et al. 2009, Takashima et al. 2009, Volpe 2011). Downstream, excitotoxicity and free radical accumulation appear to mediate the mechanisms of damage, resulting in marked astrogliosis, microgliosis, and alterations in oligodendrocyte maturation (with an initial loss of premyelinating oligodendrocytes) (Armstrong &Norman 1974, Volpe JJ 2009a,b, Volpe 2011). Importantly, similar pathological changes in the white matter are also seen in primate models of preterm birth and neonatal intensive care treatment (Inder et al. 2005).

In the most severe cases, macroscopic areas of necrosis are seen in the periventricular white matter, which result in the formation several weeks later of multiple large cysts (measuring several millimetres or more in diameter), with the appearance typically termed cystic-PVL (*figure 1.8(c)*) (Banker & Larroche 1962, Armstrong & Norman 1974, Volpe JJ 2009a,b). The original descriptions of PVL by Virchow (1867) (and later refined in a large case series by Banker & Larroche (1962)) were of focal demyelination in the white matter secondary to infarction in preterm infants of 34 weeks gestation and above, and almost certainly were describing this most severe form of the disease (Armstrong & Norman 1974, De Vries et al. 2002, Deng et al. 2008). Encouragingly, studies across a number of different countries within the developed world have consistently shown that the incidence of cystic-PVL has steadily decreased over the last 20 years, and now affects just 0.5-5% of

preterm infants born at less than 33 weeks gestation (Larroque at el. 2003, Hamrick et al. 2004, van Hassert et al. 2011, Sugiura et al. 2012). Although the neurodevelopmental outcome of cystic-PVL is highly dependent on the location of the cystic lesions, extensive lesions are invariably associated with poor outcome with up to 90% of affected infants later developing cerebral palsy, typically of a spastic diplegic type (de Vries et al. 2004, Ancel et al. 2006, van Haastert et al. 2011).

Far more common than the overt macroscopic lesions of cystic-PVL, are areas of gliotic scarring which arise from microscopic necrosis in the peri-ventricular white matter, and a more diffuse effect on white matter maturation and function, which collectively has been termed “non-cystic” PVL (Volpe JJ 2009a,b, Volpe 2011). The identification of this more subtle white matter injury in preterm infants has dramatically increased due to the greater sensitivity of neuroimaging techniques (and in particular MRI). Moreover, quantitative MR measures of this “milder” form of injury have been found to inversely correlate with neurodevelopmental outcome, suggesting that it is not entirely benign in nature (Counsell et al. 2006, Krishnan et al. 2007, Cheong et al. 2009). This form of common injury is difficult to detect with cranial ultrasound examination, and was probably present (but not recognised) in the majority of preterm infants reported to have “normal brain appearances” in historical cohorts who developed later adverse neurodevelopmental outcome (Allen 2008, Volpe 2008).

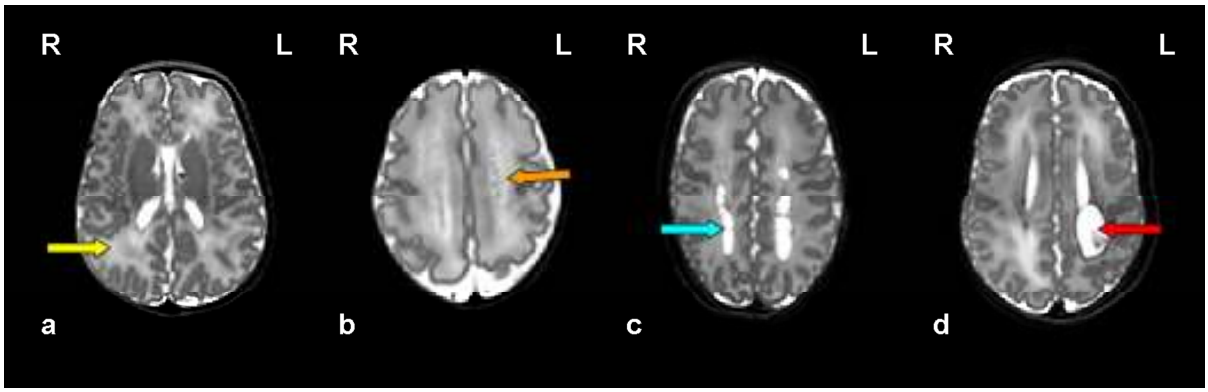

Figure 1.8: ***The spectrum of white matter pathology seen in preterm infants on T2-weighted MRI.*** White matter injury is seen in approximately 50% of all infants born prematurely; (a) The commonest lesion is Diffuse Excessive High Signal Intensity (DEHSI) in the periventricular white matter (yellow arrow); (b) low signal punctate lesions seen here in the centrum semiovale (orange arrow); (c) cystic Periventricular Leukomalacia (PVL) with multiple large cysts in the white matter (blue arrow); (d) porencephalic cyst (red arrow) arising from the roof of the left lateral ventricle following grade 4 intraventricular haemorrhage (Haemorrhagic Parenchymal Infarction (HPI)).

1.4.2.1. MRI appearances of white matter injury

MR imaging is particularly sensitive at identifying white matter abnormalities, with up to 80% of preterm infants showing increased T2 signal and decreased volume within the white matter on MR imaging at term equivalent PMA (*figure 1.8(a)*) (Maalouf et al. 1999, Dyet et all. 2006, Hagmann et al. 2009, Rutherford et al. 2010). Objective measures of white matter volume and morphometric studies have confirmed a significant reduction in white matter volume which is maintained even in adolescence (Inder et al. 2005, Giminez et al. 2006, Kesler et al. 2008, Nosarti et al. 2008). The clinical importance of increased T2 signal in the white matter (termed Diffuse Excessive High Signal Intensity (DEHSI)) is uncertain, with recent studies suggesting that the appearance does not correlate with later adverse neurodevelopmental outcome in childhood (Hart et al. 2011, Kidokoro et al. 2011). However, a clearer association between white matter signal abnormalities and outcome is identified when more specific quantitative measures derived from diffusion weighted imaging such as the ADC, FA and radial diffusivity (RD) are studied, which furthermore suggest that the

underlying pathology may involve oligodendrocyte and axonal abnormalities (Counsell et al. 2006, Krishnan et al. 2007 Cheong et al. 2009).

Punctate white matter lesions are seen in approximately 20% of preterm infants on conventional MR imaging, and can be distributed throughout the white matter in addition to the periventricular areas (*figure 1.8(b)*) (Cornette et al. 2002, Dyet et al. 2006, Rutherford et al. 2010). The aetiology is unclear, although studies utilising susceptibility weighted imaging (SWI) suggest that there may be different forms with some lesions clearly haemorrhagic in origin, while others appear to represent early gliosis and microglial infiltration (Rutherford et al. 2010, Niwa et al. 2011). Although the lesions are small and transient enough that they are not readily visible on cranial ultrasound examination and are usually no longer visible with MRI at term equivalent gestational age, some studies have suggested that they are not entirely benign, and are associated with a qualitative reduction in cortical maturation and myelination at term equivalent age (Ramenghi et al. 2007). Clinical outcome measures however suggest that neurodevelopment is not adversely affected except in those infants with a large number of punctuate lesions and/or additional cerebral pathology (Cornette et al. 2002, Dyet et al. 2006, Bassi et al. 2011).

1.4.2.2. Detailed MRI studies of white matter microstructure

Metrics derived from Diffusion Tensor Imaging (DTI) have been used in a number of studies to probe the alterations in white matter microstructure which are associated with prematurity. The fundamental premise of these studies is that healthy and appropriately developed (and/or myelinated) white matter tracts will have increased diffusion of water along the principle tract direction, with a corresponding restriction perpendicular to this, represented by a high FA and low RD (reviewed in Dudink et al. 2008). In addition to studies measuring these parameters using pre-defined regions of interest (ROIs), the recent development of advanced techniques such as Tract-Based Spatial Statistics (TBSS) have made it possible to perform whole brain, voxelwise analyses to

test detailed hypotheses across groups of patients (Smith et al. 2006, Ball et al. 2010). These studies have shown that even in the absence of overt white matter lesions on conventional MR images, significant reductions are present in the FA of the centrum semiovale, frontal white matter, and corpus callosum in preterm infants at term equivalent age in comparison to control infants (*figure 1.9*) (Anjari et al. 2007). In addition, the microstructure of the white matter has been found to be more extensively and significantly impaired in infants born at younger gestational ages, those with a history of chronic lung disease (with an oxygen requirement at 36 weeks PMA), and in those with a high lesion load of punctate white matter lesions (Anjari et al. 2007, Anjari et al. 2009, Ball et al. 2010, Bassi et al. 2011).

The possible utility of these objective measures of white matter microstructure integrity as biomarkers has been highlighted by recent studies which have demonstrated that reductions in FA correlate with standardised concurrent measures of neurodevelopmental status; such as performance in the Griffiths Mental Developmental Scale (GMDS) at 2 years, Intelligent Quotient (IQ) scores, and assessment of verbal and visual-motor integration at 12 and 16 years of age (Counsell et al. 2008, Constable et al. 2008, Mullen et al. 2011). Crucially, 2 recent studies have also found that alterations in FA at term equivalent age can be similarly correlated with neurodevelopmental outcome at 2 years of age in both ex-preterm infants and in term infants following hypoxic ischaemic encephalopathy, suggesting that it can be used as an imaging biomarker which accurately correlates with later outcome (Tusor et al. 2012, van Kooij et al 2012).

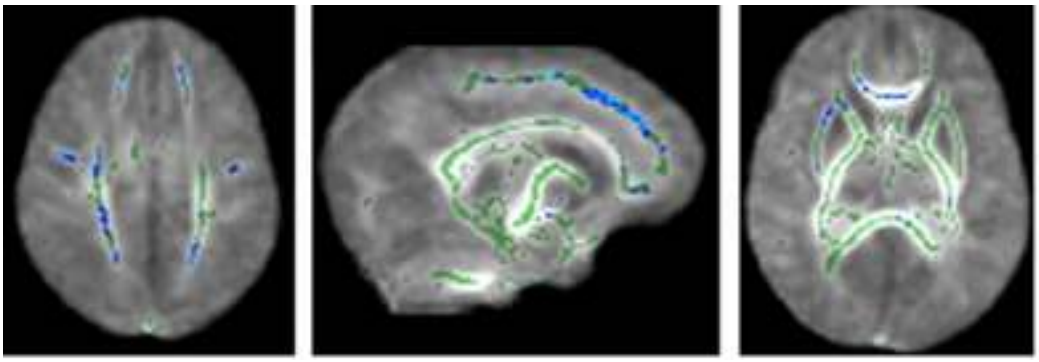

Figure 1.9: ***Preterm birth is associated with significant decreases in white matter microstructure at term equivalent age.*** Observer-independent whole brain analysis techniques such as Tract-based Spatial Statistics (TBSS) can be used to identify significant decreases (blue) in the Fractional Anisotropy (FA) of the white matter (group mean FA skeleton is shown in green) in infants born at less than 28 weeks gestation in comparison to term born controls (*Figure adapted and reproduced from Anjari et al. 2007*).

The directional information derived from diffusion DTI data can be further analysed to reconstruct white matter fibre tract pathways, and therefore to directly investigate the effects of prematurity on particular distributions of structural connectivity. Using this approach, Bassi and colleagues demonstrated a significant correlation between the FA of the optic radiations as delineated by probabilistic tractography and a visual assessment at term equivalent age (Bassi et al. 2008). Of further interest, in a later study, it was found that visual function at term equivalent age could not be predicted by the FA within the optic radiations when assessed at an earlier scan during the preterm period, suggesting that any alteration in white matter microstructure and resultant visual function was occurring as a postnatal process during the preterm period (Groppo et al. 2012). Similar correlations have been described between the cortico-spinal tracts and later motor outcome in infants with focal brain injury (Roze et al. 2012).

1.4.3. Brain growth and volume

In addition to obvious white matter axonal damage, the damage of PVL also involves accompanying neuronal damage which can be identified during the initial stages of the disease in the preterm

period, and can be seen throughout the cortex, deep grey matter and cerebellum (Ment et al. 2009, Volpe JJ 2009a,b, Lubsen et al. 2011). A recent meta-analysis of 15 MRI studies has found that very preterm infants as young adults have a significant reduction in whole brain volume and an associated increase in ventricular volume in comparison to term-born controls (de Kieviet et al. 2012). This reduction is seen throughout the brain, and in particular in several key structures including the thalamus, hippocampus, corpus callosum, cortex, and white matter (de Kieviet et al. 2012). The degree of later brain volume loss has been found to be related to the gestation of the infant at birth, and appears to be directly related to the level of neurodevelopmental and cognitive impairment (Nosarti et al. 2008). While the exact pathophysiological mechanism underlying this volume loss remains uncertain, it seems likely that a disruption to the normal patterns of intracerebral connectivity is integral to these changes (Lubsen et al. 2011, Ball et al. 2011).

1.4.3.1. Cortical volume and development

Despite a reduction in adolescence, preterm infants without a history of chronic lung disease do not have a reduced whole brain volume at term equivalent age in comparison to term-born controls (Ajayi-Obe et al. 2000, Zacharia et al. 2006, Boardman et al. 2007, de Kieviet et al. 2012). Although brain volume is preserved, morphometric MRI studies have found a specific but significant reduction in the volume, surface area and the complexity of folding of the cortex at term equivalent age; which suggests that whole brain growth failure appears to be a secondary consequence following on from these early signs of pathology (Ajayi-Obe et al. 2000, Inder et al. 2005, Kapellou et al. 2006). The importance of this period further is highlighted by studies which have found that the rate of cerebral cortical growth in the preterm period is highly predictive of cognitive ability (but not motor outcome) later in childhood at 2 and 6 years of age (Kapellou et al. 2006, Rathbone et al. 2011). Together with the known reductions in white matter integrity and volume, these findings could be interpreted as strongly supportive of the “veso-elastic tension” hypothesis of cortical gyrification as proposed by van Essen, as a reduction in the underlying white matter connectivity would be

expected to result in a decrease in the tensile forces which are proposed to cause cortical folding (van Essen 1997).

Detailed quantitative studies using computer-based morphometric techniques such as Voxel-based Morphometry (VBM) have consistently identified particular areas of specific volume loss in the prefrontal, fronto-temporal, temporal, hippocampal and cingulate areas in preterm infants in later childhood and adolescence; with these effects more profound in male subjects (Peterson et al. 2000, Kesler et al. 2008, Nosarti et al. 2008, Nagy et al. 2009, Soria-Pastor 2009). In addition, accompanying deficits are also seen in the functional skills associated with these cortical areas including reading, language, executive control and visual-spatial attention (Allen 2008, Kesler et al. 2008, Nosarti et al. 2008). Crucially, a recent study using Deformation-based morphometry (DBM) has shown that a similar pattern of volume loss in the anterior temporal lobes and orbitofrontal areas can be identified even as early as term equivalent age (*figure 1.10*) (Ball et al. 2011).

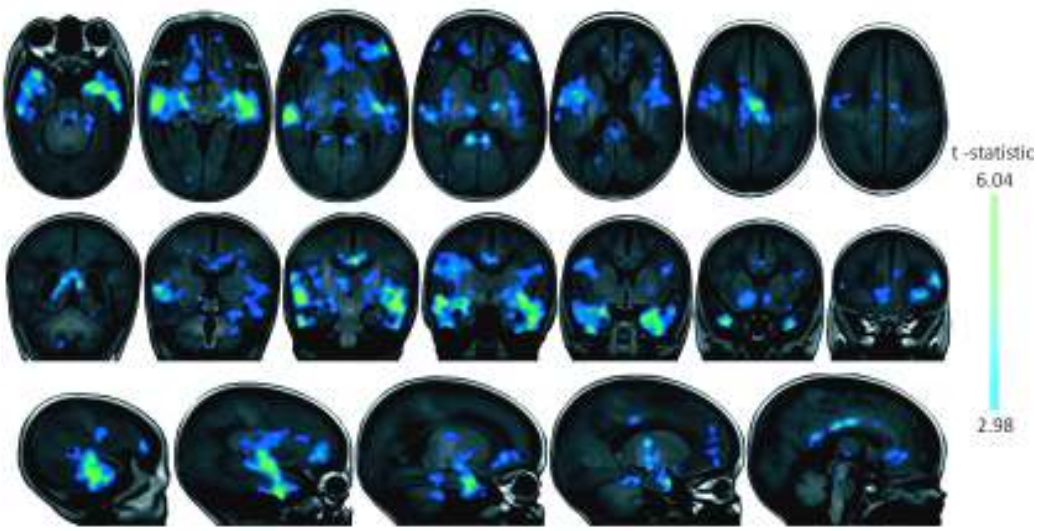

Figure 1.10: ***At term-equivalent age, there are regional reductions in brain volume which are maintained into adolescence.*** Deformation based morphometry shows that an increasing degree of prematurity at birth is associated with a decrease in volume in the anterior temporal lobes, the orbito-frontal areas, the posterior cingulate, the thalamus, and the centrum semiovale. (*figure reproduced and adapted from Ball et al. 2011*)

1.4.3.2. Thalamo-cortical connectivity

The thalamus is a key structure in determining the function of the brain, as nearly all incoming information to the cortex is relayed through the thalamus and via its associated connections (Behrens et al. 2003a, Sherman 2007, Wang et al. 2010). Within the thalamus, a distinct pattern of cytoarchitecture can be recognised from at least 2 years of age in human subjects, with specific nuclei differentiated by the pattern of anatomical connectivity with the cortex (Behrens et al. 2003a, Counsell et al. 2007, Broser et al. 2011). From the perspective of thalamocortical connectivity, the third trimester of human gestation represents a critical juncture in development and perhaps a specific window of vulnerability, as a dense network of thalamo-cortical circuitry is established through the transient subplate (Kostović & Jovanov-Milošević 2006, Ball et al. 2011).

The thalamus appears to be particularly susceptible to injury following preterm birth, as volumetric studies have found that even in the absence of severe white matter disease, infants born preterm have significant reductions in thalamic volume at term equivalent age (*figure 1.10*) (Inder et al. 2005, Boardman et al. 2006, Srinivasan et al. 2007, Ball et al. 2011). In keeping with the described trends seen in injury of other brain structures, the degree of prematurity at birth is inversely correlated with the volume of the thalamus (Inder et al. 2005, Boardman et al. 2006, Ball et al. 2011). The importance of thalamic growth and connectivity was underlined in a recent study by Ball and colleagues in which thalamic volume (controlling for the degree of prematurity at birth) was shown to predict both specific patterns of decreased brain volume, and impaired white matter microstructure in the corticospinal tracts and corpus callosum (Ball et al. 2011). In addition, a combined imaging phenotype of reduced white matter and thalamic volume at term equivalent age has been found to be highly predictive of adverse neurodevelopmental outcome at 1 and 2 years of age (Inder et al. 2005, Boardman et al. 2010).

1.4.3.3. Cerebellar growth and development

Although long known to be integral to sensori-motor function and coordination, in recent years the cerebellum has come under increasing scrutiny in neuroscientific studies as its crucial role in learning, attention, and cognitive function has become apparent (Manto & Jissendi 2012). The cerebellum is of particular interest as it has a unique pattern of connectivity and development distinct from that of the supratentorial cerebrum, and additionally undergoes a period of rapid growth during the third trimester of human gestation (Limperopoulos et al. 2005, Manto & Jissendi 2012). Injury to the cerebellum has classically been under-recognised in preterm infants, largely due to the restraints in visualisation imposed by cranial ultrasound examination (Limperopoulos & du Plessis 2006). In one cohort, cerebellar haemorrhage was identified in nearly 20% of infants with a birth weight less than 750g (Limperopoulos et al. 2005). Even in the absence of direct cerebellar injury, its growth appears to be adversely affected by preterm delivery, with a significantly reduced volume seen in adolescence in comparison to term-born controls (de Kieviet et al. 2012). However, as seen with whole brain volume measurements, a reduction is not seen at term equivalent age in the absence of supra-tentorial lesions (Shah et al. 2006, Srinivasan et al. 2007).

Recent studies have also found that cerebellar injury appears to confer a significant increase in the risk of later neurodevelopmental impairment, with one study finding that as high as 66% of infants with preterm cerebellar haemorrhage developed later neurological difficulties (including a significant increase in autistic tendencies) (Limperopoulos et al. 2007). While a single study found only a weak correlation (which was partially mediated by the degree of white matter injury) between cerebellar volume and cognitive and motor outcome (Shah et al. 2006), recent studies have identified a stronger correlation between objective measures of reduced cerebellar volume and adverse neurological outcome at 2 years (Lind et al. 2011, van Kooij et al. 2012). Moreover, the effects of impaired cerebellar growth can be life-long, as evidenced by an inverse association between

cerebellar volume and the prevalence of neuropsychological difficulties in young adulthood (Parker et al. 2008).

1.5. Summary

The human brain undergoes a dramatic and rapid, but highly structured pattern of maturation during gestational life. Disruption to these developmental processes leads to life-long neurodevelopmental difficulties, as highlighted by the marked increase in incidence seen in infants born prematurely, even in the absence of overt cerebral pathology. In-vivo neuroimaging tools, and in particular MRI techniques, have provided a wealth of new information about the underlying pathophysiology; and have identified a specific imaging phenotype which appears to result from the preterm period, and can be readily detected at term equivalent age. The application of advanced MRI tools may have the potential to act as much needed biomarkers for predicting outcome and measuring the response to therapeutic intervention.

Chapter 2

2. Functional Magnetic Resonance Imaging

Whilst a great wealth of knowledge about the structure and development of the immature brain has long come via detailed histological and macroscopic ex-vivo studies, a true understanding has been limited by the relative lack of capacity to provide information about the brain's function. In recent years, functional brain imaging techniques have become commonplace in the neuroscience and clinical communities as a means with which to gain objective information about and/or visualise "brain activity" through the measurement of the underlying or associated short-term (and often brief) physiological processes (Huettel et al. 2004). The information derived from these techniques is extremely diverse, and covers a wide spectrum of temporal and spatial resolutions. Although largely complementary, different techniques provide information which may represent both direct and indirect measures of the neuronal activity, and therefore the comprehensive integration of this multi-modal data remains a necessary but highly complex challenge. At the finest end of the resolution scale, in-vitro electrophysiology can be used to directly measure the rapid changes in neuronal membrane potential which accompany neurotransmission, at a spatial resolution as fine as in a single neuron. In contrast, in-vivo imaging techniques (such as functional MRI (fMRI) and Positron Emission Tomography (PET)) may not offer such fine spatial or temporal information, but provide a wealth of rich information which describes the activity of large populations of neurones in their natural state (Matthews 2001, Huettel et al. 2004).

Fundamental to two of the most prominent in-vivo techniques currently in use is the long-recognised principle that neuronal activity is a highly metabolic process, and that the local demand for the required substrates are provided by a rapid increase in blood flow via the dense cerebral vasculature (*reviewed in Gjedde 2001, Buxton 2009, Kim & Ogawa 2012*). The first of these techniques to reach prominence was PET, in which changes in local brain blood flow and metabolism are identified following the injection of a radioactive tracer (Sokoloff et al 1977, *reviewed in Jones &*

Rabiner 2012). Functional MRI (fMRI) overcomes some of the major disadvantages inherent to PET, as it is without exposure to ionising radiation, does not require the expensive development and storage of radioactive isotopes, and has less limitations to the temporal resolution at which data can be sampled (Matthews 2001, Huettel et al. 2004, Buxton 2009). In the last 30 years, these techniques have transformed neuroscience by offering the potential to accurately localise, measure, and characterise large-scale patterns of function in the living, working brain.

The concept of localisation and "mapping" of brain function was first proposed by Franz Joseph Gall (1758-1828) and advocated by the phrenologists of the early nineteenth century, who maintained that specific personality attributes were supported by distinct areas of the brain, and that these traits could be identified by palpating a relative increase or decrease in size as bumps or smoothness felt on the overlying skull (Simpson 2005). Despite phrenology falling out of favour later in the nineteenth century, localisation of brain function was later confirmed in the celebrated clinical case reports of Paul Broca (1824-1880) who described a series of patients suffering from expressive aphasia (loss of speech production) following damage to an area in the left lateral frontal lobe (*now known as Broca's area*) (Finger 2004, Simpson 2005). Although further cases of lesion and location-specific loss of function were reported throughout the nineteenth century (*reviewed in Frith 2007*), the next major advance in brain mapping was the detailed work of the German neurologist Korbinian Brodmann (1868-1918). Brodmann described 52 distinct subdivisions of the human cerebral cortex based on careful examination of their histological (termed "cyto-architectonic") characteristics (*translated and reproduced in Garey 1999*). Brodmann's eponymous areas are still used in current neuroscience, and in particular to classify and localise the patterns of brain activity identified in functional neuroimaging experiments. Ironically, in his original landmark monograph (*Garey 1999*), Brodmann himself concludes:

> "*One thing must be stressed quite firmly: henceforth functional localisation of the cerebral cortex without the lead of anatomy is utterly impossible in man as animals…anyone wishing to undertake physiological localisation studies will have to base his research on the results of histological localisation*".

Although functional Imaging techniques have consolidated the concept of functional localisation; the richness of the data provided has also opened new avenues into exploring the integration of function between distinct brain regions (Smith 2012). Even at rest, specific and reproducible patterns of spontaneous but highly correlated fluctuations in the fMRI signal are seen between distinct brain regions (Biswal et al. 1995, Smith et al. 2010). Characterising brain function has therefore proved to be a far more complex challenge than localisation of function alone; as an individual brain region may participate in several functions, with a given single function often requiring the co-ordinated activity of several regions which are distributed into specific topologically efficient "networks" throughout the brain (Bullmore & Sporns 2012).

Techniques such as fMRI therefore offer the clear potential to provide a new and vital dimension to our understanding of early human brain development; not only by allowing the characterisation of responses to external stimulation, but also by providing a wealth of new knowledge about the development of whole-brain neural integration and the dynamic properties of immature brain function. In the twenty years since it was first described however, fMRI has rarely been used to study human neonatal subjects, due to a history of inconsistent results and fundamental challenges with respect to both the acquisition and analysis of data. To put these difficulties in context, in this chapter of the thesis, I will outline briefly the basic principles of MR imaging, and specifically those which underlie fMRI data acquisition and the underlying physiology. I will then review in more detail the fundamentals of fMRI experimental methodology and analysis.

2.1. Basic principles of MRI

All of Magnetic Resonance Imaging is based on core principles about the magnetic properties of atomic nuclei, which were independently described by the seminal work of physicists and Nobel laureates Edward Purcell and Felix Bloch in 1946 (*reviewed in Buxton 2009*). While techniques based on this work were then used throughout the twentieth century as a powerful tool for analytical chemistry, it was then the landmark work of Nobel laureates Paul Lauterbur (1973) and Peter Mansfield (1977) which led to the application of the technique as an imaging modality, and ultimately to MRI's current status as an established tool in both clinical and scientific work.

2.1.1. Nuclear Magnetic Resonance

All matter is composed of atoms, which contain a small densely packed nucleus of neutrons and protons, and a surrounding electron cloud. Underlying the principles of Nuclear Magnetic Resonance (NMR) are two fundamental properties of atoms (Westbrook & Roth 2005, Buxton 2009, McRobbie et al. 2010):

Spin: Protons, neutrons and electrons possess an intrinsic angular momentum (or spin). The magnitude of spin cannot be changed, although the axis (the direction) of spin can be altered. In a nucleus containing an even number of protons (and neutrons) there is no net spin, as particles with oppositely orientated spins are paired together and therefore "balanced" out. In contrast, a nucleus containing an odd number of protons and neutrons will be unbalanced, and therefore has a net spin. The primary focus of the underlying physics of MRI is the hydrogen ion, as it contains a single unbalanced proton in its nucleus and therefore has a net spin; and most importantly as it is by far the most abundant atom in the human body (Westbrook & Roth 2005, McRobbie et al. 2010).

Magnetic Dipole Moment and Precession: The spin motion of an unbalanced proton generates an electric current, which causes the nucleus to behave like a bar magnet with a north and south axis (*a*

dipole), parallel to the spin axis. As a result, when placed in an external magnetic field (typically referred to as the $\mathbf{B_0}$ field), a torque is exerted on the proton as the dipole is rotated into alignment with the field. Due to its intrinsic angular momentum, the spin axis initially wobbles in a gyroscopic fashion or "precesses" around the field axis, rather than immediately aligning to it (Westbrook & Roth 2005, McRobbie et al. 2010).

The frequency of precession ($\omega 0$) (*commonly known as the Larmor frequency*) is directly proportional to the strength of the B_0 field and is defined by the Larmor equation:

$$\omega 0 = \gamma B_0 \qquad [2.1]$$

where γ is a gyromagnetic ratio specific to different atomic nuclei. While initially the dipole axis precesses around the B_0 field, over time it will gradually and eventually align, with the time constant describing this "relaxation" process designated ***T1*** (Buxton 2009, Deoni 2010). Parallel alignment with the B_0 field represents the principle of energy equilibration: as in this situation it represents the lowest energy state the dipole can achieve (with opposite alignment therefore representing the highest). The process of changing dipole orientation must therefore dissipate energy, which is typically converted to electromagnetic energy and emitted as a photon. The time taken for energy equilibration is dependent on the coupling of the dipole orientation to the random thermal motion of the molecules; in water, this coupling is weak and therefore time constant T1 is long (Buxton 2009).

In actual practice, MR techniques do not assess the properties of a single nucleus, rather a collection of nuclei within a body of tissue or fluid. At room temperature, a group of nuclei within a B_0 field, will contain a slight majority of "low-energy" state dipoles aligned to the field, and slightly less "high-energy" anti-parallel dipoles. Thus, within this group, there is a weak net magnetisation (**M**) at

equilibrium aligned to the B_0 field. While the magnitude of M is too weak for accurate measurement under normal conditions, perturbing the equilibrium state and observing the resultant changes does allow measurement, and it is this principle which provides the basis of MR signal generation (Huettel et al. 2004, Buxton 2009). This perturbation or "excitation" is achieved by the application of an external radio-frequency current generated in a coil, which produces a weak perpendicular oscillatory magnetic field (**B_1**), typically referred to as the **RF pulse**. To have this effect, the oscillatory frequency of the RF pulse must exactly match the precessional Larmor frequency of the studied atomic nuceli (usually hydrogen) (Westbrook & Roth 2005).

The basic NMR experiment (*see figure 2.1*) consists of 2 fundamental phases (Buxton et al. 2009):

1. ***The transmit phase:*** If a sample is placed within a constant B_0 field, the dipoles within it reach a state of equilibrium magnetisation which is weakly aligned to the field. A coil placed around the sample (with an axis perpendicular to B_0) can then be used to apply an excitation RF pulse, which causes an increase in high-energy state dipoles. The net effect of this increase is that M is "tipped" away from alignment with B_0, and instead precesses around the axis of B_0. The angle of this precession (termed the **flip angle (α)**) can be increased by increasing the amplitude or duration of B_1.

2. ***The receive phase:*** The precessing macroscopic magnetisation induced in the transmit phase creates a changing magnetic field, which induces an electric current in the coil in the receive phase. The induced signal (described as **free induction decay** (FID)) decreases over time as the individual dipole spins progressively move out of phase with another, with the net effect that the transverse component of M gradually decays. This decay process is exponential, with time constant ***T2***. Measurement of the induced electric current is the fundamental basis of all MR techniques.

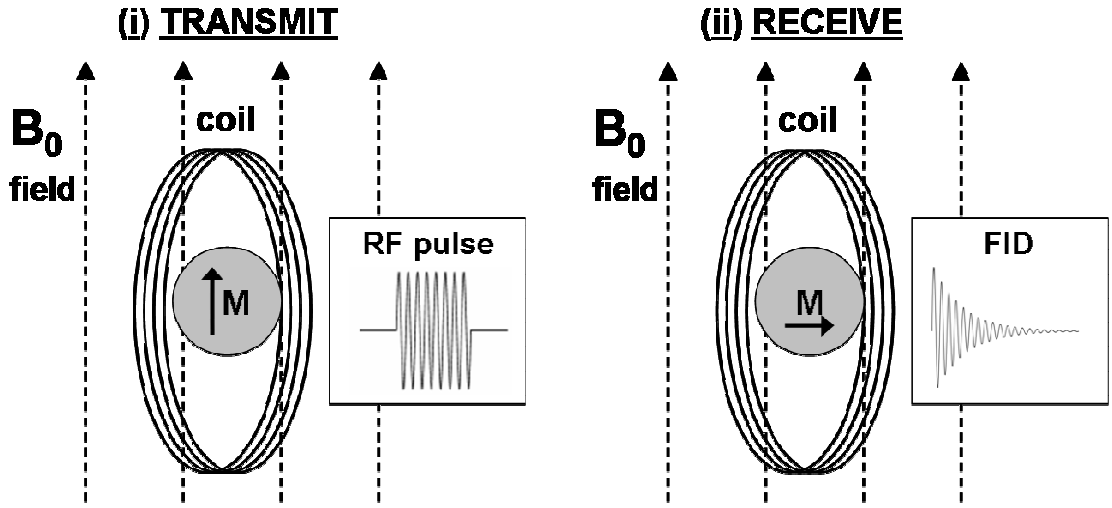

Figure 2.1: ***The Basic NMR experiment.*** A sample (grey circle) is placed inside a large static magnetic field (the B_0 field); the hydrogen ion dipoles within the sample align to the axis of the field, producing a net magnetisation (M) parallel to B_0. ***(i) In the transmit phase***: a radio-frequency oscillatory current in the coil (the RF pulse) is applied. ***(ii) In the receive phase***: as a result of the RF pulse, M has been tipped over and now precesses around the axis of B_0. The transverse component of precessing magnetisation induces an oscillatory current in the coil (the NMR signal) which decays as the spins of individual hydrogen dipoles progressively dephase (known as free induction decay (FID)). (*Figure adapted from Buxton 2009*).

2.1.2. Basics of Image contrast

Although MRI typically studies the magnetic properties of the hydrogen nucleus, the values of the time constants T1 and T2 vary greatly between different tissue types, and this forms the basis of image contrast in MRI (Westbrook & Roth 2005, McRobbie et al. 2010). The variations arise from differences in molecular motion, interaction, and energy exchange (Deoni 2010). T1 is also referred to as “spin-lattice” relaxation time, as the process of longitudinal recovery involves the exchange of energy with the surrounding tissue (which is collectively referred to as the lattice) (McRobbie et al. 2010). Differences in T2 (or “spin-spin” relaxation time) arise from interactions between the fluctuating magnetic fields of other nuclei, in addition to the main effects of the B_0 field (Deoni 2010,

McRobbie et al. 2010). These interactions lead to more rapid spin dephasing, as the Larmor equation [2.1] states that the precessional frequency is the product of a constant (the gyromagnetic ratio) and the external magnetic field. In pure water, the second hydrogen nucleus within the same water molecule (H_20) is the principle source of the additional fluctuating field. In biological systems, the hydrogen ions in water are generally bound or coexist with other much larger molecules such as polysaccharides and proteins, which have hydration layers of surface bound water molecules (and their constituent protons). Free liquids (such as CSF) have a long T2, because random thermal motion within the liquid means that the protons are subjected to a relatively homogeneous local field, as the local interactive field rapidly fluctuates and largely averages out during the motion of the unbound protons. In contrast, when bound to a large macromolecule (such as is seen in myelinated white matter), the protons experience far slower fluctuations in field, leading to an inhomogeneous magnetic field and more rapid dephasing (and a resultant shorter T2). In biological systems, T1 is invariably much longer than T2 across tissue types (*figure 2.2*).

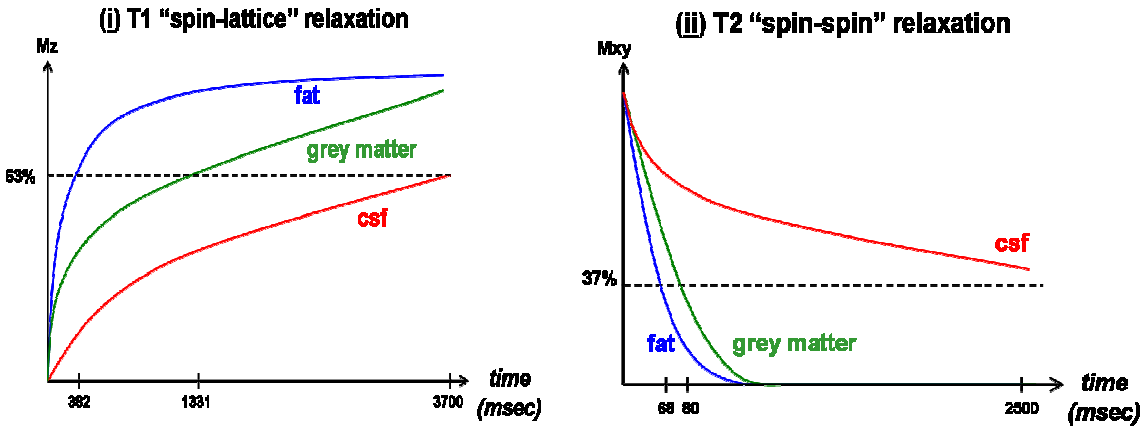

Figure 2.2: ***The value of time constants T1 and T2 varies greatly between tissues, and is the basis of tissue contrast in MRI.*** **(i):** T1 is defined as the time taken for the longitudinal magnetisation (Mz) to recover to 63% of its equilibrium value, and is considerably longer for fluid (such as CSF) in comparison to fat. **(ii):** T2 is defined as the time taken for 63% of the transverse magnetisation to decay due to spin dephasing, and is shorter when protons are bound to macromolecules such as fat. (*Axes are not to scale; values are derived from McRobbie et al. 2010*).

Tissue contrast is therefore generated by delaying measurement of the NMR signal, so that differences in T1 and T2 time can be exploited (Westbrook & Roth 2005, Buxton 2009, McRobbie et al. 2010). By applying further RF pulses to the sample before the full relaxation of M to the longitudinal axis, the tissue differences can be further exploited. The time between each RF pulse is referred to as the **repetition time** (**TR**). The contrast generated in the simplest possible MRI pulse sequence (the gradient recalled echo (**GRE**) sequence) depends only on the TR and α, and the time the FID signal is measured is defined as the centre of data acquisition (**TE**) (Buxton 2009). In actual practice, measuring signal by FID signal alone is rather inefficient and particularly susceptible to both external and internal sources of magnetic field inhomogeneity; and therefore clinical images are instead usually acquired using spin echo (**SE**) sequences, in which further (typically 180°) RF pulses are applied to refocus the rapidly delaying signal at specific echo times (by convention also designated TE) (Buxton 2009).

For a standard T1-weighted image, both the TR and TE are typically short to enhance the contrast differences (*figure 2.2(i)*): with fluid (ie: CSF) appearing dark and fat (ie: myelin) appearing bright (Westbrook & Roth 2005, McRobbie et al. 2010). The converse applies for T2-weighting, where both a long TR and TE are required to maximise the contrast (*figure 2.2(ii)*): and therefore the relatively unbound protons in slowly dephasing fluid appear bright, while the rapidly dephasing tissue (such as fat) appear dark (Westbrook & Roth 2005, McRobbie et al. 2010).

As mentioned previously, the innate flexibility and sensitivity of the technique based on the aforementioned principles of NMR, has led to the design and application of a wide variety of MRI sequences capable of measuring physiological parameters in addition to visualising anatomy. Interestingly, the physical effects which underlie these techniques were historically considered only to be sources of artefact in conventional anatomical MR imaging; but through understanding the underlying cause and taking advantage of the effect, it has been possible to develop novel and

powerful MRI tools (Buxton 2009). An example of this principle is utilising the differences in magnetisation and phase offset which occur within a slice due to the rapid inflow of blood during each TR interval, to specifically visualise the large vessel vascular tree (MR angiography) and quantitatively measure blood flow (Phase Contrast Angiography (PCA)) (Schellinger et al. 2007, Vernooij et al. 2007). The focus of this thesis: fMRI, similarly utilises the transient changes in local field inhomogeneity generated by deoxygenated haemoglobin to indirectly measure functional brain activity.

2.1.3. Image formation

To create an image, the signal must be spatially localised, and this is achieved by manipulating the local resonant frequency in different spatial locations by applying magnetic field gradients (Westbrook & Roth 2005, Buxton 2009, McRobbie et al. 2010). These gradients are produced by three gradient coils which each produce magnetic fields which vary locally in a linear manner along three orthogonal directions (*x,y,z*). Thus, when a field gradient is switched on, predictable phase offsets in spin are produced (known as phase dispersion) at different spatial locations along the gradient "slope" (Westbrook & Roth 2005). The three directions of MRI spatial encoding (x,y,z) are termed frequency encoding, phase encoding, and slice selection respectively (Westbrook & Roth 2005, Buxton 2009, McRobbie et al. 2010). By altering the resonant frequency along the z-axis, the slice selection gradient limits the effect of the RF pulse to a single slice in which the bandwidth is appropriate for excitation. Within the selected slice, the frequency encoding gradient in the x-direction generates a range of frequencies which are represented in the sum sampled signal acquired during the data acquisition window. Phase encoding occurs in "steps" in which the pulse sequence is effectively repeated at each stage of the linear y-axis gradient, and therefore represents the rate of local phase change between data acquisition windows. The acquired data is in the spatial-frequency domain (known as ***k-space***), with each data point (or voxel) containing frequency information about the entire acquired data matrix (Buxton 2009). For an image to be generated, a

two-dimensional Fourier transform is applied, which can then represent the distribution of different frequency amplitudes at each location in space (Westbrook & Roth 2005, Buxton 2009, McRobbie et al. 2010). The final image is therefore a matrix of pixels which are each associated with a volume of data (known as **voxels**), with the final resolution of the image dictated by the measured range of the frequencies in the initial k-space matrix (Buxton 2009).

2.2. fMRI

While enormous strides in the development of MRI techniques during the 1980s led to faster acquisition times and higher image quality, it was not until 1991 that the feasibility of visualising functional brain activity with MRI techniques was first described (Huettel et al. 2004, Buxton 2009). In this first study, Belliveau and colleagues demonstrated that it was possible to measure local increases in blood volume in the primary visual areas, following the injection of a ferromagnetic contrast agent (Magnevist) and a photic stimulus (Belliveau et al. 1991). While this first study established the possibility of functional brain mapping with MRI, it was in 1992 that the first fMRI experiments as used in its current form, were then reported in three independent experiments conducted by Seiji Ogawa, Kenneth Kwong, and Peter Bandettini (Bandettini et al. 1992, Kwong et al. 1992, Ogawa et al. 1992). Although a small number of investigators have reported alternative sources of image contrast for fMRI, the work described in this thesis and by far the most commonly used method is that first described in 1990 by Ogawa and colleagues at the AT&T Bell laboratories (NJ, USA) known as Blood Oxygen Level Dependent (**BOLD**) contrast (Ogawa et al. 1990a,b,c, Jasanoff 2007, Le Bihan et al. 2007, Kim & Ogawa 2012). Over the last 20 years, BOLD contrast fMRI has become the functional imaging modality of choice for the mapping, measurement and characterisation of activity in the human brain, largely owing to its non-invasive nature (without the requirement of an exogenous contrast agent) and attractive temporal and spatial characteristics (*figure 2.3*) (Kim & Ogawa 2012).

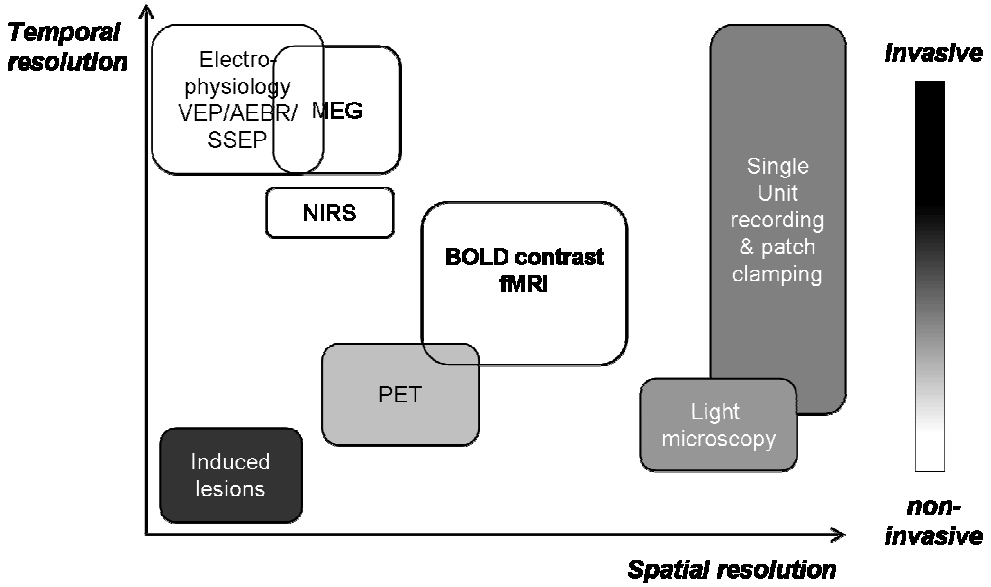

Figure 2.3: ***In comparison to other functional brain imaging techniques, Blood Oxygen Level Dependent (BOLD) contrast fMRI offers an attractive combination of relatively good temporal and spatial resolution, in addition to being non-invasive.*** (AEBR: auditory evoked brainstem responses; MEG: magnetoencephalography; NIRS: near-infrared spectroscopy; PET: positron emission tomography; SSEP: somatosensory evoked potentials; VEP: visual evoked potentials) (*figure adapted from Cohen and Bookheimer 1994*).

2.2.1. T2* effects and BOLD contrast

In biological tissue, if a typical NMR experiment is performed as described in section 2.1.1 and the FID signal is measured after a delay, it does not (as expected) decay exponentially at the rate dictated by the tissue-specific T2 (Buxton 2009). This is because the signal decreases at a faster rate than predicted due to static sources of local magnetic field inhomogeneity (in addition to fluctuating or random spin-spin interactions), with the name given to describe this apparent transverse relaxation time, **T2*** (Westbrook & Roth 2005, Buxton 2009, McRobbie et al. 2010). The effect arises as static field inhomogeneity leads to a range of precessional frequencies within the collection of studied protons, with the resultant loss of phase coherence “interfering” with and leading to a more rapid loss of net magnetisation (Buxton 2009). A particular source of the image distortion which results from the T2* effect are paramagnetic agents (those are positively susceptible to an external

magnetic field), in particular air pockets (sinuses and bowel), dense bone, and ferromagnetic blood-breakdown products (McRobbie et al. 2010). A T2* value of an imaged tissue therefore represents this apparent rate of exponential decay and can be derived from the equation:

$$I_{(t)} = I_{(t=0)}.e^{-t/T2^*} \qquad [2.2]$$

where I is the signal intensity measured at a specific time point (t).

Exploiting the magnetic susceptibility and T2* effects of a paramagnetic substance is the basis of contrast agents such as gadolinium, where a (usually intra-vascular) susceptibility difference is induced via the injection of the agent, which can therefore be exploited to enhance the visualisation of vascular-rich areas (Westbrook & Roth 2005). This same concept underlies BOLD contrast fMRI, as the magnetic properties of Haemoglobin (**Hb**) are known to change depending on its oxygen binding state, with deoxygenated Hb (**d-Hb**) containing unpaired electrons which thus render it paramagnetic (Thulborn et al. 1982, Ogawa et al. 1990a,b,c). In their seminal studies of 1990, Ogawa and colleagues elegantly demonstrated this effect in the in-vivo rat brain at 7-Tesla. By altering the concentration of inhaled oxygen and therefore the degree of blood oxygenation, marked changes in signal were observed in the large vessels of the brain using a simple GRE sequence; an effect they then termed BOLD contrast (Ogawa et al. 1990a,c). The finding that further changes in BOLD contrast could be induced by insulin-provoked hypoglycaemia and halothane anaesthesia, demonstrated that the technique was sensitive enough not only to identify transient changes in brain physiology, but also crucially suggested that it could be used as an intrinsic contrast agent for imaging brain activity (Ogawa et al. 1990b).

While the concept of paramagnetic d-Hb leading to more rapid proton spin dephasing and therefore a decrease in BOLD contrast has long been accepted; biophysical and anatomical factors render a

direct and precise modelling of the relationship extremely difficult (Buxton 2009). At increasing B_0 field strengths magnetic susceptibility increases, and consequently T2* values are seen to decrease in all tissue types with associated improvements in both signal-to-noise ratio (**SNR**) and tissue contrast (Krűger et al. 2001, Peters et al, 2007, Harmer et al. 2012). In an acquired voxel, there may be blood contained within either arteries, capillaries and/or veins, all of which may be of varying orientation and calibre. Although the intravascular compartment represents just 4% of the total cerebral tissue volume, at lower field strengths (1.5 T) a substantial fraction of the sampled changes in BOLD signal are intravascular in origin (Krűger et al. 2001, Buxton 2009). The majority of the contrast is derived from the venous side of the vasculature; as the vessels are larger in diameter, have the largest increase in volume during acute increases in blood flow (due to passive dilatation of the vessel), and suffer the largest shifts in oxygenation (Buxton et al. 1998, 2004). In addition, due to effects of diffusion on the dispersion of spins in the extravascular space, the effects of shifts in oxygenation on the observed BOLD signal are more significant in large vessels like veins than in the smaller capillaries (Ogawa et al. 1993). With increasing B_0 field strength, the proportionate contribution of the intra- and extra-vascular compartments to the BOLD signal switches, and an increasing proportion of the contrast is also derived from the capillary space (Silvennoinen et al. 2003, Harmer et al. 2012).

2.2.2. Neurovascular coupling

The terms “neural activity” and “neuronal signalling” are often used to collectively describe the membrane electrical field potential changes observed with electrophysiological techniques (Logothetis & Pfeuffer 2004). Underlying the electrical changes is a complex series of physiological processes which serve to initially generate negative free energy changes by moving the thermodynamic system (maintained by intracellular and extracellular ion concentrations) closer to equilibrium (Attwell & Iadecola 2002, Attwell & Gibb 2005, Buxton 2009). In contrast, the subsequent restoration of the ion gradients increases the free energy of the system and is therefore

a highly metabolic and time limiting process; involving the active pumping of Na^+ and Ca^{2+} ions against their natural drift, and the repackaging and processing of synaptic neurotransmitters by astrocytes (Attwell & Iadecola 2002, Attwell & Gibb 2005). This energy is provided through the consumption of adenosine triphosphate (ATP), the levels of which are maintained through the provision of glucose and oxygen to the mitochondria for oxidative phosphorylation (Buxton 2009). The majority of oxygen (98%) is carried in red blood cells bound to haemoglobin, on which it is transported throughout the body. This knowledge forms the physiological basis of the signals measured by fMRI and PET techniques, as the provision of the metabolic substrates required for neural activity must come from an external source, and is assumed to be delivered via the local vasculature (Attwell & Iadecola 2002, Logothetis & Pfeuffer 2004, Mangia et al. 2009, Cauli & Hamel 2010, Kim & Ogawa 2012, Jones & Rabiner 2012).

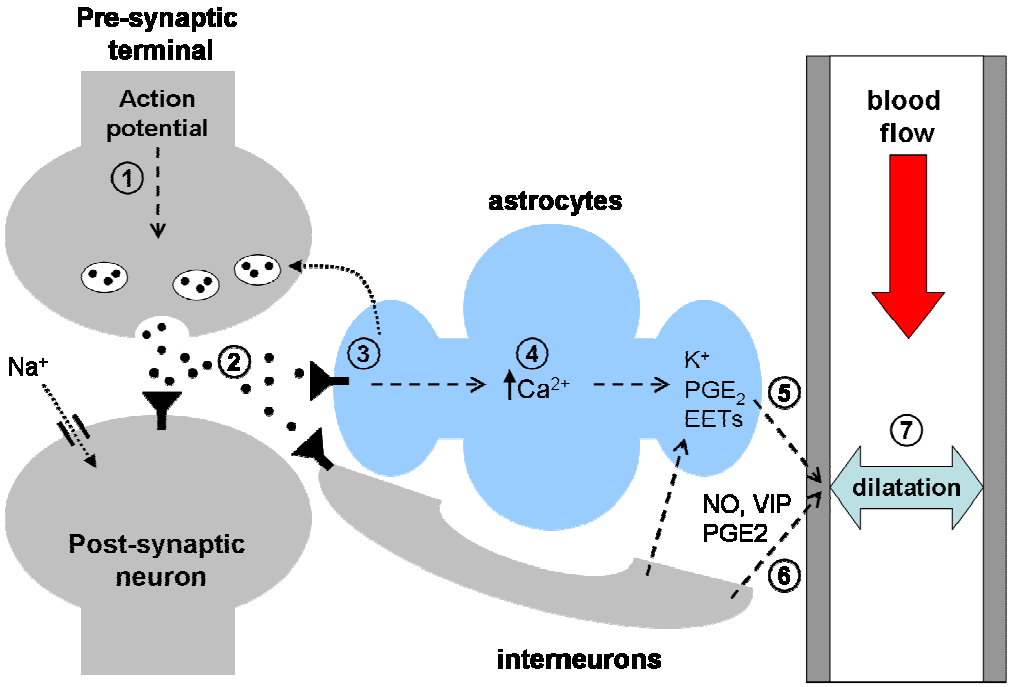

Figure 2.4: ***Neuronal signalling is accompanied by a "neurovascular coupling" cascade which culminates in a local increase in blood flow.*** (1) Arrival of an action potential in the presynaptic terminal leads to; (2) the release of neurotransmitters into the synaptic cleft and post-synaptic depolarisation via sodium (Na+) ion entry; (3) the neurotransmitter also binds to receptors on local astrocytes where it is repackaged; (4) but also

causes an increase in intracellular calcium ions (Ca^{2+}); (5) this triggers the release of agents such as potassium ions (K^+), prostaglandin E_2 (PGE_2), and epoxyeicosatrienoic acids (EETs); (6) local interneurons mediate the release of these agents from the astrocyte end-feet, but also release other agents such as nitric oxide (NO), and vasoactive intestinal polypeptide (VIP); (7) these vasodilating agents act on the smooth muscle of the local vasculature causing dilatation, and an increase in local blood flow. (*figure reproduced and adapted from Buxton 2009, Cauli & Hamel 2010*).

The cumulative terminology for the physiological processes which mediate the vascular supply of glucose and oxygen required for neural activity, is ***neurovascular coupling*** *(figure 2.4)*. The astrocyte has been found to a vital part of the "neurovascular unit", in particular through changes in intracellular Ca^{2+}; although animal studies have also suggested that it may act as an early source of lactate which may be initially used as a source of energy (Lauritzen 2005, Carmignoto & Gomez-Gonzalo 2009, Mangia et al. 2009, Attwell et al. 2010, Cauli & Hamel 2010, McCaslin et al. 2011). Increases in astrocytic intracellular Ca^{2+} lead to the release of vasoactive messengers, in particular potassium ions (K^+) and derivatives of arichidonic acid such as prostaglandin E_2 (PGE_2) and epoxyeicosatrienoic acids (EETs) (Lauritzen 2005, Cauli & Hamel 2010). The release of these substances is mediated partly through local interneurons which can also release PGE_2, in addition to other vasoactive substances including nitric oxide (NO) and vasoactive intestinal polypeptide (VIP) (Lauritzen 2005, Cauli & Hamel 2010). The net result of this signalling cascade is that over approximately 5 seconds in the adult brain, the smooth muscle of the adjacent vasculature relaxes, leading to an increase in local blood flow, and provision of the required glucose and oxygen (Buxton 2009).

Of importance to functional imaging, the main consequence of this neurovascular coupling cascade is a "functional hyperaemia" whereby the resultant increases in local cerebral blood flow (**CBF**) and slightly smaller increases in local cerebral blood volume (**CBV**) are proportionately much larger than the rise in metabolism, leading to a consequent oversupply of oxygenated Hb (**Hb-O_2**) (Fox & Raichle

1986, Buxton et al. 1998, 2004, Buxton 2009). This activity dependent local increase in diamagnetic Hb-O2 (and proportionate decrease in paramagnetic d-Hb) was first reported as a local increase in BOLD contrast in human subjects in 1992, in response to a visual stimulus (Kwong et al. 1992, Ogawa et al. 1992) and a simple motor task (Kwong et al. 1992, Bandettini et al. 1992).

2.2.3. Linking electrical activity to fMRI BOLD contrast

By measuring the haemodynamic end event of the neurovascular coupling cascade, BOLD contrast is therefore clearly an indirect measure of neural activity (Logothetis 2008). While more direct measures of electrical activity such as sensory evoked potentials and single unit recordings typically identify responses on the order of hundreds of milliseconds, the haemodynamic changes of fMRI take place over several seconds (Menon & Goodyear 2001, Logothetis & Pfeuffer 2004, Logothetis 2008). While it is tempting to believe that activity dependent increases in BOLD contrast are directly associated with an increase in the spiking output of task-specific neurons; it is more likely that changes in contrast are representative of the average metabolic requirements for a population of neurons, encompassing changes in both excitatory and inhibitory conductance, and both feedforward and feedback processing (Logothetis 2008, Lee et al. 2010). In keeping with this assertion, simultaneous BOLD contrast measurement and intra-cortical electrophysiology in the visual cortex of monkeys has found that local-field potentials (**LFPs**) were a better predictor of changes in BOLD signal than either single or multi-unit spiking activity (Logothetis et al. 2001). LFPs are thought to be representative of relatively slow neural events which reflect the combined activity of a neural population; including the weighted average of dendro-somatic synaptic signalling, spike after-potentials, and voltage-dependent membrane oscillations (Logothetis & Pfeuffer 2004, Logethetis 2008). Further compelling evidence linking neural activity and increases in BOLD contrast has also been provided by Lee and colleagues, who used optogenetic techniques to demonstrate a correlation in cell-specific responses and associated BOLD signal increases in connected downstream axonal targets (Lee et al. 2010).

2.2.4. Modelling the response to stimulation

While the first fMRI experiments sought to identify temporal changes in the BOLD contrast in sensory areas which had been selected a-priori on the basis of the stimulus type (for example the primary visual areas in the occipital lobe for a photic stimulus (Ogawa et al. 1992)), such an approach did not exploit a powerful aspect of the technique in the ability to image the whole brain. An important feature of the measured BOLD response to stimulation which makes this possible, is that it has been found to be highly reproducible within the same subject and to a specific stimulus type (Aguirre et al. 1998b, Miezin et al. 2000, Handwerker et al. 2004, 2012). Although subtle but significant variations are seen between brain regions and subjects, fundamental to fMRI analysis is the assumption that the BOLD impulse response is largely stable and retains a characteristic morphology across experiments (Friston et al. 1994a, 1995b, Hoge & Pike 2001, Handwerker et al. 2012). While a complete understanding of the physiological and biophysical origins of the features of the response function have proved elusive, an appreciation is vital so that quantitative aspects of the sampled BOLD signal can be put into perspective, and detailed modelling of the signal can be performed for accurate data analysis (Hoge & Pike 2001, Buxton et al. 2004). The most comprehensive biophysical models have typically described the BOLD response in terms of the neural activity driving dynamic changes in three physiological parameters: local CBF, CBV, and the cerebral metabolic rate of oxygen (**$CMRO_2$**) (Buxton 1998, Mandeville 1998, Buxton 2004).

2.2.4.1. The Haemodynamic Response Function (HRF)

As fMRI experiments are providing a measure of the local changes in oxygen bound Hb within the local vasculature, the observed transient and delayed changes in BOLD contrast are commonly referred to as the "**haemodynamic response**" (Hoge & Pike 2001). Following a brief period of neural activity, this localised response follows a distinct and reproducible temporal course, which has been characterised and termed the haemodynamic response function (**HRF**) (*figure2.5*) (Friston 1994a, Glover 1999, Hoge & Pike 2001).

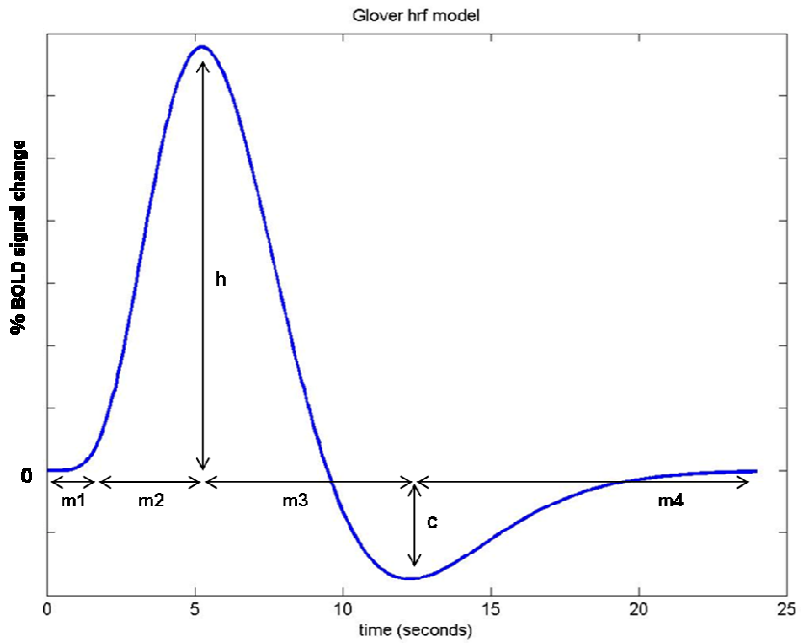

Figure 2.5: ***The canonical HRF waveform*****.** Following a brief period of neural activity, the sampled BOLD signal is seen to change in a characteristic manner. There is a brief period (approximately 2 seconds) in which the signal is not seen to rise (period m1), and during which a brief small amplitude decrease in signal may be seen (the "initial dip"). As the initial dip is typically very brief, is of a small amplitude, and is not consistently seen (particularly at lower B_0 field strengths), it is not usually included (as here) in the HRF model. The peak of the impulse response (the "positive peak") is modelled to have a lag time of approximately 5 seconds (m1+m2), with amplitude (h). The signal is then seen to drop below baseline ("the negative undershoot") approximately 10-20 seconds after stimulation (m1+m2+m3) before a return to baseline (at the end of time period m4). (*figure reproduced and adapted from Glover 1999, Woolrich et al. 2004*).

The canonical HRF can be divided into three distinct epochs (*figure 2.5*):

1. ***The time to onset and initial dip*****:** A brief delay of approximately 2 seconds following the stimulus is seen before the onset of the rise in BOLD contrast is initiated. A low amplitude "initial dip" (a brief decrease) in BOLD contrast has been reported during this short period, although it is not consistently identified in fMRI studies across different species and stimulus

types (Ernst & Henning 1994, Hu & Yacoub 2012). This initial dip is more reliably seen and appears to be of larger amplitude at higher B_0 field strengths (3-Tesla and above) and with increased stimulus intensity (Ernst & Henning 1994, Hu et al. 1997, Yacoub & Hu 2001, Buxton et al. 2004, Yeşilyurt et al. 2008, Hu & Yacoub 2012). It has been postulated that this period may best localise the area of neural activity as it may represent an immediate faster rise in local metabolism which occurs before the larger but more spatially dispersed increase in blood flow (Malonek & Grinvald 1996, Buxton et al. 2004, Hu & Yacoub 2012). In keeping with this are the early increases in d-Hb seen during the equivalent early post-stimulus time period in the cat brain with optical techniques (Malonek & Grinvald 1996).

2. ***The positive peak***: The local oversupply of Hb-O_2 associated with task induced hyperaemia leads to a robust increase in BOLD contrast with a peak in signal seen approximately 5-7 seconds (range in reported studies 4-10 seconds) after stimulus onset (Friston et al. 1994a, 1995b, Buxton et al. 1998, 2004, Glover 1999, Handwerker et al. 2004, Yeşilyurt et al. 2008). Although subtle differences in both the lag time and amplitude of the peak response are observed between different subject populations and brain regions, the amplitude is typically measured as approximately 2-3% above the baseline signal level (Friston et al. 1995b, Glover 1999, Handwerker et al. 2004). A reliable peak in signal has been described following stimuli as brief as 5 milliseconds, with the amplitude of the response rising with both increasing stimulus duration and intensity (Yeşilyurt et al. 2008, Hirano et al. 2011). The effect has been elegantly shown using depth-resolved optical imaging and in-vivo two-photon microscopy to be predominately caused by increases in local CBV following rapid increases in CBF resulting from local arteriolar dilation (Hillman et al. 2007).

3. ***The post-stimulus negative undershoot***: Approximately 10-20 seconds after stimulus cessation, the BOLD response is seen to decrease and drop again below baseline for a

prolonged period of up to 60 seconds (Frahm et al. 1996, Buxton et al. 1998,2004, Mandeville et al. 1998, Chen & Pike 2009b, van Zijl et al. 2012). While this decrease in BOLD contrast is likely to relate to a rise in local d-Hb, the origin of this change remains controversial, but is generally postulated to arise from 3 possible sources; (i) a transient decoupling between the CBF (which has returned to baseline) and an ongoing increased $CMRO_2$ resulting in an increase in the oxygen extraction fraction (Frahm et al. 1996, 2008, Dechent et al. 2011), (ii) a temporal mismatch between the rapid changes in CBF and the slower prolonged (predominately venous) CBV response due to underlying differences in vessel wall compliance (Buxton et al. 1998, 2004, Mandeville et al. 1998), or (iii) an undershoot (brief decrease) in local CBF following the rapid increase associated with the positive peak (Chen and Pike 2009a, 2009b).

Of importance to fMRI methodology and data analysis, the HRF has been found to have specific and predictable characteristics which are largely consistent across subject groups. One important assumption common to fMRI experiments and analysis techniques is that overlapping HRFs will sum in a roughly linear fashion, such that the BOLD response to a prolonged stimulus can be predicted in a relatively simple manner (Friston et al. 1994a, Boynton et al. 1996, Dale & Buckner 1997). The supposition that a linear transform model can relate the average neural activity to the BOLD response is intrinsically attractive, as the direct relationship between the stimulus and the induced neural response is likely to be highly non-linear (Boynton et al. 1996). In keeping with this, Boynton and colleagues also found that both the magnitude and duration of the neural activity appears to be independently related to the respective parameters of the resultant BOLD response (Boynton et al. 1996, Donaldson & Buckner 2001). In addition to simplifying fMRI data analysis (see section 2.3.4.), these traits allow great flexibility in the design of stimulation patterns for fMRI studies (Donaldson & Buckner 2001). While these assumptions are largely accepted and now commonly applied in the fMRI field, recent biophysical models and fMRI studies using short stimulus durations (event-related

experimental paradigms, see *section 2.3.3*) have suggested that the BOLD response is not entirely linear in character, particularly at longer durations when the response would be generally over-predicted in amplitude (Buxton et al. 1998, Friston et al. 1998b, Mandeville et al. 1998, Yeşilyurt et al. 2008, Hirano et al. 2011).

2.2.4.2. Biophysical models of the BOLD haemodynamic response

The description of functional hyperaemia in the seminal work of Fox and Raichle (1986) highlighted the importance of the large increases in local CBF associated with neural activity, and led to early interpretations of the BOLD haemodynamic response to relate solely to changes in CBF (Buxton 2012). However, while this assumption could relate the positive peak of the haemodynamic response to a marked increase in local CBF, it is unable to explain the other features of the HRF, notably the initial dip and post-stimulus negative undershoot (Buxton et al. 1998, Mandeville et al. 1999). By historical convention, normalised CBV (v(f)) was previously thought to be related to the normalised CBF (f) in a steady-state relationship under a power law (with an exponent δ=0.38) proposed by Grubb and colleagues (Grubb et al. 1974):

$$v(f) = f^{\delta} \qquad [2.3]$$

While this relationship appears valid at rest, a key study by Mandeville and colleagues demonstrated in the rat brain, that the Grubb relationship is not valid during the short time period that follows stimulus-induced brain activity, as the local CBV recovery to baseline is significantly delayed in comparison to the CBF (Mandeville et al. 1998). These findings led to the first widely accepted and comprehensive biophysical model of the BOLD contrast response described by Buxton and colleagues, termed the “balloon model” (Buxton et al. 1998). Under this model, the BOLD effect was related to temporal changes in d-Hb and the CBV, with an additional effect of the oxygen extraction fraction. A fundamental concept of the model was the relatively slow time course of CBV change,

which was proposed to be analogous to the expansion and subsequent slower contraction of an inflating and deflating balloon (Buxton et al. 1998). Such behaviour can be logically explained by the relative differences in intra-luminal musculature and vessel compliance which are inherent to the arteriole and venous sides of the local circulation: with active changes in the arteriole diameter responsible for rapid changes in CBF, and the resultant passive stretching and dilation of the venous side responsible for the delayed increase in CBV (Buxton et al. 1998, 2004, 2012). These concepts were also essential to the "Windkessel" model independently described by Mandeville and colleagues (1999).

In recent years, the development of novel quantitative MR techniques has allowed the direct measurement of some of these specific physiological parameters, and has allowed investigators to probe the concepts proposed in the original balloon model (*figure 2.6*) (*reviewed in Buxton 2012*). Arterial Spin Labelling (ASL) in particular provides a direct measurement of local changes in CBF, and therefore allows a non-invasive means to formally assess the relationship with the BOLD response and indirectly calculate the $CMRO_2$ (Hoge 2012). These studies have challenged the long-held belief that $CMRO_2$ is tightly coupled to CBF, and have found the relationship to be highly variable, with neural factors driving both $CMRO_2$ and CBF levels in a parallel (but independent) way rather than metabolism alone (Griffeth & Buxton 2011, Buxton 2012). In addition, there is mounting evidence that the physiology underlying the post-stimulus undershoot does not consist solely of slow CBV recovery, but is likely to be a multi-factorial process; consisting also of an additional transient undershoot in CBF (Chen & Pike 2009a,b), and/or a prolonged local elevation in $CMRO_2$ which outlasts the stimulus-induced increases in CBF (Frahm et al, 2008, Dechent et al. 2011, Hua et al. 2011). Furthermore, although direct in-vivo visualisation of the vasculature with 2-photon microscopy has confirmed that active dilation of the arteriole compartment is responsible for the rapid rise in CBF and the positive peak of the HRF, a "ballooning" effect was not observed in the venous compartment (Hillman et al. 2007). An additional complicating factor is that improvements in

the spatial resolution of fMRI have also suggested that there are depth-specific differences in the BOLD haemodynamic response, indicating that there are cortical-layer specific differences in neurovascular coupling (or an over-reliance on the venous compartment in the generation of BOLD contrast) which therefore further complicates attempts to create a comprehensive descriptive model (Jin et al. 2008, Siero et al. 2011, Pimental et al. 2012).

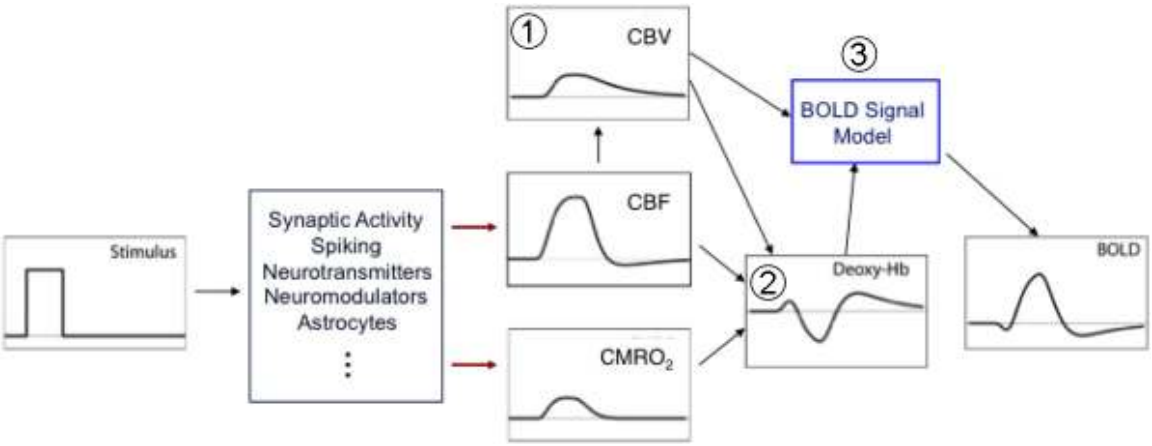

Figure 2.6: ***The modified balloon model proposed by Buxton (1998, 2012).*** The initial balloon model described the haemodynamic response as a deterministic function of dynamic changes in local cerebral blood flow (CBF). Work since that time has suggested that neural activity drives both the CBF and the cerebral metabolic rate of oxygen ($CMRO_2$). The key components of the model are: (1) A slow and delayed recovery of cerebral blood volume (CBV) governed principally by the passive dilation of the venous system (the "balloon" effect); (2) A model describing the dynamic change in deoxygenated-Hb (Deoxy-Hb) with respect to CBF, CBV and $CMRO_2$; (3) A model for the conversion of changes in and CBV and Deoxy-Hb into the final observed BOLD response. (*figure reproduced and adapted from Buxton 1998, 2012*).

2.2.4.3. Induced changes in the BOLD response

While the HRF has been found to be generally reproducible across subjects under normal physiological conditions, further clues as to the underlying physiology have been provided through

investigating the effects of induced changes in cerebro-vascular dynamics and under pathological conditions. Caffeine is known to act as a potent vasoconstrictor, with intake leading to a significant reduction in baseline (and global) CBF. This effect has been shown to be associated with an increase in the temporal dynamics of the CBF response, with the resultant effect that the BOLD response is seen to evolve more rapidly; with a loss of the initial dip (and a decrease in the time to onset), an increase in the positive peak amplitude, and a significant shortening in the time taken to reach the positive peak (*figure 2.7(i)*) (Liu et al. 2004, Behzadi & Liu 2006, Perthen et al. 2008, Chen & Parrish 2009). In contrast, carbon dioxide (CO_2) is known to act as a potent cerebral vasodilator and therefore induced hypercapnia (an increase in the partial pressure of CO_2 in the blood) has been shown to increase baseline CBF (and to a lesser extent CBV) with no associated change in the $CMRO_2$ (Chen & Pike 2010a,b). These changes result in the converse effect to caffeine; an increase in the baseline BOLD signal contrast with a decrease in the positive peak amplitude and lengthening of the time to peak (*figure 2.7(ii)*) (Cohen et al. 2002).

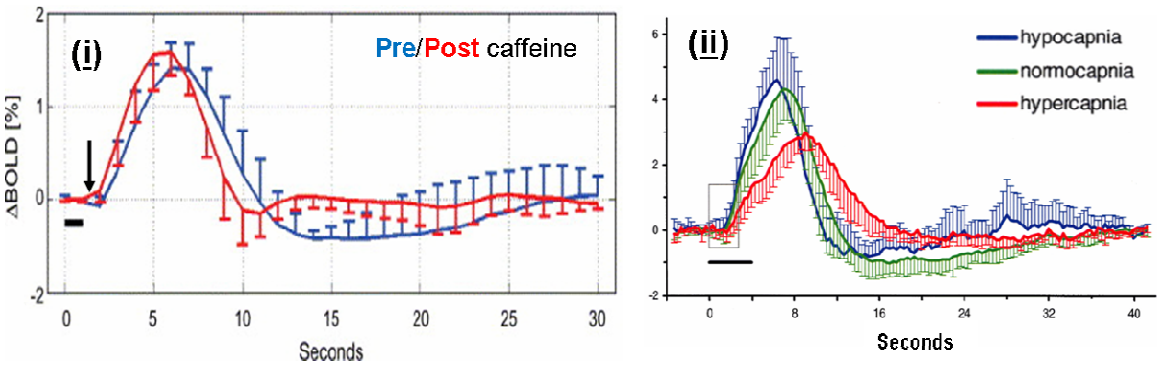

Figure 2.7: ***Changes in the BOLD haemodynamic response can be induced by agents which alter baseline cerebral blood flow (CBF).*** **(i):** Caffeine lowers baseline CBF, and results in faster and higher amplitude BOLD responses to a brief stimulus (occurring during the time period marked with a horizontal black bar). Of interest, caffeine also causes a loss of the initial dip (arrowed) and a decrease in the post-stimulus undershoot amplitude (*figure reproduced from Liu et al. 2004*); **(ii)**: In contrast, hypercapnic conditions (raised CO_2) results

in a higher baseline CBF, and the converse effect, with slower and lower amplitude BOLD responses (*figure reproduced from Cohen et al. 2002*).

While it is tempting to widely apply fMRI techniques to infer the functional effects of intra-cerebral pathology, the previously described physiological effects on the BOLD response suggest that the results must be treated with caution: as it remains unclear whether any identified differences are a true effect of the pathology directly on neural activity, or may represent indirect alterations to the associated neurovascular coupling and/or vascular dynamics (D'Esposito et al. 2003, Buxton 2009). If the pathology is purely vascular in origin, (such as unilateral occlusive cerebrovascular disease), a predictable delay and reduction in amplitude of the BOLD response is seen in the abnormal side (Carusone et al. 2002). However, in patients with assumed unilateral microvascular disease (diagnosed by the presence of lacunar infarction), a similar delay and reduction in response was seen even in the unaffected hemisphere, in keeping with a more diffuse underlying pattern of vascular pathology (Pineiro et al. 2002). Furthermore, the effects of vascular pathology may lead to such a marked reduction in CBF that the temporal SNR (tSNR) of the fMRI experiment becomes insufficient to identify any BOLD response at all (Bonakdarpour et al. 2007). During epileptic discharges, the HRF is seen to differ markedly from the canonical response, although neurovascular coupling appears to be preserved even during the pathological events (Hamandi et al. 2008, Masterton et al. 2010). Through presumed decreases in vascular compliance and reactivity, old age has been found to also be associated with a decrease in SNR, the spatial extent of the activation, the amplitude of responses, and an altered timecourse with a delayed recovery to baseline (D'Esposito et al. 2003, Richter & Richter 2003).

2.3. fMRI methodology

The aforementioned principles of BOLD contrast and the haemodynamic response to stimulation therefore form the essential foundations of fMRI, upon which experiments can be designed, data analysed, and patterns of activation identified. An important consideration is that as a result of these factors, the temporal resolution of the technique is always likely to be largely restricted by the technical and physical limitations of MR signal generation and acquisition, and the timescale of the physiology underlying the haemodynamic response (Donaldson & Buckner 2001). Regardless, other key factors still allow for great flexibility in fMRI study design; including high sensitivity to even extremely brief patterns of stimulation, the relatively predictable and linear behaviour of the haemodynamic response, and the spatial specificity offered by the acquisition of whole-brain images (Boynton et al. 1996, Friston et al. 1998a, Matthews 2001, Yeşilyurt et al. 2008, Hirano et al. 2011).

While a major advantage of fMRI is that data is acquired for the whole brain and sampled at relatively frequent time intervals, this necessarily renders data analysis a highly statistical process as a result of the enormous amount of data generated and the high degree of noise inherent to the technique (Friston et al. 1994a, Huettel et al. 2004, Buxton 2009, Monti 2011). Central to the framework of analysis is a number of key assumptions about the nature of the data (including those mentioned previously), with conformity to these principles preserved through several pre-processing steps which are generally considered to now be standard to the analysis (Friston et al. 1994a, Smith et al. 2004, Monti 2011). These steps in addition to further statistical correction techniques, are vital to avoid potential sources of bias common to the data (Smith 2001, Monti 2011).

A number of open-source fMRI processing packages have been developed and refined over the last 20 years, and are widely applied across the neuroscience community for data analysis, the most common of these being SPM, AFNI, BrainVoyager and FSL (Ashburner 2012, Cox 2012, Goebel 2012, Jenkinson et al. 2012). The work of this thesis was predominately carried out with tools within

FMRIB's software library (**FSL**) (http://www.fmrib.ox.ac.uk/fsl/); and therefore unless otherwise stated, the described methods are as implemented therein (Smith et al. 2004).

2.3.1. Image acquisition

The basis of BOLD fMRI is therefore that temporal differences in image contrast are induced by changes in an endogenous contrast agent (d-Hb), and that these changes can be accurately localised to an area of "functional" activity (Ogawa 1990b). This means that relatively rapid image acquisition is highly desirable, thereby allowing the study of dynamic changes in the signal throughout the brain, and to minimise possible artefacts induced by subject motion during the study period (Bandettini 2001, Huettel et al. 2004, Buxton 2009). Thus, the ideal image acquisition sequence for fMRI would be capable of sampling data quickly, offer a high SNR so that tissue dependent differences in contrast can be identified, and collect images of high spatial resolution so the activation can be well localised to a defined region of anatomy (Bandettini 2001, Buxton 2009). Unfortunately in practice, due to the very nature of MR imaging, the steps necessary to optimise each of these aspects are in direct conflict with one another, making this goal generally unachievable (Westbrook & Roth 2005, McRobbie et al. 2010). The SNR of 2-Dimensional (2D) MR image is defined by the following equation, where K is a constant largely dependent on the strength of the main B_0 field; the term "measurements" represents the number of signal components used in the Fourier reconstruction of a voxel (and is therefore proportionate to voxel size and the number of excitations); and "bandwidth" refers to the range of frequencies used to sample the MR signal (and is inversely proportional to the sampling time and therefore TR) (Elster 1994):

$$\text{SNR} = K * (\text{voxel size}) * (\sqrt{\text{measurements}}) / (\sqrt{\text{bandwidth}}) \qquad [2.4]$$

Given this relationship, to maintain SNR at faster image acquisition times, it is clear that the spatial resolution must be sacrificed (*figure 2.8*) (Elster 1994, Westbrook and Roth 2005).

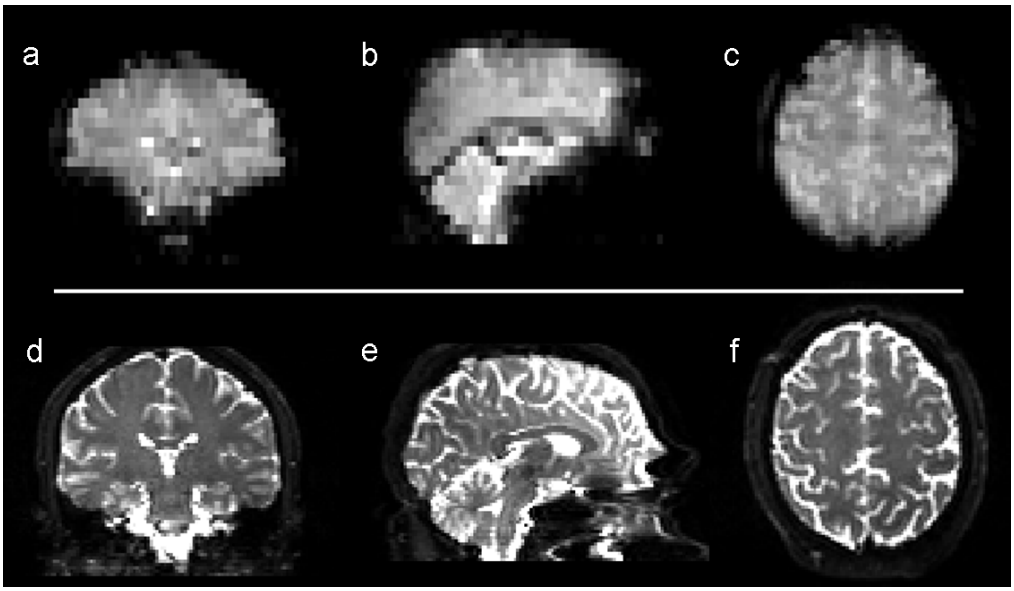

Figure 2.8: ***Echo-Planar Imaging (EPI) sequences are commonly used to acquire fMRI data of good temporal resolution, but relatively poor spatial resolution.*** On the top row are images in the coronal, sagittal, and axial planes with an EPI sequence of spatial resolution (voxel volume: 55.75mm^3), with a whole brain image acquired every 1.5 seconds. In comparison, the equivalent T2-weighted images of the same subject (bottom row) show greater tissue contrast and spatial resolution (6.125mm^3), but the whole image has been acquired over 2 minutes 17 seconds.

In the most basic MRI sequence (as described in 2.1), the collection of data corresponding to each step in the phase encoding direction will follow a new RF excitation pulse, and therefore the acquisition of an entire image may take several minutes (depending on the acquired matrix size in the y-direction and the TR) (Buxton 2009). In a typical fMRI study, it is desirable to acquire a whole brain image every few seconds, and therefore this approach is clearly insufficient. The most commonly used solution to this problem is to use Echo-Planar Imaging (**EPI**) sequences, as first described in the seminal work of Peter Mansfield (1977). The basic theory of the EPI sequence is that rapid switching of the gradients can generate a "train" of gradient echoes, such that the entire phase-encoding measurements of the image can be done following a single excitation pulse (and therefore are often referred to as "single-shot" techniques) (Mansfield 1977). The switching of the

gradients means that the k-space sampling trajectory scans in alternating directions from one phase-encode line to the next (known as a “Cartesian” trajectory) (Mansfield 1977, Westbrook & Roth 2005, McRobbie et al. 2010).

In addition to dramatically increasing the data sampling rate, a further major advantage of an EPI sequence is that each image is representative of a brief “frozen” epoch in time, therefore greatly reducing image artefacts which can arise in anatomical images due to physiological motion (such as pulsatile vessel flow, swallowing, and large respiratory movements) (Bandettini 2001, Buxton 2009). However, by nature of the EPI sequence itself, the images are predisposed to other specific artefacts, some of which can be potentially severe and lead to bias or data loss. These include: “Nyquist ghosting” (where the alternating directions of k-space sampling lead to a weak image of the brain shifted by half an image frame and wrapped around to the other side in the phase-encoding direction); areas of marked low signal or “signal drop-out” (which arise due to intrinsic field gradients generated in areas where there is a marked difference in magnetic susceptibility between adjacent tissues, such as between an air-filled sinus and the neighbouring brain); and distortions due to “off-resonance effects” (as phase offsets caused by subtle alterations in the frequency of precession arising from differences in the chemical binding of the hydrogen nuclei cannot be “reset” as there is only a single RF pulse) (Jezzard & Clare 1999, Westbrook & Roth 2005, Buxton 2009, McRobbie et al. 2010).

To maximise T2* effects (and therefore BOLD contrast), a simple GRE EPI sequence is commonly used for fMRI data acquisition as described in the very first studies described by Ogawa and colleagues (Ogawa et al. 1990a,b,c, 1992, Bandettini 2001, Buxton 2009, Harmer et al. 2012). The traditional GRE EPI sequence is generally considered to be sensitive to BOLD contrast due to changes in magnetic susceptibility in all of the vascular compartments, but in particular the large venous compartment (Ogawa et al. 1993, Bandettini 2001, Silvennoinen et al. 2003, Buxton 2009). In

comparison, it is postulated that less commonly used SE EPI sequences may be more specific to the area of neural activity as they may be detecting signal changes in the smaller vessels (and particularly capillaries), as static dephasing of the signal around the large vessels will in theory be refocused by the 180° pulse (Bandettini et al. 1994, Bandettini 2001, Harmer et al. 2012). However, SE EPI sequences are significantly less sensitive to BOLD contrast, and therefore imaging at very high field strength (7 Tesla and above) has been necessary to detect significant differences in the activation pattern between the two sequences (Harmer et al. 2012).

2.3.2. Data pre-processing

An fMRI data set therefore comprises a series of BOLD contrast weighted whole brain images, which have been sampled at a rate defined by the sequence TR. By convention, the 3D image acquired at a single time point is referred to as a **volume** (Friston et al. 1994a). For a given spatial location (for example a single voxel) the dynamic changes in the measured BOLD contrast signal through the entire data acquisition period can be best represented as a signal timeseries (Friston et al. 1994a, Monti 2011). By thinking of the data in this way, it is possible to understand the principles which underlie data pre-processing, and explain how fMRI data is amenable to statistical analysis and modelling.

Data pre-processing represents a series of essential steps performed prior to the analysis proper which serve to prepare the raw data for statistical analysis by reducing noise and removing clear sources of potential bias (Friston et al. 1994a, Smith 2001b, Monti 2011). The importance of reducing noise is emphasised when it is considered that in a typical fMRI experiment, the induced change in BOLD contrast may be just 0.5-5% above baseline level, while fluctuations due to noise alone may be as much as 0.5-1% (Donaldson & Buckner 2001, Smith 2001b). The steps outlined in this section are those as performed in the work of this thesis, and as implemented largely by default in FSL. The attached text is purposely explanatory, and other than where directly relevant to this

thesis, intentionally does not discuss the relative merits or drawbacks of techniques implemented in other fMRI analysis software packages.

2.3.2.1. Slice acquisition time correction

Although a single data volume is assumed to be representative of the sampled BOLD signal at a particular timepoint, the image is actually acquired one slice at a time throughout the specified TR interval (Smith 2001b, Huettel 2004). Thus if an image is acquired from the bottom slice upwards using a sequence TR of 3 seconds, the BOLD signal at the top of the brain is measured close to 3 seconds after that measured at the base of the brain. If uncorrected, this effect can have a marked effect on the later analysis which assumes that all of the data within a volume is acquired at the same instant in time (in FSL this is assumed to be halfway through the TR interval) (Smith 2001b). This correction is typically achieved in practice by phase shifting the signal timeseries in all of the voxels within a slice using temporal interpolation (Huettel et al 2004). In FSL, this shift is done using Hanning-windowed sinc interpolation (Smith 2001b). By nature of the techniques, the interpolation will always be more effective for data collected at short TRs, although the need for it to be performed is more pressing for data collected at longer TRs (Huettel et al. 2004).

2.3.2.2. Motion correction

If it is considered that a key premise of fMRI analysis is that a given BOLD signal timeseries is derived from a single spatial location, then it is apparent that head motion represents a very important possible confound and source of potential bias (Brammer 2001, Huettel et al. 2004). This effect is particularly profound in areas with high-contrast boundaries such as is seen around the cortex on the surface of the brain, where even a small movement may lead to signal being derived from an entirely different source (such as CSF) during the course of timeseries acquisition (*figure 2.9*). The significance of motion as a confound for the technique as a whole, was highlighted in an early study by Hajnal and colleagues, where it was demonstrated that even tiny amounts of movement

(particularly those correlated with the timing of the stimulus) can lead to significant changes in local signal intensity which may be interpreted falsely as neural activity (Hajnal et al. 1994).

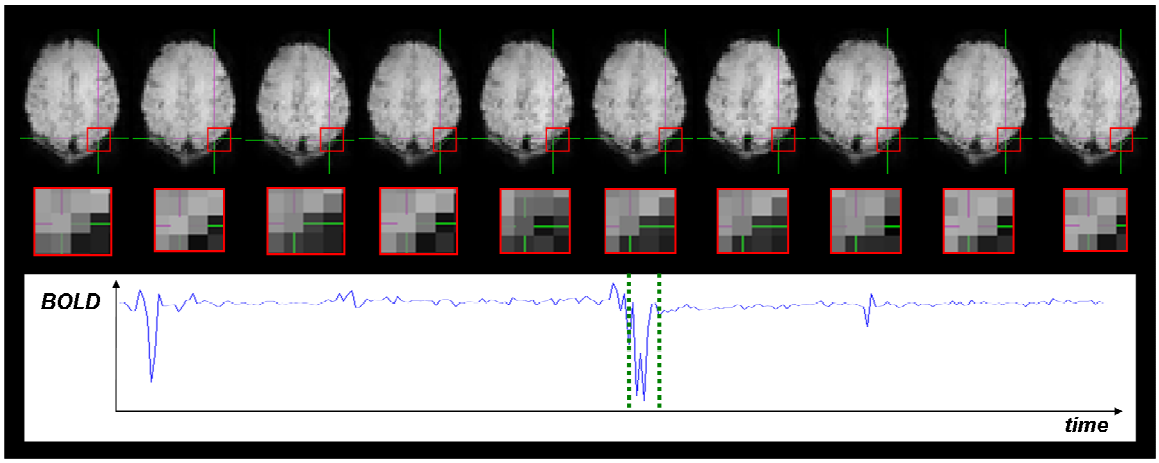

Figure 2.9: ***Head motion can have a marked confounding effect on fMRI data.*** In the above example data, a subtle rotation of the subject's head (*shown in the axial plane, top row*) can be seen during this selected portion of the data. On closer view, this movement can be seen to have a profound effect on the measured BOLD signal in voxels on the edge of the brain (*middle row, contained within the red box*). In the cross-haired voxel, this effect causes a marked drop in BOLD contrast during the corresponding the time period, which is sustained even after the movement itself has finished (*bottom row, between the green dashed lines*).

A crude initial screen of the raw images are often done immediately after acquisition and large amounts of head motion can be visualised by watching a video-loop of the data, which may suggest that data should be discarded prior to further analysis (Brammer 2001). For the purposes of motion correction, the head is considered to be a rigid body (ie: while there may be changes in position and orientation during the acquisition period, it is assumed there are no changes in shape) (Friston et al. 1995a, 1996, Brammer 2001, Jenkinson et al. 2002, Huettel et al. 2004). Within the FSL environment, this process is carried out with MCFLIRT (Motion Correction using FMRIB's Linear Image Registration Tool) (Jenkinson et al. 2002). Each individual brain image volume is aligned or "co-registered" by computing the image transformation (usually 6 parameters: 3 translation estimates (in the x,y,z directions) and 3 rotation estimates (around the x,y,z axes)) required to match it to a specified

“template” or “target” image (in FSL this is automatically selected as the middle volume of the data acquisition) (Friston et al. 1995a, Brammer 2001, Jenkinson et al. 2002). This process also has the advantage of providing quantitative measures of head displacement in the 6 specified parameters, which can also be used to accurately identify the timing of movements to guide removal of corrupted periods of data, and to recognise possible bias when comparing results between groups (Brammer 2001, Jenkinson et al. 2002).

Although this process of rigid-body realignment correction will therefore produce fMRI data consisting of volumes which should be spatially identical to one another, significant (and more complex) residual effects still remain in the data (Friston et al. 1996, Brammer 2001, Muresan et al. 2005). Even small displacements can have profound effects on the measured BOLD signal intensity, particularly if they occur “through-plane” (ie: movement which causes an area to be displaced in and out of an acquired slice) (*figure 2.9*) (Friston et al. 1996, Muresan et al. 2005). These effects have been termed “spin-history” artefacts, and occur as a result of the change in position within the external magnetic field disrupting the tissue’s steady-state magnetisation, thereby modifying the measured signal (Friston et al. 1996). Furthermore, until a new state is reached, the altered signal intensity will propagate into the subsequent acquired volumes, regardless if no further displacement occurs in that period (Friston et al. 1996, Muresan et al. 2005). Although various methods of direct spin-history artefact correction have been proposed, this is not done within FSL as the relationship between movement and signal intensity is highly complex, with a single pattern of movement resulting in vastly different (and unpredictable) patterns of signal change across the brain (Friston et al. 1996, Brammer 2001, Jenkinson et al. 2001, Beckmann & Smith 2004).

The estimated displacement vectors derived from the rigid-body realignment can be used as confound variables in the later data analysis, based on the assumption that abhorrent changes in the image intensity will be linearly related to the measured head motion and therefore can be regressed

out (Brammer 2001). This method is limited in its effectiveness, as there areas in the brain which move independently under normal conditions (such as areas with physiological pulsation) and therefore violate the rigid body assumption, and due to the profoundly non-linear relationship between head motion and BOLD contrast (Brammer 2001, Beckmann et al. 2004). An alternative and perhaps preferable method is to use a blind source separation technique such as Independent Component Analysis (ICA) to identify and filter out patterns of structured noise within the signal (such as in areas containing pulsating arteries, and changes related to patterns of head motion) (*see section 2.3.4.3*) (Beckmann et al. 2004).

2.3.2.3. Distortion correction

As described previously (*section 2.3.1*) images acquired with an EPI sequence are particularly predisposed to particular forms of geometric distortion, especially those due to magnetic field inhomogeneity induced by differences in susceptibility in adjacent tissues (Jezzard & Clare 1999, Westbrook & Roth 2005, Buxton 2009, McRobbie et al. 2010). This inhomogeneity can be characterised and a B_0 "field map" created by calculating the difference in signal phase between two images which have been acquired at different echo times (Jezzard & Balaban 1995). This field map can then be used to "unwarp" the fMRI data by applying cost-function masking thereby ignoring areas of high signal loss (Jezzard & Balaban 1995). In the adult brain, signal drop-out is common in the inferior frontal and temporal areas due to the presence of large air-filled sinuses adjacent to the brain (Jezzard & Clare 1999, Buxton 2009). In the preterm and term neonate, these areas of signal drop-out are not significant as the sphenoidal and frontal sinuses are not yet pneumatised, and therefore this step was not felt to be necessary for the data described in this thesis (Abidelli et al. 2011).

2.3.2.4. Intensity normalisation

Large scale changes in the global signal intensity of the brain can be corrected by "intensity normalisation", whereby the BOLD signal in each volume is effectively "normalised" to have the same mean intensity (Friston et al. 1994a, Smith 2001b). This is done by calculating the mean intensity of each separate volume, and then rescaling the data such that each individual volume has a mean intensity instead defined by a preset constant (Friston et al. 1994a). This step is carried out routinely in the widely used Statistical Parametric Mapping fMRI analysis package (SPM, http://www.fil.ion.ucl.ac.uk/spm/), but is not automatically done in FSL, and was not performed in the work of the thesis, as it has been shown to potentially lead to false patterns of functional "deactivation". This effect occurs because stimulus induced activation may cause large increases in signal intensity, which therefore raise the overall volume mean, forcing the signal in other "non-activated" areas of the brain to be negatively correlated with the stimulus (Aguirre et al. 1998a, Smith 2001b). Large scale drifts in the data are instead corrected by high-pass temporal filtering (*section 2.3.2.6*), and scaling is performed by a single factor ("grand mean scaling") to effectively normalise the data and allow intra and inter-subject comparison (Smith 2001b).

2.3.2.5. Spatial filtering

A low pass spatial filter is typically applied to fMRI data, with the net consequence the images are effectively "blurred" prior to further analysis (Smith 2001b, Huettel et al. 2004). While it initially appears counter-intuitive to actively reduce the spatial resolution of the data, this process serves two important functions: firstly to increase the SNR of the data (as although SNR is inherently low in fMRI data, it is spatially correlated across distinct areas due to the patterns of functional localisation and vascular supply in the brain), and secondly to reduce false positive rates due to the large number of data points generating multiple comparison statistical problems in the later analysis (Friston et al. 1994b, Huettel et al. 2004). Spatial smoothing is therefore only worthwhile if the eventual cluster of identified activity is predicted to be larger than the extent of the smoothing. This

process is achieved in FSL by convolution of each data volume with Gaussian process filters, the width of which determines the extent of blurring to be carried out (Smith et al. 2001).

2.3.2.6. Temporal filtering

Temporal filtering is then carried out on the BOLD signal timeseries of each individual voxel following the previously described stages of pre-processing. This can be done at both the high and low ends of the frequency spectrum to remove unwanted timeseries artefacts which are unquestionably not related to the experimental signal of interest (Friston et al. 1994a, Smith 2001b, Huettel et al. 2004). High-pass filtering is used to remove low frequency drifts in the data, such as those caused by "scanner drift" (due to gradual changes in the scanner magnetic field during the acquisition), slow movements of the subject's head, and aliased physiological effects (such as subject breathing) (Friston et al. 1994a, Smith 2001b). Low-pass filtering can also be used to remove high frequency noise (such as that caused by vascular pulsation), but has a potential downside in that the power of the later analysis may be reduced due to an effective "smoothing" of the timeseries response (and in particular a dampening of high amplitude rapid responses) (Smith 2001b). In FSL, high pass filtering is applied automatically to data; but low pass filtering is not, so as not to reduce the strength of the signal of interest.

2.3.3. Study design

In a prototype fMRI experiment, the optimal stimulation paradigm would induce robust and repeatable BOLD contrast changes in discrete areas of the brain, and at a frequency which can be easily distinguished from artefactual signal changes (Bandettini et al. 1993, Friston et al. 1994a, Donaldson & Buckner 2001, Henson 2003). In general, it is assumed that a brief stimulus will induce a BOLD signal response which is identical to the canonical HRF (Friston et al. 1994a). A further key assumption is that the characteristics of the measured BOLD responses will be highly predictable in nature, in particular with overlapping haemodynamic responses summing in a roughly linear fashion

(*see section 2.2.4.1*) (Boynton et al. 1996, Dale & Buckner 1997). It is therefore possible to model a predicted BOLD response for a given experiment by convolution of the known HRF with a simple model which describes the experimental design in terms of the timing of stimulation or task (Friston et al. 1994a).

In general, fMRI experimental paradigms can be classified into two forms: (*figure 2.10*) (Donaldson & Buckner 2001, Henson 2003, Huettel et al. 2004, Amaro & Barker 2006, Monti 2011):

Block Paradigms: consist of "blocks" of constant stimulation or task which are interspersed with blocks of rest, with several repetitions of this cycle repeated during the experiment (*figure 2.10(a)*) (Bandettini et al. 1993, Donaldson & Buckner 2001, Henson 2003). The prolonged nature of the activity block means that this form of design is generally unsuitable for studying stimuli which the subject may habituate to, and tasks in which predictability must be avoided such as those which require higher cognitive functioning (Poellinger et al. 2001, Donaldson & Buckner 2001, Huettel et al. 2004, Amaro & Barker 2006).

Event-related Paradigms: consist of individual brief "events" of stimulation or task, with either a constant or random rest period between events (Buckner et al. 1996, Dale 1999, Bandettini & Cox 2000, Donaldson & Buckner 2001, Henson 2003). This takes advantage of fMRI's relatively good temporal resolution, with the further advantage that time-locking and averaging of the signal will allow the accurate quantification of haemodynamic responses and characterisation of the HRF (*figure 2.10(b)*) (Buckner et al. 1996, Friston et al. 1998a, Dale & Buckner 1997, Buxton et al. 2004). Moreover, several different forms of event can be randomised into a single experimental design, allowing studies of simultaneous sensory processing and integration, which also avoids the problems of prediction in studies of cognitive processing (*figure 2.10(c)*) (Dale & Buckner 1997, Donaldson & Buckner 2001, Amaro & Barker 2006).

The choice of paradigm therefore depends on the aims of the study; with block designs most suited for detecting patterns of activation (due to the large amplitude responses), and event-related designs most suited for estimating the haemodynamic response (Dale 1999, Buxton 2009). A block design is comparatively insensitive to the shape of the HRF, as the plateau of the response is dependent on the area under the HRF curve, while the shape affects only the transitional rest periods (Buxton 2009). In contrast, in an event-related design, although individual responses may appear to vary greatly during data acquisition (assuming that noise is random), time-locked averaging within a cluster of activated voxels can systematically characterise both the shape and amplitude of the haemodynamic response, analogous to the theory behind evoked electrophysiological responses (Buckner et al. 1996, Dale & Buckner 1997, Miezin et al. 2000). An important drawback is that the sensitivity and efficiency of such an event-related design can be relatively poor (due to the infrequent pattern of stimulation and low amplitude response) particularly if a regular and large inter-stimulus interval (ISI) is used, although simulations have suggested that both factors can be maximised at an ISI of 12-15 seconds (Dale 1999, Bandettini & Cox 2000, Miezin et al. 2000). A further strategy is to randomise the stimulation pattern which will both increase efficiency by allowing a greater number of events, and theoretically increase the sensitivity due to the additive effects of overlapping responses (*figure 2.10(c)*) (Dale & Buckner 1997). Another alternative and an extremely powerful approach is to "jitter" the presentation timing throughout different timepoints within the TR interval, so that a composite haemodynamic response can be reconstructed from the time-locked data (Miezin et al. 2000, Donaldson & Buckner 2001, Henson 2003).

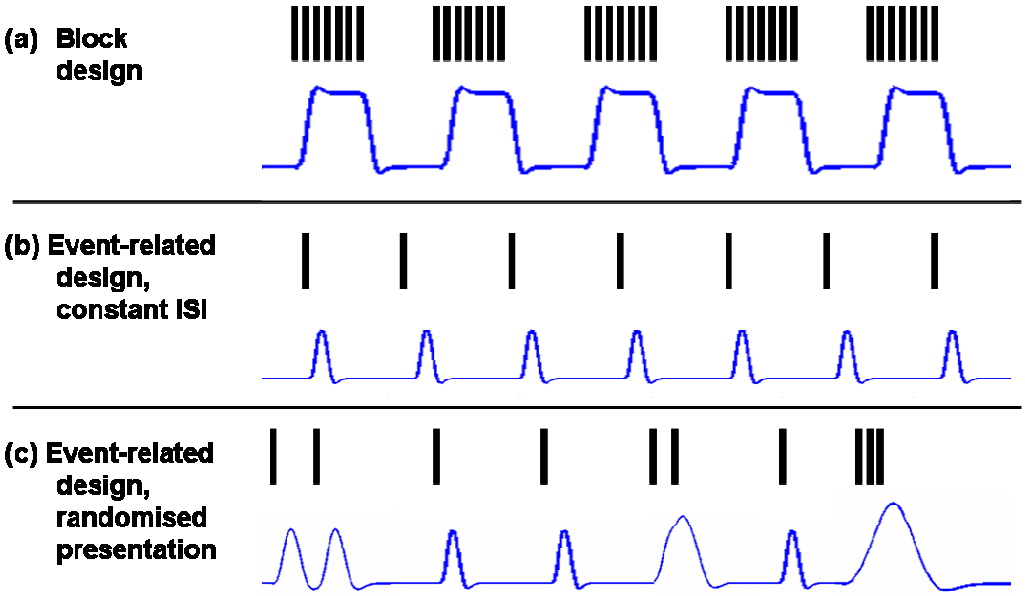

Figure 2.10: ***fMRI experimental design and efficiency:*** (a): In the block design, periods of constant or repetitive stimulation (black bars represent timing of stimulus) are presented, with robust large amplitude responses as a result of linear summation of successive HRFs (blue represents theoretical BOLD signal timeseries); (b): In an event-related design, individual events are presented intermittently in this case with a constant inter-stimulus interval (ISI). Responses are therefore identical to a single HRF; (c): Stimulus presentation can also be randomised (including with different stimulus types), with overlapping HRFs assumed to sum in a linear fashion, thus increasing both sensitivity and efficiency in comparison to a simple event-related design with a constant ISI.

2.3.4. Principles of data analysis

Taking the basic principles outlined in the previous sections, an fMRI data set can therefore be thought of as a set of cuboid elements (voxels) of a pre-specified size, each of which has an associated BOLD signal timeseries containing as many timepoints as volumes and of a sampling frequency as specified in the fMRI acquisition sequence (Friston et al. 1994a, Monti 2011). It is further assumed that neural activity will be associated with a local increase in BOLD signal following a temporal delay of approximately 5-8 seconds (Bandettini et al. 1993). In the first fMRI studies, patterns of functional activation were identified by the simple subtraction of the images acquired during rest from those during stimulation, in a manner identical to that used in PET data analysis

(Belliveau et al. 1991, Bandettini et al. 1992, Kwong et al. 1992, Ogawa et al. 1992). In 1995, Friston and colleagues first introduced the idea of taking advantage of the known and reproducible properties of the BOLD response by using a General Linear Model (GLM) framework to perform a statistically robust analysis (Friston et al. 1995b,c). Although alternative methods of analysis have been proposed (in particular those which are free from the possible constraints of a model), the simplicity and flexibility of the GLM makes it intrinsically attractive, and it remains as the basic framework on which nearly all task-driven fMRI data analysis is still performed (Monti 2011, Poline & Brett 2012).

2.3.4.1. The General Linear Model (GLM)

The GLM assumes that the measured data can be explained by a model which is formed by the linear sum of weighted known data (Poline & Brett 2012). As the timeseries of each voxel is analysed independently, the standard GLM is a "univariate" analysis; although the later statistical inference steps are typically "multivariate" to identify biologically plausible clusters of activated voxels (Smith 2001a). Therefore for a single voxel timeseries y(t), the standard GLM is expressed as:

$$y(t) = \beta_1 * x(t) + c + \varepsilon \qquad [2.5]$$

where x(t) is the predicted response (formed from a convolution of the design paradigm and the HRF as described in section 2.3.3), c is a constant representing the baseline BOLD signal, ε is the error in the model fit, and β_1 is a "*parameter estimate*" which scales the design x(t) to the actual observed response y(t) (Friston et al. 1995b,c). This simple formulation can be easily extended to incorporate experimental designs which consist of two or more types of stimuli, by simply summing in extra design models ($x_1 \ldots x_n$) and their associated parameter estimates ($\beta_1 \ldots B_n$) (Friston et al. 1995c, 1998, Smith 2001a):

$$y(t) = \beta_1 * x_1(t) + \beta_2 * x_2(t) + \ldots + \beta_n * x_n(t) + c + \varepsilon \qquad [2.6]$$

This approach also allows nuisance variables (such as the estimated head motion parameters as described in section 2.3.2) to be included into the model as confound regressors (Smith 2001a). The GLM is usually formulated in matrix notation, which allows all of the parameter estimates to be grouped into a single vector β, and all of the explanatory models to be grouped into a single matrix X (often termed the "*design matrix",* where each column represents an individual model) (Friston et al. 1995c, Smith 2001a). The aim of this first stage of analysis is therefore to identify if the unknown parameter β differs significantly from zero, and in doing do effectively determine the degree to which the predicted response X can explain the variance in the actual response Y (Monti 2011). This is typically solved using a simple linear regression method which aims to minimise the residuals in the fit such as Ordinary Least Squares (OLS) (Woolrich et al. 2001). It is generally assumed that ε is uniformly normally distributed, and is independent to the design matrix (Woolrich et al. 2001).

The calculated parameter estimate is then converted to a more meaningful statistical value, by compared it to the uncertainty in the estimation (Smith 2001a). In FSL, this is done by first dividing the estimated β by its standard error (SE) (calculated from the residual noise after model fitting) to generate a t-statistic, which is then further converted to a normally distributed z-statistic (Smith 2001a, Woolrich et al. 2001). An important effect at this stage in the analysis is timeseries autocorrelation, due to unaccounted correlated patterns of intrinsic noise (such as those related to residual motion artefact, vessel pulsation, breathing movement, MR hardware related) which violate the assumptions of the GLM, and lead to biased estimates of error variance (Worsely & Friston 1995, Bullmore et al. 1996, Woolrich et al. 2001). In FILM (FMRIB's Improved Linear Model) this is avoided by performing "pre-whitening" on the data; whereby the autocorrelation is estimated and corrected using a regularised non-parametric algorithm prior to calculating the model parameters (Woolrich et al. 2001).

A statistical map of the brain is thus produced from the GLM, with an individual statistical value for each voxel of the brain derived from the GLM analysis of the individual timeseries (Friston 1994a, Smith 2001a). To identify "activated" regions of the brain, a further statistical inference or "thresholding" step is then required to classify voxels at a given level of significance (Friston 1994a). The potential for false positive classification (due to the enormous number of voxels in a brain image) is avoided by performing a correction for multiple comparisons; and as "real" patterns of activity are assumed to occur over a group of voxels, by taking into account the spatial extent of contiguous clusters of activation (in FSL this is done using gaussian random field theory) (Smith et al. 2001a, 2004, Genovese et al. 2002, Nichols & Hayasaka 2003). A consideration (and potential source of bias) at this final stage of the analysis is the relatively arbitrary nature of thresholding, as a suitable level of significance must be selected by the investigator (Genovese et al. 2002, Smith & Nichols 2009, Nichols 2012).

2.3.4.2. Higher level group analysis

An important attribute of fMRI is that once normalised, the data is amenable to the combined analysis of multiple data sets of repeated sessions within the same subject or across different subjects (Holmes & Friston 1998, Smith 2001a). Not only can this potentially increase the overall sensitivity of an experiment (as noise is assumed to be random and will not be consistent between sessions or subjects), but also importantly allows the formal statistical comparison of responses to different stimuli or tasks, and between different populations of subjects (Holmes & Friston 1998). A group analysis is typically referred to as a "higher-level" analysis, as it is often performed on the statistical maps derived from the analysis of individual subject data sets (which are therefore also termed "lower-level" analyses). For functional data sets to be combined across a population of subjects, they must first be spatially normalised by alignment to a common image space which compensates for individual differences in brain anatomy and orientation (Jenkinson 2001, Brett et al.

2002). In adult study populations, this process of registration to a "*standard reference space*" is commonly done to a widely available resource such as the MNI152 brain (Montreal Neurological Institute 152 brain), onto which a number of labelled brain atlases can be applied (Mazziota et al. 2001, Jenkinson 2001).

Higher level analyses on spatially normalised data can be generally classified into three groups, with the choice of analysis dependent on the study populations and the specific study question (Nichols & Holmes 2002, Mumford & Nichols 2006, Mumford & Poldrack 2007):

Fixed-effects: In this form of analysis, it is assumed that the average response within each subject is equal, with the variance derived from errors within a session (Friston & Holmes 1998, Mumford & Nichols 2006). A fixed-effects analysis is therefore sensitive to the activation pattern only within the studied group, but the findings are not representative of the wider population from which the group was drawn, as cross-session and cross-subject variance is not taken into account in the modelling (Mumford & Nichols 2006).

Mixed-effects: An alternative which allows the analysis results to be interpreted as representative of the wider population, is to include both the within session variance (the fixed-effects) and the cross session variance (the random-effects) into the higher level analysis model (Beckmann et al. 2003, Mumford & Nichols 2006, Mumford & Poldrack 2007). A drawback to this approach is that it is intuitively more conservative at identifying group patterns of activation, and is unsuitable for small groups of subjects where cross session variance may be overstated (Mumford & Poldrack 2007).

Permutation methods: While the first two approaches follow on from the framework of the GLM and assume that the data is drawn from a parametrically distributed population, a further approach is to use a permutation test which makes no assumptions about the data (and noise) distributions

(Nichols & Holmes 2002). This conceptually simple approach has been shown to outperform some of the more traditional parametric methods, and is particularly suitable in situations where a non-standard approach is required (such as TBSS, where the white matter tracts studied may be highly irregular and variable in shape) (Hayasaka & Nichols 2004, Smith et al. 2006).

2.3.4.3. Independent Component Analysis (ICA)

An entirely distinct approach to traditional GLM based analysis methods is to use a multivariate and model-free technique such as Independent Component Analysis (ICA). The principles of the technique originate in classical signal processing, whereby it is assumed that measured data is generated from a mixture of underlying independent signals of interest via a complicated process. It is clearly apparent how this premise is applicable to fMRI data, particularly given the large variety of potential sources of noise (McKeown et al. 1998, Beckmann & Smith 2004, Beckmann 2012). In FSL, a probabilistic ICA model is implemented in MELODIC (Multivariate Exploratory Linear Optimised Decomposition into Independent Components) (Beckmann & Smith 2004). Here, the entire data set is thought of as a single 2D matrix of space (with each voxel representing a different column) and time (with each row representing a different timepoint or volume of data). This matrix can then be decomposed into two new matrices, one in which the timecourse of a component is represented in different columns; and the other in which the spatial representation of each component is represented in rows (Beckmann & Smith 2004). In FSL, the vital extra steps of noise variance normalisation and statistical inference are implemented by the addition of probabilistic principal component analysis and thresholding with Gaussian mixture modelling (Beckmann & Smith 2004).

The resulting spatial components may represent a map of stimulus related functional activity, task-unrelated intrinsic brain activity, or possible sources of artefact (Beckmann et al. 2004, 2005, 2012). In task-driven fMRI experiments, ICA techniques are of particular use to identify and remove artefactual signals, such as those likely to be related to intrinsic physiological factors (vessel

pulsation, respiratory movement) and head motion (*see section 2.3.2.2*) (Beckmann & Smith 2004). A further and particularly valuable application of ICA techniques is in the identification and study of resting state networks, where coherent patterns of low frequency correlated activity in fMRI data are seen even under conditions where no stimulus or task has been performed by the subject (Biswal et al. 1995, Beckmann et al. 2005).

2.4. Summary

By exploiting the changing magnetic properties of haemoglobin induced by its oxygen binding state, fMRI offers a non-invasive (but indirect) way of visualising and quantifying in-vivo brain activity. Following stimulation, neural activity initiates a cascade of neurovascular coupling which leads to a local vascular response, and an increase in the BOLD signal measured by a T2* weighted MRI sequence. In addition to avoiding the potentially harmful effects of ionising radiation, fMRI offers further advantages through the relatively good (and adaptable) temporal and spatial resolution which are inherent to MRI techniques. The measured BOLD signal response to stimulation is reproducible across sessions and subjects, with the canonical impulse response termed the haemodynamic response function (HRF). fMRI data analysis is a statistical process, which has been carefully refined in the last 20 years to account for possible sources of noise, and to avoid false positive results. This has the additional benefits of allowing both great flexibility to the technique in study design and extended analysis, and the combination of data sets to systematically identify within and between group patterns of brain activity.

Chapter 3

3. fMRI studies of the newborn brain

In the 20 years since Ogawa and colleagues first described BOLD contrast, the widespread application of fMRI techniques has begun to allow investigators to accurately map and characterise the functional organisation of the brain, and furthermore to probe more complex issues such as the underlying patterns of connectivity between different regions during particular tasks and at rest (Ogawa et al. 1990, Kim & Ogawa 2012). Coupled with its non-invasive nature and excellent safety profile, these attributes would seemingly make fMRI extremely suitable for studying the infant brain, and further suggest that it could hold the potential to add a vital new dimension to our understanding of the developing CNS (Seghier et al. 2006, Smyser et al. 2011).

Despite this, there have only been a relatively small number of fMRI studies which have reported reliable functional responses in neonatal subjects to simple visual, auditory, and tactile stimuli (*reviewed in Seghier et al. 2006, 2010*). Notable among these studies are prominent differences in the study population (with infants of markedly different age and clinical characteristics included in a single group), the use of sedative medication, and the imaging sequence parameters. With this in mind, it is perhaps unsurprising that these studies have all reported inconsistent results, with the most prominent controversy relating to the amplitude of the functional responses, with early studies reporting (in contrast to the typical adult response) a localised decrease in BOLD signal (termed "***negative BOLD***").

In this chapter of the thesis, I will review the current literature of existing fMRI studies in early infancy. I will then attempt to identify some of the key questions and challenges which are likely to be pertinent for developing the technique and its successful application for studies of the vulnerable neonatal population.

3.1. Reported studies in the literature

A PubMed search using the keywords “infant” “neonate” and “functional MRI” identifies only 22 relevant studies in early infancy, with a further 9 studies of resting state fMRI connectivity alone (*table 3.1*). The first description of the use of BOLD contrast in a MRI study of unwell neonates was reported by Toft and colleagues in 1995, who described changes in BOLD contrast in response to an induced difference in the partial pressure of carbon dioxide (pCO_2) following adjustment of the mechanical ventilation rate (Toft et al. 1995). While this study initially demonstrated the feasibility of measuring dynamic changes in BOLD contrast in neonates, it was then shortly afterwards in 1996 that the first task-driven fMRI experiments in young infants were reported by Peter Born and colleagues, who used a simple visual stimulus to study BOLD responses in young infants in a series of studies over a range of ages from a few days to 4 years (Born et al. 1996, 1998, 2000, 2002b). Like these early studies, the majority of later studies have also utilised a visual stimulus (*figure 3.1(a)*), and slightly more than half of the studies (58%) have used a pharmacological sedative agent. Approximately one third of the reported studies identified predominately negative BOLD responses, with a further one third reporting positive responses, and the further third identifying either responses of both type or a shift in amplitude with increasing age (*figure 3.1(b)*).

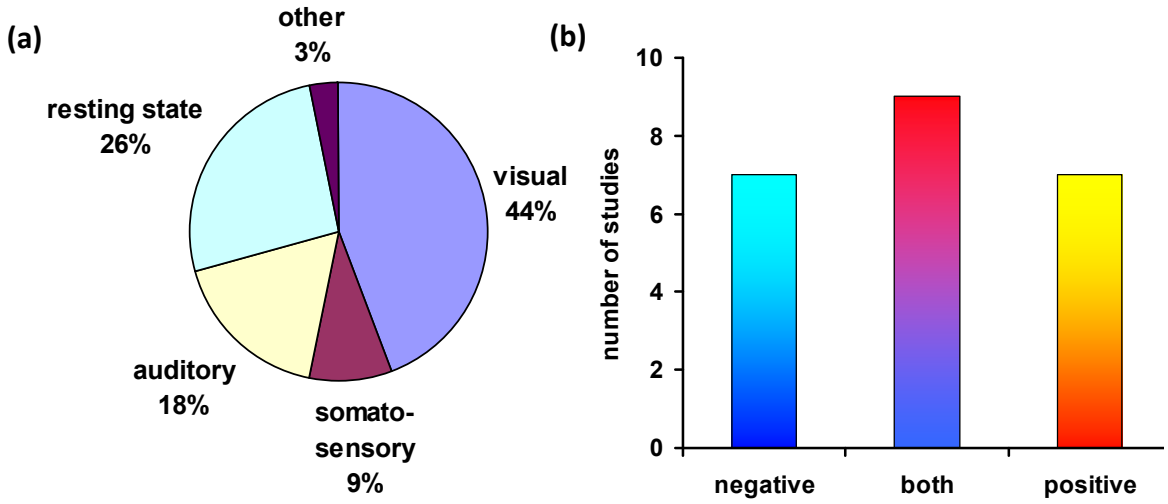

Figure 3.1: (a) ***A total of 31 fMRI studies in early infancy have been reported in the literature.*** Of these, the largest proportion (44%) have utilised a visual stimulus, although an increasing number of recent studies have investigated functional connectivity at rest with no stimulus. **(b)** ***Prominent inconsistency is found in the amplitude of induced BOLD fMRI responses in early infancy.*** While approximately a third of studies report predominately negative and positive BOLD responses only, a further third has described an equal distribution. This includes 5 studies which suggest that the amplitude changes from positive to negative at 8 weeks of age post-term.

Study (Authors, year of publication)	Stimulus type	Study population size (number discarded); (Age, range)	Sedation (type)	MR sequence parameters						BOLD responses (identified, amplitude)
				B_0 field strength (Tesla)	Spatial resolution (x*y*z) mm	TE (msec)	TR (msec)	Flip Angle (degrees)	Length of sequence (minutes, seconds)	
Altman & Bernal, 2001	Visual (31); Auditory (38)	38 (2) (2months to 9 years old) *MRI scan clinically indicated*	chloral hydrate (10/38) pheno-barbitone (28/38) propofol (1/38) alprazolam (2/38)	1.5	3.75*3.75* not written	60	3750	60	3 min 7 sec	*Visual*: 1/31 positive; 28/31 negative; 2/31 no response *Auditory*: 26/38 positive; 0/38 negative; 12/38 no response
Anderson et al. 2001	Auditory	14 (6) ex-preterm and control (33 to 47.5 wks PMA)	None	1.5	3.125*3.125* not written	60	5000	Not written	12 min	5/14 positive 9/14 negative 0/14 no response
Blasi et al. 2011	Auditory (language)	21 controls (3 to 7 months)	None	1.5	3.5*3.5*5	57	3000	90	16 min	21/21 positive

Born et al. 1996	Visual	7 (6 weeks to 36 months *MRI scan clinically indicated*	Chloral hydrate (6/7)	1.5	3.125*3.125*4	66	4000	Not written	6.5 min	6/7 negative 1/7 not known
Born et al. 1998	Visual	17 (5) (3 days to 48 months)	Chloral hydrate (9/12)	1.5	3.125*3.125*4	66	4000	Not written	6.5 min	1/12 positive 10/12 negative 1/12 no response
Born et al. 2000	Visual	9 preterm (32-61wks); 14 visual deficit (52-338wks); 8 others (54-179wks)	Chloral hydate (5/9); (13/14); (6/8)	1.5	1.5-.8*1.5-.8*4	66	2500	90	4 min	*Preterm*: 3/9 positive; 3/9 negative; 3/9 no response *Visual deficit*: 1/14 positive; 13/14 negative Others: 2/8 positive; 5/8 negative; 1/8 no response
Born et al. 2002	Visual	4 (1 visual deficit) (4-71 months)	Chloral hydrate (4/4)	1.5	1.8*1.8*4	66	2500	Not written	4 min	4/4 negative
Dehaene-Lambertz et al. 2002.	Auditory (language)	20 (10) control infants (2-3 months old)	none	1.5	3.1*3.1*4	60	3333	Not written	3 min	20/20 positive
Doria et al. 2010	Resting state	62 (12) (29-43 weeks PMA)	Chloral hydrate (30/74)	3	2.5*2.5*3.25	45	1500	90	6 min 34 sec	n/a

Erberich et al. 2003	Somato-sensory; Visual	6 (1) (34-58 weeks PMA) *MRI scan clinically indicated*	Chloral hydrate (7/7)	1.5	3*3*3	40	3000	85	3 min (each hand)	*Somatosensory*: 6/6 positive (coexistent 5/6 negative) *Visual*: 6/6 positive (coexistent 6/6 negative)
Erberich et al. 2006	Somato-sensory	24 (18) Ex-preterm (38-49 weeks PMA); 6 controls (3-9 months)	Chloral hydrate (50/50)	1.5	2.8*2.8*3	60	3000	90	3 min (each hand)	Positive and negative responses seen in all subjects: positive predominately seen in contralateral hemisphere
Fransson et al. 2007	Resting state	12 ex-preterm infants (39+1 to 44+2 weeks PMA)	Chloral hydrate (12/12)	1.5	2.8*2.8*4.5	50	2000	80	10 min	n/a
Fransson et al. 2009, 2011	Resting state	19 (2) control infants (39+2 to 41+5 weeks PMA)	none	1.5	2.8*2.8*4.5	50	2000	80	10 min	n/a
Gao et al. 2009	Resting state	20 neonates (24 +/- 12 days); 24 1-year olds; 27 2-year olds	None	3	4*4*4	32	2000	Not written	5 min	n/a
Gao et al. 2011, 2012	Resting state	51 neonates (23 +/- 12 days); 50 1-year olds; 46 2-year olds	none	3	4*4*4	32	2000	Not written	5 min	n/a
Heep et al. 2009	Somato-sensory	5 (3) ex-preterm infants	Chloral hydrate	3	1.88*1.88 *3.59	35	2600	90	3 min 20 sec	1/5 positive 4/5 negative

		(38-39 weeks PMA)	(8/8)							
Konishi et al. 2002	Visual	16 (<8weeks); 11 (8 to 22 weeks) *MRI scan clinically indicated*	Pheno-barbitone (27/27)	1.5	3.4*3.4*6-7	50	3000	90	2 min 6 sec	*Lateral Geniculate Nucleus* (*LGN*): 27/27 positive *Primary visual cortex*: <60 days positive, >60 days negative
Lee et al. 2012	Visual	65 (19) preterm (30.5 +/- 2.7 weeks PMA); 23 (5) term (41.2 +/- 2.6 weeks PMA)	none	1.5	2.5*2.5*4	60/130	3000	90	3-3.5 min	*Preterm*: 4/65 positive; 61/65 no response *Term*: 19/26 positive; 7/26 no response
Lin et al. 2008	Resting state	38 neonates (2-4 weeks); 26 1-year olds; 21 2-year olds	none	3	4*4*4	32	2000	Not written	5 min	n/a
Marcar et al. 2004	Visual	11 (<5-years old); 10 (5-12 years old)	Midazolam, Sevoflurane anesthesia	2	2*4.1*5.5	58	2000	90	3 min 20 sec	Both positive and negative responses (proportion not documented)
Martin et al. 1999	Visual	58 (17); 8 neonate; 14 infants (1 month to 1-yr); 29 (1 to 6-yrs old); 7 (6 to 12-yrs old)	Pheno-barbitone (28/58); Chloral hydrate (12/58); halothane (9/58)	2	1.7-.9*1.7-.9*5	40	100	20	8 min	*0-4 months*: 6/18 positive; 5/18 negative; 7/18 no response *4-40 months*: 4/25 positive; 12/25 negative; 9/25 no response *40+ months*: 13/25 positive; 8/25 negative, 4/25 no response

Morita et al. 2000	Visual	8 (<60 days) 8 (60-361 days) *MRI scan clinically indicated*	Pheno-barbitone (16/16)	1.5	3.4*3.4*6-7	50	3000	90	2 min 6 sec	*LGN*: 16/16 positive *Primary visual cortex*: <60 days positive; >60 days negative
Muramoto et al. 2002	Visual	20 (22): 10 (<8 weeks); 10 (8-32 weeks) *MRI scan clinically indicated*	Pheno-barbitone (20/20)	1.5	1.72*1.72 *6	50	3000	90	5 min 6 sec	<8 weeks positive >8 weeks negative
Perani et al. 2010	Auditory (music perception)	18 (3) control infants (0-3 days)	none	1.5	3.75*3.75*3	40	3000	Not written	7 min	15/18 positive 3/18 negative
Perani et al. 2011	Auditory (language)	15 control infants (0-3 days)	none	3	2.81*2.81*3	40	3000	Not written	8 min 3 sec	15/15 positive
Smyser et al. 2010	Resting state	90 (8): 10 (<30 weeks PMA); 16 (30-34 weeks); 36 (34-38 weeks); 28 (38-42 weeks); 10 term control	none	3	2.4*2.4*2.4	28	2910	90	10 min	n/a
Seghier et al. 2004	Visual	1 (50 weeks PMA)	Chloral hydrate	1.5	1.9*1.9*4	40	2000	80	4 min (repeated 3 times)	Negative responses, and “inverse gamma” impulse response in event-related experiment

Toft et al. 1995	Changes in pCO_2	5 clinically unwell infants (31+6 to 47 weeks PMA)	All infants ventilated – anesthetic agent not documented	1.5	0.8*1.6*3 (single slice)	60	82	40	21 to 29 min	Hyperventilation associated with decreases in pCO_2 and decreases in BOLD contrast
Yamada et al. 1997	Visual	6 (<8 weeks); 9 (8 to 54 weeks) *MRI scan clinically indicated*	Pheno-barbitone (15/15)	1.5	1.7*1.7*5 (5 slices)	50	3000	90	5 min 6 sec	<8 weeks positive >8 weeks negative
Yamada et al. 2000	Visual	16 (<8weeks); 11 (8 to 22 weeks) *MRI scan clinically indicated*	Pheno-barbitone (27/27)	1.5	1.7*1.7*5 (5 slices)	50	3000	90	5 min 6 sec	<8 weeks positive >8 weeks negative

3.1.1. Visual Stimulation

Including the first studies of Born and colleagues, there have been a total of fourteen fMRI studies using a visual stimulus in neonatal and young infant subjects. Of interest, it is also striking that the greatest variability in results also appears to be seen in these studies, with large differences reported between studies and in comparison to adults in both the site and amplitude of the identified BOLD responses. Some of this inconsistency may arise from the relatively wide age ranges of the subjects included in these studies, as infants as old as 48 months of age have been grouped with some as young as just a few days (Born et al. 1996, 1998). A further confounding effect is that different clinical populations have also been included in single groups, with some healthy control infants born at term gestational age, grouped with others born prematurely, or even with some infants with a clear clinical indication for a brain MRI scan such as hydrocephalus (Born et al. 1996, 1998, 2000, 2002b, Yamada et al. 1997, 2000, Morita et al. 2000, Altman & Bernal 2001, Konishi et al. 2002, Muramoto et al. 2002). Comparison between groups is also complicated by the varying use of pharmacological sedation, with studies from Japan all utilising intravenous phenobarbitone (Yamada et al. 1997, 2000, Morita et al. 2000, Konishi et al. 2002, Muramoto et al. 2002), in contrast to those from Europe which have mostly used chloral hydrate (Born et al. 1996, 1998, 2000, 2002b, Seghier et al. 2004).

Common to the majority of visual fMRI studies is the use of a simple block stimulation paradigm; similar to that used by Born et al. (1996) in their first study, where they presented an 8 Hertz (Hz) flickering light stimulus for 24 seconds interspersed with 24 seconds of rest (darkness) to 7 infants (aged 6 weeks to 36 months) all of whom had been sedated with chloral hydrate (100-150mg/kg) (Born et al. 1996). In contrast to the canonical positive BOLD response seen in the primary visual cortex and along the calcarine fissure in adult subjects, Born described a counter-intuitive task induced decrease in BOLD contrast in all 6 of the infants in whom responses were identified, with the activity also localised to the

more anterolateral regions of the occipital lobe (Born et al. 1996). An identical study protocol was then extended to a larger study group of 17 subjects, with similar findings with the exception being a positive BOLD response seen in a single 4 week old healthy infant (Born et al. 1998). Two further studies from the same research group also identified similar patterns of response in infant populations with a clinically diagnosed visual deficit (Born et al. 2000, 2002b).

These findings led to Born and colleagues proposing that a "negative BOLD" response may represent a normal stage in early brain development when the increased metabolic demands of a higher synaptic density are not met by the task-driven increase in local CBF (Born et al. 1996, 1998, 2000). They attempted to address this issue directly in an interesting study reported in 2002, by simultaneously acquiring quantitative local perfusion data using a FAIR (flow sensitive alternating inversion recovery) sequence (Born et al. 2002b). In four studied adults, the local CBF was seen to increase accordingly with task-induced increases in BOLD contrast, but in the four studied infants (age range 4 months to 71 months) decreases in both the FAIR and BOLD signals were seen during the flickering light stimulation (Born et al. 2002). Although this could be interpreted as showing a task-induced decrease in CBF, the authors were cautious in concluding this due to the relatively poor SNR of the FAIR images (Born et al. 2002b). Of particular interest, in a separate study, Born and colleagues found that a strobing light stimulus on closed eyelids also induced a negative BOLD response and decrease in CBF (assessed with $H_2{}^{15}O$ PET) even in adults during slow-wave sleep, suggesting that the behavioural state of the subject is also a principal factor in the control of the induced response (Born et al. 2002a).

During the same time period, five studies were reported from a group in Japan utilising a similar 8Hz flickering light stimulus and a block stimulation paradigm (Yamada et al. 1997, 2000, Morita et al. 2000, Konishi et al. 2002, Muramoto et al. 2002). An intriguing finding consistent to all of these studies was

that of positive BOLD responses in the lateral geniculate nucleus (LGN), while the responses in the calcarine fissure appeared to switch amplitude from positive to a predominately negative response after 8 weeks of corrected postnatal age. The authors also suggested that their findings could be explained by an age-dependent increase in metabolism due to presumed increases in synaptic density at that developmental juncture, with the most marked increases suggested to occur in the primary visual areas as opposed to the LGN (Yamada et al. 2000, Morita et al. 2000). By applying the existing models of Buxton and Mandeville, the group also attempted to simulate the infant BOLD response and again postulated that a developmental increase in $CMRO_2$ was responsible for their findings (Buxton et al. 1998, Mandeville et al. 1999, Muramoto et al. 2002). However, in the absence of other information, a number of large and perhaps incorrect assumptions were made in this modelling including a stable relationship between CBF and CBV throughout development (and identical to adults), and the direct use of several constants (which may be invalid when relating to the neonatal brain) in the original Buxton Balloon model formulation (Buxton et al. 1998).

A further important study is that of Seghier and colleagues (2004), who studied the functional response to a 2 Hz flashing light stimulus, in a single sedated 13 week infant who had suffered a large left perinatal arterial stroke. They found no BOLD response in the pathological hemisphere (in which they also found no optic radiation using DTI tractography), and a negative BOLD response in the unaffected (presumed healthy) hemisphere (Seghier et al. 2004). Perhaps most significantly, they also performed a study using an event-related paradigm to allow an exact measurement and characterisation of the HRF. In their patient, they found a negative impulse response (which they termed an “inverse gamma function”) which mirrored the canonical adult response, with the lowest signal seen at 5-7 seconds (*figure 3.2*)((Seghier et al. 2004).

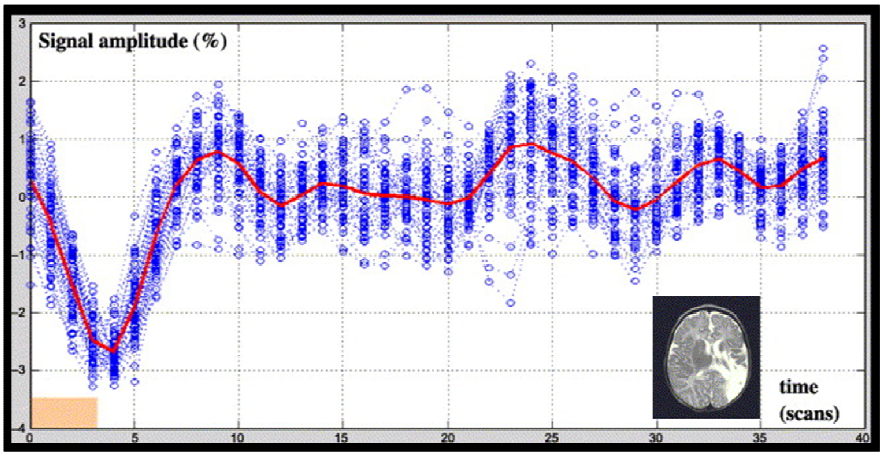

Figure 3.2: ***Using a visual stimulus and an event-related study design, Seghier and colleagues characterised an "inverse gamma" haemodynamic response function in a 13 week old infant.*** The subject had suffered a large perinatal arterial stroke in the left hemisphere (shown in inset picture), and functional responses were only identified in the "healthy" hemisphere. Following a 2Hz flashing light stimulus lasting 4.5 seconds, the BOLD signal was seen to decrease with the minimum signal seen at approximately 5-7 seconds (x-axis shows scan volume number, acquisition TR was 1.5 seconds) (*figure adapted and reproduced from Seghier et al. 2004*).

Most recently, Lee and colleagues described an fMRI study in a large cohort of preterm and term equivalent neonates using a 1 Hz flickering light stimulus (Lee et al. 2012). They were able to identify BOLD responses in just 5% of their preterm population and 73% of their term population, and did not identify any negative BOLD responses (Lee et al. 2012). Although newborn infants behaviourally can be shown to be visually attentive (for example, showing a preference for looking at images of faces) and immature visual evoked potentials can be demonstrated in some infants as young as 24 post-menstrual weeks, the authors concluded that fMRI is probably not an appropriate modality for studying visual function in preterm infants (Lee et al. 2012). A crucial consideration is that the findings of this study and those described above, may support the theory that at least some early visual activity occurs via the subcortical extra-geniculo-calcarine system (Johnson 1990). These theories further advocate that

functional activity in the primary visual areas not fully established until 2-3 months of age, and therefore may be highly relevant to the reported inconsistencies (Johnson 1990).

3.1.2. Sensori-motor stimulation

There have been 3 reported studies which have used a somatosensory stimulus to elicit fMRI responses in neonatal subjects (Eberich et al. 2003, 2006, Heep et al. 2009). In an initial pilot study of seven neonatal patients (age range 34 to 58 weeks PMA) with intracerebral pathology (hydrocephalus and white matter injury), Erberich and colleagues (2003) used a manually inflated rubber bulb fixed into the palm of their subjects' hands to passively move the fingers during 30 second blocks of activity. They were able to identify both negative and positive BOLD responses in the hemisphere contralateral to the side of stimulation, although in four of the subjects the predominant cluster was seen in the supplementary motor area (SMA) (Erberich et al. 2003). The same group utilised an identical stimulus and design paradigm in a much larger study of 42 (24 successful) prematurely born subjects imaged at term equivalent PMA and 6 control infants (imaged at 3-9 months of age) (Erberich et al. 2006). Of interest, the data in this study was analysed using a standard GLM approach, with the block stimulation paradigm convolved with the canonical adult HRF. At term age they were able to identify both negative and positive BOLD responses, with a clear preponderance towards positive activity in the contralateral hemisphere and 36.4-43.8% of infants showing a bilateral pattern of activation (Erberich et al. 2006). The great potential for fMRI to characterise patterns of functional development was highlighted by the findings in the smaller group of older infants, all of whom showed exclusively contralateral patterns of positive activity (Erberich et al. 2006).

The findings of Erberich's work were in contrast to that of Heep and colleagues (2009) who also studied somatosensory responses in a group of 8 (5 successful) ex-preterm infants studied at term equivalent

PMA. In response to passive movement of the forearm (induced by manually lifting the arm using Velcro fixed wrist straps) they reported a predominately bilateral pattern of negative BOLD activity in their study group, with a single infant showing a bilateral positive pattern of activity (Heep et al. 2009). The authors concluded that their study suggested that in the neonatal period, a negative and bilateral BOLD response should be considered normal, as the infant with positive responses was later found to have mild motor developmental delay at 4-6 months of age (Heep et al. 2009).

3.1.3. Auditory stimulation

Six studies have reported the use of an auditory stimulus, and of interest positive BOLD responses were identified in nearly all of the reported subjects (Altman & Bernal 2001, Anderson et al. 2001, Dehaene-Lambertz et al. 2002, Perani et al. 2010, 2011, Blasi et al. 2011). This effect was particularly clear in the study of Altman & Bernal (2001) who studied the BOLD response to both visual and auditory stimulation in 40 infants (38 successful) aged 2 to 9 months of age; with exclusively positive BOLD responses seen to an auditory paradigm consisting of 30 second stimulation blocks containing recordings of the infants' mother's voice, and a negative BOLD response seen in the majority to a flashing light stimulus.

Recent studies have further confirmed that positive BOLD responses can be robustly identified in the primary auditory cortex of young infants to both language and musical stimulation (Perani et al. 2010, 2011, Blasi et al. 2011). A particularly intriguing finding in these studies is that subtle but significant differences in the pattern of activation could be identified between vocal and non-vocal environmental auditory stimuli, and that responses were even sensitive to the "emotional" pitch of the presented voice (Blasi et al. 2011). In newly born term control infants, Perani and colleagues have also reported sensitivity to auditory stimuli as subtle as music dissonance and speech intonation (Perani et al. 2010, 2011). The findings of these studies suggest that even in very early life, the auditory system is

sufficiently mature to differentiate complex stimuli, and further imply that the developmental trajectories of functional activity may differ markedly between anatomical regions and sensory systems.

3.1.4. Resting state connectivity

A number of recent studies have sought to characterise the correlated patterns of functional activity at rest in early life (Fransson et al. 2007, 2009, 2011, Lin et al. 2008, Gao et al. 2009, 2011, 2012, Doria et al. 2010, Smyser et al. 2010). This approach is intrinsically attractive for studying the developing brain, as not only does it provide exciting information about the maturation of integrated system-wide brain activity, but it also requires no stimuli and potentially is relatively free from the limitations of analysis inherent to traditional GLM methods (Smyser et al. 2011). In adults at rest, a repertoire of 10-20 resting state networks can be reliably identified with a variety of analysis tools, in spatially distinct but presumably functionally connected brain regions (Smith et al. 2009). Although consistently identified across a variety of patient groups and mental states, the exact role of these networks remains unclear and is vigorously debated in the literature. Studies in neonatal subjects have similarly found that resting state networks can be readily identified at term equivalent PMA suggesting that large scale neural organisation is present in the resting brain even in early life (Fransson et al. 2007, 2009). These include complete facsimiles of the adult networks in the primary visual areas, the somatosensory and motor cortices, the primary auditory areas, cerebellum and premotor areas (Fransson et al. 2007, 2009, Doria et al. 2010. Smyser et al. 2010).

An area of particular interest is the longitudinal development of the resting state networks, with a clear maturational pattern visible through the preterm period (equivalent to the third trimester of in-utero life). Identifiable but fragmented networks can be identified at 30 weeks PMA, which are then seen over the subsequent last weeks of gestation to progress to the more complex long-range and bilateral

networks characteristic to the adult brain (*figure 3.3*) (Doria et al. 2010, Smyser et al. 2010). These findings are fascinating as they support the notion that a dramatic developmental increase in brain connectivity and organisation takes place around the time of birth, as suggested by the histological findings of rapid neural growth and synaptogenesis (Kostović & Jovanov-Milošević 2006).

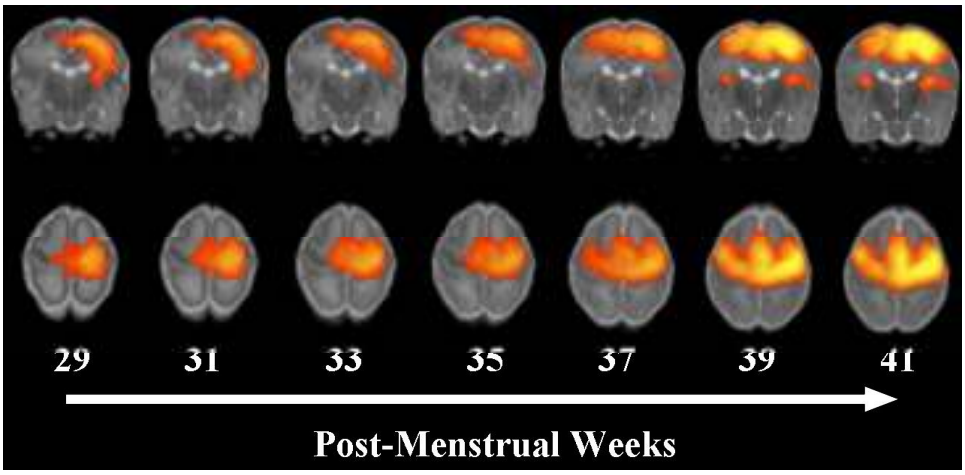

Figure 3.3: ***Development of the motor "resting state network" during the preterm period.*** The network can be clearly seen to progress from a unilateral representation at 29 weeks PMA, to a bilateral but spatially dispersed network at 35-37 weeks PMA, and finally to a well localised bilateral network with a clear pattern of connectivity between the left and right peri-rolandic cortices at 41 weeks PMA identical to that seen in the brains of adult subjects (numbers correspond to post-menstrual age (PMA) in weeks) (*Figure has been published in Arichi et al. 2011*).

A topic worthy of more detailed discussion is the Default Mode Network (DMN) or "task-negative" network which encompasses a group of discrete brain regions; the medial prefrontal cortex, the posterior cingulate gyrus and adjacent precuneus, and the inferior lateral parietal lobules (Raichle et al. 2001, Buckner et al. 2008). As many of these structures are traditionally thought of as playing a role in memory retrieval and higher cognitive functioning, the DMN has been implicated to play a role in "internally focused tasks" such as autobiographical memory retrieval and envisioning the future

(Buckner et al. 2008). The network is unique as it is seen to specifically “deactivate” (ie: develops a task related decrease in BOLD contrast) during goal-orientated tasks (Raichle et al. 2001). Moreover, decreased DMN activity and connectivity between the “hubs” of the network have been described in pathological states such as schizophrenia and autism (Garrity et al. 2007, Assaf et al. 2010). Although initial resting state fMRI studies did not identify the DMN in newborn infants, later studies have found it to be present at term equivalent PMA, and furthermore have described a maturational trend of increasing connectivity amongst the network hubs (Gao et al. 2009, 2011, 2012, Doria et al. 2010). These fascinating findings call into question the accepted function of the network, or may suggest that newborn infants are having self-referential thoughts at an age well before they appear to have attained the levels of recognisable cognition which are typically associated with “independent thought” (Lagercrantz & Changeux 2009).

3.2. Potential but major challenges

The small body of existing fMRI studies of the newborn brain have therefore yielded exciting and potentially important insights into the functional activity and organisation of the maturing brain. Not only do they hint that the neonatal brain contains a richer and more complex architecture of functional activity than that previously thought of, but they may also offer a new understanding of the effects of congenital and acquired brain injury, and moreover to the nature of the BOLD contrast itself. However, this enthusiasm is tempered by the clear limitations present in these previous studies, which may in part explain the conflicting results reported both within and between studies.

A major and important possible cause of such inconsistency is that many of the previous fMRI studies have used sequences and analysis techniques directly taken from equivalent adult studies. While this choice may have seemed logical at the time of study, it is apparent now that a number of fundamental

differences exist in both the biological and functional make-up of the immature brain, which suggest that they may have contributed to the aberrant findings.

3.2.1. Practical considerations

Successful MR image acquisition in neonates is a technically and practically challenging process, due to their potentially fragile clinical status and inherently uncooperative behaviour (Pennock 2001, Merchant et al. 2009). Newborn infants (and particularly those born prematurely) are susceptible to episodes of bradycardia and/or oxygen desaturation, and therefore require careful physiological monitoring during the period of data acquisition (Merchant et al. 2009). Adequate hearing protection is necessary due to the significant acoustic noise generated by the rapid switching of the gradient coils during image acquisition, with this effect greatest in fast acquisition techniques such as EPI (Merchant et al. 2009).

Head motion during image acquisition is a major cause of data corruption and potential bias, and has been shown to introduce systematic but false patterns of connectivity in functional data (*see section 2.3.2.2*) (Hajnal et al. 1994, Power et al. 2012, Satterthwaite et al. 2012, van Dijk et al. 2012). This issue is of particular importance in infant subjects who cannot follow instructions to remain still and moreover may become distressed in the alien environment of the MR scanner. One of the simplest techniques to try and overcome this, is to use head immobilisation techniques such as vacuum-evacuated bead filled bags and packing foam (Pennock 2001, Merchant et al. 2009). It is generally preferable that the infants are asleep during image acquisition, which is typically achieved either through feeding and swaddling the infant ("feed and wrap" technique) or with pharmacological sedation (Edwards & Arthurs 2011). However, while a systematic review has supported the effectiveness and safety of sedative medication for neonatal MR examination, it should be born in mind that there is a lack of similar systematic evidence to suggest that feed and wrap techniques are sufficient for consistently good image quality

(Edwards & Arthurs 2011). An important caveat is the unknown effect of sedative agents directly on the functional activity of interest; with possible effects on the neural activity itself, the neurovascular coupling, and the baseline vascular parameters (Galliard et al. 2001, Seghier et al. 2006, Harris et al. 2011).

3.2.2. Study population

Data collection of studies involving infant subjects is a challenging task, with strict ethical protocols and constraints limiting the study populations and methods. As a result, the majority of reported fMRI studies have grouped patients together into single groups which may cover a broad range of ages and a variety of clinical abnormalities (*see table 3.1*). Only a few studies have been able to report functional responses in adequately sized groups of healthy infants delivered at full term gestation, and it is of interest to note that all have been able to identify robust patterns of positive BOLD activation (Dehaene-Lambertz et al. 2002, Fransson et al. 2009, Perani et al. 2010, 2011, Blasi et al. 2011). This is of particular significance as differing degrees of brain development and clinical pathology are likely to profoundly affect both the spatial and temporal characteristics of the BOLD response, with the sensitivity of any subsequent group analysis likely to be markedly decreased by the increased variance present in the data.

3.2.3. Choice of Image acquisition parameters

An issue fundamental to the EPI sequences generally used to acquire fMRI data is the maximisation of the inherently low SNR, with the necessary trade-off between improved temporal resolution and a decrease in spatial resolution a resulting effect (*see section 2.3.1*). This issue is very pertinent to fMRI studies of neonatal subjects, where a number of factors if unaccounted for may contrive to decrease SNR and therefore the ability to reliably detect functional responses.

Throughout early human development, marked maturational changes in the appearances of the brain are seen on MRI as cellular density increases and water content decreases (*see chapter 1*) (Battin & Rutherford 2002, Counsell et al. 2003). It is therefore unsurprising that in addition to clear maturational trends in tissue-specific properties such as T1 and T2, marked differences are also present in T2* values (*see figure 3.4*) (Rivkin et al. 2004, Lee et al. 2012). This is of particular significance as the SNR for a simple GRE fMRI sequence is generally considered to be maximised when the TE is equal to the T2* value of the tissue of interest (Bandettini et al. 1994). T2* values are estimated to be approximately 60-70 msec in the adult brain at 1.5T, with these values significantly decreasing at higher B_0 field strengths (Bandettini et al. 1994, KrŰger et al. 2001, Peters et al, 2007, Harmer et al. 2012). Two studies have suggested that the T2* values of cortical tissues in preterm infants is approximately 3 times longer than in the adult, with the value at term equivalent PMA still significantly increased at 100-130 msec (Rivkin et al. 2004, Lee et al. 2012). This is of particular relevance as the majority of the reported neonatal fMRI studies have used TEs suitable for adult subjects (in the range of 40 to 66 msec) (*see table 3.1*).

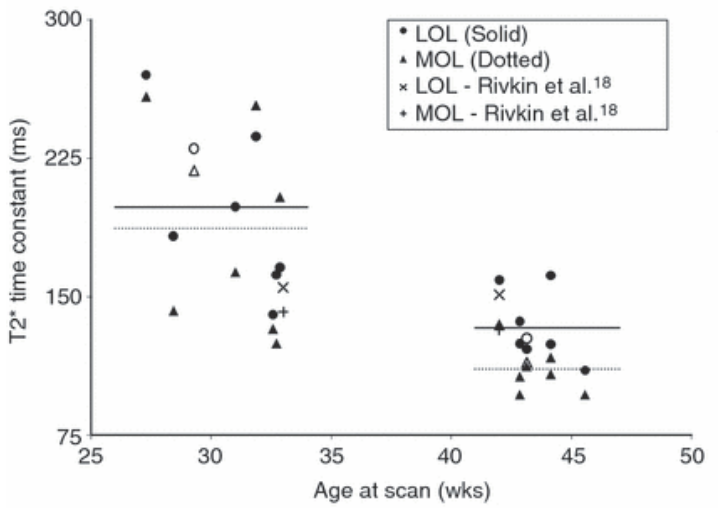

Figure 3.4*: T2* values are prolonged in the preterm brain, and decrease with age.* At 1.5 Tesla, two studies have shown that quantitative T2* values in the lateral and medial occipital lobes (LOL and MOL respectively) are

significantly longer in neonates than those in the adult brain which in comparison are usually approximately 60-70msec (Rivkin et al. 2004, Lee et al. 2012) (*figure reproduced from Lee et al. 2012*).

The majority (71%) of reported studies were carried out at low field strength (1.5T), and have used a relatively reduced spatial resolution in an attempt to preserve image SNR (*see table 3.1*). While a voxel size of 39-80 mm^3 is commonplace in adult fMRI studies and is generally sufficient to provide good anatomical localisation of activity, it is likely to cause marked partial volume effects (in which a single voxel contains information about more than one tissue type) when imaging the markedly smaller neonatal brain. This effect is not insignificant as particular tissue types have a very prolonged T2* values in the neonatal brain (in particular the immature white matter), and furthermore as the area where the activity is presumed to occur (the cortex) is anatomically bordered by an area where no activity is presumed to occur (the CSF) (Rivkin et al. 2004). An additional consideration is that at 1.5T, the BOLD effect appears to predominately arise from the intravascular compartment and therefore is disproportionately sensitised to the larger venous vessels which have the largest shifts in volumes and oxygenation following activity (*see section 2.2.1*) (Buxton et al. 1998, 2004, 2009, Krűger et al. 2001). Known developmental differences in vessel density and wall compliance may therefore have a more significant effect on BOLD contrast dynamics at lower B_0 field strengths (Norman & O'Klusky 1986, Gilles 2001, Harris et al. 2011).

3.2.4. Stimulation paradigms

A key issue in neonatal fMRI study design is the choice of stimulus, which must be of significant magnitude to elicit a functional response whilst being gentle enough in nature not to rouse or distress the studied infant. The stimulus must be developmentally appropriate for the age of the study population and suitable to be performed during sleep. These factors may be pertinent to the

interpretation of the reported neonatal fMRI studies which used a visual stimulus, where both the developmental stage and sleep status of the subjects may have contributed to the uncertainty about the results (Born et al. 2002a, Lee et al. 2012). To prevent bias and improve sensitivity, the stimulus should ideally be consistently repeatable in both timing and amplitude (and if possible synchronised with image acquisition), with most recent studies therefore favouring a fully automated approach. Designing and manufacturing the stimulation apparatus is not trivial, as the equipment must be completely metal-free for the MR scanner environment and preferably can be controlled remotely from the MR scanner control room (Gassert et al. 2008).

3.2.5. Data Analysis

While a number of fMRI data analysis packages are widely available and are used throughout the reported literature, none have been developed specifically with neonatal or paediatric subjects in mind. This is of importance as the optimal parameters for the pre-processing steps (such as the size of the filters in the spatial and temporal smoothing) which are considered standard in adult fMRI analysis are unknown for data derived from infants.

In a standard univariate GLM analysis, the specification of the design matrix is key to the analysis and can profoundly affect the analysis statistics and outcome (*see section 2.3.4.1*) (Friston et al. 1995b,c). In the adult brain, it is customary to account for the true temporal characteristics of the BOLD functional response (including it's smoothness and delay in onset) by producing the design matrix from the convolution of the stimulation paradigm with a waveform representative of the canonical HRF (Bandettini et al. 1993, Friston et al. 1995b,c, Monti 2011, Poline & Brett 2012). Crucially, even subtle changes in HRF morphology have been found to significantly affect the results of fMRI data analysis (Aguirre et al. 1998b, Handwerker et al. 2004). With the exception of the single study of Seghier and

colleagues (2004), there have been no studies which have attempted a systematic characterisation of the HRF in neonatal life, and therefore the appropriate model for use in the GLM is not known. Previous fMRI studies of the newborn have not accounted directly for this uncertainty, and instead have either used a classical GLM approach with convolution of the canonical adult HRF into the design matrix (Dehaene-Lambertz et al. 2002, Erberich et al. 2003, 2006, Perani et al. 2010, 2011), or have used a simple image subtraction approach (Born et al. 1996, Lee et al. 2012). This issue is therefore of fundamental importance to the field of neonatal fMRI, as the morphology of the HRF in the neonatal brain is more than likely to differ from the canonical adult form, as marked differences in the underlying vascular physiology are known to occur during infant brain development (reviewed in Volpe 2008).

A major advantage of fMRI techniques is that between session and between subject data can be combined into a single analysis to identify robust patterns of activity with far greater sensitivity and specificity than a single data set (Holmes & Friston 1998, Smith et al. 2001a). For this to be done, the individual subject data must be accurately registered to a common standard space (Jenkinson et al. 2001). In the neonatal brain, the relatively simple cortical folding and vastly different tissue contrast properties can lead to great difficulties with accurate image registration, which is further compounded by an even lower image resolution relative to brain size (Aljabar et al. 2008, 2011, Ball et al. 2010). Moreover, given the marked developmental changes in brain size and shape which occur in the neonatal period, it is clearly inappropriate to register infant functional data either directly to any of the existing adult standard brain templates, or to a single infant template if the study population covers a range of post-menstrual ages (Kuklisova-Murgasova et al. 2010, Serag et al. 2012).

3.3. Summary

Despite the great potential of the technique to offer a new window into our understanding of early brain development, there have been only a limited number of BOLD fMRI studies in neonatal subjects over the last 15 years. These studies have demonstrated the feasibility of the technique, and have confirmed that functional localisation is present even in the immature brain. Unfortunately, a great deal of uncertainty still remains about the nature of BOLD responses in this population, with a number of older studies suggesting that a negative BOLD response is normal in early infancy. The possible explanation for this ambiguity is likely to be multi-factorial, and includes fundamental aspects of study design, image acquisition, and data analysis.

Chapter 4

4. Thesis Aims and Hypotheses

The work of this thesis was motivated by the themes summarised in the first three introductory chapters: firstly by the process of attempting to understand early human brain development; and moreover how premature birth can adversely affect it and ultimately lead to life-long pervasive neurodevelopmental difficulties (*reviewed in chapter 1*). The widespread application of MRI techniques both in the clinical and neuroscientific environments, has led over the last 20 years to the development and application of fMRI, which provides an exciting means with which to non-invasively measure and characterise in-vivo brain activity with a greater combination of spatial and temporal resolution than previously possible (*reviewed in chapter 2*). Despite this, fMRI has not been widely applied to studies of neonatal subjects, and has a disappointing history of contradictory results with an underlying background of inconsistent study design, methodology, and analysis techniques (*reviewed in chapter 3*).

4.1. Thesis study plan

I therefore planned the studies described in this thesis with the over-arching goal of attempting to optimise fMRI techniques specifically for use with neonatal subjects. To try and achieve this, two main studies were envisioned, with the first intended to test the feasibility of the technique using a simple somatosensory stimulus, to accurately and reproducibly detect patterns of functional activation in neonatal subjects. Thus, in this first study, targeted adaptations and simple restrictions were applied to address some of the possible sources of inconsistency, so that a truly systematic fMRI study could be carried out in a defined neonatal population. The second study was designed to then investigate more deeply whether one of the fundamental principles of fMRI, that of a robust and (intra- and inter-subject) consistent haemodynamic response function (HRF) holds true during the rapid sequence of brain development which occurs during the preterm and neonatal period. The characterisation of a

population-specific HRF is likely to be vital for the future application of the technique, as alterations in the waveform can profoundly affect some of the basic assumptions integral to both fMRI study design (that of the linearity and time-scale of the response), and analysis (of timing and linear behaviour in the standard GLM). Through a number of smaller experiments, I sought to directly investigate some of the characteristics of the neonatal HRF (specifically the behaviour of overlapping impulse responses), and expand on the knowledge gained about the development of motor function in the neonatal brain. Lastly, I aimed to address whether the findings of the main studies (and specifically that of the emperical age-specific HRF) could be applied to further fMRI studies of other functional brain systems, and to study the effect of acquired and focal perinatal brain pathology on the pattern of functional responses.

4.2. Thesis Aims

The aims of the thesis were therefore to:

- Perform a systematic fMRI study with neonatal subjects, and in doing so to test the feasibility of the technique for identifying accurate and reproducible patterns of functional brain activity.
- Investigate whether fMRI can be used to characterise and investigate developmental aspects of brain activity in infants through all stages of the preterm and neonatal period.
- Characterise the morphology and development of the HRF in the premature and neonatal human brain.
- To investigate whether the application of an age-specific HRF would significantly improve the analysis of fMRI data.
- Test the flexibility and potential of the technique to study functional brain activity induced by a variety of sensory stimuli, and in pathological brain states.

4.3. Thesis Hypotheses

The work of this thesis was driven by the following hypotheses:

- Well localised and positive BOLD functional responses can be identified in the neonatal brain using appropriate study design, methodology, and analysis.
- The neonatal HRF differs significantly from the canonical adult waveform.
- A systematic maturational trend exists in the morphology and parameters of the HRF during early human brain development.
- The application of an age-appropriate HRF in the analysis of neonatal fMRI data will greatly improve the identification of functional responses.
- The use of optimised fMRI techniques based on the findings of this thesis will allow the study of activity in other functional brain systems in the neonatal brain.

Chapter 5

5. Characterising functional responses to hand movement with fMRI in neonatal subjects

Functional MRI holds the exciting potential to provide novel information about both the functional and clinical status of an infant, and a means with which to non-invasively gain a wealth of new information about in-vivo brain development. In all of these respects, the rapidly maturing brain of the premature infant is a compelling focus for study; as little is known about the functional capacity of these infants; there is a clear need to address the increased risk of adverse neurodevelopmental sequelae; and in comparison to a growing fetus, their premature exposure to ex-utero life allows not only an easier route for detailed study but also a means with which to observe and test the effects of external stimulation on brain development.

The somatosensory cortex was chosen as the ideal substrate for a stimulus based fMRI experiment in the preterm brain because the major anatomical landmark of the primary motor and somatosensory cortices (the central sulcus) can be readily identified from at least 26-28 weeks PMA (van der Knaap et al. 1996, Battin et al. 1998, Battin & Rutherford 2002), and as robust evoked responses to peripheral somatosensory stimulation have been described with multimodal techniques in both preterm and term neonates (Erberich et al. 2006, Vanhatalo & Lauronen 2006, Nevalainen et al. 2008, Kusaka et al. 2011). In addition, the stimulus itself can be conceptually relatively simple, with the peripheral effects (ie: hand movement) easily visualised by the investigator.

The goal of this first study was therefore to directly address some of the inconsistencies and challenges identified through review of the previously reported studies, and in doing so to test the feasibility of carrying out an accurate and reproducible fMRI study with neonatal subjects.

5.1. Somatosensory system development in early human life

Somatosensory information in the human body is processed via a multifaceted system, which receives and communicates peripheral information from a range of receptors in various tissue types (such as the skin, muscle and joints) for central interpretation predominately in the primary somatosensory cortex of the contralateral hemisphere (Purves et al. 2001, Rees et al. 2010). This information is transmitted via two distinct ascending "three neuron" pathways which handle different forms of sensory information: the dorsal columns for fine touch, proprioception, and vibration; and the lateral spinothalamic tracts for pain, temperature, and some touch information (*figure 5.1*) (Tawia 1992, Purves et al. 2001, Rees et al. 2010).

The dorsal column system is fed via a diverse collection of low threshold encapsulated cutaneous mechanoreceptors and muscle spindle and tendon organ receptors, all of which are innervated by large myelinated fibres (Purves et al. 2001, Rees et al. 2010). These fibres ascend the spinal cord and synapse in the dorsal column nuclei of the medulla, from where the medial leminscus then decussates the signal to the contralateral side of the CNS, terminating in the ventral posterior aspect of the thalamus (Rees et al. 2010). In contrast, pain and temperature information first enters the system via a family of nociceptors, thermoreceptors and unencapsulated tactile receptors which then send signals to the dorsal horn of the spinal cord via both myelinated and unmyelinated fibres (Purves et al 2001, Fitzgerald 2005). The "second" neuron of this system then immediately decussates to the contralateral spinal cord and travels upwards as the lateral spinothalamic tracts (Purves et al. 2001). Both systems reach an eventual target in the ventral-lateral thalamus, from where the thalamo-cortical projections relay the information to the primary somatosensory cortex located posterior to the central sulcus. The sensory representation of the body is classically depicted in the cortical "homunculus" with the feet and legs located at the top of the map, and with certain "sensitive" areas of the body appearing to be

enormously over-represented in comparison to their true physical size such as the hands, face, and mouth (Purves et al. 2001).

While information about the first stage of somatosensory system development in the human is sparse, it has been shown that reflex movements to an external stimulus can be demonstrated with in-utero fetuses as young as 6-7 weeks GA (Tawia 1992). The developmental timetable of pain pathways is slower and more dispersed with some of the projections appearing to be amongst the last to mature in the spinal cord (Fitzgerald 2005). Though induced electrical activity in the brainstem has been observed at 10 weeks GA, synaptic connections and differentiation into a "primary sensory area" within the immature cortical plate is not seen until around 18-20 weeks GA (Tawia 1992, Rees et al. 2010). At this stage however, thalamo-cortical connections are far from established with their growth through the subplate and immature cortex taking place continuously through the third trimester of gestation (Kostović & Jovanov-Milošević 2006). The maturation of these connections appears to correlate with the gradual transformation of diffuse and undefined SSEPs in preterm infants of 25 weeks PMA, to the more locally restricted and distinct responses recorded after 29-30 weeks PMA (*section 5.1.2*) (Taylor et al. 1996, Vanhatalo & Lauronen 2006).

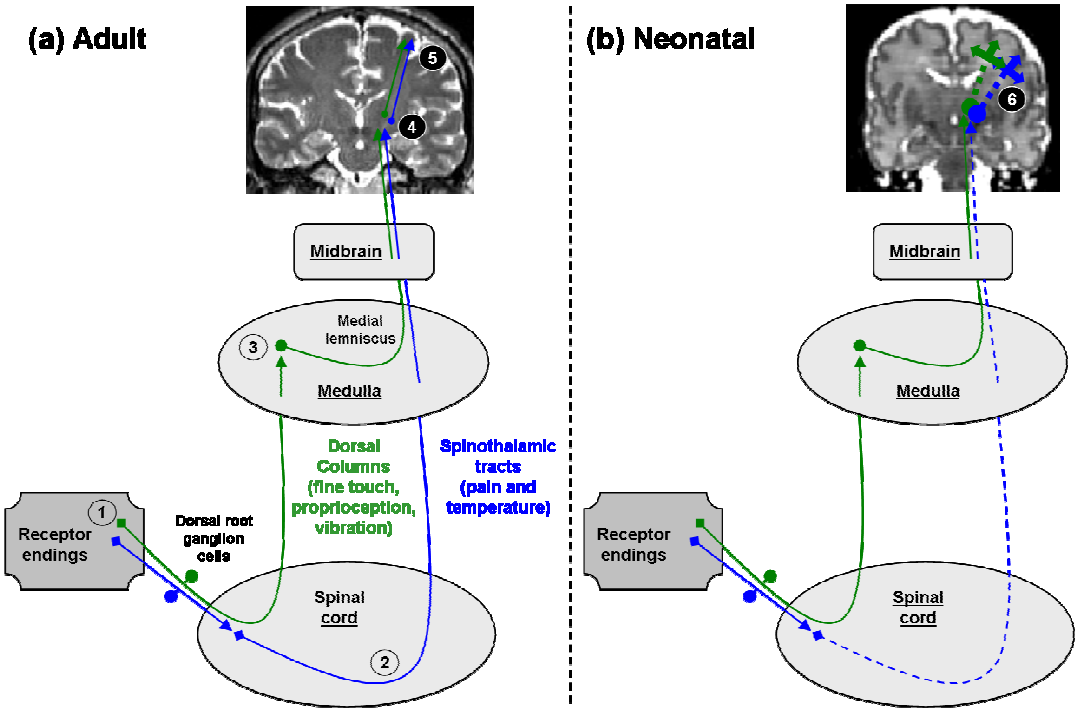

Figure 5.1: (a) ***The adult ascending somatic sensory system:*** Stimulation in the peripheral receptor endings (1) is communicated up to the brain via two separate "three-neuron" routes. Pain and temperature (and some fine touch) information is carried via the lateral "spinothalamic tracts" (blue) with decussation occurring at the level of the spinal cord (2). Fine touch, joint position (proprioception) and vibration sensory information is carried up the "dorsal columns" (green) with decussation occurring at the level of the medulla via the medial lemniscus (3). Axons from both pathways then pass through the midbrain and terminate at the ventral posterior thalamus (4). The thalamus then projects axons out to the primary somatosensory cortex, immediately posterior to the central sulcus (5). **(b)** ***In the developing system of the preterm infant,*** the ascending dorsal column pathways are present and decussate at the medulla from 19-20 weeks gestation. Pain receptors are present as are the neurons to the spinal cord, but the spinothalamic tracts which then conduct the signal centrally continue to develop through the preterm period. In the brain, throughout the third trimester the axons from the thalamus are still growing through the immature white matter and subplate (6).

5.1.1. Studies of somatosensory function in neonates

Functional activity has been demonstrated in the somatosensory system in the neonatal brain with a number of different assessment modalities, confirming that the pathways are both present and capable of conducting signals from the periphery to the central structures responsible for processing the information in the developing brain. It has long been known that the primary electrical activity induced by a somatosensory stimulus (SSEPs) can be reliably detected in the neonatal period, even at the cot-side using a relatively simple one or two channel system (George & Taylor 1991, Karniski et al. 1992a,b, Pike & Marlow 2000, Vanhatalo & Lauronen 2006, Vanhatalo et al. 2009). In the preterm period, SSEPs have been described in infants as young as 25 weeks PMA, although the timescale and morphology of the typically triphasic responses are markedly different than those classically recognised in the adult CNS (Taylor et al. 1996, Vanhatalo et al. 2009). A general maturational trend is seen with increasing age, associated with a decrease in the latency of the initial deflection, a relative decrease in the prominence of the later slow-wave response, and a shortening of the overall duration of the response, all of which have been attributed to myelin associated increases in conduction time (Karniski et al. 1992b, Taylor et al. 1996, Vanhatalo & Lauronen 2006). The spatial location of the electrophysiological response has been found to be well circumscribed and is consistently first seen in the cortical hemisphere contralateral to the stimulus (Karniski et al. 1992b, Vanhatalo & Lauronen 2006). It has been suggested that SSEPs may be of value in the clinical setting as they have been found to have a high specificity for predicting adverse outcome in term infants following perinatal asyphxia, and in predicting Cerebral Palsy (CP) in preterm infants (de Vries et al. 1992, Gibson et al. 1992, Taylor et al. 1992, Pike & Marlow 2000). While some authors have therefore advocated the more widespread use of SSEPs as a prognostic tool (Vanhatalo & Lauronen 2006, Vanhatalo et al. 2009), the general enthusiasm is tempered somewhat by the relatively poor sensitivity (around 40-60%) of the technique (particularly in preterm infants) and an inability to predict the degree of later impairment (de Vries et al. 1992, Pike & Marlow 2000).

A number of recent studies have also been able to describe the reliable measurement of somatosensory evoked magnetic fields (SEFs) by MEG in neonatal subjects (Pihko & Lauronen 2004, Lauronen 2006, Nevalainen et al. 2008, Pihko et al. 2009). While both EEG and MEG provide information about the electrical activity of the cortical neurons, MEG has the advantage of being relatively unaffected by the differences in conductance which can arise from variations in the skull thickness and over the fontanelle areas (Pikho et al. 2009). Developmental studies in preterm infants have also described maturational changes in the latency, amplitude, and morphology of SEFs, with the characteristic adult response not seen until 2 years of age (Pihko & Lauronen 2004, Lauronen 2006, Pihko et al. 2009). MEG can also potentially yield greater spatial information than EEG, with a detailed study in full term neonates describing a pattern of responses across the somatosensory system with the first and largest response occurring invariably in the contralateral primary somatosensory cortex (Nevalainen et al. 2008).

Near Infrared Spectroscopy (NIRS) and Topography have also been used to investigate the characteristics of the cortical haemodynamic response following passive motor stimulation in sleeping newborn infants (Isobe et al. 2001, Hintz et al. 2005a, Kusaka et al. 2011). Of interest, NIRS can provide a quantitative measure of both Hb-O_2 and d-Hb, which were found to rise and fall respectively during passive movement of the infants' knees and elbows, which would be in keeping with a positive BOLD response had it been visualised by fMRI (Isobe et al. 2001, Kusaka et al. 2011). While the three previous fMRI studies using a somatosensory stimulus with a population of neonatal subjects have all been able to identify BOLD responses, there was marked inconsistency as to both the spatial localisation and amplitude of the responses (*see section 3.1.2*) (Erberich et al. 2003, 2006, Heep et al. 2009). In the first study of Erberich and colleagues, a single preterm infant of 34 weeks PMA was included in their cohort of 7 patients, in whom they were able to identify a large cluster of positive BOLD response in the contralateral perirolandic area with further areas of negative BOLD change seen in the ipsilateral

hemisphere and the frontal areas (Erberich et al. 2003). In a later more extensive study of infants at term equivalent PMA, they found an interesting pattern of both contralateral and ipsilateral responses of mixed amplitude, with slightly less than half of the infants showing a bilateral response (Erberich et al. 2006). In contrast, a later study by Heep and colleagues found entirely conflicting results with predominately negative and bilateral BOLD responses in a relatively small (5 subjects) cohort of ex-preterm infants studied at term equivalent PMA (Heep et al. 2009).

5.2. Study aims and hypotheses

The hypothesis of this study was that well localised positive BOLD responses could be identified with fMRI in the neonatal brain using appropriate adjustments to the experimental design, methods and analysis.

I aimed to directly address some of the challenges and inconsistencies which were identified in existing fMRI studies in the newborn period, and which may have led to the previous reporting of discrepant results. By addressing these challenges, I then aimed to investigate somatosensory system development in early human infancy by characterising the pattern of BOLD responses during the preterm period, and to then compare it with those detected in ex-preterm infants at term equivalent PMA and in control infants born at full term.

5.3. Methods and materials

The study was approved by the Hammersmith Hospitals Research Ethics Committee (code: H0707/101). Written parental consent was obtained prior to all sessions of data acquisition, following a detailed discussion with myself or one my colleagues about the aims of the work and the study procedures. All of the data was anonymised following collection (and labelled with a study number identifier), and stored in encrypted and firewall protected file systems.

5.3.1. Study population

All of the subjects included in this study were recruited from the Neonatal Intensive Care Unit or postnatal wards of the Queen Charlotte and Chelsea Hospital, London during a period of 12 months between 2008 and 2009. The study group consisted of: 13 preterm infants; 19 ex-preterm infants who were scanned at term equivalent PMA; and 8 healthy control infants who were born at full term gestational age (*see table 5.1*). Clinical details including antenatal, birth and postnatal care were recorded for each patient, and a neurological assessment was carried out (Mercuri et al. 2005). Infants with extensive IVH diagnosed on cranial ultrasound examination (grade 3 with ventricular dilatation, or grade 4 with parenchymal involvement, (*see section 1.4.1,* (Levene & de Crispgny 1983)), other focal intracerebral parenchymal lesions, hydrocephalus, congenital brain malformations or metabolic disorders were excluded from the study group. All of the infants were assessed to be clinically safe for scanning prior to the data acquisition by a trained paediatrician.

The ex-preterm infants were invited for a day admission to the Children's Ambulatory Unit, Hammersmith Hospital following discharge from the Neonatal Intensive Care Unit. On attendance, all of the infants were clinically examined by a paediatrician, and the use of oral sedation was discussed with the infants' parents. If consent was given, a form was signed, and oral sedation (chloral hydrate 30-50

mg/kg) was administered approximately 20 minutes prior to the MRI scan. Sedation was given to 15 of the 19 ex-preterm infants, but to none of the premature infants and only 1 of the term control infants. In those infants in whom it was felt it was not suitable for sedation to be given and/or the parents did not consent for its use, a milk feed was given (either via nasogastric tube or orally) prior to the MRI scan, the infant was swaddled in blankets, and encouraged to sleep naturally ("feed and wrap"). 2 of the preterm infants were receiving respiratory support with nasal continuous positive airway pressure (nCPAP) at the time of scanning, while a further 4 required low flow supplementary oxygen (range 50-100cc) via nasal cannulae. One ex-preterm infant required supplementary oxygen via nasal cannulae at the time of scanning. There were no adverse incidents during the data acquisition period in any of the subject groups.

Patient group	*n*	Gestational age at birth in weeks + days Median (range)	Post-menstrual age at scan in weeks + days Median (range)	Birth weight in grams Median (range)	Birth head circumference in centimetres Median (range)	Number of infants receiving sedation prior to scan	Number of hours of mechanical ventilation Median (range)	Number with blood culture positive sepsis in the neonatal period	Number of infants with intra-ventricular haemorrhage
Preterm	13	29+4 (25+4 - 34+0)	31+1 (27+1 – 35+3)	1037 (795 – 2374)	26.5 (22 – 33)	0	0.5 (0 – 120)	1	Grade 1: 0 Grade 2: 0 Grade 3: 0 Grade 4: 0
Term control	8	40+3 (36+3 – 41+6)	40+4 (36+5-43+0)	3571 (2176 – 4242)	34.5 (32 – 28.9)	1	0 (0 – 0)	0	Grade 1: 0 Grade 2: 0 Grade 3: 0 Grade 4: 0
Ex-preterm at term equivalent age	19	30+5 (25+4 – 36+0)	42+0 (39+0 – 44+6)	1050 (795 – 2430)	27.5 (22 – 33)	15	0.5 (0 – 126)	1	Grade 1: 3 Grade 2: 0 Grade 3: 0 Grade 4: 0

Table 5.1: ***The study population, with corresponding birth and clinical characteristics.*** (*table published in Arichi et al. 2010*).

5.3.2. Image acquisition

MR imaging was performed on a Philips Achieva 3T system (Best, Netherlands) with a standard eight channel phased array "birdcage" head coil, located on the Neonatal Intensive Care Unit in the Queen Charlotte and Chelsea Hospital (*figure 5.2(a)*). All scans were performed by a specialist radiographer and at least one clinician trained in neonatal resuscitation. The infants' temperatures, arterial oxygen saturations and heart rates were monitored throughout the scan (*figure 5.2(b)*). Ear protection was used in all infants in the form of dental putty and adhesive ear muffs (Minimuffs, Natus Medical Inc, San Carlos CA, USA), and the head was immobilised using a polystyrene bead filled pillow from which the air was evacuated.

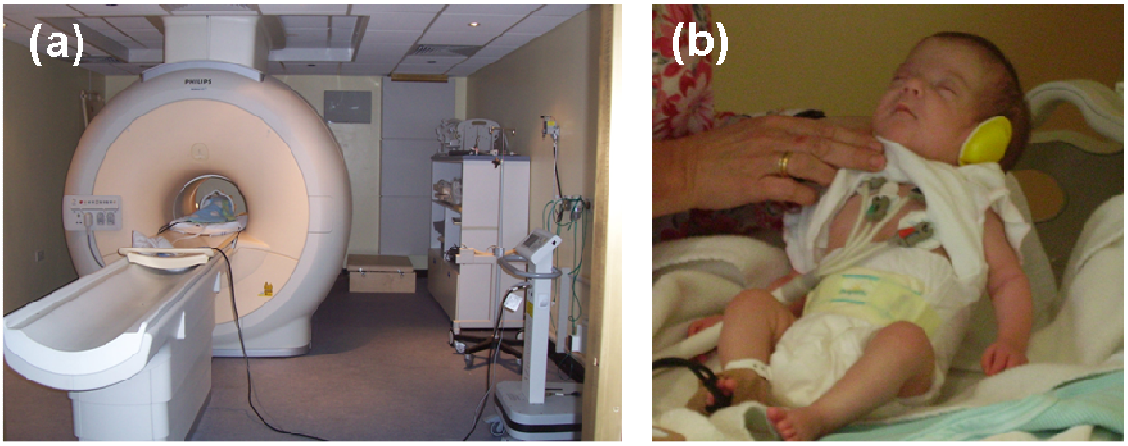

Figure 5.2: ***(a) Images were acquired on a 3-Tesla Philips MRI scanner in the neonatal intensive care unit, Queen Charlotte and Chelsea Hospital. (b) The infants' physiological parameters were monitored throughout the period of data acquisition*****.** Prior to the scan, acoustic protection was applied (dental putty and adhesive ear muffs), ECG leads were applied to the chest, a temperature monitoring lead was fixed into the axilla, and an oxygen saturation probe was fitted to the foot. (*Figure 2(b) courtesy of Serena Counsell*)

3D dual echo-weighted (proton density and T2-weighted), and 3D MPRAGE T1-weighted images were acquired for all infants to provide clinical information and to act as a high resolution image with which

the functional data could be registered (*parameters shown in table 5.2*, (Merchant et al. 2009)). All structural images were also reviewed and fully reported by a Neonatal Neuroradiologist, and any resultant clinical implications were fully discussed with parents and relevant members of the clinical team.

Sequence	TE (ms)	TR (ms)	Slice thickness (mm)	Matrix	FOV (mm)	Time	SPL-max/dBA	SAR W/kg	Other
3D MPRAGE	4.6	17	0.8	256×256 135 slices	210	4 min and 21 s	103	0.4	Flip angle 13°
Multi-slice dual echo T2-W fast spin echo	160 & 16	11,712	2 (slice gap −1)	256×256	220	4 min and 40 s	99	3	Echo train length 16
Single shot echo planar diffusion tensor imaging (32 direction)	49	9000	2	128×128	224	5 min and 50 s	98	1.3	*b* value 750 s/mm^2
Single shot fast spin echo	160	22,200	2	224×178	220	7 min	93	3.2	4 loops in one signal average TSE length 60
fMRI	45	1.5	3.25	80×64	256	6 min and 30 s	94	0.4	Flip angle 90°

TE: echo time; TR: repetition time; FOV: field of view; SAR: specific absorption rate; SPL-max: maximum sound pressure level; MPRAGE: Magnetisation prepared rapid gradient-echo.

Table 5.2: ***Pulse sequence parameters for the routine neonatal MRI examination at the time of study.*** For optimal image quality, sequences were repeated as necessary, but the total duration of the MR examination was limited to 60 minutes (*table reproduced from Merchant et al. 2009*).

Functional MR data was acquired with an EPI sequence lasting a total of 6 minutes and 30 seconds with the following parameters; TR 1500 msec, TE 45 msec, flip angle 90°, 22 slices, matrix 80*64, voxel size 2.5 mm^2, slice thickness 3.25 mm, slice gap 0.75mm, and total 256 volumes. 4 “dummy scans” which are not included in the final image analysis were included at the start of each fMRI sequence to ensure spin system steady state was reached prior to data acquisition. DTI data was also acquired from 9 infants (2 preterm, 2 term control and 5 ex-preterm) during the same image acquisition session as the fMRI data. Data was acquired with a single shot EPI sequence lasting 5 minutes and 50 seconds in 32 non-collinear directions with a b-value of 750 s/mm^2 and the following parameters; TR 9000 msec, TE 49 msec, matrix 128*128, voxel size 1.75mm^2, slice thickness 2mm.

5.3.3. Somatosensory stimulus

The somatosensory stimulus was designed and manufactured in collaboration with the Human Robotics Group of the Bioengineering department, Imperial College London. The initial design was in large part inspired by the work of Erberich and colleagues, who used an inflatable rubber bulb placed in their subjects' palms to passively open and close the hand (Erberich et al. 2003, 2006). A major limitation of the stimulus utilised in their work was that it was manually controlled, which is likely to have lead to an inconsistent pattern of stimulation, involving aspects such as the time of onset, amplitude, and frequency.

Working in close collaboration with a bioengineering MSc student (Amélie Moraux), a simple somatosensory stimulus suitable for fMRI experiments of neonatal subjects was designed and implemented with the following specifications:

- Completely metal free and fMRI compatible (Gassert et al. 2008).
- Able to provide stimulation synchronised with fMRI acquisition.
- Able to induce custom passive motor stimulation patterns at a controlled amplitude and frequency to elicit robust functional responses.
- To be able to monitor the operation of the stimulus remotely to ensure consistent stimulation was occurring and that no potentially harmful events could occur.
- Light and small enough to avoid the infant suffering movement restriction and/or discomfort.
- Mechanically safe to avoid distress or possible harm to the infant.
- Able to be easily cleaned to prevent infection spreading from one infant to another.

5.3.3.1. Stimulus design and architecture

The somatosensory stimulus consisted of a tailor-made inflatable balloon, a control box and customisable software (*see figure 5.3*). As an additional safety feature, a locking emergency stop button was attached to the control box. The control box contains a pressure regulator valve controlled by software on a standard PC, both of which are connected to the MRI scanner via a Data Acquisition Card (DAQ) (National Instruments, Austin TX, USA) (*figure 5.4*). The DAQ allows integration of the control box and software with the MRI scanner "sync" port via a standard coaxial cable and BNC connector (Bayonet Neill-Concelman connector). Precise stimulation timing and synchronisation with functional image acquisition is therefore possible as this connection can be used to detect the transistor-to-transistor logic (TTL) pulse emitted by the scanner (if specified in the set-up of the MR acquisition sequence; usually set to occur at the start of each TR).

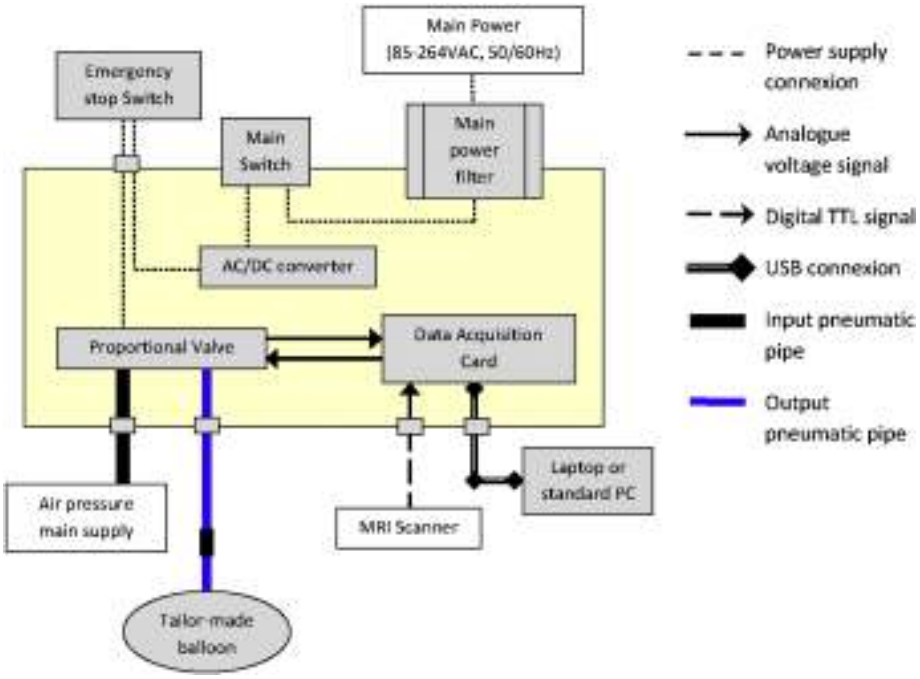

Figure 5.3: ***Schematic diagram of the device used to create the somatosensory stimulus during the fMRI image acquisition***. Synchronisation with the MRI scanner was achieved via the Data Acquisition Card within the control

box outside the examination room. Somatosensory stimulation is achieved by Inflating the balloon (placed in the subject's right hand) resulting in passive finger extension, with deflation resulting in flexion. (*figure published in Arichi et al. 2010*).

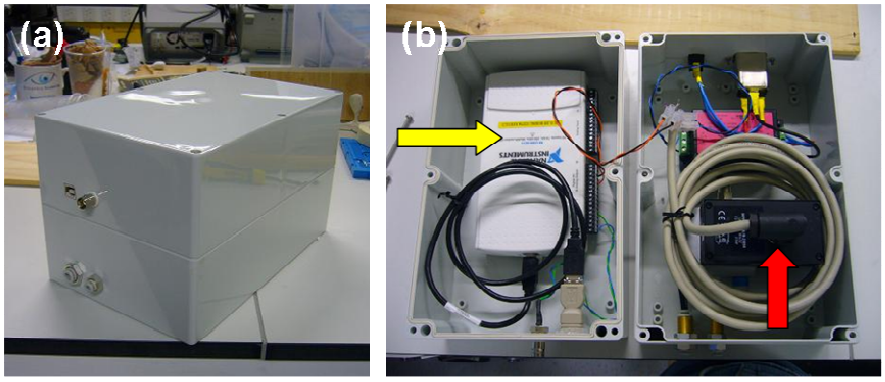

Figure 5.4: ***(a) The stimulus control box is kept in the scanner console room.*** **(b)** ***Precise measurement and control of the stimulus is achieved with a data acquisition card (yellow arrow), and a pressure regulator valve (red arrow).***

The balloon is composed of 2 layers of latex around a nylon mesh, which allows it to inflate in a uniform (and controlled) manner, and to be easily cleaned (*see figure 5.5(a); the manufacturing process of the balloon stimulus is described in appendix a*). The balloon itself is entirely metal free, with inflation and deflation possible via a 7m plastic pipe connected to the control box outside the examination room. The control box is connected to the medical air wall supply, with opening and closing of the pressure regulator valve within responsible for control of the balloon inflation/deflation. Three sizes of balloon were developed for neonatal, 2 year old infant, and adult subjects, based on initial plaster casts made from the hands of age-appropriate volunteers.

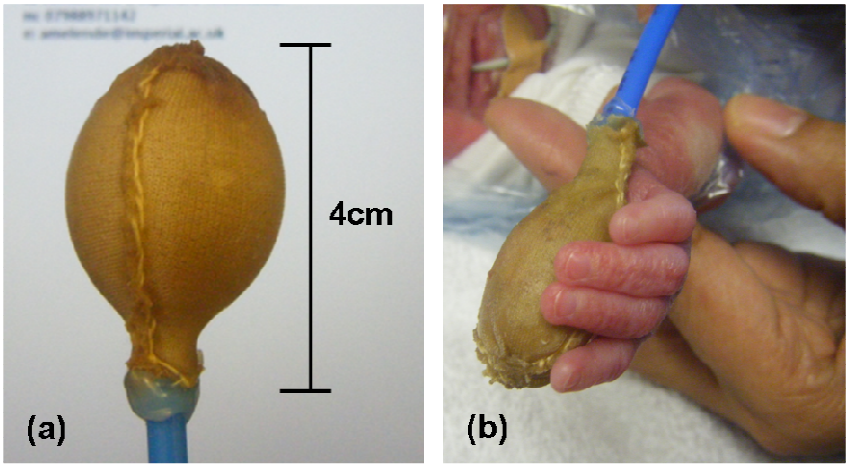

Figure 5.5: (a) ***A custom made inflatable balloon was developed as a MR safe somatosensory stimulus.*** The balloon is composed of 2 layers of latex around a nylon mesh. **(b)** ***Prior to image acquisition, the appropriately sized balloon was placed in the right hand of the subject***. To prevent the balloon slipping out during image acquisition, it was loosely strapped in with a self-adhesive bandage (not shown).

Prior to each MRI session, the balloon was sized and placed in the right hand of each subject (*see figure 5.5(b)*). To prevent the balloon from slipping out the subjects hand during the MRI scan, a loose self-adherent strap was applied around the subject's hand (Coban, 3M, St. Paul MN, USA). Inflation of the balloon resulted in passive extension of the fingers, while deflation allowed flexion. Using the software interface on the PC (*described in 5.3.3.2*), the amplitude of balloon inflation was adjusted appropriately for hand size (balloon volume range 1.2cm^3 – 3.1cm^3).

5.3.3.2. Stimulus control

Precise control of the pattern of stimulation was achieved with a customisable programme developed within the Labview software environment (v8.1 2009, National Instruments, Austin TX, USA). Via the DAQ, the software allows the complete integration of the acquired information (from the scanner, air supply, and the device itself). Programmes developed with Labview have a "front panel" window which

can act as a Graphical User Interface (GUI), allowing the simple selection of the stimulation parameters (in this case: the frequency, amplitude, and length of stimulation) (*figure 5.6*). In addition, a real-time graph representing the air pressure output from the control box is included on the front panel to allow the investigator to monitor the operation of the stimulus. The stimulus can be stopped either via the front panel interface, or by pressing the emergency button if necessary.

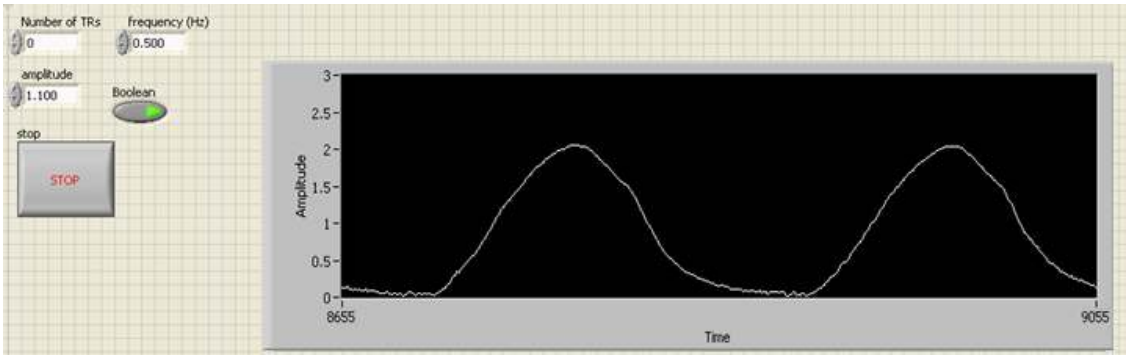

Figure 5.6: ***The front panel of the Labview programme acts as a GUI for the investigator***. The stimulation parameters (frequency, amplitude, length) can be specified in the boxes on the top left of the interface. The graph shows the air pressure output from the pressure regulator valve responsible for balloon inflation. This allows the investigator to monitor the timing and amplitude of the stimulation, and helps to ensure subject safety.

5.3.3.3. Experimental design

Prior to use with human subjects, it was confirmed that the device was completely MR safe and compatible (Gassert et al. 2008). It was first tested on three healthy adult volunteers to ensure that characteristic patterns of functional activation could be identified (*figure 5.7*). Using a simple block stimulation paradigm, a large cluster of functional activation could be identified in the primary somatosensory cortex contralateral to the side of stimulation in all three subjects. In addition, as has been described in a number of previous fMRI studies of the somatosensory system, additional areas of

activity were also seen in the ipsilateral somatosensory cortex, the supplementary motor area, the premotor cortices, and the cerebellum (Bandettini et al. 1992, Hirano et al. 2011, Harmer et al. 2012).

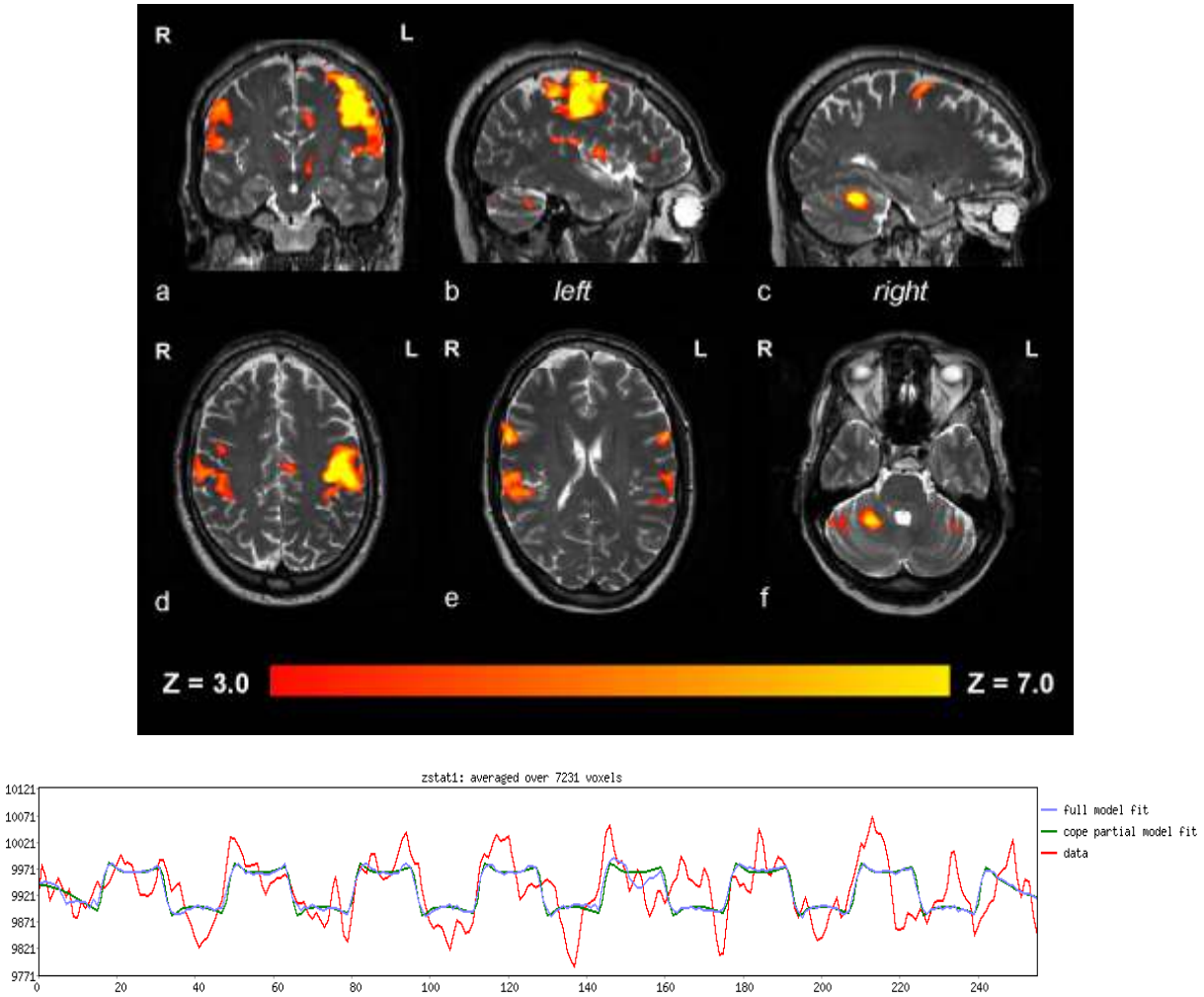

Figure 5.7: ***The somatosensory stimulus was found to produce characteristic patterns of intra-cerebral activation in a healthy right handed 54 year old volunteer.*** Following passive motor stimulation of the right hand, a large cluster of functional activity could be seen in the contralateral (left) primary somatosensory cortex (images a,b,d); in addition smaller clusters of activity were seen in the ipsilateral somatosensory cortex (images a,c,d), the bilateral premotor cortices (image e), the supplementary motor area (image d), and the ipsilateral cerebellum (images c,f). In the corresponding BOLD signal timeseries (average derived from the most significant cluster of activity), the data (red) can be seen to closely fit the design matrix (model fit shown in blue).

For the full study, a simple block stimulation paradigm was chosen and programmed onto the PC interface, with alternating periods lasting 24 seconds each (16 TRs) (*figure 5.8*). During each "on" period, the subject received a periodic sinusoidal inflation/deflation stimulus at a frequency of 0.33 Hz. A sinusoid waveform was chosen to obtain a smooth pattern of progressive inflation/deflation in the balloon. The rate of stimulation was empirically chosen so as to provide a gentle pattern of stimulation which would not unduly cause the baby discomfort; and to allow sufficient time for the desired volume of balloon inflation and then complete deflation to occur. During each "off" period, the balloon was kept in deflation by complete closure of the valve in the control box. A total of 8 blocks of stimulation were presented during the 6 minute and 30 second image acquisition sequence.

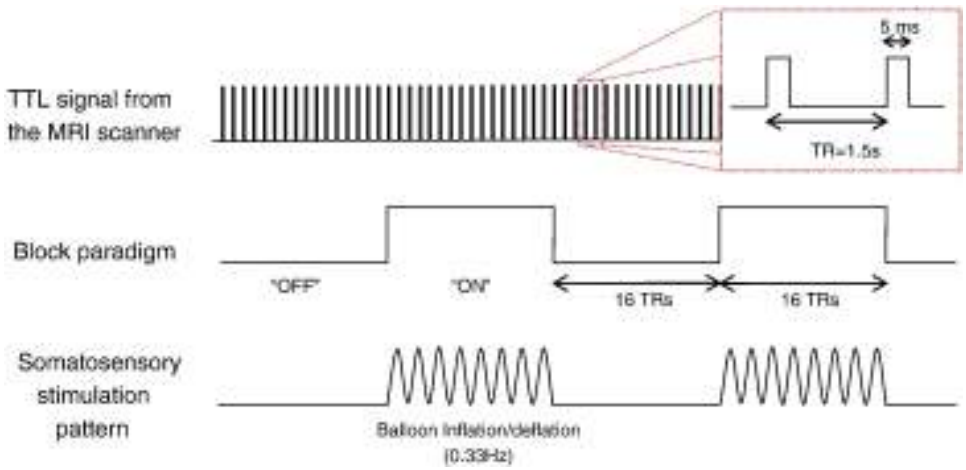

Figure 5.8: ***A simple block paradigm was used for the somatosensory stimulus.*** Equal periods of 24 seconds activity ("on") were alternated with period of rest ("off"). The initiation of the stimulus was synchronized with the scanner TR via detection of the TTL pulse produced. During periods of activity, the balloon inflated and deflated with a sinusoidal waveform at a frequency of 0.33 Hz. (*figure published in Arichi et al. 2010*).

5.3.4. fMRI data analysis

All data was analysed off-line using tools implemented within FSL (FMRIB, Oxford, UK, www.fmrib.ox.ac.uk/fsl, Smith et al. 2004).

5.3.4.1. Individual subject analysis

Individual subject "lower-level analysis" was performed using FEAT (FMRI Expert Analysis Tool, version 5.98). Pre-statistics processing steps were applied to all data sets as implemented in FEAT v5.98 (*see section 2.3.2*); including slice-timing correction (for slice acquisition from the bottom slice up), non-brain tissue removal (using BET (Brain Extraction Tool v2.1)), spatial smoothing (FWHM 5mm), global intensity normalisation and highpass temporal filtering (cut-off 50 seconds) (Woolrich et al. 2001, Jenkinson et al. 2002). Data sets were assessed and corrected for motion using MCFLIRT (FSL's intra-modal motion correction tool) which estimates absolute and relative displacement through the entire image time-series (Jenkinson et al. 2002). If the motion was found to be isolated specifically to either the start or end of the sequence, then the relevant volumes were deleted and the analysis adjusted accordingly to account for any change in stimulation phase or total sequence length. Following appropriate deletion, the minimum number of volumes used for analysis was 128 (or 4 full blocks of stimulation and rest). Additional data denoising was performed using MELODIC version 3.0 (Model-free FMRI analysis using Probabilistic Independent Component Analysis (PICA) v3.0 (Beckmann and Smith 2004)). Independent components were assessed for their spatial representation and frequency power spectrum, and those that were judged to represent physiological noise or motion artefact were then filtered from the data prior to further statistical analysis.

A general linear model (GLM) was used to define the observed data using a convolution of the experimental design (box-car function of the time course of somatosensory stimulation) and an optimal

basis set representing a dispersion range of possible HRF waveforms generated using FLOBS (FMRIB's linear optimal basis sets, v1.1) (*see section 4.3.4.2*) (Woolrich et al. 2004). The detected motion estimates (translations and rotations) were included in the GLM analysis as confounding variables. Parameter estimates for each of the explanatory variables and basis functions were then convolved in the GLM, and then converted to a t-statistic image by dividing by the relevant standard error (which is derived from residual noise after the complete model fit). The t-statistic image was then converted to a z-statistical score image, and a threshold of 2.3 with a corrected cluster significance level of $p<0.05$ was then used to generate spatial maps of activated voxels on an individual subject level. For visualisation purposes, all of the activation maps were registered to the individual subject's high resolution structural T2-weighted image using FMRIB's linear image registration tool (FLIRT) version 5.5 (Jenkinson 2002).

5.3.4.2. Linear Basis sets

Given the uncertainty with respect to the appropriate choice of HRF for fMRI analysis with neonatal subjects (*see section 3.2.5*), an optimal set of linear basis functions representing a dispersion range of possible HRF waveforms was convolved in the GLM instead of the canonical HRF (Woolrich et al. 2004). Although there are a number of different implementations of the technique (within different functional imaging analysis software packages), the principle is as first described by Friston and colleagues (1995b) (Lindquist et al. 2009). The technique is possible as the linear combination of basis functions (convolved with the model of stimulation) can be done within the GLM framework, thereby allowing flexibility as to the onset and parameters of the measured response in a given subject and greatly increasing analysis sensitivity (*reviewed in Steffener et al. 2010, Monti 2011*). A typical example of this approach is the use of a temporal derivative function, which individually does not model a recognised functional response, but in linear combination with the canonical HRF will model a delay in onset and/or an initial dip in the response (Friston et al. 1995b, 1998a).

In this work, this was achieved with the FLOBS toolkit, as implemented in FSL (Woolrich et al. 2004). This approach randomly samples the delay and height parameters from a pre-specified range (in this study, the default range of values was used) and then generates various possible HRF waveforms. A set of "optimal" basis functions is then created using principal component analysis to maximally span the subspace of the previously generated HRF samples. As standard (and in this study), three basis functions are usually generated (*as shown in figure 5.9 below*). Statistical analysis of the functional data is then performed for each individual voxel of the data set, and the best fit for the data can be identified via a weighted linear combination of the basis functions in an F-test. The FLOBS technique has the advantage of avoiding a potential and major drawback of basis functions which is the modelling of non-sensical HRF shapes, but still allows a large span of the possible HRF subspace (*figure 5.9(b)*) (Woolrich et al. 2004). Of importance, this also allows equal fitting of different shaped HRFs (such as those with an initial dip or deep post-stimulus undershoot) without bias towards a predefined shape.

While the use of basis functions greatly improves analysis sensitivity, it can potentially lead to less statistical power and fewer degrees of freedom (Lindquist et al. 2009). A further limitation is that the ideal method of aggregating or comparing data in a group analysis is still not clear; with some investigators advocating including only the results derived from the primary basis function (thus negating the advantages gained from using them in the lower level analysis) (Steffener et al. 2010, Monti 2011). To avoid this drawback, the higher level analysis in this study was performed using permutation methods (rather than a more traditional GLM based method), which allowed the lower level complete F-test statistical maps to be used for group level inference (*see section 2.3.4.2*) (Nichols & Holmes 2002).

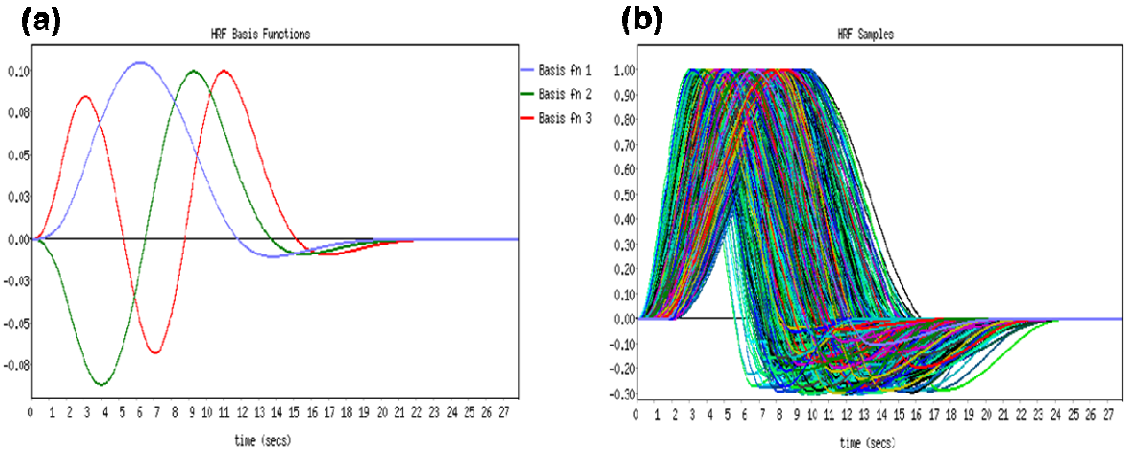

Figure 5.9: To allow the analysis to have flexibility for the possible differences in HRF shape, linear basis functions were used in the GLM analysis. **(a)**: ***Three basis functions were generated using FLOBS (FSL's linear optimal basis sets);*** with the primary basis function (blue) representing the canonical response, the second (green) representing the temporal derivative which allows for variation in response onset, and the third (ref) representing a dispersion derivative which allows for variation in the temporal spread and rate of response. **(b)**: ***The weighted combination of these three basis functions can maximally span the possible HRF subspace***; to avoid the modelling of non-sensical HRF waveforms, FLOBS "constrains" the samples using principal component analysis.

5.3.4.3. Standard template registration

At the time of conducting this study, there was no widely available neonatal "standard" brain template MR image. Given that marked structural and development changes are known to occur from birth through to adulthood, it was clearly inappropriate to register the functional data to any of the existing standard adult brain templates (Battin et al. 1998, Battin & Rutherford 2002, Kuklisova-Murgasova et al. 2011, Serag et al. 2012). To address this problem, 2 custom neonatal brain templates were constructed by the non-linear transformation of high resolution T2-weighted images. The preterm standard brain template was generated from 13 subjects (median PMA 33 weeks and 4 days, range 33+1 to 35+6); and the corresponding term PMA standard brain template was generated from 19 ex-preterm at term equivalent PMA subjects (median PMA 40 weeks and 2 days, range 39+4 to 42+6). The infants used for

the construction of these templates were from a separate cohort than those studied in this fMRI experiment. The T2-weighted images of ex-preterm infants were used for the term standard brain template generation, as it has been shown previously that brain volume and growth is preserved in clinically healthy ex-preterm infants at term corrected gestational age, provided there is no evidence of chronic problems such as bronchopulmonary dysplasia (Boardman et al. 2007). The T2-weighted image of each of the subjects was registered into stereotaxic space by a non-affine co-ordinate transformation as implemented in FNIRT version 1.0β (FMRIB's non-linear image registration tool). The resultant images were then averaged, and single template images were generated for the two subject groups (*figure 5.10*).

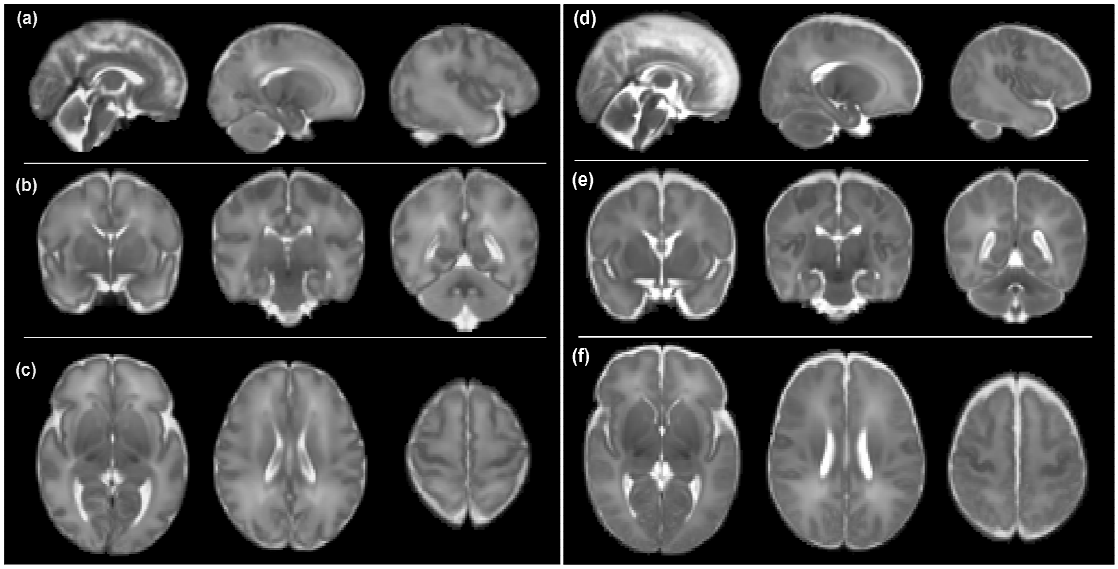

Figure 5.10: ***Custom neonatal brain templates were made to act as a standard space for the higher level functional analysis*.** The templates were made by non-linear registration of T2-weighted neonatal images into stereotaxic space and then averaging. Two templates were made, for the preterm (rows a,b,c) and term equivalent PMA groups (rows d,e,f).

5.3.4.4. Higher level analysis

Higher level group analysis was performed using FSL Randomise version 2.1, which utilises permutation methods for inferring trends in statistical maps where the null distribution is unknown (Nichols & Holmes 2002). This approach was suitable for this study, as not only was the data sampled from a population of unknown distribution, but also as it circumvents the potential problems of aggregating results derived from lower-level analyses using basis functions (Steffener et al. 2010, Monti 2011). The individual subjects' F-test statistical images were first registered to the appropriate custom template brain using linear registration. These were then combined to form a single 4D data set, and 5000 permutations of the data were then generated. A non-parametric one sample t-test was then used to identify suprathreshold clusters with 5mm of variance smoothing. A false discovery rate (FDR) calculation was used to correct for multiple comparisons with a p-value threshold of $p<0.05$.

5.3.5. Probabilistic tractography

To further probe the anatomical plausibility of the fMRI results, the structural connectivity of the identified clusters of activity were qualitatively assessed using DTI probabilistic tractrography. The DTI data was pre-processed and analysed using the FMRIB diffusion toolbox (FDT, version 2.0) implemented in FSL (Smith et al. 2004). Image artefact secondary to eddy current distortions were minimised by affine registration of the DT images to the "b0 image" (the first non-diffusion weighted volume of the sequence, also referred to as the "reference volume"). Images were brain-extracted to remove all non-brain tissue using the Brain Extraction Tool (BET) and fractional anisotropy (FA) maps were then generated using a diffusion tensor model as implemented in DTIFIT (Behrens et al. 2003b). Local diffusion directions were then calculated using BEDPOSTX (Bayesian Estimation of Diffusion Parameters Obtained using Sampling Techniques, X stands for modelling crossing fibres) which runs Markov Chain Monte Carlo sampling to build voxel-wise diffusion parameter distributions (Behrens et al. 2003b, 2007).

Probabilistic tractography was then performed using the maximally activated voxel from the fMRI GLM analysis as a seed area (following linear registration into diffusion space).

5.4. Results

Functional data was collected from 13 preterm infants, of which 2 data sets were later discarded due to image and motion artefacts associated with the nCPAP respiratory support required during the scan. 11 infants were therefore included in the analysis; with a median GA of 30 weeks and 4 days at birth (range 25+4 to 34+0), a median PMA of 33 weeks and 4 days at the time of scanning (range 29+1 to 35+3), a median birth weight of 1225g (range 795g to 2374g), and a median head circumference of 27.2cm (range 22cm to 33cm). The youngest infant from whom data was successfully collected was of PMA 29+1 weeks at the time of scanning.

Data was also collected from 19 ex-preterm infants at term equivalent PMA, of which 1 infant was excluded due to the presence of diffuse white matter abnormality, significant ventricular asymmetry and cerebellar abnormalities, following intraventricular haemorrhage and subsequent venous infarction during the preterm period. 18 infants were thus available for analysis of median GA at birth of 30 weeks and 5 days (range 25+4 to 36+0), with a median PMA at the time of scanning of 42 weeks (range 39+0 to 44+6), a median birth weight of 1305g (range 795g to 2374g) and median head circumference at birth of 26.6cm (range 22cm to 33cm). Eight control infants who were born at term GA were also scanned, of whom 2 were excluded due to excessive motion throughout the data set. The remaining 6 infants included in the analysis were of median GA 40 weeks and 3 days at birth (range 36+3 to 41+6), median PMA 40+4 days at the time of scanning (range 36+5 to 43+0), median birth weight 3586g (range 2176g to 4242g), and median birth head circumference 35cm (range 32cm to 38.9cm).

The median absolute head displacement in the sedated subjects was 0.19mm (total 16 subjects, range 0.05 – 3.54mm), as compared to 0.79mm in the un-sedated subject group (total 22 patients, range 0.08 – 6.54mm). In the 4 patients discarded from the analysis for excessive motion (all of whom were un-sedated during image acquisition), the median absolute displacement was 3.09mm (range 1.52 – 6.52mm).

5.4.1. Preterm group

Following stimulation of the right hand, clusters of well localised positive BOLD contrast activation were identified in the contralateral (left) primary somatosensory cortex of 9 of the 11 preterm infants (*example shown in figure 5.11(a,b)*), with predominately negative BOLD responses seen also in the contralateral somatosensory cortex in the remaining two infants (PMA at scanning: 34+1 weeks and 30+1 weeks). A pattern of bilateral positive responses in both primary somatosensory cortices was seen in only 1 of the 11 infants (PMA at scanning 31+3 weeks). A large contralateral cluster of positive BOLD activity was identified posterior to the central sulcus in the putative primary somatosensory cortex of the youngest infant from whom data was successfully collected (29+1 weeks PMA) (*figure 5.11(c)*).

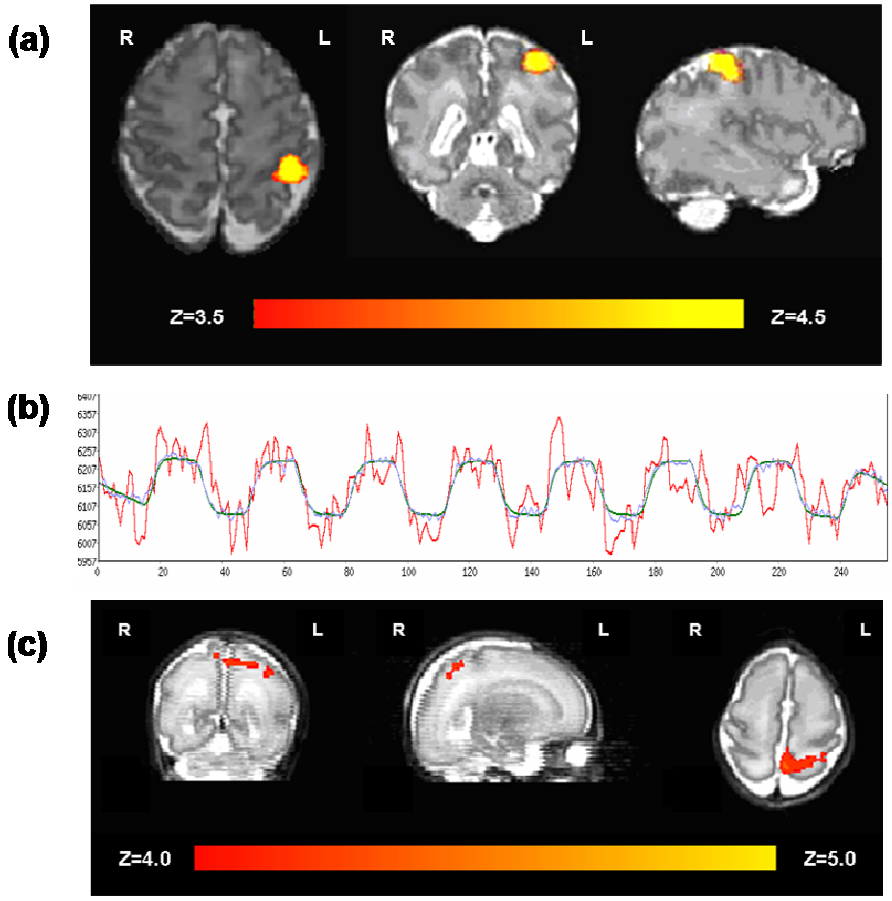

Figure 5.11: ***Example fMRI results in individual preterm subjects following passive movement of the right hand.*** The thresholded statistical maps (with a corrected cluster significance of $p<0.05$) have been overlaid on the subject's own T2-weighted image. **(a)** ***In a 34+2 weeks PMA infant (born at 33+5 weeks),*** a well localised cluster of positive BOLD activity can be seen in the contralateral primary somatosensory cortex. **(b)** ***In the corresponding timeseries***, the data from the cluster of activity (red trace) can be seen to rise during periods of stimulation (model fit shown in blue). **(c)** ***A large area of contralateral positive BOLD activation could also be seen in the youngest infant (29+1 weeks PMA, born at 27+1 weeks PMA).*** (*figure (c) has been published in Arichi et al. 2010*).

The group analysis of 11 preterm infants (*figure 5.12*) identified a small but extremely well localised cluster of positive BOLD activation in the contralateral primary somatosensory cortex only with a median percentage signal change during stimulation of 1.0% (range -2.9% to +2.5%). No additional areas

of co-activation could be significantly identified in any of the associative motor areas. A group analysis specifically for negative BOLD responses (by aggregating the inverse contrast of the primary basis function) did not identify any significant clusters.

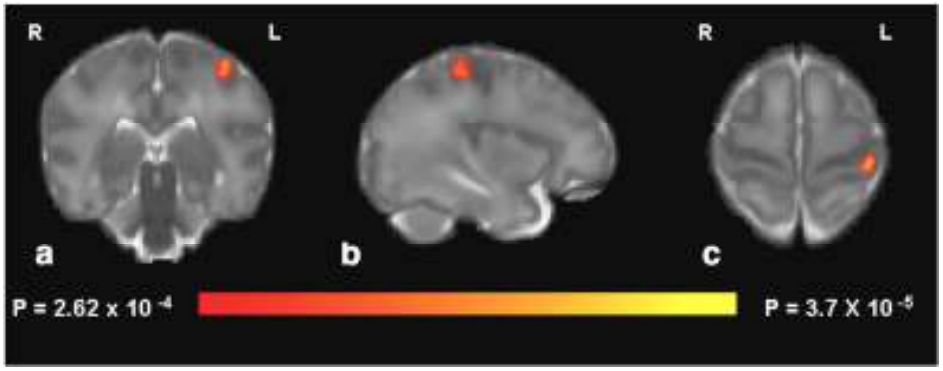

Figure 5.12: ***Group analysis of 11 preterm infants*** (median PMA at scan 33+4 weeks). The results of a FDR corrected t-test performed using non-parametric permutation methods have been overlaid on a custom T2-weighted brain template. A well localised cluster of positive BOLD functional activation was seen only in the contralateral (left) primary somatosensory cortex. (*figure has been published in Arichi et al. 2010*).

5.4.2. Term Control group

fMRI data was successfully acquired from 6 healthy infants born at full term gestation, one of whom was sedated for the period of scanning. The group analysis of the 6 patients identified a cluster of positive BOLD activation in the contralateral left primary somatosensory cortex. In addition, a central area of activation in the SMA, and a further small area of activity in the cerebellum were also identified (*figure 5.13*). A median percentage signal change during stimulation of 0.8% (range -0.9% to +2.0%) was seen in the group.

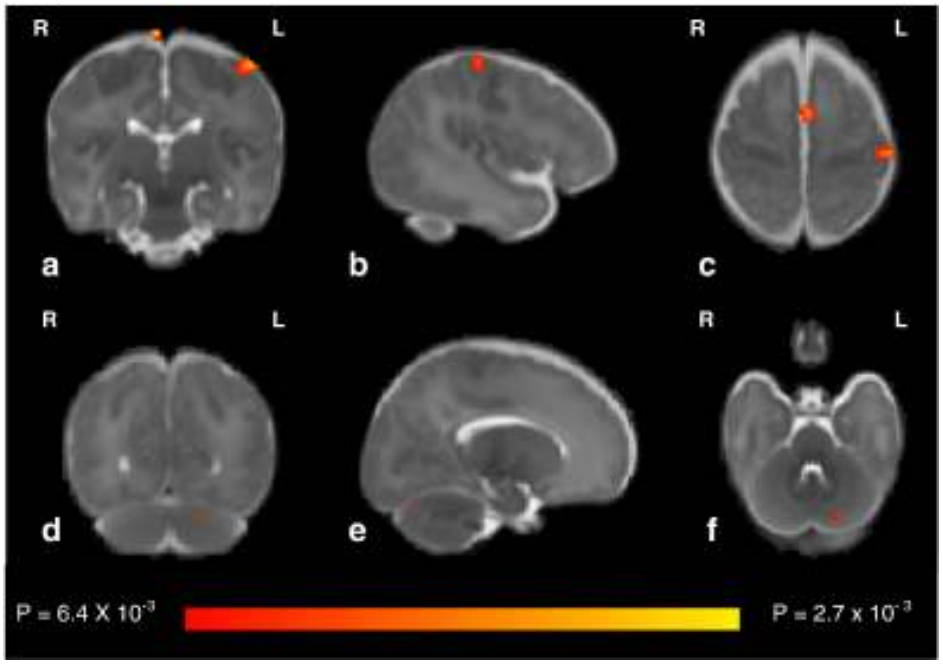

Figure 5.13: Group *analysis of 6 healthy full term control infants* (median PMA at scan 40+3 weeks). In addition to the main cluster of activity seen in the left primary somatosensory cortex, additional areas of activity are also seen in the supplementary motor area (figure c) and the cerebellum (d,e,f). (*figure has been published in Arichi et al. 2010*).

5.4.3. Ex-preterm at term equivalent PMA group

All of the ex-preterm infants at term equivalent age had a detailed neurological examination performed at term CGA by an experienced paediatrician, and none were found to have either significant or focal neurological deficits at the time of scanning (Mercuri et al. 2005).

A BOLD response was observed in the contralateral primary somatosensory cortex in all 18 of the ex-preterm infants who were scanned at term equivalent PMA. Of these, 8 infants (44.4%) displayed bilateral activity in both primary somatosensory cortices. 14 of the 18 infants had a predominately positive BOLD response in the primary somatosensory cortex contralateral to the side of stimulation (78%). Group analysis identified an area of contralateral positive BOLD activation in the primary

somatosensory cortex, with a median percentage signal change of 0.7% (range -3.5% to +1.8%) during periods of activity (*figure 5.14*). In contrast to the other study groups, a coexisting cluster of negative BOLD signal change was also seen in an overlapping area in the contralateral somatosensory cortex, as well as in the contralateral primary motor area (*figure 5.14, images a,b,c*). Ipsilateral activity was seen posterior to the central sulcus, but inferior to that seen on the contralateral side, in an area which may correspond to the secondary somatosensory cortex (*figure 5.14, images a,d,g*). In addition, activity was also identified above the sylvian fissure in the inferior premotor cortex on the contralateral side (*figure 5.14, images b,e*), in the contralateral basal ganglia (*figure 5.14, image f*), and ipsilateral cerebellum (*figure 5.14, images h,i*).

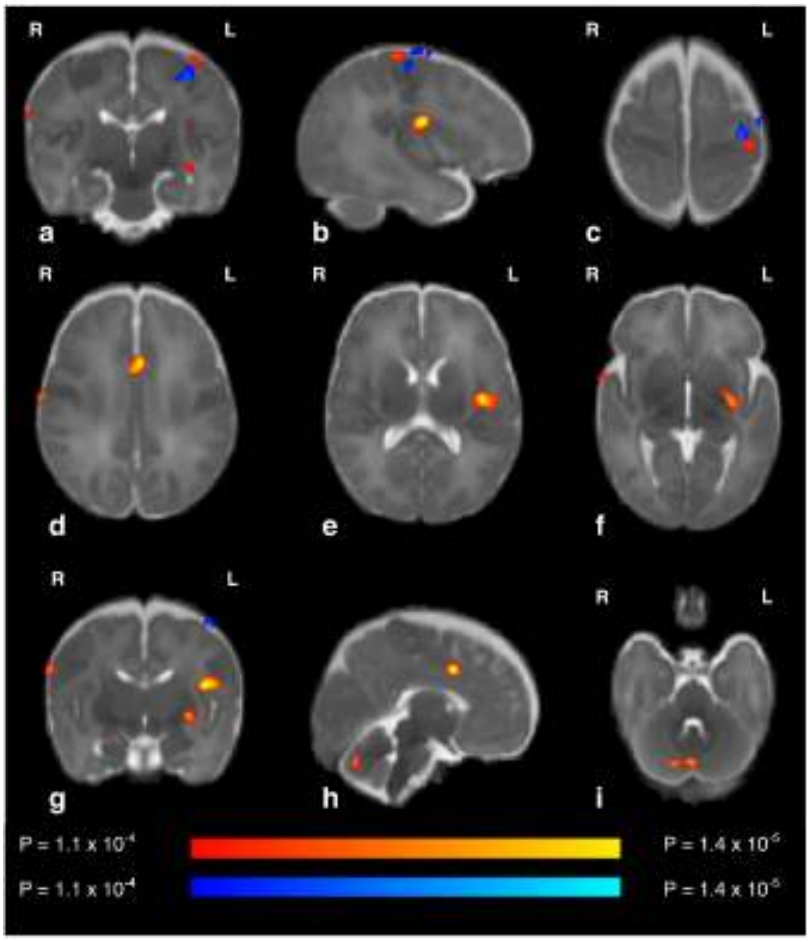

Figure 5.14: ***Group analysis of 18 ex-preterm infants studied at term equivalent PMA*** (median PMA at scan 42 weeks). A more widespread pattern of activation can be seen in this study group, and in contrast to the other study groups, co-existing clusters of both positive (red-yellow) and negative (blue) BOLD responses were identified. A well localised cluster of positive activation is present in the contralateral (left) primary somatosensory cortex; in addition, a small overlapping area of negative BOLD response can also be seen on the contralateral side both anterior and posterior to the central sulcus (*images a, b, c*). Activity is also present in the ipsilateral inferior post-central gyrus (*images a, d, g*), in the midline SMA (*images d, h*), in an area superior to the sylvian fissure in the contralateral cortex (*images b,e*), the contralateral basal ganglia (*images f, g*), and the ipsilateral cerebellum (*images h, i*). (*figure has been published in Arichi et al. 2010*).

A small number of infants (5) had both a preterm and term equivalent MRI scan performed. In these individual subjects, as seen in the group analysis, the pattern of response was seen to increase with age, with additional areas of response seen in the ipsilateral hemisphere and SMA (*figure 5.15*).

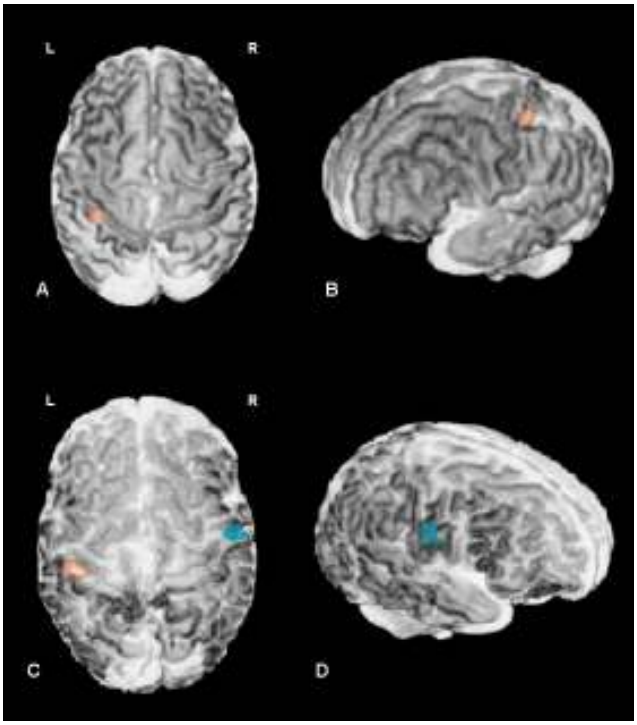

Figure 5.15: ***3D-rendered T2-weighted MR images of the same preterm infant studied at 34+2 weeks PMA and at term equivalent PMA.*** A striking increase in the folding of the cortical surface can be seen to have occurred over just 6 weeks of ex-uterine life. In the preterm period (images A,B), a single cluster of positive BOLD response (red) can be seen in the left somatosensory cortex. At term equivalent PMA (images C,D), in addition to this cluster in the left hemisphere, an area of negative BOLD response (blue) was also seen inferiorly and anteriorly in the ipsilateral hemisphere. (*note: as images have been rendered in 3D, they are not shown orientated in the radiological convention*).

5.4.4. Probabilistic tractography

In a small subset of patients on whom it was possible to acquire both fMRI and DTI data of high quality, the structural connectivity of the functional results was further assessed qualitatively by performing probabilistic tractography. This was done with DTI data collected from 9 infants; 2 preterm infants of median GA 28+6 weeks at birth and PMA 32+2 weeks at scanning; 2 term control infants of median GA 39+0 weeks at birth and PMA 39+5 weeks at scanning; and 5 ex-preterm infants at term equivalent PMA of median GA 27+1 weeks at birth and PMA 42+0 weeks at scanning. The probabilistic tractography from a seed area defined as the maximally activated voxel from the fMRI analysis identified significant and well localised connectivity distributions running from the area of functional activation, through the PLIC, and down to the ipsilateral cerebral peduncle. These distributions therefore followed the known pathway of the cortico-spinal tract (*figure 5.16*). Visually, the pattern of connectivity appeared to be more dispersed at term equivalent PMA, with a significant part of the distribution seen to cross the midline via the corpus callosum (*figure 5.16, images d,e,f*). In comparison during the preterm period, the connectivity distribution appeared to be simpler, with the main pathway appearing to only follow the trajectory of the cortico-spinal tract (*figure 5.16, images a,b,c*). The mean fractional anisotropy (FA) was seen to increase within the identified tracts from 0.169 (range 0.152-0.180) in the preterm group, to 0.193 (range 0.191-0.194) in the term control group, and 0.219 (range 0.185-0.244) in the ex-preterm group.

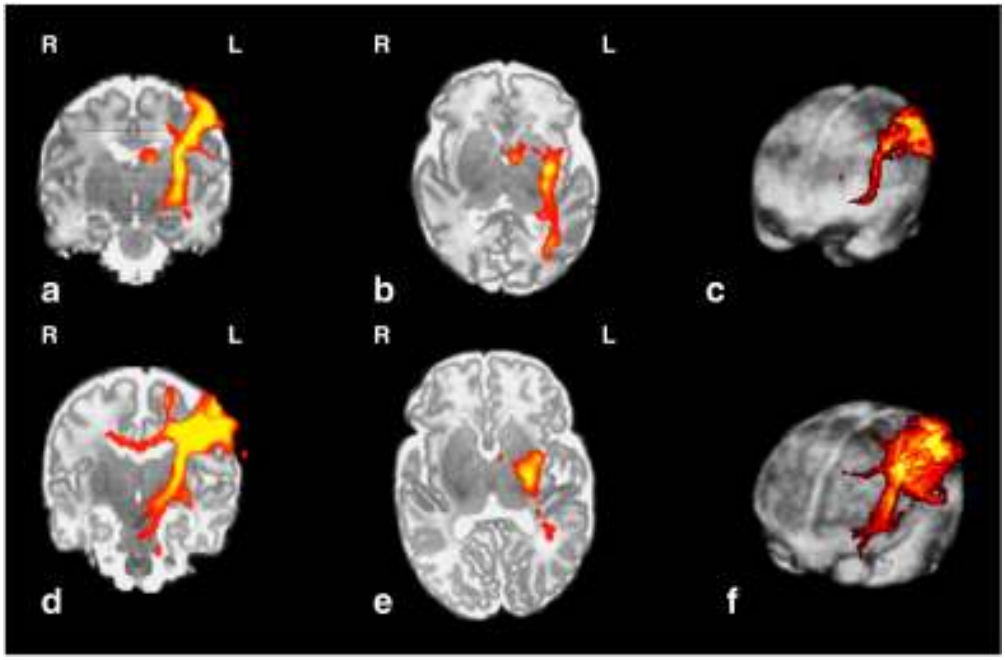

Figure 5.16: ***The anatomical plausibility of the fMRI results was confirmed by performing DTI probabilistic tractography using the maximally activated voxel from the functional analysis as a seed area***. In a preterm infant (35+3 weeks PMA), a significant and well localised connectivity distribution was identified running from the area of functional activation in the cortex, down through the PLIC (*images a,b,c*). In comparison, at term equivalent PMA, a more diffuse pattern of interhemispheric connectivity is seen, with a clear pathway across the corpus callosum in addition to the primary tract.

5.5. Discussion

In this first study, it was shown that through the combination of a carefully designed (and appropriate) stimulus and an adapted image processing and analysis pipeline, it is possible to identify well localised BOLD responses with fMRI in neonatal subjects. In the majority of infants, robust positive BOLD responses were identified as demonstrated by the findings of the more systematic group analyses. In addition, we were able to demonstrate for the first time using fMRI, well localised and reliable BOLD responses in the primary somatosensory cortex of premature infants. Furthermore, at term equivalent PMA, the results suggested a maturational tendency towards increasing bilaterality and complexity in the pattern of activation.

5.5.1. Development of somatosensory activation

Consistent and well localised patterns of functional activation were identified following somatosensory stimulation in neonatal subjects, both during the preterm period and at term equivalent PMA. Of interest, the results of this first study of preterm infants do not support either the hypothesis that hemispheric lateralisation increases linearly in the first few months of life, or the suggestion that an extensive bilateral representation in the more immature brain is replaced by exclusive contralateral localisation at 3 to 9 months (Erberich et al. 2006). In the preterm subject group, we were able to identify robust patterns of unilateral (and contralateral) activation, and not the widespread bilateral responses predicted by that hypothesis. Moreover, while previous studies of infants at term equivalent PMA have found mixtures of either predominately positive or negative BOLD responses with unilateral and bilateral activation (Erberich et al. 2003, 2006, Heep et al. 2009), the equivalent groups in this study showed a consistent pattern of predominately positive BOLD response in the contralateral somatosensory cortex with associated involvement of the supplementary and premotor areas, compatible with the complex patterns of response seen in studies of older children and adults (Mall V et

al. 2005, Guzzetta A et al. 2007). The findings of this study are in agreement with those described in a recent neonatal MEG study which found a principal response in the contralateral primary somatosensory cortex, with later responses seen inferiorly in the bilateral secondary somatosensory cortices (located inferiorly, adjacent to the sylvian fissure) and less consistently in the ipsilateral primary somatosensory cortex (Nevalainen et al. 2008).

Although performed on a relatively small subset of only 9 infants, it was possible to further provide anatomical validation of the identified functionally active regions with probabilistic tractography. At term equivalent PMA, a far more diffuse connectivity distribution was identified, suggesting that a maturational increase in structural connectivity may underlie the more complex pattern of functional responses. The somatosensory and motor systems are known to display a marked capacity for neural plasticity, with the development of the appropriate pathways largely dependent on regular tactile and proprioceptive stimulation which provide feedback during infancy (Fox & Wong 2005). It is also known that during the third trimester of gestation, thalamo-cortical axons are still establishing connections through the highly vascular subplate zone, with cortico-cortico and transcallosal connections yet to be fully established (Kostović & Jovanov-Milošević 2006). The activity-dependent maturation of these pathways may in part explain the results of this study as the relatively “simple” preterm system has not yet developed the more complex intra- and inter-hemispheric projections seen in later life.

5.5.2. Explaining negative BOLD

In contrast to a number of previous fMRI studies in early infancy, we were able to identify predominately positive BOLD responses across all of our subject groups, which are generally consistent with the results seen in adult fMRI studies (*see chapter 3*) (Bandettini et al. 1992, Hirano et al. 2011, Harmer et al. 2012). In this study, I aimed to address some of the possible sources of inconsistency

present in previous studies, and therefore carry out a thorough and systematic study. Clinical and developmental variance was accounted for by intentionally restricting the age ranges of the study groups, and by excluding all infants with possible clinical confounders. Methodologically, somatosensory stimulation was performed using a developmentally appropriate device which was reliable and consistent, fully synchronised with image acquisition, and could be carefully controlled. In the analysis, a set of linear basis functions was used to provide a flexible characterisation of the HRF within a traditional GLM analysis, a custom made neonatal brain template was used to allow a higher level analysis, and then a non-parametric permutation technique was implemented to reduce the effects of between subject variance and noise and identify group patterns of activity.

In the term equivalent PMA infant group analysis, we were able to identify co-existent patterns of negative BOLD response in addition to the expected clusters of positive BOLD response. The identification of negative BOLD accompanying canonical positive BOLD responses is not exclusive to paediatric studies, with animal and adult data suggesting they are a concomitant component of the normal response to stimuli together with the well described positive activity (Allison et al. 2000, Smith AT et al. 2000, 2004, Shmuel et al. 2002, 2006, Kastrup et al. 2008, Klingner et al. 2010). Historically, negative BOLD responses were frequently disregarded by investigators as noise artefacts, and were often not properly accounted for in the analysis (as they will not be identified unless the inverse response is specifically modelled for in the GLM, or checked for in the results). There is a degree of evidence to support this stance, as negative BOLD responses have been shown to be readily identified in areas devoid of neural tissue, where they may simply reflect increases in blood volume within the large ependymal and pial veins which lie along the sulci and adjacent to the CSF (Bianciardi et al. 2011).

As opposed to the transient periods of negative BOLD contrast seen before and after the positive peak during the canonical HRF (which are thought to arise from increased oxygen extraction and venous ballooning), it has been postulated that prolonged periods of negative BOLD contrast may actually reflect neuronal inhibition (Shmuel et al. 2006). In adult studies, unilateral median nerve stimulation has been found to cause ipsilateral negative BOLD responses in the primary somatosensory cortex (together with the expected contralateral positive BOLD response) suggestive of functional neuronal suppression rather than behavioural (selective) inhibition alone (Kastrup et al. 2008, Schäfer et al. 2012). Moreover, this neuronal inhibition has been shown to be associated with local arteriolar vasoconstriction, and decreased tissue perfusion and oxygenation (Devor et al. 2007, Schäfer et al. 2012). The amplitude of this ipsilateral negative BOLD effect has been shown to be directly linked to the strength of the initial somatosensory stimulus, with a stronger stimulus intensity leading to more negative and dispersed responses suggestive of greater neuronal inhibition (Klingner et al. 2010).

A further suggestion is that the negative BOLD effect can be explained by a “haemodynamic steal effect” arising from the redistribution of blood in neighbouring cortical areas during a period of activity (Shmuel et al. 2002). This theory has largely fallen out of favour as negative BOLD responses are frequently seen in areas that are clearly remote to those with positive activation (and therefore have entirely independent vascular supplies) (Smith et al. 2004, Kastrup et al. 2008). A recent study however has suggested that the negative and positive BOLD responses are not physiologically independent and may interact, although the positive response will always predominate (Klingner et al. 2011). The findings in the term equivalent PMA group analysis may fit in part with the haemodynamic steal hypothesis as both overlapping and adjacent negative BOLD responses were seen together with the expected positive activation.

5.5.3. Study limitations and implications

Sedation was used in the majority of ex-preterm infants scanned at term equivalent PMA, and cannot be disregarded as a potentially significant confounder. While a number of MRI studies have not used sedative medication and reported using “feed and wrap” techniques alone, increased head motion leads to the quality of the imaging (particularly for very motion sensitive EPI sequences) in naturally sleeping infants to be markedly poorer and a large number of data sets are often discarded as a result. It could be argued that this in itself represents a further form of bias as the infants which would then remain in the analysis represent a self-selecting group of “non-moving” infants (in whom it is not possible to say that they are neurologically identical to those that moved: as reduced movement itself may represent a particular pattern of brain activity or neurological status). Such an effect has been demonstrated in cognitively impaired adults, who were found to be move significantly more than control subjects, thus leading to clear bias (Wylie et al. 2012). The effects of head motion on fMRI data are not insignificant, as a number of studies have now shown that systematic but false patterns of correlation and connectivity can be identified when it is not appropriately dealt with (Power et al. 2012, Satterthwaite et al. 2012, van Dijk et al. 2012). The basic challenge therefore is to choose an appropriate balance between the potential bias of the direct effects of sedative medication against those derived from head motion and/or the subsequent self-selection of unmoving infants.

Although sleep state has been shown to affect the latency and duration of SSEPs in newborn infants, the responses have been shown still to be consistently identified with both electrophysiological and MEG techniques (Pihko & Lauronen 2004, Nevalainen et al. 2008). While sedation in adults with pentobarbital has been shown to cause marked changes in cerebral blood flow and therefore significantly affect the amplitude of the detected BOLD signal (Martin et al. 2000), chloral hydrate sedation does not appear to affect either the underlying neural response to stimulation or the associated neurovascular coupling. In

clinical practice, chloral hydrate sedation is commonly used when recording auditory evoked responses (AEBR) and has been found to not affect either the amplitude or character of the responses (Avalonitou et al. 2011). Furthermore, in the rat brain mild to moderate doses of intravenous chloral hydrate do not affect either the power spectrum of the resting EEG or the character/parameters of visual evoked potentials (VEP) (Sisson & Siegel 1989). Previous fMRI studies in neonates have also attempted to address these concerns, with no significant differences identified between unsedated and chloral hydrate sedated infants in either the distribution of resting state networks or qualitatively in response to visual stimulation (Born et al. 1998, 2000, Doria et al. 2010).

It is also worth considering the inflation of the balloon in our somatosensory stimulus provided both finger proprioceptive and local pressure stimulation in the palm, and therefore the patterns of identified activation cannot be generalised as a response pattern to either of the sensations individually. Stimulated active motor activity may also have contributed to the detected signals, although a grasp reflex activated during rest periods by the stimulus would not be expected to involve intracerebral structures. In addition, it may not be possible to easily disentangle this possible effect as a previous study in older children did not detect a significant difference in activation between active and passive motor tasks (Guzzetta et al. 2007).

All stimulus-based fMRI studies in children are largely limited by the fact that an adult-derived HRF model is frequently assumed to be appropriate for convolution into the GLM analysis. Given the significant differences in key physiological parameters such as CBF, CBV, $CMRO_2$ are known to exist throughout the early stages of brain development, it is likely that the HRF following sensory stimulation in newborns is different in shape when compared to adults (Greisen 1986, Miranda et al. 2006, Roche-Labarbe et al. 2010, 2012, Varela et al. 2012). In this first study we attempted to account for the possible

developmental differences in the characteristics of the HRF by using a set of linear basis functions in our analysis, but this increase in sensitivity would have been accompanied by an associated loss of specificity and a loss of statistical power (Woolrich et la. 2004, Lindquist et al. 2009, Steffener et al. 2010, Monti 2011). A further possibility would be to have analysed the data using a data driven (and therefore model free) approach, such as ICA (Beckmann & Smith 2004, Beckmann 2012).

5.6. Study conclusions

Using targeted adaptations and planning to the study design and population, the form and pattern of stimulation, and the data analysis, we were able to demonstrate that robust patterns of positive BOLD response can be identified in the neonatal brain with fMRI. The findings of this study represent the first description of well-localised patterns of somatosensory cortical activation in a group of infants during the preterm period. The potential of the technique to greatly deepen our understanding of early human brain development was highlighted by the finding that a maturational trend towards an increasingly complex pattern of functional responses could be seen at term equivalent PMA. Furthermore, this apparent increase in functional connectivity was associated with qualitative increases in structural connectivity in a small subset of patients assessed with DTI probabilistic tractography.

Chapter 6

6. Characterisation of the HRF in the preterm and neonatal period

A fundamental premise of fMRI study design and data analysis is that the BOLD contrast response to a brief stimulus is consistent and reproducible across experimental runs and subjects (*see section 2.2.4.1*) (Friston et al. 1994a, 1995b, Boynton et al. 1996, Aguirre et al. 1998b, Miezien et al. 2000, Handwerker et al. 2004). The modelled canonical impulse response is traditionally termed the Haemodynamic Response Function (HRF); and is typically convolved with the experimental paradigm to form the design matrix of the GLM analysis, thereby accounting for the true temporal characteristics of the induced BOLD response (and in particular the delay in onset) (*see section 2.3.4.1*) (Friston et al. 1994a, Boynton et al. 1996).

In the third trimester of gestation and first months of postnatal life, the human brain is known to undergo a dramatic but structured sequence of maturation, with the effect of these developmental changes on the haemodynamic response to stimulation largely unknown (Battin & Rutherford 2002, de Graaf-Peters & Hadders-Algra 2006, Seghier et al. 2006, Harris et al. 2011). In the last study I attempted to account for this uncertainty by convolving a set of linear basis functions in the GLM instead of the canonical function; therefore allowing a degree of flexibility for possible developmental differences in response latency and amplitude (*see section 5.3.4.2*) (Woolrich et al. 2004, Steffener et al. 2010, Monti et al. 2011). However, while the use of basis functions may greatly improve the sensitivity of the analysis, there are also associated drawbacks; in particular a loss of specificity and an inability to easily aggregate the results for a higher level analysis (Steffener et al. 2010, Monti et al. 2011). Furthermore, an implicit knowledge of the HRF is necessary for effective fMRI study design, and in particular event-related study designs where the assumed latency and overall length of the responses are integral to the paradigm (*section 2.3.3*) (Buckner et al. 1996, Dale 1999, Bandettini & Cox 2000). The motivation for this second

study was therefore the realisation that a definitive characterisation of the HRF in the neonatal period was likely to be vital, not only to resolve some of the remaining ambiguity surrounding the amplitude of responses, but also to aid the design of future fMRI studies.

6.1. The effect of inter-subject HRF variability on fMRI analysis

While the key features of the HRF (a delay before onset, a rise in BOLD signal culminating in a "peak" response, and a post-stimulus undershoot) are invariably consistent across all adult subject groups and stimulus types, several studies have now shown that a wide range of differences can be present both within and between subjects in the response latency, width, shape, and magnitude (*figure 6.1*) (Aguirre et al. 1998b, Miezen et al. 2000, Handwerker et al. 2004, Lindquist et al. 2009, Handwerker et al. 2012). In addition, for a given subject, there does not appear to be any clear relationship between these HRF parameters (ie: a particular response magnitude cannot be used to infer the latency) (Miezen et al. 2000). When explored in more detail, HRF variability has been found to be minimised within a single subject scanned on the same day but in different scanning sessions, and (unsurprisingly) is greatest between different subjects (Aguirre et al. 1998b). The origins of this variability are largely unknown, and are likely multi-factorial encompassing external and internal influences (such as caffeine intake and particular disease states), and either or a combination of both neural and vascular factors (Handwerker et al. 2012). In awake task-engaged adults, there is also mounting evidence that endogenous non-sensory neural activity (related to anticipation, attention, and task structure) almost certainly contributes to the detected haemodynamic response, which may be better estimated by taking this distinct additional signal into account (Jack et al. 2006, Sylvester et al. 2007, Cardoso et al. 2012).

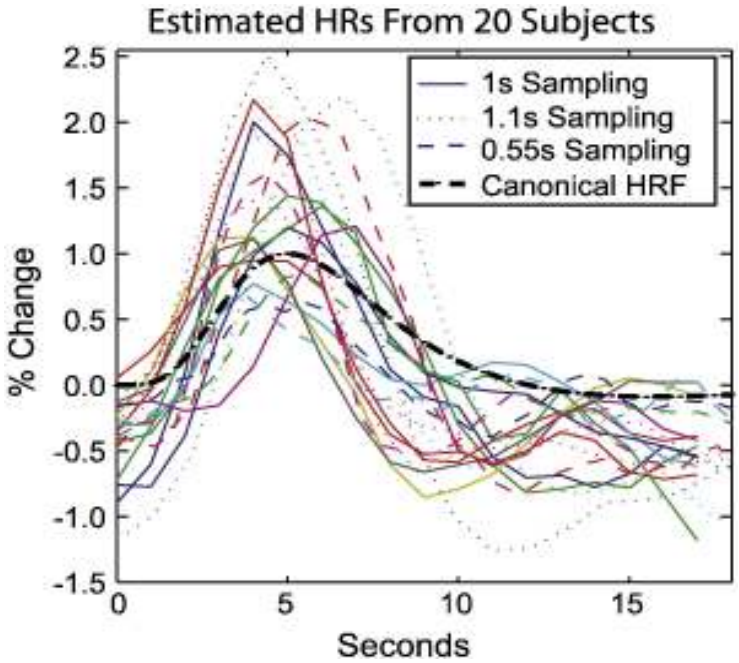

Figure 6.1: ***There is natural HRF variation across a group of subjects, even when the study group population and pattern of stimulation is tightly controlled.*** In this study, HRFs were sampled from a region of interest in 20 healthy young adult volunteers performing a simple button pushing experiment. When unaccounted for, these differences were shown to lead to a significant increase in analysis false negatives (*figure reproduced from Handwerker et al. 2004*).

The importance of this variability was largely unnoticed in early fMRI studies, as by nature of the sustained pattern of stimulation and induced responses, the classic block experimental paradigm tends to be relatively forgiving with respect to the exact model of the HRF (Aguirre et al. 1998b, Henson 2003, Uludağ 2008, Lindquist et al. 2009, Handwerker et al. 2012). This is not the case however for an event-related experimental paradigm, which largely relies on the assumption that the detected BOLD response will be identical to that of the canonical HRF (Buckner et al. 1996, Dale & Buckner 1997, Friston et al. 1998a, Dale 1999, Miezen et al. 2000, Henson 2003). In an elegant study by Handwerker and colleagues (2004), it was shown that considerable inter-subject HRF variability exists even with a tightly controlled study population and stimulus, and further demonstrated that just a 2 second misestimate of the HRF

time to peak can lead to a 38% decrease in the fit magnitude of the GLM analysis. Natural HRF variation can therefore have significant effects on the sensitivity of an analysis, largely due to the potential increase in false negative results (Handwerker et al. 2004, 2012, Uludağ 2008, Lindquist et al. 2009). These findings have led some investigators to suggest the relatively inefficient solution that a separate experiment should be included in all fMRI experiments so that a subject (and task) specific HRF can be identified (Aguirre et al. 1998). However, the preferred approach adopted by the majority of the fMRI community to account for HRF variability, is (as done in the first study of this thesis) to include basis functions in the GLM analysis (Friston et al. 1995b, Woolrich et al. 2004, Lindquist et al. 2009).

6.1.1. Maturational changes in the HRF in childhood and old age

There have been only a few studies which have aimed to systematically characterise the effect of normal aging on BOLD haemodynamic responses (Galliard et al. 2000, Altman & Bernal 2001, Richter & Richter 2003, Schapiro et al. 2004). A consistent finding in fMRI studies of children is that the spatial extent of the patterns of activation appears to decrease with age, suggesting that an increase in functional localisation is an important component of brain maturation (Galliard et al. 2000, Altman & Bernal 2001, Doria et al. 2010, Smyser et al. 2010). A decrease in activation cluster size also appears to be present at the opposite end of the spectrum in old age; although this is likely to be mediated by an entirely different set of biological processes including degenerative decreases in synaptic and microvascular density, and differences in vascular reactivity (D'Esposito et al. 1999, Huettel et al. 2001, D'Esposito et al. 2003). Old age is also associated with a decrease in the magnitude of the measured BOLD responses (D'Esposito et al. 1999, 2003); but this trend has been shown to be reversed in childhood where a linear increase in BOLD response magnitude was described in an extensive study of 332 children between 4 and 19 years of age during both a language and motor task (Schapiro et al. 2004).

Subtle changes specifically in HRF morphology have been described during normal aging; with an earlier trailing edge of the positive peak together with a more significant undershoot period seen in healthy younger subjects (7-20 years old) relative to a group of "older" subjects (>30 years old) (Richter & Richter 2003). In a study of epileptic patients in childhood and adolescence, the latency time to the positive peak of the HRF associated with epileptic discharges was found to be significantly longer in their youngest subjects (3 months to 2 years old) in comparison to all of the older subject groups (up to 18 years old) (Jacobs et al. 2008). Although during young adulthood there appears to be no significant relationship between the latency time and increasing age, it has been shown to be prolonged at ages greater than 50 years of age (Taoka et al. 1998, Richter & Richter 2003). This apparent delay in response has been interpreted as supporting theories which suggest that the age related differences in BOLD response are predominately secondary to decreases in cerebral vessel wall compliance (D'Esposito et al. 2003).

6.1.2. HRF development in early life

Marked developmental changes in cerebro-vascular haemodynamics are known to occur in the brains of newborn infants in the first few days to months following delivery (*reviewed in Volpe 2008*). Using a diverse range of measurement techniques, marked developmental increases have been described in the majority of the major intra-cerebral physiological parameters (including the global CBF, CBV and $CMRO_2$) throughout the preterm and neonatal period (Chugani & Phelps 1986, Greisen 1986, Altman et al. 1988, Edwards et al. 1988, Wyatt et al. 1990, Meek et al. 1998, Miranda et al. 2006, Roche-Labarbe et al. 2010, 2012, Varela et al. 2012). The effect of these maturational changes in physiology on the morphology of the HRF is unlikely to be trivial, given that induced alterations in any or all of these baseline parameters has been found to markedly affect the canonical adult response (*see section 2.2.4.3*) (Cohen et al. 2002, Liu et al. 2004, Chen Y & Parrish 2009, Chen J & Pike 2010a,b).

Characterisation of the HRF with BOLD fMRI during human infancy has been described in a single 3 month old infant following a large perinatal stroke, where a negative waveform was observed in the unaffected (and presumed healthy) hemisphere using a visual stimulus (*see section 3.1.1 and figure 3.2*) (Seghier et al. 2004). No haemodynamic response could be detected in the abnormal hemisphere, in which the optic radiation was also found to be impaired with DTI tractography (Seghier et al. 2004). Interestingly, at 20 months of age, compensatory neuronal plasticity was demonstrated in the same infant, who was found to have developed a negative BOLD response in the pathological hemisphere (identical to that of the unaffected hemisphere) with an associated structural recovery of the previously absent optic radiation (Seghier et al. 2005). However, while the findings of these studies are fascinating, the pathological status of the subject means that they are probably not generalisable to the neonatal population as a whole.

The work of this study was in large part motivated by the findings of Colonnese and colleagues (2008), who performed a developmental study of somatosensory system electrophysiological and BOLD fMRI responses in the immature rat brain. Using electrical forepaw stimulation, they were able to elicit positive BOLD contrast responses from postnatal day 11-13, which equates to approximately 28-32 weeks in human gestation (Clancy et al. 2001, Colonnese et al. 2008). They further found a systematic maturational trend in the key parameters of the sampled HRF, with increasing age characterised by an increase in the peak amplitude of BOLD responses, larger and more widespread responses, and co-activation of the ipsilateral cortex and supplementary areas in addition to the primary sensory areas (*figure 6.2(a)*) (Colonnese et al. 2008, Chan et al. 2010). In addition, LFP recordings and BOLD contrast were also found to show a progressive decrease in the time to peak response with increasing age (*figure 6.2(b)*) (Colonnese et al. 2008). Developmental increases in the upregulation of carbonic anhydrase

activity were found to be fundamental to the observed maturational trends, suggesting that the control of resting CBF plays a key role in these changes (Colonnese et al. 2008).

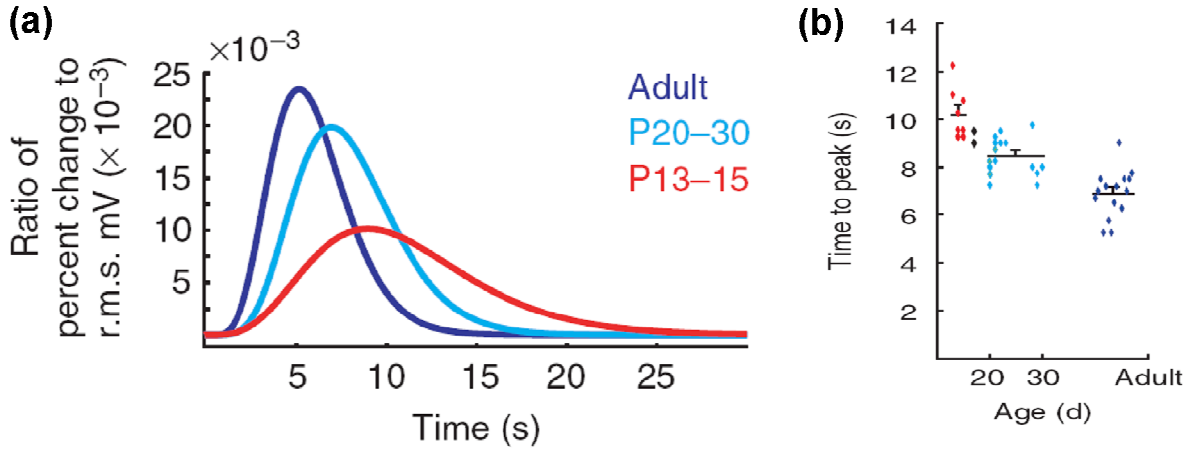

Figure 6.2: (a) ***In the rat somatosensory cortex, the HRF shows a systematic pattern of maturation during early postnatal life.*** An increase in amplitude and shortening of the time to peak response can be seen from the youngest P13-15 rats (equivalent to human 32 weeks PMA) to the mature adult. The HRFs in this study were derived from the minimisation of the observed data fit with a model derived from the measured LFPs. **(b)** ***A significant shortening of the time taken to achieve the peak response amplitude was clearly evident with increasing age.*** (Black bars represent group mean and error bars: one standard error from the mean) (*Figures reproduced from Colonnese et al. 2008*).

6.2. Study aims and hypothesis

The aim of this study was therefore to systematically characterise the ontogeny and morphology of the haemodynamic response to neural stimulation before and after the normal time of birth. Given that the use of sedative medication could represent a significant confounder in this study, I also aimed to resolve this ambiguity by directly measuring the effects of induced sedation on baseline CBF.

I hypothesised that the neonatal HRF would differ from the canonical adult model; and further that there would be a systematic maturational trend akin to that seen in the developing rat brain (Colonnese et al. 2008). I then planned to apply the empirically derived HRFs into the analysis of real fMRI data, with the hypothesis that the use of an age-appropriate HRF would significantly improve the identification of functional responses in a traditional GLM analysis of fMRI data.

6.3. Materials and methods

The work was approved by the Hammersmith Hospitals Research Ethics Committee (code: H0707/101). As in the previous study, written parental consent was obtained prior to all of the sessions of data acquisition, following a detailed discussion with myself or one my colleagues about the aims of the work and the study procedures. All of the data was anonymised following collection (and labelled with a study number identifier), and stored in encrypted and firewall protected file systems.

6.3.1. fMRI Study population

All of the neonatal subjects in this study were recruited from the Neonatal Intensive Care Unit and Postnatal wards at the Queen Charlotte and Chelsea Hospital, London, UK during a period of 18 months between 2010 and 2011. A total of 19 preterm infants and 22 infants at term equivalent PMA were scanned. Data sets were excluded from the analysis if the sequence was not able to be completed (due to the subject waking), or due to excessive motion throughout the period of data acquisition. The final study group (*see table 6.1*) therefore consisted of 10 preterm infants scanned at median 34+4 weeks PMA (range 32+3 to 35+3 weeks) (9 male; median age at delivery 33+2 weeks PMA (26-34+3 weeks); median weight 1890g (1560-2360); and median HC 30.07cm (28-33)); and 15 infants scanned at term equivalent PMA (median age at scan 41+1 weeks PMA (38+1 to 44+0 weeks)) (5 male; median age at delivery 34+1 weeks (26+3-41+1); median weight 3035g (2385-4770); median HC 35cm (31-36.8). 12 of

the infants studied at term equivalent PMA had previously been born prematurely. In addition, 10 healthy adult volunteers (median age 31.5 years (22-54 years), 5 male, all right-handed) were scanned using the same sequence and stimulation paradigm as those used in the neonatal subjects. Clinical details including antenatal, birth and postnatal care were recorded for each infant subject, and a detailed neurological assessment was carried out on all term equivalent PMA subjects by an experienced practitioner (Mercuri et al. 2005). Infants were excluded from the study group with the same criteria as described for the previous study (*see section 5.3.1*).

The clinical assessment and subject preparation prior to data acquisition in the MRI scanner was identical to that described in the last study. In those infants whose parents had given signed consent, oral sedation (chloral hydrate 30-50 mg/kg/dose) was administered approximately 20 minutes before scanning. This was given to 13 of the 15 term equivalent PMA infants, but to none of the premature infants. There were no adverse incidents during the data acquisition period in any of the subject groups.

Group	Number of subjects (male)	Post-menstrual age at scan (median, range)	Gestational age at birth (median, range)	Weight (median, range)	Head circumference (median, range)
Preterm infant	10 (9)	34+4 weeks (32+3-35+3)	33+2 weeks (26+0-34+3)	1890 grams (1560-2360)	30.07 cm (28-33)
Term Infant	15 (5)	41+1 weeks (38+1-44+0)	34+1 weeks (26+3-41+1)	3035 grams (2385-4770)	35 cm (31-36.8)
Adult	10 (5)	31.5 years (22-54)	n/a	Not recorded	Not recorded

Table 6.1: ***The study population of subjects included in the final analysis of the HRF characterisation experiment.*** (*table published in Arichi et al. 2012*).

6.3.2. fMRI image acquisition

MR imaging was performed on the Philips Achieva 3-T system (Best, Netherlands) with an eight channel phased array head coil, in the Neonatal Intensive Care Unit at the Queen Charlotte and Chelsea Hospital, London. As described previously, all of the scanning sessions were attended by either myself or a trained paediatrician colleague, and the infants' temperatures, oxygen saturations and heart rates were monitored throughout the scan (Merchant et al. 2009). A high resolution T2-weighted image and a 3D MPRAGE T1-weighted image were acquired for each of the infants for review by a Neonatal Neuroradiologist (*as described in section 5.3.2*).

fMRI data was acquired with a single shot EPI sequence lasting 8 minutes and 37 seconds (parameters: (TR) 500msec; (TE) 45msec; (flip angle) 90 degrees; (matrix) 64*64; (resolution(x*y*z))

3.125*3.125*4mm, total 1000 volumes). For this study, a relatively short TR was chosen as a faster sampling rate has been shown to be extremely important when attempting to accurately characterise the HRF waveform particularly with respect to identifying the time to response onset and peak (Miezen et al. 2000, Handwerker et al. 2004). To allow for such an improvement in temporal resolution, the spatial resolution of the acquisition sequence must be decreased so as to preserve adequate image SNR (see *equation 2.4, section 2.3.1*). Therefore, the strategy utilised for this study was not to acquire whole brain images, but rather to obtain only a limited (but relevant) field of view, with a further increase in voxel size from the sequence parameters utilised in the last study. This reduced field of view (consisting of just 6 axial slices) was placed above the level of the corpus callosum to give coverage of the peri-rolandic cortex (*figure 6.3*). An identical scan protocol was used for both the adult and neonatal subjects.

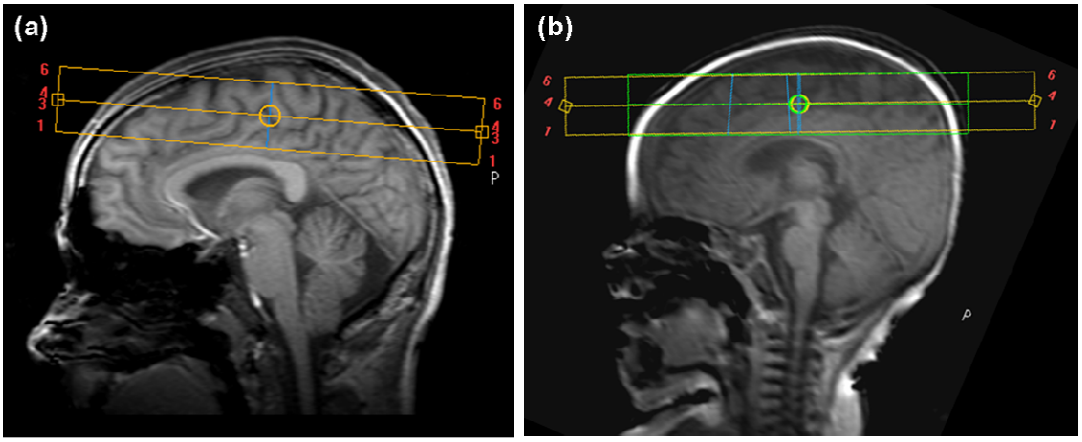

Figure 6.3: (a) ***So as to acquire rapidly sampled data while attempting to preserve image SNR, a greatly reduced sequence FOV of just 6 axial slices was used to acquire data.*** The FOV was positioned above the level of the corpus callosum so as to give coverage of the peri-rolandic cortex (excompassing the primary motor and somatosensory areas) where the primary BOLD responses were anticipated to be induced. **(b)** ***An identical sequence was utilised for both adult and neonatal subjects.*** (Orange box represents acquisition FOV, green box represents the planned shim box).

6.3.3. fMRI experimental design

An event-related experimental design has been demonstrated in a number of previous studies to be suitable for accurately sampling and characterising the HRF in a manner analogous to measuring evoked responses with electrophysiological techiques (Buckner et al. 1996, Friston et al. 1998a, Dale & Buckner 1997, Aguirre et al. 1998b, Bandettini & Cox 2000, Miezen et al. 2000, Handwerker et al. 2004). In this study, a simple event-related design was therefore used with a fixed ISI to acquire a sampled BOLD HRF following a brief (1 second) stimulus during which the subject's right hand was moved passively. Characterisation of the HRF using such a brief stimulus was felt to be achievable, as robust changes in BOLD contrast have been described and used to characterise the HRF using stimuli as brief as 0.1-0.3msec (Hirano et al. 2011, Yeşilyurt et al. 2010). To ensure full recovery of the BOLD signal to baseline, a relatively long 40.5 second inter-stimulus interval was used, during which time the BOLD signal was sampled during TR (every 500msec). While inefficient, an experimental design with a fixed ISI was felt to be suitable for this study so that no assumptions would need to be made about the linear effects of overlapping responses (Dale & Buckner 1997, Bandettini and Cox 2000). In the 1000 volumes acquired, a total of 12 complete stimulation and rest epochs were presented.

Somatosensory stimulation was fully synchronised to the image acquisition, and was elicited using the tailor-made inflatable balloon as described in detail in the last study. To allow an event-related experiment to be performed, a simple series of adaptations were made to the Labview control programme, so that the timing of stimulation (according to the acquisition TR number) can be specified by inserting a 1 column text matrix in the front panel window.

6.3.4. fMRI data analysis and HRF model fitting

All of the fMRI data was initially analysed using tools implemented in the FMRIB Software library (FSL, Oxford, UK, www.fmrib.ox.ac.uk/fsl) (Smith et al. 2004). Each functional data set was first visually examined for excessive motion artefact and image distortion, and data sets were discarded accordingly. When the motion was found only to be isolated to a particular time period during the acquisition, then the specific blocks of data affected by motion were removed from the analysis. This was done as systematic but false correlations in fMRI data are seen as a result of motion artefact despite standard registration and motion estimate regression techniques (*section 2.3.2.2*) (Hajnal et al. 1994, Power et al. 2012, Satterthwaite et al. 2012, van Dijk et al. 2012). Particular attention was placed on removing motion artefact which was specifically associated with the timing of the stimulus, which would have markedly affected the analysis and later model fitting (*figure 6.4*). The remaining contiguous blocks of data were only included in the final analysis if greater than 40% of the entire data acquisition remained (representing a minimum of 5 peristimulus epochs).

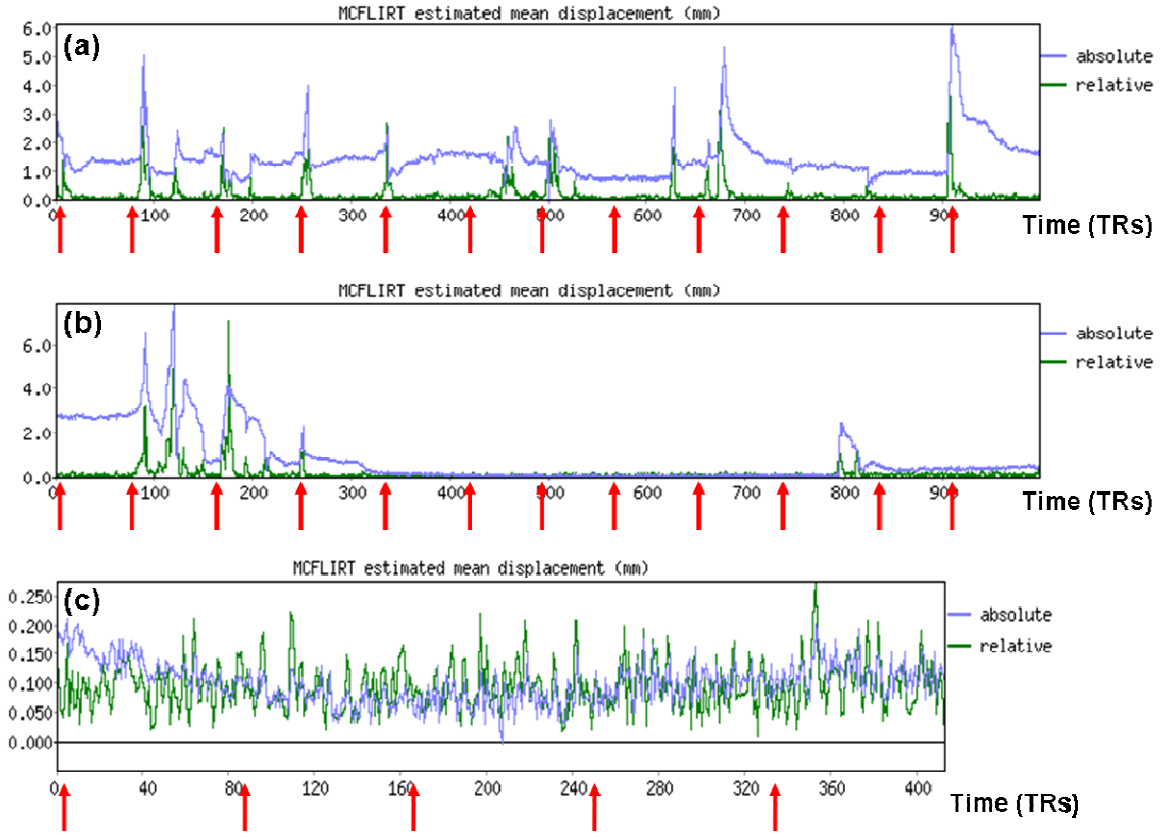

Figure 6.4: ***Estimated mean displacement plots created by FSL's MCFLIRT motion correction toolkit.*** The red arrows along the x-axis denote the timing of stimulation during the period of data collection (x-axis represents time in TRs, y-axis represents estimated mean displacement in mm). **(a):** ***In an unsedated preterm infant who was excluded from the study population***, the periods of movement are clearly associated with the stimulation paradigm. **(b): I*n a sedated term infant*,** there is a burst of large movement at the start (up to volume 300) and a smaller burst (volume 800) towards the end of the data acquisition. **(c)** ***Deletion of the motion corrupted sections of the data results in a trace from a shortened block of data*** in which there is no clear association between the stimulus and the estimated head motion.

All of the data was first processed using FEAT (fMRI Expert Analysis Tool, v5.98) and standard pre-statistics processing steps were applied as described in the last study (Jenkinson et al. 2002, Woolrich et

al. 2001). A highpass temporal filtering cut-off of 50 seconds was used as it was assumed that the total duration of a single haemodynamic response would not exceed this limit (Smith 2001b). Head motion parameters were not included as confound regressors in the analysis, and data de-noising was only performed in this study using MELODIC (Model-free FMRI analysis using Probabilistic Independent Component Analysis (PICA, v3.0) (Beckmann and Smith 2004)). Time-series statistical analysis in FEAT was carried out using FMRIB's improved linear model (FILM) with local autocorrelation correction (Woolrich et al. 2001); with a GLM used to define the observed data using a convolution of the experimental design and a set of optimal basis functions generated using FLOBS (*see section 5.3.4.2*) (FMRIB's linear optimal basis sets, v1.1) (Woolrich et al. 2004). For the generation of the basis set, a range of parameters was specified which could allow for a greater range in the delay and height of the HRF than the default limits set for typical adult data. As in the previous study, the parameter estimates for each of the explanatory variables and basis functions were then convolved into the GLM, converted to a t-statistic image by dividing by the relevant standard error, and finally to a z-statistical score image at a threshold of 2.3 with a corrected cluster significance level of $p<0.05$.

The BOLD signal time-series was extracted and averaged from a ROI which was defined as voxels above the 90th centile in z-score within the cluster of activation in the contralateral primary somatosensory cortex. This cluster was identified with the complete fit of the data derived from an F-test combination of the parameter estimates from the individual basis functions. The time-series was averaged across the peristimulus period and then normalised by converting the data to a percentage signal change (relative to the baseline, defined as the time-points across the 2 seconds prior to stimulus onset). A subject specific percentage signal change (relating to the presumed peak of the HRF) was then calculated using the following equation (http://mumford.fmripower.org):

$$\% \text{ signal change} = \frac{(100 * (\text{p-p height}) * (\text{parameter estimate})}{(\text{baseline signal})} \quad [6.7]$$

where the *p-p height* is the peak to peak height of the event in the model (*see appendix for shell script written and used for this purpose*).

For each individual subject and the group analysis, the converted peristimulus data was then fitted with a linear combination of two gamma distribution functions (or a "*double gamma function*"):

$$h(t) = \rho 1 * G(\mu_1, \sigma_1^2) - \rho 2 * G(\mu_2, \sigma_2^2) \quad [6.8]$$

using a robust non-linear least squares fit (trust-region algorithm) in the curve-fitting toolbox implemented in MATLAB (2009b, The Mathworks, Natick, MA USA). In this model, the HRF as a function of time is defined as h(t); where $G(\mu,\sigma)$ is a gamma distribution parameterised by its mean (μ) and variance (σ), and $\rho 1$ and $\rho 2$ are scalars responsible for the relative proportions of the positive and negative components (Boynton et al. 1996, Glover 1999). The use of two gamma distribution functions for modelling the HRF has been widely described in the literature, and has been found to provide a reasonable characterisation of all of the key positive (positive peak) and negative (initial dip and undershoot) features of the HRF (*figure 6.5*) (Boyton et al. 1996, Friston et al. 1998a, Handwerker et al. 2004, Lindquist et al. 2009).

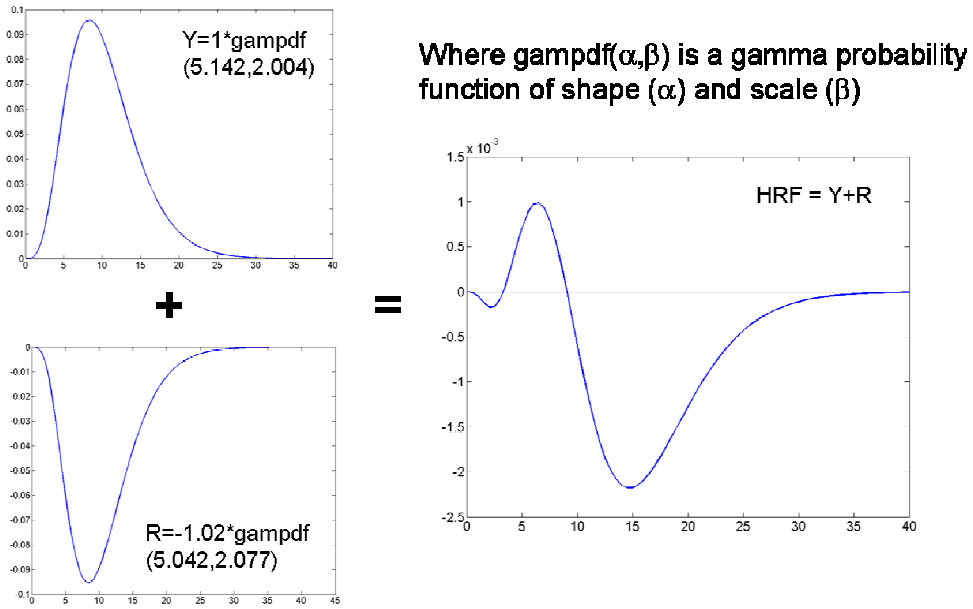

Figure 6.5: The linear combination of two gamma distribution functions can be used to model both the positive and negative features of the HRF. An optimised fit (and in particular the relative proportions of the two functions) can therefore allow the positive peak (in this case modelled by positive gamma Y), an initial dip (modelled by the first section of negative gamma R), and a post-stimulus undershoot (the later section of R) to all be included in the final HRF model.

6.3.5. Global CBF estimation

Animal and adult fMRI work have demonstrated that changes in the HRF peak amplitude and time to peak can be artificially induced by the experimental manipulation of baseline CBF (Cohen et al. 2002, Colonnese et al. 2008, Chen J & Pike 2009a,b, Chen Y & Parrish 2009). To investigate if the administration of chloral hydrate could have been responsible for any observed differences in HRF morphology, global CBF was measured from a separate cohort of 14 healthy term born infants who were then subdivided into two groups (those who were sedated with low dose chloral hydrate medication (30-50mg/kg/dose) prior to scanning, and those who were not) (*see table 6.3*). Infants who had required neonatal resuscitation or had any abnormalities (as described above in the fMRI study

population) were ineligible for this study. The infants were paired by PMA at the time of scan, as it has previously been shown that CBF increases in the first few days and months following delivery (Greisen 1986, Meek et al. 1998, Miranda et al. 2006, Varela et al. 2012).

Global CBF measurement data was acquired using an optimised Phase Contrast Angiography (PCA) sequence (Varela et al. 2012). A multi-slice inflow arteriogram ((TR) 21msec; (TE) 6msec; (matrix) 160*132; (resolution(x*y*z)) 1*1*1mm) was performed for geometrical planning of the PC flow measurement sequence. Flow data was acquired using a sequence previously developed and optimised specifically for neonatal subjects ((TR) 7msec; (TE) 4.2msec; (flip angle) 10°; (resolution(x*y*z)) 0.6*0.6*4.0mm; (maximal encoding velocity (v_{ENC})) 120 cm/sec) (Varela et al. 2012). The acquisition plane for this sequence was positioned at the level of the sphenoid bone, where the internal carotid and basilar arteries are approximately parallel and simultaneous flow measurements can be done using a single imaging plane and encoding velocity along the through-plane direction (*figure 6.6*) (Buijs et al. 1998, Varela et al. 2012).

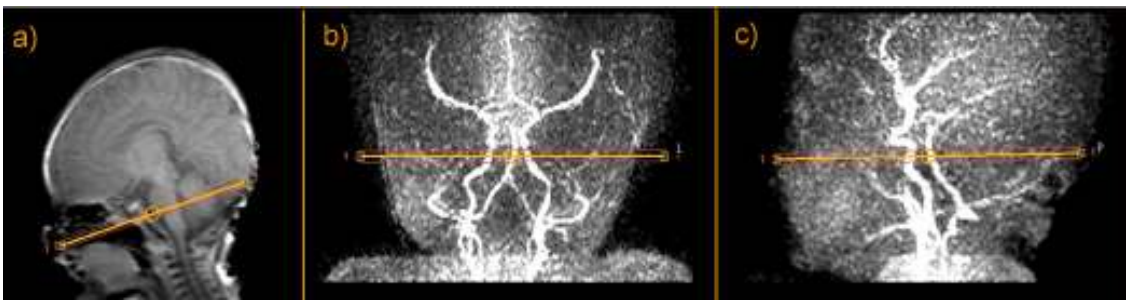

Figure 6.6: (a) ***Phase Contrast Angiography (PCA) data was acquired in a single axial slice placed to allow measurement of all three of the major arteries providing blood flow to the brain*****. (b,c)** ***A multi-slice inflow arteriogram was first performed for planning*****.** The internal carotid arteries and the basilar artery can be seen to be roughly parallel to one another, and approximately perpendicular to the acquisition slice in the maximum

intensity projections of the inflow arteriogram in the coronal and sagittal planes. (*figure reproduced from Varela et al. 2012*).

Instantaneous flux was measured for each cardiac phase and artery, using a time-resolved ROI method (Q-flow Philips image analysis package, release 2.3.5.0 (Philips Corporation, Best, Netherlands)). The mean velocity across the ROI was multiplied by vessel area to give an estimate of instantaneous flux, and flow in the vessel calculated from the mean of the instantaneous flux across the cardiac cycle (*figure 6.7(a,b)*). Total flow to the brain was obtained by summing blood flow in the two internal carotid arteries and the basilar artery. Whole brain volume was measured from high resolution T2-weighted images, following tissue segmentation using in-house software. Each subjects' T2-weighted images were first bias-field corrected using FAST v4.1 (FMRIB's automatic segmentation tool (Zhang et al. 2001)). The corrected image was then aligned to a 4D neonatal atlas using non-linear registration as implemented in IRTK (Image Registration Toolkit; www.doc.ic.ac.uk/~dr/software/) (*figure 6.7(c)*) (Rueckert et al. 1999, Kukilsova-Murgasova et al. 2011). The CSF and extra-cerebral tissue was subtracted from the segmented image, and then whole brain volume was then computed in mm^3. Global CBF in ml/100g/min was then calculated by dividing the total flow to the brain by the brain volume with a further correction for brain density (1.05 g/mL in neonates) (Delpy et al. 1987).

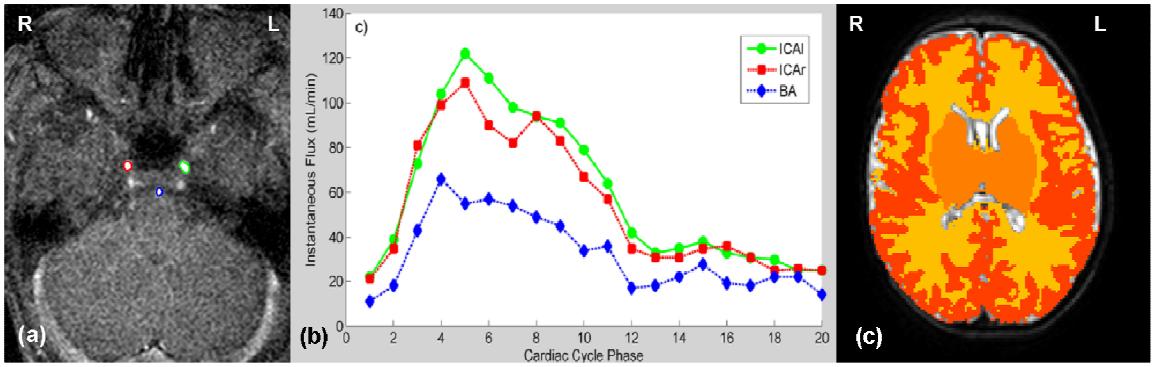

Figure 6.7: (a) ***Global Cerebral Blood Flow (CBF) analysis was performed using a time-resolved region-of-interest (ROI) method.*** The individual vessels (right internal carotid artery (red), left internal carotid artery (green), basilar artery (blue)) were manually delineated and then propagated across the cardiac cycle. ***(b) This allowed quantification of the instantaneous flux across the cardiac cycle in the three vessels of interest.*** **(c)** ***The calculated flow was then divided by the brain volume, which was computed using an automated segmentation tool*** (*figure (b) reproduced from Varela et al. 2012*).

6.3.6. Application of empirical HRFs to experimental data

To test the value of the HRF waveforms derived in the main study, they were then applied into the GLM analysis of 6 preterm (median age 34+0 weeks PMA (range 32+2-34+5)) and 6 term equivalent PMA (median age 40+5 weeks PMA (39+0-43+3)) infant data sets from the study group described in the previous study. The block experimental design (24 seconds of activity interspersed with 24 seconds of rest) was convolved with the age-specific HRF waveform into the GLM using the parameters derived from the HRF characterisation study. Standard pre-processing steps and data analysis (as described previously) were performed using FEAT v5.98, and z-statistical score images were generated with a threshold of 2.3 and corrected cluster significance of $p<0.05$. Each of the individual subject statistical maps was then registered to a custom-made neonatal template for higher level analysis using linear registration (*section 5.3.4.3*) (Jenkinson et al. 2002, Smith et al. 2004). A fixed-effects model was then applied to identify group means, and perform a paired t-test on the lower-level statistical images.

6.4. Results

Following passive motor stimulation of the right hand lasting 1 second, clusters of positive BOLD functional activation were identified in the contralateral (left) primary somatosensory cortex in all 3 subject groups (*figure 6.8*). As observed in the developing rat brain and in the last study, a trend towards co-activation of the ipsilateral primary somatosensory cortex and associated sensori-motor areas such as the supplementary motor area was seen with increasing age (Colonnese et al. 2008, Chan et al. 2010). To maintain consistency across the 3 different subject groups, HRF characterisation was performed using the BOLD signal time-series from a region of interest (ROI) in the contralateral cortex only (*figure 6.9*).

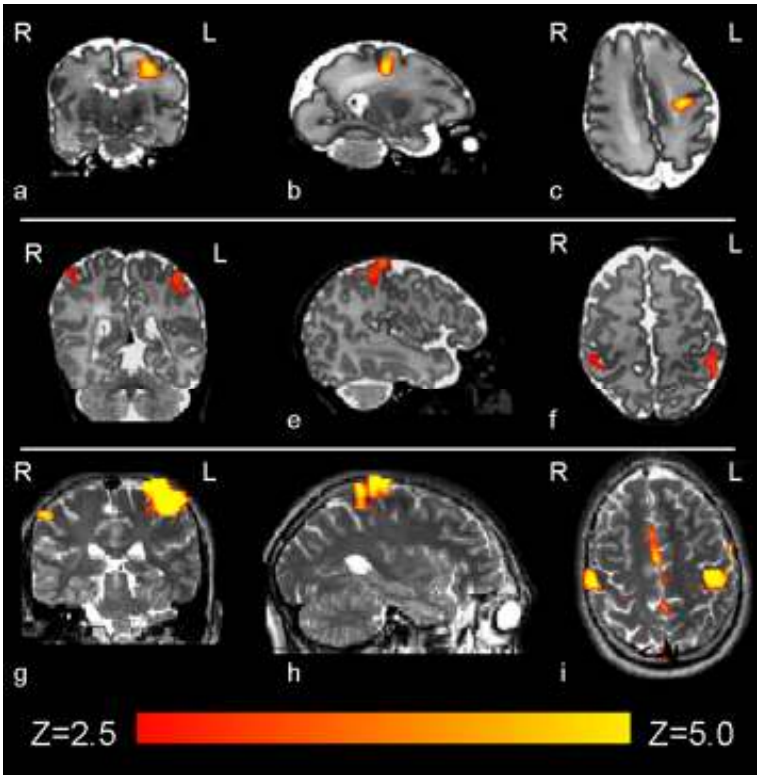

Figure 6.8: ***Identified clusters of functional activation following passive motor stimulation of the right hand.*** Thresholded statistical maps with a corrected cluster significance of p<0.05 have been overlaid on the subjects own T2-weighted image. ***(top row; a,b,c): In a 32+3 PMA week preterm infant***, a large cluster of positive BOLD

activation can be seen only in the contralateral (left) hemisphere. ***(middle row; d,e,f): At term equivalent age*** (PMA 41+1 weeks), a bilateral pattern of activation was more commonly seen. ***(top row; g,h,i): A healthy 24 year old adult*** also shows a smaller clusters of activation in the ipsilateral somatosensory cortex and centrally in the supplementary motor area, in addition to the primary cluster in the contralateral hemisphere. (*figure published in Arichi et al. 2012*).

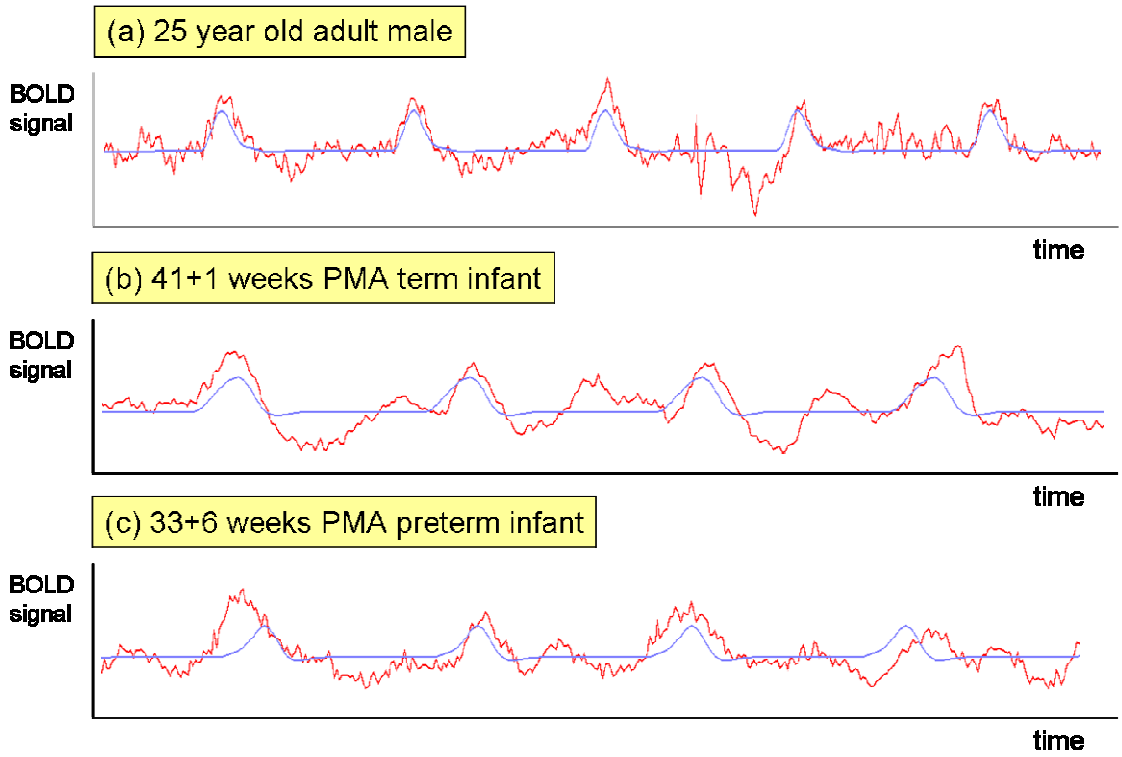

Figure 6.9: ***Example BOLD signal timeseries averaged across a region of interest (ROI) in the contralateral primary somatosensory cortex.*** The ROI was defined as voxels >90th centile in z-score in the cluster of activation. The data (red trace) is shown with the corresponding GLM model (blue trace).

6.4.1. HRF characterisation

Following analysis, ROI idenfitication, and extraction of the data timeseries, it was possible to characterise a HRF for each subject. Although there was HRF shape variability between subjects within a group, with some subjects for example showing an initial dip or deeper post-stimulus undershoot, all had an easily identified positive peak response at some point during the waveform. When the BOLD signal timeseries was extracted from a region of interest placed in an area where activation was not identified in the GLM analysis (eg: the frontal lobe), no systematic change in signal or any clear HRF waveform was seen when averaged around the peri-stimulus period (*figure 6.10*).

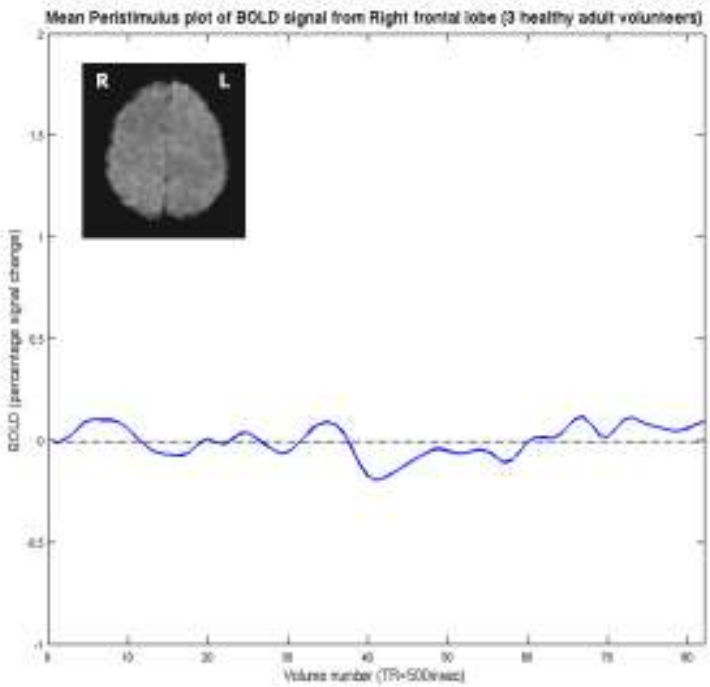

Figure 6.10: ***A HRF waveform was not recognised when a ROI was placed in an area which was not identified as activated in the initial GLM analysis.*** In these 3 adult subjects, the ROI was randomly placed in the right frontal lobe (red area, inset picture), and the BOLD signal timeseries (blue) extracted, and averaged around the peristimulus period (with the stimulus occurring at time-point 0).

By identifying the parameter estimates for each of the separate basis functions, and performing a simple linear sum, it is possible to "deconvolve" and extract the form of the HRF which was used in the final GLM fit. When this was done however, it was clear that this method favours a characterisation of the positive peak response only (*figure 6.11*). The averaged peristimulus timeseries data was therefore instead fitted with a double gamma distribution function using the curve fitting toolbox implemented in MATLAB. This was done as a separate process so as to provide an independent and best model fit without any of the possible constraints imposed by the GLM fit.

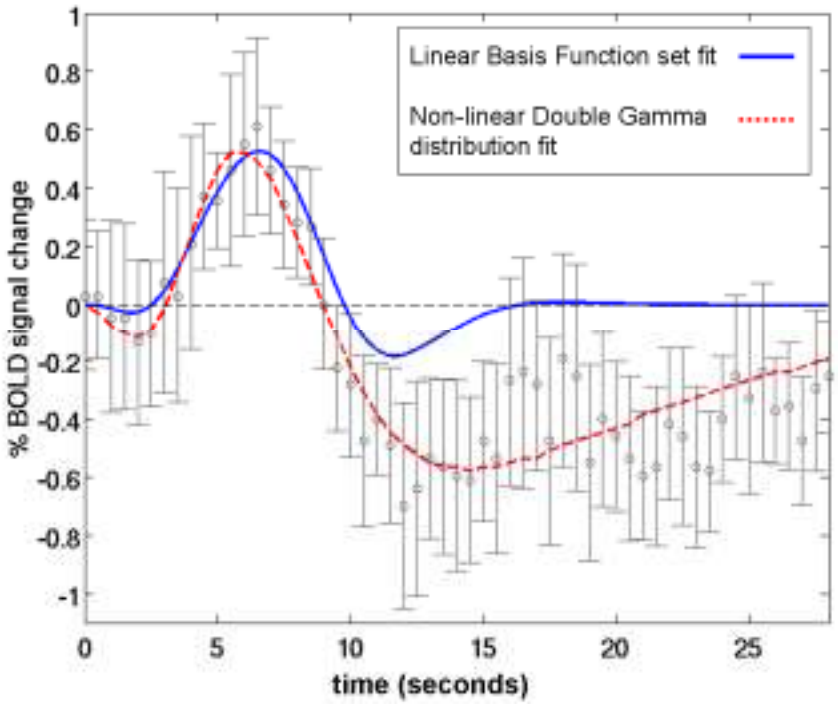

Figure 6.11: ***The peristimulus data in a single infant at term equivalent PMA (40+1 weeks), was fitted with a double gamma distribution.*** This fit (red) was done independently of the GLM analysis using a non-linear least squares fit. The data fit performed by the GLM using a linear combination of three basis functions (blue) is good at characterising the positive peak of the data, but does not adequately model the other features of the HRF, such as in this case where there is a deep and prolonged post-stimulus negative undershoot. The circles represent the data mean (sampled BOLD signal converted to percentage signal change relative to baseline) at each timepoint, with errorbars representing one standard deviation (SD) from the mean.

6.4.1.1. Adult Group

In the adult group (n=10), the parameters and morphology of the sampled HRF waveforms were in agreement to those described in the literature (*figure 6.12*) (Aguirre et al. 1998b, Glover 1999, Miezen et al. 2000, Handwerker et al. 2004). The median time to the positive peak was 5.38 seconds (range 4.5 to 9), with a median peak amplitude of 1.63 % signal change (range 0.78 to 2.93) (relative to the pre-stimulus baseline BOLD signal), and median positive peak to undershoot ratio 0.23 (range 0 to 0.69).

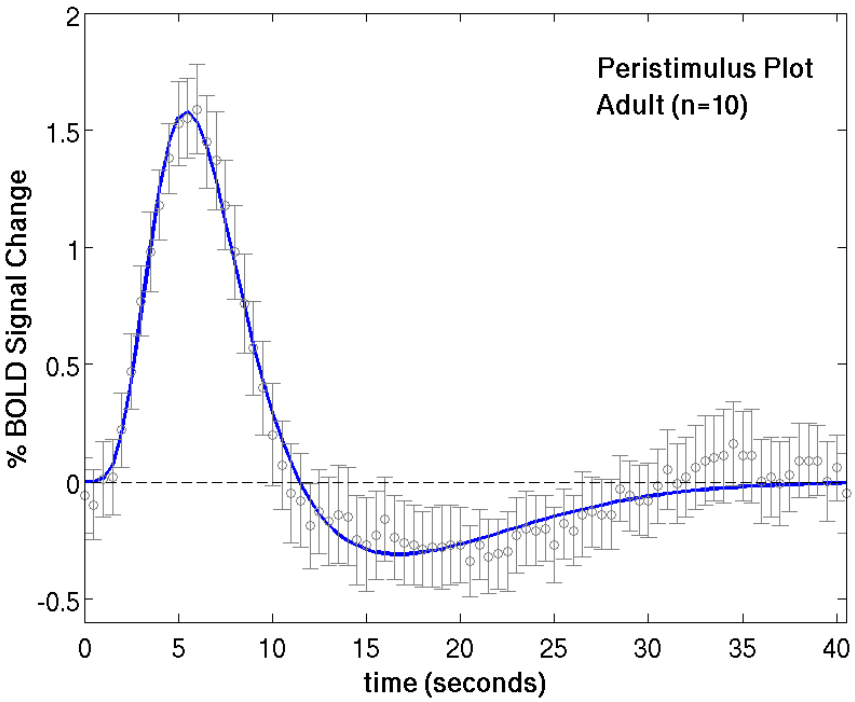

Figure 6.12: ***The sampled HRF in the adult group (n=10, median age 31.5 years) was in agreement with the parameters and shape as reported in the literature***. The mean % BOLD signal change (relative to the pre-stimulus baseline signal) at each timepoint (circles) is shown fitted with a double gamma probability distribution function (blue trace). The error bars represent 2 standard errors of the mean. Somatosensory stimulation (hand opening and closing) occurred at time point 0 and lasted a total of 1 second. (*figure published in Arichi et al. 2012*).

6.4.1.2. Term equivalent PMA infant group

The HRF waveform in the term equivalent PMA infant group (n=15) had a median time to the positive peak of 7.0 seconds (range 3 to 9 seconds) (*figure 6.13*). The median peak amplitude was 0.54% (range 0.27 to 1.42%), and the negative undershoot to positive peak ratio 0.49 (range 0 to 3.31).

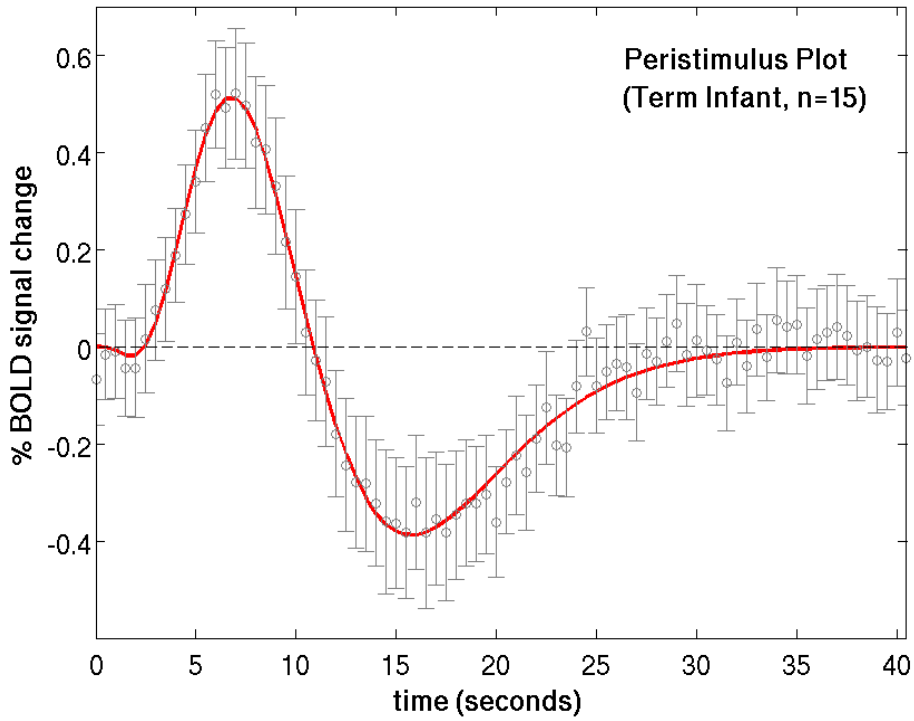

Figure 6.13: ***The sampled HRF in the term equivalent PMA infant group (n=15, median PMA 41+1 weeks).*** In comparison to the canonical HRF, there is a deep negative post-stimulus undershoot period. (*figure published in Arichi et al. 2012*).

6.4.1.3. Preterm infant group

The median positive peak amplitude of the preterm infants (n=10) was 0.52%, (range 0.19 to 0.99) with a relatively shallow undershoot period (ratio to the positive peak: 0.15 (range 0 to 0.62)) (*figure 6.14*). The median time to the positive peak was 11.25 seconds (range 8.5 to 16).

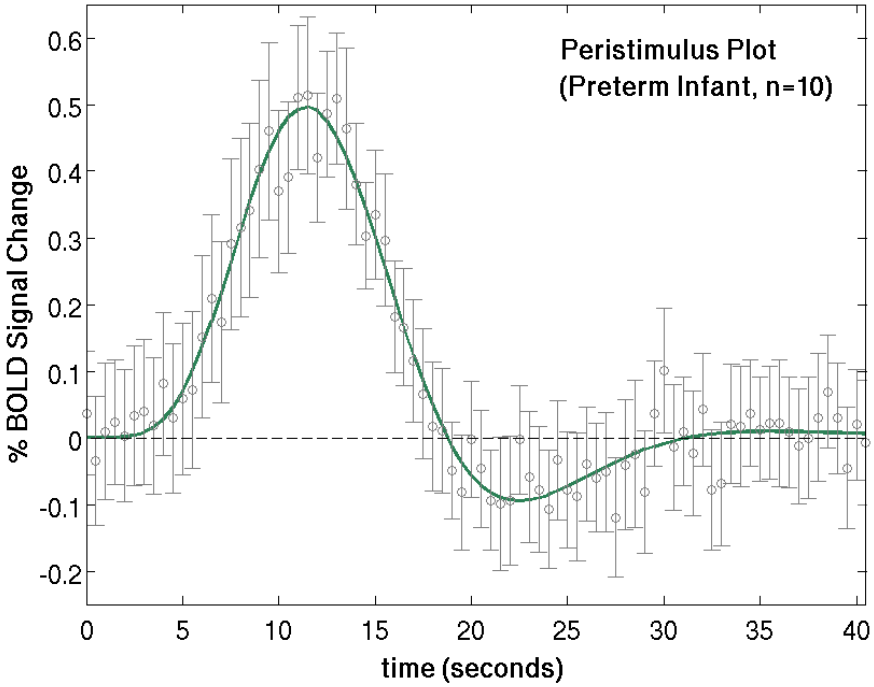

Figure 6.14: ***The sampled HRF in the preterm infant group (n=10, median PMA 34+4 weeks).*** (*figure published in Arichi et al. 2012*).

6.4.1.4. Characterising HRF development

A clear developmental trend in the shape parameters of the HRF can be identified from the described data, characterised by a reduction in the time to positive peak and an increase in positive peak amplitude with increasing age (*table 6.2, figure 6.15*).

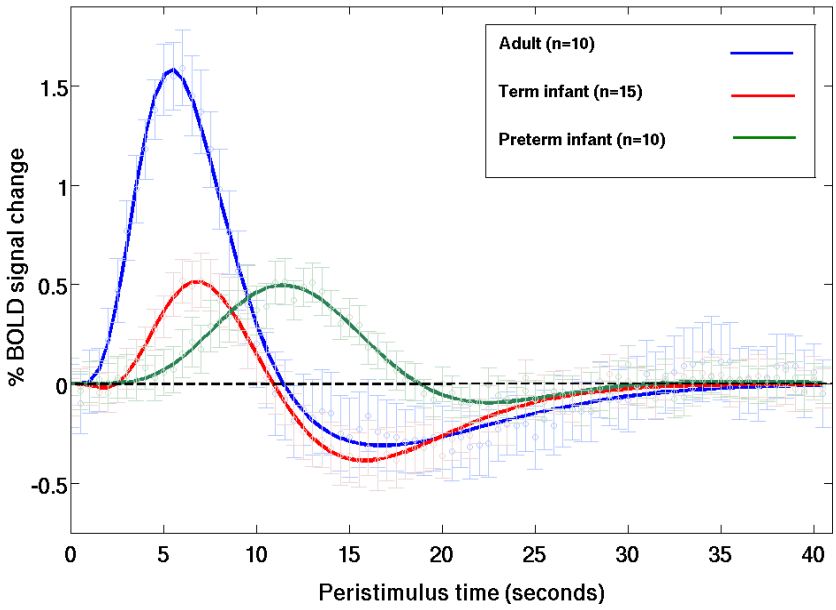

Figure 6.15: ***A systematic developmental trend in HRF morphology.*** With increasing age, a trend towards a shortening of the time to the positive peak, and an increase in positive peak amplitude can be seen. The negative post-stimulus undershoot period is noticeably deeper at term equivalent PMA (*figure published in Arichi et al. 2012*).

Group	n	Time to positive peak (median, range; seconds)	Positive peak amplitude (median, range; % BOLD signal change)	Undershoot to positive peak ratio (median, range)
Preterm infant	10	11.25 (8.5 – 16) **	0.52 (0.19 – 0.99) **	0.15 (0 – 0.62)
Term equivalent PMA infant	15	7.0 (3 -9) *	0.54 (0.27 – 1.42) **	0.49 (0 – 3.31) *
Adult	10	5.38 (4.5 – 9)	1.63 (0.78 – 2.93)	0.23 (0 – 0.69)

Table 6.2: ***Summary of the sampled HRF parameters across the 3 study groups.*** (* p<0.05, ** p<0.001 Mann-Whitney Wilcoxon test in comparison to adult group, Holm-Bonferroni correction for multiple comparisons). (*table published in Arichi et al. 2012*).

In comparison to the adult group, the HRF waveform in the term equivalent PMA infant group has a significantly longer time to peak (p<0.05: Mann-Whitney-Wilcoxon test, Holm-Bonferroni correction for multiple comparisons), a significantly smaller positive peak amplitude, and significantly deeper negative undershoot period (*figure 6.16*). The median positive peak amplitude of the preterm infants was similar to those of the term equivalent PMA infants, although a proportionately shallower undershoot period can be seen. A highly significant lengthening in the median time to the positive peak at 11.25 seconds is seen in the preterm infants in comparison to both the adult and term infant groups (p<0.01) (*figure 6.16(c)*). The median ratio of the post-stimulus negative undershoot to the positive peak amplitude was found to be significantly different between the term equivalent PMA infant group with both the preterm (p<0.05) and adult groups (p<0.05) (*figure 6.16(b)*). No significant difference was found between the adult group and preterm infant group in the ratio of the negative undershoot to the positive peak (p=0.8331).

A particularly interesting aspect of the developmental trend was the striking shortening of the time to the positive peak of the response with increasing age. In the neonatal subjects, this relationship can be seen to follow an inverse exponential trend; with increasing PMA associated with a decrease in the time taken to reach the positive peak of the HRF (*figure 6.17*).

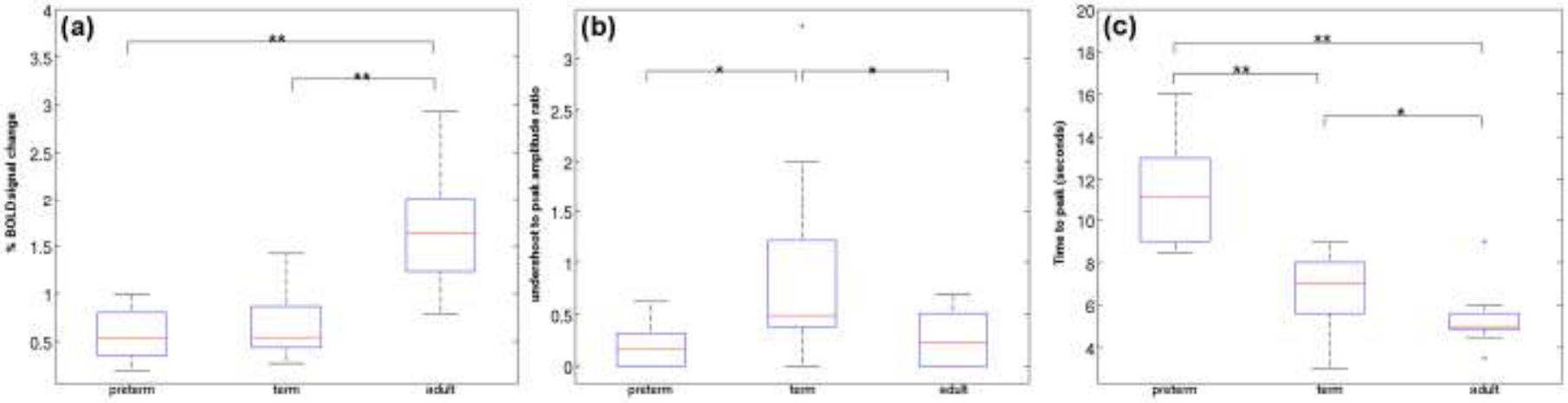

Figure 6.16: (a) ***There was a highly significant difference in the amplitude of the HRF positive peak between both neonatal groups and the adult group.*** There was no significant difference between the preterm and term equivalent PMA infants (Boxplots: box represents 25th and 75th centiles and central line the group median; outliers denoted by '+' symbol; Mann-Whitney Wilcoxon test with Holm-Bonferroni correction for multiple comparisons, $p<0.05$ *,$p<0.01$ **)). **(b):** ***The ratio of the negative HRF undershoot to the amplitude of the positive peak was significantly deeper in the term infant group in comparison to both the preterm and adult groups.*** **(c):** ***One of the most striking findings was that of a highly significant trend towards a reduction in the time taken to achieve the positive HRF peak with increasing age.*** (*figure published in Arichi et al. 2012*).

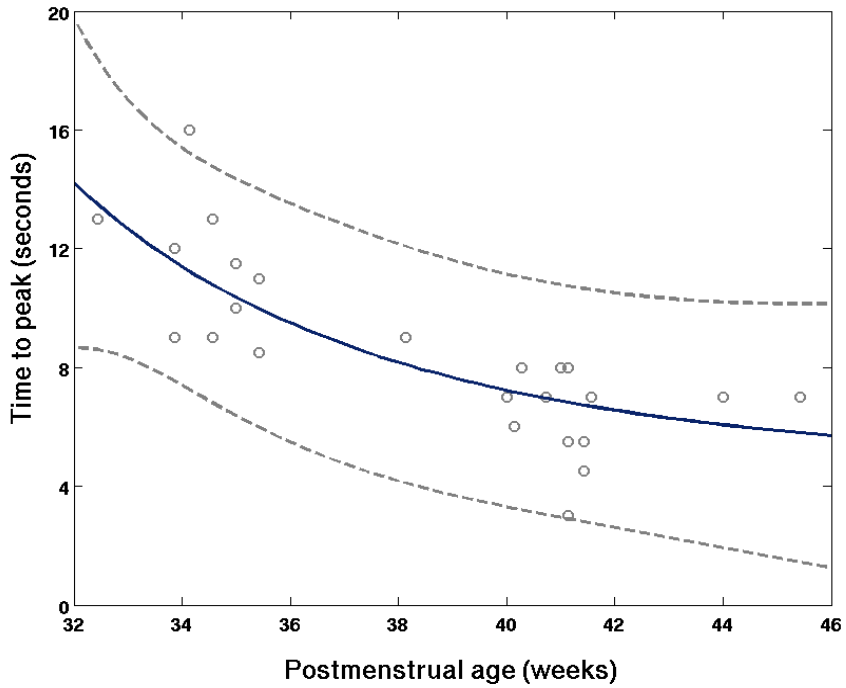

Figure 6.17: ***Within the neonatal subjects only, an inverse exponential relationship is seen between post-menstrual age (PMA) in weeks and the time taken to reach the positive peak of the response (in seconds).*** (r^2= 0.6479; dashed lines represent 95% population confidence intervals). (*figure published in Arichi et al. 2012*).

6.4.2. Global CBF estimation

Global CBF data was acquired from a total of 14 healthy infants who were born at full term gestation and then subdivided into two paired groups (those who were sedated for scanning and those who were not) by PMA at the time of scan. There were no significant differences between the two groups in the age of the infants at scan (Mann-Whitney-Wilcoxon test: p=0.5198); the weight (Wilcoxon signed rank test: p=0.3750); occipito-frontal head circumference (p=0.8438); or brain volume (p=0.1562) (*table 6.3*). Sedation was not found to affect the global mean CBF, with no significant difference between the paired sedated (median: 22.40ml/100g/min) and unsedated groups (median: 20.78ml/100g/min) (Wilcoxon paired signed rank test: p=0.4688). The CBF values measured in this study were in good agreement with

those previously described using diverse measurement techniques (Edwards et al. 1988, Greisen 1986, Roche-Labarbe et al. 2010, 2012, Varela et al. 2012).

Group	Post-menstrual age at scan (median, range)	Weight (median, range)	Head circumference (median, range)	Brain volume (median, range)	Global Cerebral Blood Flow (median, range)
Sedated (n=7)	41+3 weeks (38+1-43+4)	3700g (3115-3920)	35.5cm (34-36.5)	400.8ml (368.0-444.0)	22.40ml/100g/min (19.15-26.78)
Unsedated (n=7)	40+3 weeks (38+4-43+0)	3500g (2652-3944)	35.5cm (34-36.7)	388.0ml (324.0-446.5)	20.78ml/100g/min (19.20-28.87)

Table 6.3: ***Sedative medication has no significant effect on global CBF as measured by MR Phase Contrast Angiography (PCA).*** The infants in the global CBF estimation study were paired by PMA at scan, and separated into two groups: those who were sedated for scan and those who were not. In addition to there being no significant difference between the two groups in the measured global CBF, there were also no significant differences between the paired groups in any of the birth or clinical characteristics. (*table published in Arichi et al. 2012*).

6.4.3. Application of the empirical HRF models to experimental data

To test the value of the derived HRF models the empirical waveforms were then convolved into the GLM analyses of independent data collected from 12 infants from the population studied in the last study using a block paradigm of somatosensory stimulation (*chapter 5*). In 6 preterm subjects, a fixed effects GLM analysis following convolution of a preterm age-appropriate HRF waveform into the lower level subject analyses, identified a large but well localised cluster of positive BOLD functional activation in the primary somatosensory cortex contralateral to the side of stimulation (left hemisphere) (*figure 6.18(a)*).

In contrast, when the same analysis was performed with convolution of the empirical adult HRF, only small areas of negative BOLD were identified in the left peri-rolandic region, with no significant areas of positive signal activation (*Figure 6.18(b)*). In agreement with these findings, a direct comparison of the two types of analysis (a paired t-test on the effect-size estimates) identified a highly significant and well localised cluster in the left primary somatosensory cortex (*figure 6.18(c)*). This marked difference can be seen in the BOLD signal timeseries in an exemplar study (*figure 6.19(a)*) where convolution of the experimental design with the preterm infant HRF is shown to markedly improve the model fitting to the BOLD signal data from the identified cluster of activation with correlation coefficient 0.8407 and sum of squared errors (SSE) 1.9013, in comparison to the canonical adult HRF (correlation coefficient 0.3496, SSE 8.0755).

This process was repeated in a group of 6 infants at term equivalent PMA. In an exemplar study (*figure 6.19(b)*) convolution with the age appropriate term infant HRF waveform can be seen to improve the fit to the data with a correlation coefficient of 0.9096 and SSE 1.5775, in comparison to 0.9055 and SSE 3.0254 using the canonical adult HRF. Convolution of the term infant derived HRF and adult subject derived HRF with the experimental model identified similar clusters of positive functional activation most significantly in the left somatosensory cortex, but with co-activation of the ipsilateral right somatosensory cortex (*figures 6.18(d,e)*). Despite the slight improvement in the model fit of the data, the paired t-test did not identify any significant areas of difference between the two forms of analysis (*figure 6.18(f)*).

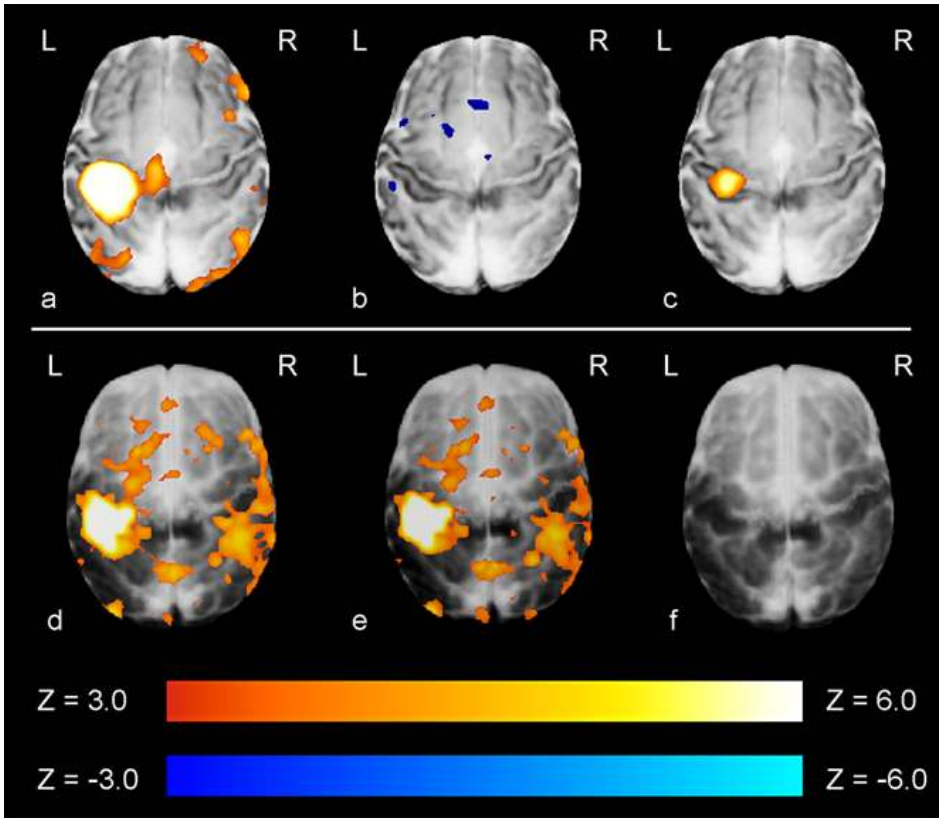

Figure 6.18: ***The application of an age appropriate HRF model significantly improves the identification of functional activity in preterm infants. Preterm infant group (top row: a,b,c):*** (a) A large cluster of positive activation was identified in the contralateral somatosensory cortex when an age-specific HRF model was convolved into the GLM analysis in a group of 6 preterm infants; (b) this was not seen when the analysis was repeated using the canonical adult t-test analysis was performed on the statistical maps derived from the lower level analyses. (c) The difference between the two forms of analyses as tested by a paired t-test is a significant and well localised area of functional activity in the primary somatosensory cortex. ***Term equivalent infant group (bottom row: d,e,f):*** (d) Significant clusters of functional activity were identified when both the age-specific and (e) canonical adult HRF models were convolved into the GLM analysis of 6 infants at term corrected PMA; (f) There was no significant difference between the two forms of analysis on a paired t-test analysis. (*figure published in Arichi et al. 2012*).

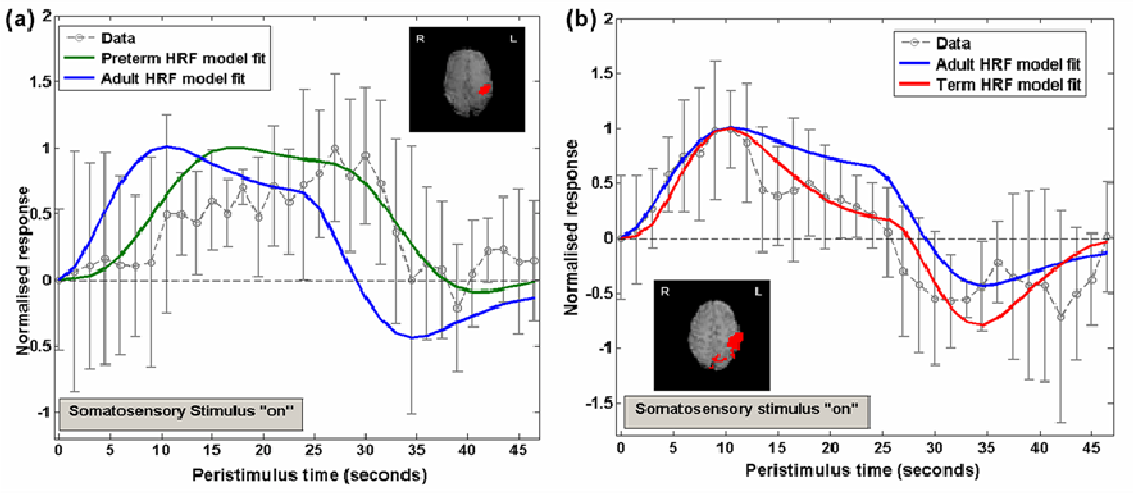

Figure 6.19: ***Example peristimulus BOLD timeseries data derived from clusters of activation (inset pictures, red) identified following passive motor stimulation of the right hand.*** **(a)** ***In a preterm infant,*** the age-specific HRF can be seen to greatly improve the model fit (green), as the peak in contrast occurs much later than would be predicted using the adult HRF (blue). (Grey bar represents the time period (24 seconds) that the somatosensory stimulus was applied, circles represent data mean, and error bars represent 1SD from the mean) **(b)** ***In an infant at term equivalent PMA***, the age-specific HRF improves the model fit (red) by incorporating the deeper undershoot period seen following the positive peak. (*figure published in Arichi et al. 2012*).

6.5. Discussion

Using a combination of optimised fMRI scanning parameters, an appropriate and precise somatosensory stimulus, and an event-related experimental design, the morphology of the BOLD contrast HRF waveform was characterised in the developing human brain. As described in the rat brain (Colonnese et al. 2008), a systematic maturational change in the morphology and parameters of the HRF was seen, both in terms of the time-to-peak and overall magnitude of the response. In addition, it was found that at term equivalent PMA, global CBF is unchanged by low-dose pharmacological sedation suggesting that the observed differences cannot be ascribed to the use of sedation but are more likely secondary to true developmental changes in intra-cerebral physiology. The potential improvement in accuracy yielded from the use of an age-appropriate HRF model convolved into the GLM analysis was demonstrated in two infant groups, with a significant effect seen when applied to preterm infant functional data.

6.5.1. Developmental changes in neurovascular coupling

In comparison to the canonical form seen in the mature adult brain, the amplitude of the HRF positive peak was found to be significantly less in the developing neonatal brain, regardless of PMA. In addition, the time taken to attain the positive peak amplitude of the HRF was found to decrease significantly with increasing age. The physiological reasons underlying these differences are likely multi-factorial, involving many stages of the neurovascular coupling cascade which ultimately culminate in the haemodynamic changes responsible for the BOLD contrast response (*see section 2.2.2*) (Attwell & Iadecola 2002, Logothetis & Pfeuffer 2004, Buxton 2009, Mangia et al. 2009, Cauli & Hamel 2010, Harris et al. 2011, Kim & Ogawa 2012). Due to limitations inherent to studying the in-vivo human infant brain, the effects of developmental changes on these processes have not been extensively investigated; and many of the detailed measures common to calibrated fMRI experiments in adult subjects and animal models are not applicable to this population (Galliard et al. 2001, Harris et al. 2011).

Of note, robust electrophysiological responses to simple somatosensory stimuli can be elicited at a significantly younger age than reliable BOLD signal responses have been described in both animal and human subjects (Taylor et al. 1996, Vanhatalo & Lauronen 2006, Vanhatalo et al. 2009). Although it is unlikely that neural activity in very immature subjects is occurring without the vascular provision of the required metabolic substrates, it does suggest that marked differences in the dynamic coupling of the neural activity and vascular response must underlie some of the trends in HRF morphology identified in this study. The neurovascular coupling cascade is thought to involve multiple signaling pathways encompassing perivascular astrocytes, vasoactive chemical agents, and direct neuronal connections (Attwell & Iadecola 2002, Buxton 2009, Cauli & Hamel 2010, McCaslin et al. 2011). Changes in astrocyte-mediated processes may be of particular significance as animal studies have found marked increases in number, size and local connectivity at an age which corresponds to the human age groups studied in this work (Kaur et al. 1989, Harris et al. 2011).

6.5.2. Trends in cerebral haemodynamics in early life

A localised increase in CBF is known to be the key to the positive peak of the BOLD response through the change in signal which results from an increase in local oxygenated haemoglobin (Hb) (Buxton et al. 2004, Hillman et al. 2007, Buxton 2009, Chen & Pike 2009a,b). Arterial Spin Labelling (ASL) experiments have demonstrated that the local CBF time course following stimulation closely mirrors that of the BOLD HRF, and furthermore have suggested that a feedback mechanism may contribute to a post-stimulus suppression in CBF which correlates with the HRF post-stimulus negative undershoot (Chen & Pike 2009a,b). Global decreases in CBF following caffeine administration have been shown to lower the baseline BOLD signal, increase the percentage signal change of BOLD responses and shorten the time to peak (Chen Y &Parrish 2009, Liu et al. 2004, Perthen et al. 2008); while increases in CBF caused by the cerebral vasodilating effects of carbon dioxide have been shown to result in the converse (*see section*

2.2.4.3) (Cohen et al. 2002, Chen & Pike 2010a,b). These alterations are known to occur in the context of unchanged neurophysiological and metabolic parameters (Matsuura et al. 2000, Chen and Pike 2010a) and have therefore been proposed to be primarily due to the linking of arteriolar compliance as a function of baseline CBF (Liu et al. 2004).

Global CBF is known to increase dramatically during early human development, with preterm infant brain values approximately half that of a full term infant, with a further twofold increase in adult life (Greisen 1986, Edwards et al. 1988, Meek et al. 1998, Roche-Labarbe et al. 2010, 2012, Varela et al. 2012). Given that such a systematic rise in baseline CBF would be expected to induce HRF changes similar to hypercapnia, the trends observed in the results of this study are therefore likely secondary to developmental changes in the capacity of the local arterioles to increase local CBF through the neurovascular coupling cascade. This would be in keeping with histological studies which suggest that the human foetal cortical microvasculature develops radially from the superficial leptomeningeal vessels, with muscularisation of the extrastriatal arterioles and capillary beds not established until close to term equivalent PMA (*see section 1.2.6*) (Kuban & Gilles 1985, Norman & O'Klusky 1986, Kamei et al. 1992, Gilles 2001). Cerebral vessel density and volume has been shown to approximately double from the newborn to adult primate cortex, with the bulk of this change occurring at the capillary level, with this increase in vessel density likely to translate to a faster and higher amplitude local CBF response (Risser et al. 2009).

Near-Infrared Spectroscopy (NIRS) studies have shown that quantitative measures of CBV remain unchanged both throughout the preterm period and during the first weeks after full term gestation (Wyatt et al. 1990, Franceschini et al. 2007, Roche-Labarbe et al. 2010, 2012,). This would suggest that the empirical steady-state relationship (*Grubb's power law, equation [2.3]*) between whole brain CBV

and global CBF seen in adults may differ or does not have a constant exponent during the preterm and neonatal period (Grubb et al. 1974, Buxton et al. 2004). A constant CBV coupled to an increasing CBF through the late preterm to term infant period would lead to a shortening in the mean transit time (MTT) of Hb-O_2 when considered in the context of tracer kinetics as expressed by one of the Stewart-Hamilton equations (Meier & Zierler 1954, Elwell et al. 1997, Buxton 2009):

$$MTT = CBV/CBF \qquad [6.9]$$

A reduction in the MTT would therefore in part explain the shortening of the time taken to achieve the positive peak of the HRF seen with increasing PMA in our neonatal population.

A proportionately deeper post-stimulus undershoot was seen in the term infant subjects, despite a similar positive peak amplitude throughout the neonatal period. It has been suggested that the undershoot period may reflect a transient increase in d-Hb due to a temporal mismatch between the CBF and draining venous CBV response due to differences in vessel wall compliance (Buxton et al. 1998, 2004; Chen and Pike 2009a). In the context of established biomechanical models such as the Balloon Model, a deep post-stimulus undershoot could be explained by an initially stiff post-capillary-bed venous compartment which becomes compliant after prolonged expansion, leading to the volume outflow of the system resembling a hysteresis loop (*section 2.2.4.2*) (Buxton et al. 1998, 2004, 2009). Alternatively, there is also recent evidence to suggest that it is transient decoupling between the CBF and a sustained post-stimulus increase in the local cerebral metabolic rate of oxygen ($CMRO_2$) which results in d-Hb accumulation and therefore a decrease in BOLD signal (Dechent et al. 2011, Hua et al. 2011). In the neonatal brain, the latter effect may predominate as marked increases in neuronal density and integration occur in the late preterm to term infant period, with these changes correlating with the

significant maturational rises in $CMRO_2$ which have been quantified with NIRS and PET (Altman et al. 1988, Chugani & Phelps 1986, Roche-Labarbe et al. 2010, 2012).

6.5.2. Possible effects of sedative medication

In this study (as in the last study), induced sedation with chloral hydrate was used in the majority of the term infant subjects, who are more prone to motion and may become distressed during image acquisition in comparison to preterm infants. Although sedation with chloral hydrate has been found not to affect either the identification or topology of either induced functional activity or resting state networks in neonatal subjects, the potential effects directly on the underlying neural activity and vascular physiology have not been formally assessed (Born et al. 1998, 2000, Doria et al. 2010). In this study, it was felt that the benefits of sedation in avoiding the potential confounding effects of stimulus associated head motion and inefficient data collection, outweighed the concerns generated by this uncertainty.

Sedation does not appear to affect electrophysiological responses, and neurovascular coupling has been found to be preserved even during light anaesthesia (Sisson and Siegel 1989, Avalonitou et al. 2011, Huttunen et al. 2008). It has been suggested that sedative medication, and in particular phenobarbitone, may alter baseline CBF and therefore may be responsible for the inconsistent findings in previous infant fMRI studies (Lindauer et al. 1993, Joeri et al. 1996, Martin et al. 2000, Rivkin et al. 2004, Seghier et al. 2006). This effect is of particular relevance as the control of baseline CBF was shown to be key to the maturational trends in the HRF identified in the developing rat brain (Colonnese et al. 2008).

In this study, I found that chloral hydrate sedation does not affect baseline CBF in a paired sample of healthy infants born at full term gestation. It therefore seems unlikely that the observed maturational

differences between the groups of this study can be ascribed to the increased use of sedation in the term equivalent PMA group. Although it is not possible to completely exclude a possible effect of chloral hydrate on local haemodynamics, animal data suggests that very high doses of the active compound (2,2,2-trichloroethanol) in chloral hydrate acts as an agonist of non-classical K^+ channels in smooth muscle cells, leading to induced increases in local CBF and uncoupling with an unchanged $CMRO_2$ (Uematsu et al. 2009, Parelkar et al. 2010). This effect would therefore not be in keeping with the deep negative undershoot period observed in the sedated term infants. In the future, if novel motion-resistant image acquisition and analysis techniques can be optimised, it may be possible to perform a HRF characterisation study in unsedated infants to definitively answer this question. Critical information may also be gained with quantitative CBF techniques such as ASL, which can provide an exact measure and timecourse of local CBF responses (Chen & Pike 2009a,b). In addition, recent studies have suggested that ASL may provide more specific spatial information with reduced inter-subject variance in comparison to BOLD fMRI responses (Pimental et al. 2012).

6.5.3. Study design, limitations and implications

Although an event-related fMRI design with a widely-spaced constant ISI is relatively inefficient at both detecting activity and HRF estimation (Dale & Buckner 1997, Handwerker et al. 2004, Murphy et al. 2007), it was chosen in this study as particular assumptions could not be made, in particular whether overlapping impulses would sum in a linear fashion (Bandettini & Cox 2000, Buxton et al. 2004, Gu et al. 2005). The initial analysis of the data was done using a set of linear basis functions which allowed flexible HRF modelling; an approach which is particularly suitable in subjects where alterations may occur due to physiological and/or clinical factors (Woolrich et al. 2004, Steffener et al. 2010, Monti 2011). However the increased sensitivity is accompanied by a loss of specificity as evidenced by the differences in data model fitting when compared to an independent non-linear least squares fit.

The term equivalent PMA infant study group consisted mostly of subjects whom had been born prematurely (12/15), and although the findings of the last study suggest that functional activity is well localised regardless of the gestational age at birth, further work will be required to identify any more subtle effects on HRF morphology which may result from preterm birth. An important consideration is that the HRF characterised in this study is potentially representative of BOLD responses only in the primary somatosensory cortex. This is of relevance as the canonical HRF model in adults was originally derived from experiments using a visual stimulus, and further characterisation studies have now demonstrated that subtle differences exist in distinct brain regions using different stimulus types which can lead to an increase in false negative results (Friston et al. 1994a, Miezin et al. 2000, Handwerker et al. 2004). Further work to characterise this inter-region variability is of particular importance in the neonatal brain, as resting state fMRI studies have shown that different neural networks appear to develop at different rates; with the auditory system seemingly maturing before others (Doria et al. 2010, Smyser et al. 2010).

The benefits of an age-appropriate HRF for convolution into the GLM analysis was demonstrated in this study in two example preterm and term infant groups. This effect was most marked in the preterm infant group, where a cluster of positive activation in the primary somatosensory cortex was only identified when an age-appropriate HRF was used in the GLM design model, incorporating the significantly longer time taken to achieve the positive peak. In the term equivalent PMA infant group, a large area of positive functional activation was identified irrespective of the HRF model used, and a significant difference was not seen when comparing the age-specific and adult canonical HRF models. This is explained by the relative similarity in the time to the positive peak of the term equivalent PMA infant and adult HRFs, which will lead to a similar positive overshoot time regardless of the proportionately deeper undershoot period. However, if the linear summation behaviour of the HRF

holds true, then at shorter inter-stimulus intervals than used in this work, the rise rate and amplitude of BOLD signal change would be significantly reduced should the next period of stimulation occur during the undershoot (McClure et al. 2005).

It is notable that no significant areas of negative BOLD response were identified in either subject group using an age-appropriate HRF model. Negative BOLD responses were most commonly reported using a visual stimulus and in later infancy (approximately 3 months of age and above) where it has been postulated that increasing neuronal energy demands exceed the available supply of oxygenated hemoglobin (*see section 3.1.1*) (Yamada et al. 1997, 2000, Morita et al. 2000, Konishi et al. 2002, Muramoto et al. 2002, Seghier et al. 2004). The results of this study suggest that a positive BOLD response is the developmental norm in the neonatal somatosensory system, but further systematic characterisation throughout childhood would be required before the hypothesis of a developmental switch in response amplitude can be conclusively accepted.

6.6. Study conclusions

In this study, the BOLD contrast HRF in the healthy human brain before and around the normal time of birth was characterised, and a developmental trend in early human HRF morphology was identified, similar to that seen in the rodent brain. The data therefore provide evidence that the marked changes in brain structure during the third trimester of human development are also accompanied by a sequence of maturation in the brain's haemodynamic response to stimulation. These maturational changes are likely to be due to both probable developmental alterations in the underlying neurovascular coupling, and known changes in cerebrovascular physiology. The findings further demonstrate that BOLD fMRI responses can be reliably identified in neonatal subjects, and demonstrate a means to significantly improve the accuracy of analysis in neonatal fMRI studies. Induced pharmacological sedation with

chloral hydrate was found not to affect the baseline CBF, and therefore this effect is unlikely to explain the observed trends. Although the effects of sedation on local CBF responses cannot be completely excluded, the described HRF parameters are still relevant for future fMRI studies, particularly in those involving sedated subjects. Further unanswered questions from the results of this study are whether they can be extrapolated and applied to fMRI studies of other neural systems, and if the HRF displays the same linearity at this developmental juncture as is assumed to occur with the canonical adult form.

Chapter 7

7. Further work and applications

It is hoped that the findings of the studies described in the last two chapters of this thesis will be valuable to aid the planning and carrying out of future neonatal fMRI studies, and thereby add an exciting new dimension to our knowledge of the normal and pathological sequences of human brain development. For this to be possible, there remain a few questions which could not be definitively answered in the main studies of this thesis, but for which I have performed some simple preliminary studies to explore the underlying principles. I have been fortunate to have been working with a number of enthusiastic and highly skilled collaborators, notably in the bioengineering department at Imperial College London, with whom we have begun to establish the applicability of the presented findings by performing further fMRI studies of neonatal subjects with novel patterns of stimulation and following brain injury. In this chapter of the thesis I have collated together a brief description and some of the early results of these studies to represent both some of the unresolved issues (and the possible experiments which may be necessary to answer them) and the potential for future applications of the techniques.

7.1. Further investigation of the neonatal HRF

This small set of simple experiments was performed as additional detailed studies are likely to be essential to definitively understand how (and whether) the characterised HRF can be incorporated into future fMRI studies. These steps are necessary as the ubiquitous use of the canonical HRF within the fMRI community is based on certain assumptions which may not be valid in the immature neonatal brain. Two of these premises are described and tested here: firstly that the shape and characteristics of the HRF are consistent between brain regions and stimulus types, and secondly that overlapping HRFs will sum in a predictable linear fashion.

7.1.1. Characterising the neonatal HRF to auditory stimulation

In the adult brain, subtle variations in the induced haemodynamic responses have been described between distinct brain regions with different forms of stimulation (Miezen et al. 2000, Handwerker et al. 2004). It is possible that this effect may be even more pronounced in the neonatal brain where particular neural systems are thought to mature at different rates, and this may be a key contributor to the ambiguity surrounding the results of previous neonatal fMRI studies (*see chapter 3*). Indeed, resting state fMRI studies have hinted towards such a trend, with the auditory network seemingly establishing a mature bilaterally distributed appearance earlier than others (Doria et al. 2010).

With this in mind, the HRF in the auditory functional system was characterised in 3 healthy adult volunteers (2 male, ages 29, 34 and 44 years old), using a simple auditory tone stimulus presented through MR safe head-phones (MR confon GmbH, Magdeberg, Germany). fMRI data was acquired and analysed in an identical manner as described in chapter 6 of this thesis, with the exception of the placement of the acquisition field of view (over the primary auditory areas). As expected, the sampled HRF was found to have similar characteristics to that sampled from the primary somatosensory cortex, with a time to the positive peak of approximately 5 seconds, a post-stimulus negative undershoot, and a total duration of approximately 30 seconds (*figure 7.1*). Of note, the peak amplitude of the sampled HRF appears to be greatly reduced in comparison to both that of the somatosensory system and the canonical HRF (which was first derived from the visual cortex), which may be due to the modulatory effects of the background MR scanner gradient noise.

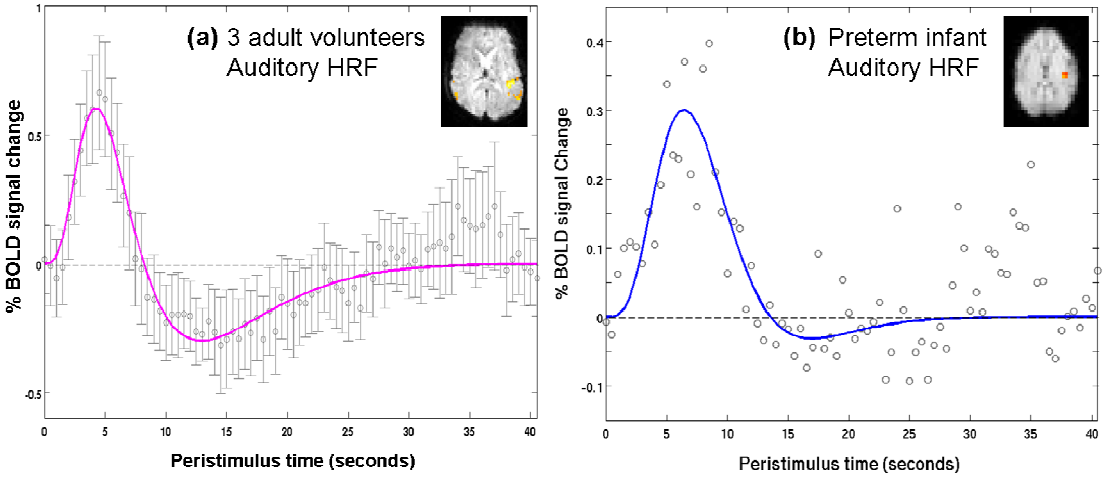

Figure 7.1 ***The HRF sampled using a simple auditory stimulus.*** **(a):** ***In 3 adult volunteers the sampled HRF resembles that of the canonical waveform.*** Circles represent data mean, error bars represent 2 SEM. The data has been fitted with a double gamma function model. Inset pictures represent the identified clusters of functional activity. **(b):** ***In a 33+1 week PMA preterm infant, the fitted HRF appears to peak much earlier than that characterised in the somatosensory system.***

This auditory HRF characterisation experiment has been successfully performed in a single preterm infant (33+1 weeks PMA). In keeping with the findings of the somatosensory experiment and the pilot adult data, a robust increase in BOLD contrast was observed with a characteristic pattern of overall signal change resembling the HRF. Although the peak of this HRF is again delayed in comparison to that sampled from an adult, it occurs much more rapidly (approximately 7 seconds) in comparison to the somatosensory system (11.25 seconds), which may indeed hint towards greater developmental maturity in the putative auditory system at this juncture (*figure 7.1(b)*). If this is truly the case, then it may also partly explain why the majority of the reported neonatal fMRI studies using an auditory stimulus have been able to consistently identify positive BOLD responses (Altman & Bernal 2001, Dehane-Lambertz et al. 2002, Perani et al. 2010, 2011, Blasi et al. 2011). This intriguing data therefore suggests that further HRF characterisation may be necessary for the successful application of fMRI in studies of different and

distinct functional systems, with the additional benefit of providing exciting new knowledge about the sequence of functional maturation in the newborn brain.

7.1.2. Exploring the Linearity of the neonatal HRF

The linearity of the BOLD response is a fundamental concept in fMRI methodology and analysis, as the assumed summation of overlapping responses is integral to predicting the measured responses in the context of the GLM (Boynton et al. 1996, Dale & Buckner 1997, Donaldson & Buckner 2001).

7.1.2.1. The effect of varying the interstimulus interval

In an event related experiment, overlapping responses are presumed to sum in a linear fashion, such that two events which occur in close succession lead to a larger evoked response (Boynton et al. 1996, Dale & Buckner 1997, Henson 2003). The design of the HRF characterisation study in this thesis was based on the premise that events spaced far apart in time will each evoke a single response identical to that of the HRF (Dale 1999, Bandettini & Cox 2000, Miezin et al. 2000). If the linearity of the response holds true, then it could be extrapolated that the amplitude of the evoked response should be affected by the baseline signal when it initiates, and potentially decreased if it occurs during the post-stimulus negative undershoot (McClure et al. 2005). While this decrease in signal is only likely to be very small in an adult subject (due to the proportionately high amplitude of the positive peak of the response), in a neonatal subject this effect can be profound. At an ISI of 30 seconds, it can be seen in simulated data that the HRF shape is relatively preserved in all 3 subject groups as there has been sufficient time for the signal to recover to baseline levels (*figure 7.2(a)*). At a 20 second ISI, the amplitude of the HRF peak would be predicted to decrease, particularly in both the adult and term equivalent PMA infant groups, due to the effects of the preceding undershoot signal (*figure 7.2(b)*). Of note, in the term equivalent PMA infant group, this effect would lead to the ratio of the positive to negative components of the HRF

reaching closer to 1; and further to no response at all being detected in the preterm infant group at a timepoint equivalent to the peak response in the other two groups. It has been proposed that for adult subjects, HRF detection efficiency is optimal at an ISI of 12-15 seconds (Bandettini & Cox 2000). At an ISI of 12 seconds in neonatal subjects however, the simulation suggests that this would result in a "block" like pattern of constant response in the preterm infant subject, while no response at all would be predicted in the term equivalent PMA group at the adult peak response timepoint (*figure 7.2(c)*).

This effect has been investigated in 2 pilot studies conducted on a 31 year old healthy adult volunteer, and a 42+1 week PMA (term equivalent) infant (*figure 7.3*). In the adult, a typical HRF was sampled using an event-related design with somatosensory stimulation at an ISI of either 40 or 12 seconds (*figure 7.3(a)*). In keeping with the expected linearity of overlapping responses, the positive peak amplitude is seen to be slightly reduced with an ISI of 12 seconds. In the term equivalent PMA infant, an approximation of the HRF is sampled with an ISI of 28.5 seconds, with a peak response at 7.5 seconds, as seen in the HRF characterisation study (*figure 7.3(b)*). However, at an ISI of 12 seconds, a recognisable response can no longer be identified, as predicted by the simulated data, due to the linear summation of a new response initiating during an ongoing deep negative post-stimulus undershoot.

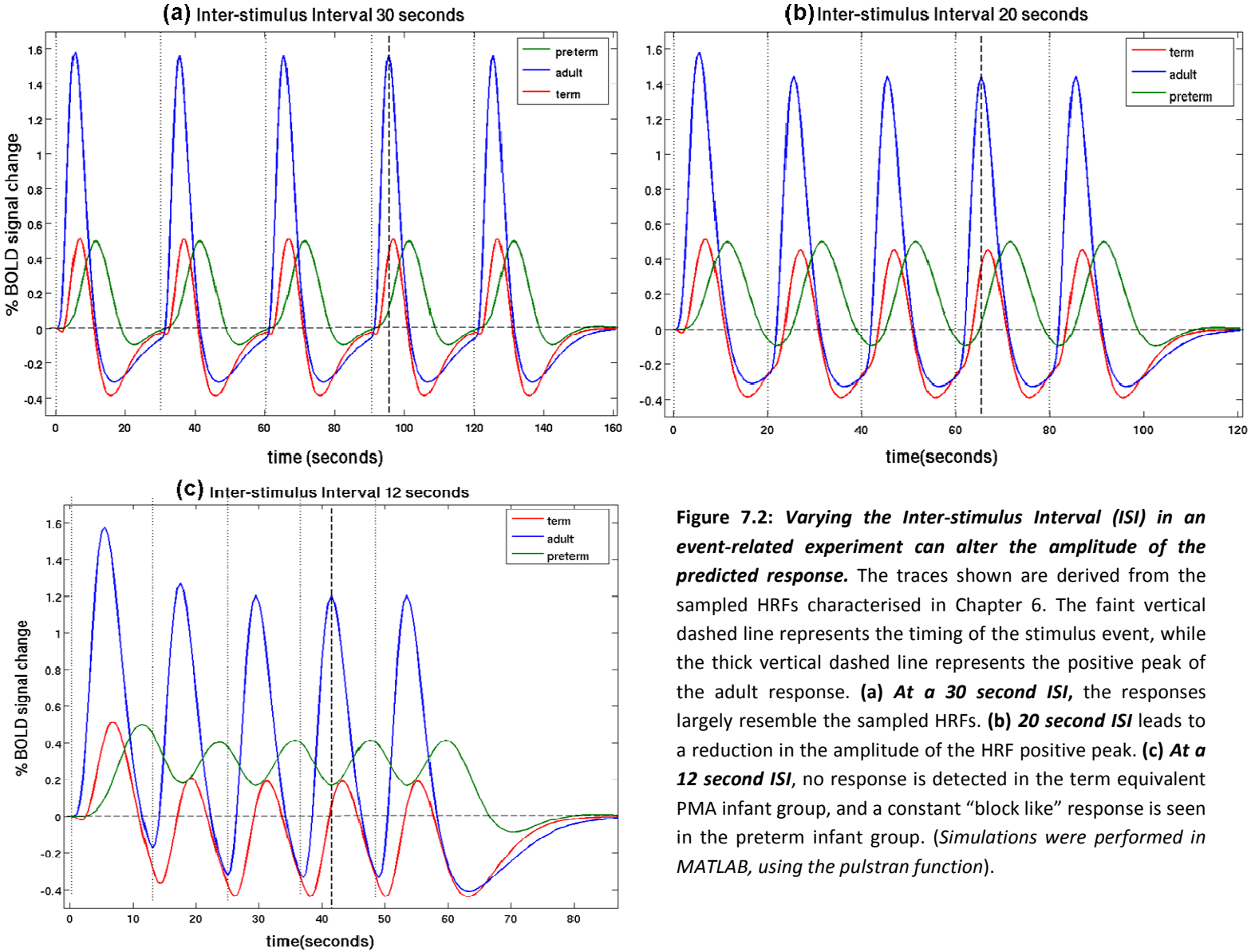

Figure 7.2: ***Varying the Inter-stimulus Interval (ISI) in an event-related experiment can alter the amplitude of the predicted response.*** The traces shown are derived from the sampled HRFs characterised in Chapter 6. The faint vertical dashed line represents the timing of the stimulus event, while the thick vertical dashed line represents the positive peak of the adult response. **(a)** ***At a 30 second ISI,*** the responses largely resemble the sampled HRFs. **(b)** ***20 second ISI*** leads to a reduction in the amplitude of the HRF positive peak. **(c)** ***At a 12 second ISI***, no response is detected in the term equivalent PMA infant group, and a constant "block like" response is seen in the preterm infant group. (*Simulations were performed in MATLAB, using the pulstran function*).

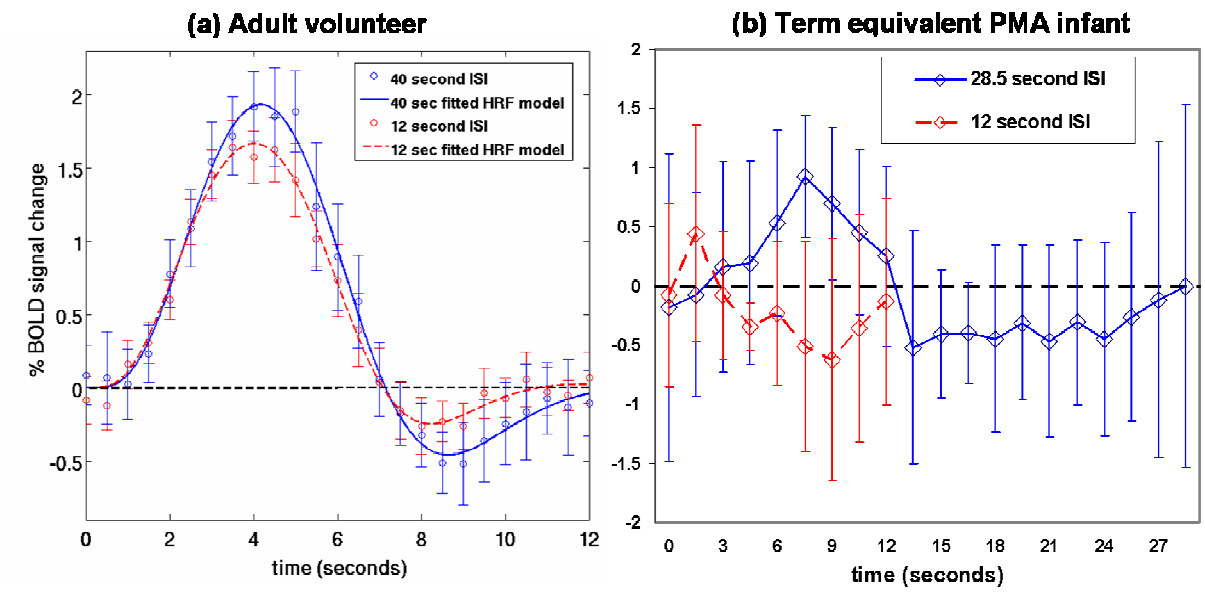

Figure 7.3: ***The detected BOLD response is reduced by a shorter ISI, in keeping with linear summation of overlapping responses.*** **(a):** ***In an adult volunteer,*** somatosensory stimulation induced a response identical to that of the typical HRF at both a 40 second (blue) and 12 second (red) ISI, but the positive peak amplitude of the response is decreased at a 12 second ISI due to the effects of the previous post-stimulus negative undershoot. **(b)** ***This effect is more profound in a term equivalent PMA infant.*** At an ISI of 28.5 seconds, the detected response is that of a typical HRF; but at an ISI of 12 seconds, the response appears to be abolished due to the linear effects of the previous undershoot. Data points represent data mean, error bars represent 2 SEM.

7.1.2.2. HRF summation in block paradigms

Linearity is also implicitly assumed when modelling the predicted response in a block design fMRI experiment in the context of the GLM (Boynton et al. 1996, Donaldson & Buckner 2001, Henson 2003). Under these assumptions, the summation of the overlapping responses during a "block" of repetitive stimulation would be predicted to result in a sustained and high amplitude BOLD response (Donalson & Buckner 2001, Hoge & Pike 2001). Moreover, a higher frequency of events during the block of stimulation would also be predicted to result in a higher amplitude but slightly delayed response (Boynton et al. 1996). In simulated data, this effect would be predicted to be consistent across all 3 of

the subject groups investigated in this thesis (*figure 7.4*). Of note, these simulations do not take into account a probable upper threshold (which has been demonstrated in the visual system) in both the amplitude of the BOLD response and the frequency at which a difference can be distinguished by the nervous system (Yeşilyurt et al. 2008).

In example data derived from somatosensory stimulation of the wrist (*see section 7.2.1.1*), it can be seen that the assumed linearity of the real BOLD data does not match that of the predicted responses. In a single adult volunteer, a higher stimulus frequency does indeed lead to a marked increase in the amplitude of the response (although not to the magnitude predicted) (*figure 7.4(d)*). In the two infant subjects however, there is only a slight increase in the response amplitude in the preterm infant, but no apparent effect in the term equivalent PMA infant (*figure 7.4(e,f)*). The peak of the response does however appear to be delayed at higher stimulus frequencies as predicted in the simulations. Given that this data is derived from single subjects, it is not appropriate to assume that it is representative of the population as a whole. However, it does suggest that further detailed studies of this effect will be necessary to understand if the behaviour of the neonatal HRF conforms to the assumed linearity of the canonical adult HRF.

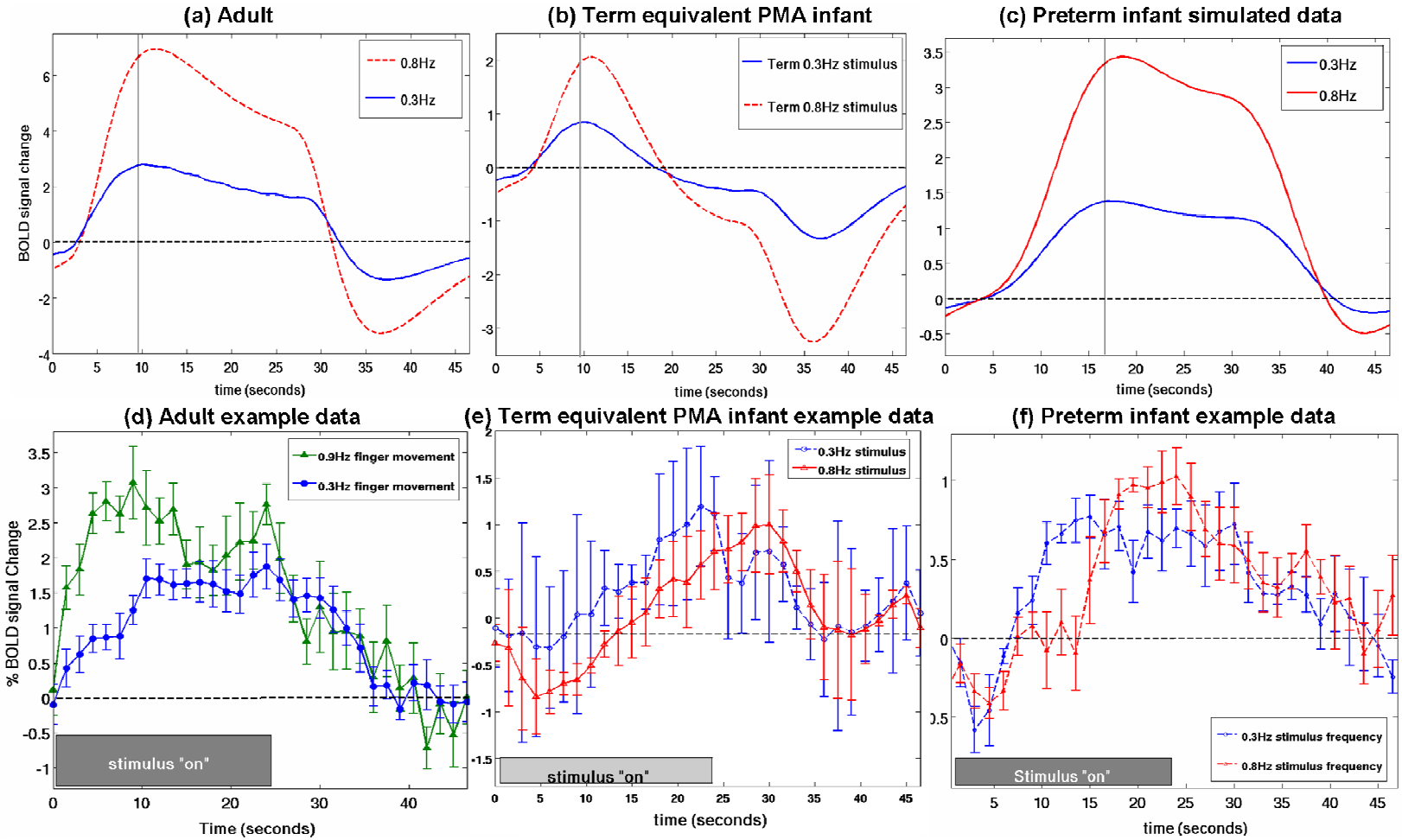

Figure 7.4: ***The effect of varying the stimulus frequency on the timing and amplitude of BOLD responses*****. (a,b,c (top row)):** ***In simulated data*****,** the linear summation of the responses at a higher stimulus frequency would be expected to evoke larger and slightly later responses in all 3 of the subject groups. Vertical line represents peak response at 0.3Hz. **(c,d,e (bottom row)):** ***Example data*** suggests that this may not be the case in neonatal subjects; where the onset of the response does appear delayed with a higher stimulus frequency, but the amplitude is not significantly increased.

7.2. Novel applications for fMRI studies of the newborn brain

It is hoped that the findings of this thesis will allow further detailed fMRI studies to be performed in neonatal subjects. This will be vital to only provide new information about the developing brain, but moreover to understand the applicability (and flexibility) of the findings to other sensory systems and stimulation paradigms. Some of this work-in-progress has yielded extremely promising results, which are briefly presented here.

7.2.1. Further characterisation of the immature motor system

While the results of the first study described in this thesis hint towards the exciting potential that fMRI can offer for gaining a deeper understanding of the development of early human somatosensory system, the stimulus used in biological terms could be considered relatively non-specific as it is likely to provide both a local pressure and proprioceptive stimulus across several joints and more than one peripheral dermatome. In addition, by nature of their relatively uncooperative (and uncommunicative) behaviour, it is unknown how much active (ie: that initiated by the subject) movement and/or resistance to the induced movement could have contributed to the detected responses.

With these considerations in mind, a further stimulation device has been designed, manufactured, and implemented in collaboration with the bioengineering department at Imperial College London. This device is based on similar principles to those of the balloon interface, but was designed specifically to provide gentle proprioceptive stimulation of only the wrist through induced flexion and extension driven by pressurised air (*figure 7.5(a)*). As previously, the rate and amplitude of the movement can be carefully controlled by the investigator through the software interface. By applying a combination of the lessons learnt from the initial study, an age-appropriate HRF, and the new stimulation device, we have been able to collect robust and reproducible fMRI data in a cohort of 14 preterm infants (median PMA

at scan 34+1 weeks (range 31+0 to 34+5). In this group of infants (as with the balloon interface), passive movement of the right wrist was found to evoke a well localised and unilateral pattern of positive BOLD activation in the contralateral primary somatosensory cortex (*figure 7.5(b,c,d)*).

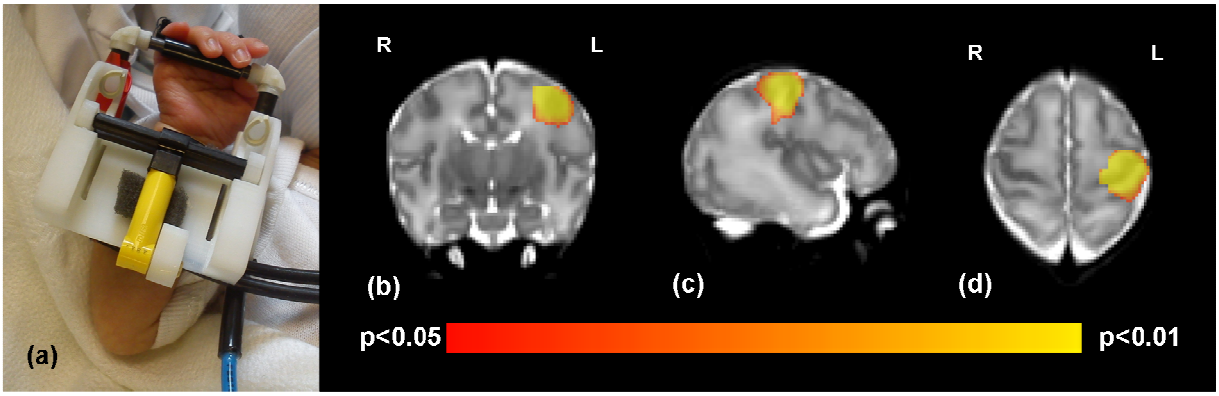

Figure 7.5: ***The novel wrist stimulation device designed for further studies of the developing motor system in neonatal subjects.*** **(a)** ***Photograph of the device fitted on a 34+3 week PMA preterm infant.*** It can be easily fitted on a neonatal subject without causing any discomfort, is MR safe, and weighs just 35g. Extension and flexion of the wrist is initiated by the piston (yellow) driven by pressurised air. **(b,c,d):** ***The group analysis of 14 preterm infants (median PMA 34+1 weeks) following stimulation of the right wrist,*** shows a large but well localised cluster in the peri-rolandic area in the contralateral cortex. The results of a non-parametric t-test, generated with permutation methods and threshold-free cluster enhancement (TFCE) have been overlaid on an age-appropriate template brain.

Although a newborn infant can be seen to make spontaneous movements with their trunk and limbs, little is known about the control or initiation of these movements (Prechtl 2001). While it is generally accepted that these movements do not appear purposeful, the quality of the movements can be qualitatively assessed and has been described to follow a recognisable sequence of ontogeny in the first few months of life (Prechtl et al. 1993, 2001, Hadders-Algra 2004, Lagercrantz & Changeux 2009). Deviations in either the normal pattern of movement (both quality and quantity) or sequence of maturation, have been found to be correlated with later adverse neurodevelopmental outcome (Prechtl

et al. 1993, Hadders-Algra et al. 1999, Ferrari et al. 2011). In the mature brain, movements are initiated in the primary motor cortex (anterior to the central sulcus) and transmitted to the contralateral side of the body via the corticospinal tracts (Purves et al. 2001). In early life, the corticospinal tracts are known to be present from approximately 24 weeks gestation; but are thought to serve a very different predominately inhibitory and sensory role in the immature motor system, with functions such as the inhibition of peripheral stretch reflexes, mediating muscle tone, reinforcing tactile reflexes, and the early individualisation of finger movements (Eyre 2001, Sarnat 2003, Martin 2007).

The accurate characterisation and quantification of spontaneous movements in the developing neonate is therefore of great interest to both the clinical and developmental neuro-biology communities. The described novel wrist interface has a segmented fibre-optic position sensor integrated into the moveable arms of the device, which can provide extremely precise position feedback information (with a maximum error of just $\pm 1.1^{o}$). The spontaneous movements of the infant's wrist during fMRI data acquisition can therefore be measured, convolved with the age-appropriate HRF, and entered into the GLM analysis as a further design matrix. The considerable potential of this approach can be seen in an exemplar study of an infant studied at 33+4 weeks PMA. "Passive" movement (ie: that induced by the device) of the right wrist was found to elicit a cluster of well localised functional activity in the primary somatosensory cortex posterior to the central sulcus, while surprisingly the spontaneous "active" movements (ie: those initiated by the infant) were found to be associated (as in the adult) with functional activity anterior to the central sulcus in the presumed immature primary motor cortex (*figure 7.6)*. Further validation of this result was provided by performing DTI probabilistic tractography from the identified clusters of activation, which confirmed that the area associated with spontaneous movements appeared to be connected to the midbrain via the corticospinal tract running through the PLIC (*figure 7.6(c)*).

The combination of fMRI and the innovative robotic wrist interface device thus offers the unique prospect of a true understanding of the developing relationship between cortical activity and movements in newborn infants during normal brain maturation and following localised injury.

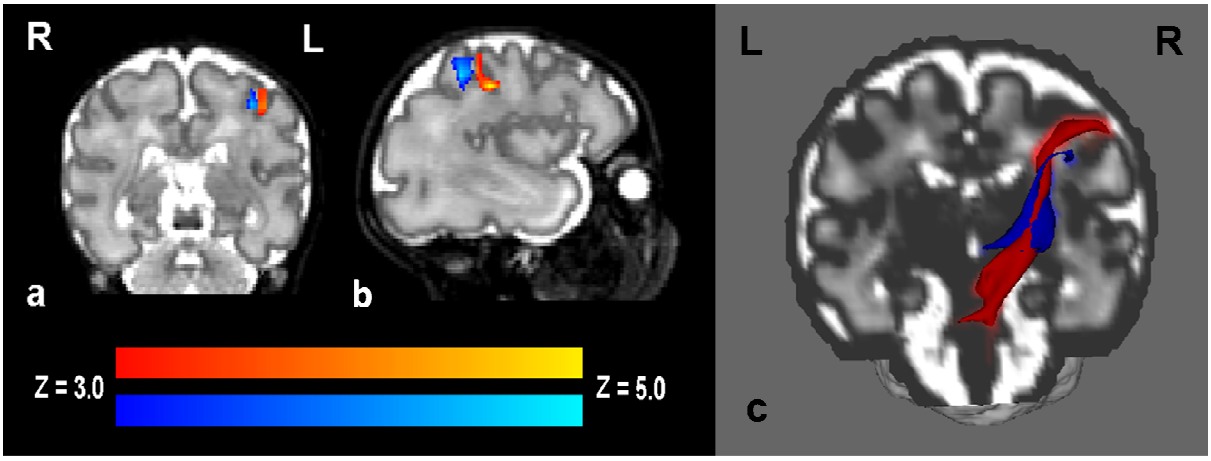

Figure 7.6: ***Functional activity associated with passive (blue) and active (red) movements of the right wrist.*** **(a,b):** ***Well localised clusters of positive BOLD functional activity can be seen posterior to the left central sulcus (blue) in the primary somatosensory cortex, and anterior (red) in the primary motor cortex.*** The cluster corrected statistical maps from the two different conditions have been overlaid on the subject's own high resolution T2 image. **(*c*):** ***The findings of the functional data are validated by the connectivity distributions derived with DTI probabilistic tractography***. The pathways from the "active" motor cluster (red) follow the path of the cortico-spinal tracts (through the posterior limb of the internal capsule (PLIC) and down to the cerebral peduncle. In contrast, the pathway from the "passive" cluster (blue) also passes through the PLIC, but then terminates at the level of the thalamus, as would be seen in the thalamo-cortical tracts.

7.2.2. The Olfactory system

The neural systems that underlie the development of olfaction around the time of birth are not well understood. Behavioural studies of infant olfaction have suggested that neonates can distinguish

between pleasant and aversive smells, and furthermore that familiar smells (such as breast milk) may have a calming effect during painful procedures (Bingham et al. 2007, Nishitani et al. 2009). A recent functional NIRS study has described greater responses in neonatal subjects in the frontal areas to the smell of breast milk in comparison to formula milk, suggesting that the neural correlates of this behaviour may be amenable to functional neuroimaging (Aoyama et al. 2010). In the mature brain, primary olfaction is processed inferiorly in the piriform cortices, with higher level processing such as smell association and discrimination processed in the thalamus, orbito-frontal, cingulate, and insular areas (Savic 2002). Functional MRI (fMRI) is therefore an ideal tool for understanding olfaction in the early brain, as activity can be identified in both cortical and subcortical areas.

An fMRI compatible "olfactometer" was designed and made based on similar principles to those described in adult fMRI studies (Popp et al. 2004, Johnson & Sobel 2007), with particular care placed on limiting infective risk between subjects. The general theory of an olfactometer is relatively simple: delivery of pressurised air through 3 odour chambers (each containing a small amount of liquid odorant) is regulated via the computer controlled opening of valves. The smell is then presented through nasal cannulae fitted to the infant prior to the image acquisition (*figure 7.7(a)*). To minimise infective risk, all of the components distal to the control valves were composed of readily available medical equipment, which could be easily disposed of between subjects.

In pilot data using this equipment and a formula milk odour stimulus, it has been found that sedated infants at term equivalent PMA age show well localised patterns of positive BOLD response in the primary olfactory areas at the base of the brain (*figure 7.7(b)*). Of interest, the term equivalent PMA infant somatosensory HRF was found to be appropriate for data derived with this stimulus type, with the

predicted design model closely fitting the data timeseries within the identified cluster of activity (*figure 7.7(c)*).

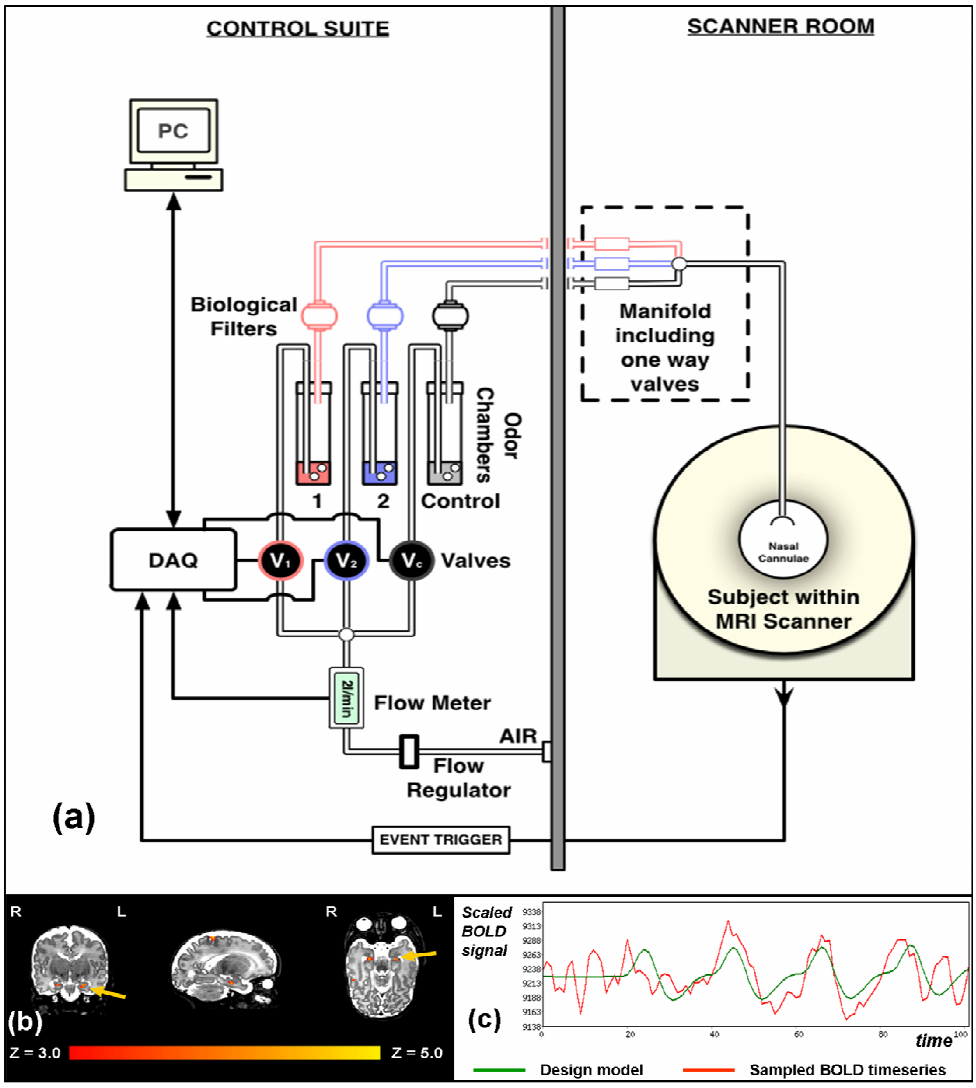

Figure 7.7: ***The neonatal olfactometer.*** **(a):** ***Schematic diagram of the control box, and presentation manifold.*** The control box contains an air flow regulator, meter and valves, and as with other stimulation devices is kept within the MR scanner console room. Pressurised air is bubbled through the stimulus odorant liquids within the odour chambers, thereby presenting the vaporised odour to the subject inside the scanner examination room. **(b):** ***Well localised positive BOLD responses in the piriform cortices were identified in a term equivalent PMA infant following stimulation with formula milk (orange arrows).*** **(c):** ***The BOLD contrast timeseries (red) can be seen to***

closely fit the design model (green) which is derived from the pattern of stimulation and the population appropriate HRF. (*figure (a) courtesy of Richard Gordon-Williams*).

A truly exciting aspect of future studies using the fMRI-compatible olfactometer will be the possibility of investigating a newborn infant's ability to distinguish smells; and in particular those that are familiar or "comforting" (such as the mother's breast milk) in contrast to those that are aversive or associated with unpleasant events (such as those associated with the clinical environment). The results of such a study may have great implications with respect to our understanding of the development of associative behaviour and cognitive capability in newborn infants.

7.3. fMRI in the study of perinatal brain injury

Acquired brain injury during the perinatal period has been described in a number of clinical case reports to have a profound effect on the growing and developing neonatal brain (Johnston 2009, Staudt 2010). In these infants, multi-modal neuro-imaging studies have found fascinating evidence of the early brain's increased capacity for neural plasticity with compensatory patterns of novel neural organisation still apparent later in childhood (Staudt et al. 2002, Fair et al. 2006, Basu et al. 2010, van der Aa et al. 2011a). The ability of the child to compensate and the eventual clinical outcome appear to depend on a number of factors including the type, timing, and location of the original injury (Staudt et al. 2010). The addition of quantitative information derived from diffusion-based MRI data in early infancy has been described to offer prognostic information with greater sensitivity and specificity than anatomical MR imaging alone (van der Aa 2011b, Roze et al. 2012). By providing information about the locality of brain activity, fMRI is ideally suited to add further insights into both the processes of compensatory plasticity and the prediction of later outcome. That said, an important caveat is that the pathology itself may have effects

(particularly in the acute phase of the disease) directly on the haemodynamic response and/or cause image artefacts, which may make interpretation difficult (Amemiya et al. 2012).

Early data collected from 2 preterm infants studied at term equivalent PMA and 1 year of age, suggest that compensatory patterns of functional activity and structural connectivity can already be identified in neonatal life, and further suggest that this information may offer dramatic new insights into the mechanisms of neural organisation during early brain development (*figure 7.8*). Functional somatosensory stimulation of the hand contralateral to the brain lesion was found to elicit positive BOLD responses in the abnormal hemisphere, which was displaced due to the presence of the area of damage. In both cases, DTI tractography from the cluster of functional activation found clear connectivity distributions which circumvented the porencephalic cyst, and which were later consolidated at follow-up imaging at 1 year of age.

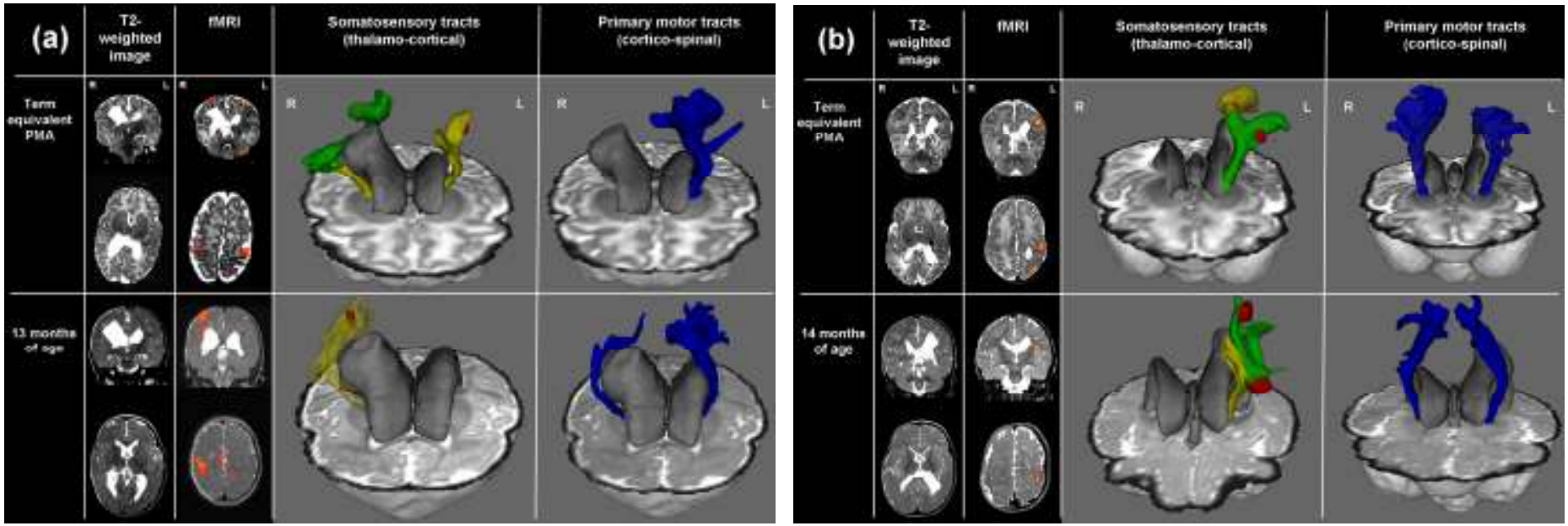

Figure 7.8: ***The combination of fMRI and DTI probabilistic tractography can offer new insights into the development of functional and structural activity following perinatal brain injury.*** Both infants were born preterm, and developed large porencephalic cysts following HPI in the perinatal period (on the right side in infant (a), and left in (b)). The infants were imaged at term equivalent PMA, and at approximately 1 year (corrected) of age. **(a):** ***In this infant at term age, right hand stimulation resulted in bilateral functional responses, with the derived tracts deviating around the cyst.*** A CST could not be delineated in the pathological hemisphere. At 13 months of age, functional responses are seen in the contralateral hemisphere only, with a thin CST; neurologically the infant has developed a dense right hemiplegia. **(b):** ***In this infant, functional responses are seen in the contralateral (left) hemisphere at term age, with the thalamo-cortical tracts passing over and around the left-sided porencephalic cyst***. There is relative preservation of the CST. At 14 months, functional responses are still seen on the left only. Although there is atrophy of the left thalamus, the PLIC is preserved, as evidenced by the symmetrical appearance of the CSTs, and the infant has had a good neurological outcome with mild asymmetry only.

Additional insights into early brain development and organisation may also come from characterising the functional and structural effects of pathology acquired at different developmental junctures, with greater patterns of plasticity seen in particular pathways in ex-preterm infants as adolescents (Johnston 2009, Staudt et al. 2010). Further work however, will be vital to investigate the effects of brain pathology (both acquired and congenital) on BOLD haemodynamic responses, and to assess the sensitivity and specificity of the technique as a potential biomarker of later outcome. Although the usefulness of aggressive rehabilitative therapy in this population remains controversial (Blauw-Hospers & Hadders-Algra 2005), the possible use of fMRI as a tool for monitoring the effectiveness of therapeutic intervention remains an exciting prospect.

7.4 Summary

This chapter highlights the potential that fMRI holds for adding striking new insights into our understanding of early human brain development and pathology. While the early results from these studies are far from conclusive, they importantly suggest that the findings of the main studies described in this thesis can be applied to further fMRI studies of the neonatal brain.

Chapter 8

8. Thesis Conclusions

The main findings of the work presented in the thesis were:

- Blood Oxygen Level Dependent (BOLD) contrast functional MRI (fMRI) can be used to identify robust, reproducible and well localised patterns of brain activity in human infants during the preterm period and through to term equivalent post-menstrual age.
- The typical amplitude of the induced BOLD response is positive in this population with a specific range of stimuli.
- The morphology of the Haemodynamic Response Function (HRF) in the neonatal period differs significantly from the canonical adult HRF.
- A systematic maturational trend exists in the parameters of the HRF during the neonatal period, which is likely due to developmental changes in neurovascular coupling.
- The application of an age-appropriate HRF into the data analysis significantly improves the identification of functional responses.

The work of this thesis was planned and carried out with the foremost goal to identify and address some of the possible sources of inconsistency in previously reported neonatal fMRI studies, and in doing so explore whether fMRI techniques could be applied to accurately and reliably characterise functional brain activity in early human life. This was achieved by firstly performing a systematic study with specific and targeted adaptations (including a custom designed somatosensory stimulus) in a cohort of preterm and term equivalent PMA infants; and then secondly by characterising the typical response to a brief stimulus, as knowledge of the underlying function (the HRF) is fundamental to fMRI methodology and data analysis. Together, these studies demonstrate that through a combination of appropriate study design, methodology, and analysis; reproducible and positive BOLD contrast responses can be identified in neonatal subjects. Furthermore, the BOLD contrast haemodynamic response to stimulation was found to be fundamentally different in early

life in comparison to the typical adult response, suggesting that the technique is both sensitive and specific enough to provide detailed information about early human brain development. Lastly, the promising early results of work in progress demonstrates the possibility that the findings can be applied to study neonatal brain activity with other forms of stimulation, and in subjects who have suffered perinatal brain injury.

It was clear when reviewing the literature of previously reported neonatal fMRI studies that the greatest unresolved issue has been that of “negative BOLD”, and specifically whether such responses are a normal developmental stage in early human infancy (Born et al. 1996, Yamada et al. 1997, 2000, Seghier et al. 2006). Whilst areas of negative BOLD are now recognised as a normal component of the functional response in adult fMRI studies, they are thought to represent complex integrative processes such as neural inhibition and modulation, rather than the primary response itself (Schmuel et al. 2006, Kastrup et al. 2008, Klingner et al. 2010, Schäfer et al. 2012). In contrast, in infants it has been postulated that a rapid rise in synaptic density in the first few months of postnatal life leads to an increased metabolic requirement which is insufficiently met by the vascular supply of oxygen, leading to an accumulation of d-Hb (and a negative BOLD response) in the primary area of activity (Born et al. 1996, Yamada et al. 2000, Muramoto et al. 2002). In the studies of this thesis, the predominant nature of the identified BOLD responses was positive. Furthermore, it was found that the HRF in early infancy has a significantly delayed but undoubtedly positive peak, with a marked negative post-stimulus undershoot evident at term equivalent PMA. Whilst previous studies in the literature have convolved the canonical HRF with the stimulation paradigm in a traditional GLM analysis, it was found here that the identification of functional activity is significantly altered by using an age-appropriate HRF. Thus, the ambiguous findings of the previously reported studies may in part be explained by the inappropriate assumption that the neonatal haemodynamic response would be identical to that of the mature adult.

A major contributor to the negative BOLD effect may have been that the imaging in a number of those historical studies was performed at 1.5 T, which would have led to a significantly reduced SNR, and a greater sensitivity to the intravascular (and particularly venous) compartment in which a delayed timecourse and accumulation of d-Hb may occur (Buxton et al. 1998, 2009, Krűger et al. 2001, Bianciardi et al. 2010). A possible way to formally quantify the intravascular contribution to the BOLD signal would be to add bipolar gradient pulses (as used in diffusion MR sequences) to suppress the signal derived from the rapidly flowing (and large displacing) blood in large vessels (Buxton 2009). It may also be that negative responses are specific to the visual system only, and occur only at a specific age; neither of which were directly studied in this thesis (Yamada et al. 1997, 2000, Muramoto et al. 2002, Seghier et al. 2004). An important insight may come through a characterisation of the underlying neurochemistry; as a recent series of intriguing studies have described a negative correlation in adults between the baseline level of GABA (as measured by MR-spectroscopy) and the amplitude and dispersion of the BOLD response (Muthukumaraswamy et al. 2009, 2012, Donahue et al. 2010). This effect may be of great pertinence to the neonatal brain, where certain receptor subtypes are relatively over-expressed, and GABA itself is conversely known to be the predominant excitatory neurotransmitter (Luján et al. 2005, Ben-Ari et al. 2007, Briggs & Galanopoulou 2011).

While every effort was made to account for all of the possible sources of inconsistency in the neonatal fMRI literature, there remain some unresolved issues which it was not possible to conclusively address. It may be possible to improve the SNR of the imaging sequence by quantifying T2* in the neonatal cortex at 3T; as it is generally considered to be maximised when the TE of the acquisition sequence is matched to the T2* value of the tissue of interest (Bandettini et al. 1994). Values have been found to be significantly raised in the neonatal period at 1.5T, but while this effect will certainly be less marked at higher B_0 strengths, such measurements have not formally been done in the neonatal brain (Bandettini et al. 1994, Rivkin et al. 2004, Harmer et al. 2012, Lee et al.

2012). A further prominent issue is the use of induced pharmacological sedation, which remains a controversial topic within the field. While possible neurotoxic effects have been implicated in animal studies with anaesthetic agents such as ketamine and isoflurane, at present there is no evidence to suggest that this is the case with milder agents such as the chloral hydrate used in this thesis (Mellon et al. 2007). Although it was found that chloral hydrate does not affect baseline CBF, there nevertheless remains the possibility that it has a direct effect on the local neurovascular coupling and the resultant vascular reactivity. However, it could be argued that the findings of this thesis are undoubtedly of operational value, as the use of sedation in infant MRI studies will likely be necessary until such a time that the imaging sequences and analysis techniques have sufficiently advanced to counteract the considerable confounding effects of subject head motion.

A number of studies have recently reported the collective use of multiple sources of functional MRI data; including the physiological manipulation and quantitative measurement of local CBF, CBV, and estimated $CMRO_2$, collectively known as "calibrated fMRI" (*reviewed in Hoge 2012*). While the considerable challenges inherent to imaging the neonatal brain mean that the implementation of such an approach is likely to be fraught with difficulty, the information it may provide could be crucial in definitively understanding the true physiology of neurovascular coupling and therefore the nature of BOLD responses in the neonatal brain. As an example, the measures of local CBF provided by ASL have been found to be as sensitive and perhaps even more specific than BOLD contrast, and therefore may be more representative of the coupled vascular response to neural activity (Hillman et al. 2007, Pimentel et al. 2011). Moreover, if true measures of the underlying vascular and metabolic parameters can be acquired, then it may be possible to put the neonatal BOLD response in context within a biophysical model of the BOLD response, or generate a new comprehensive model specific to the population (Buxton 2012).

An intrinsically attractive aspect of fMRI is that it has a number of attributes (in particular the quantitative nature of the BOLD signal, the relative experimental flexibility, and the reproducible dynamic signal properties across different subjects) which make it ideal for the application of higher level statistical testing and mathematical modelling. This has allowed the fMRI community to begin to attempt the complex process of accurately mapping and characterising the functional organisation of the brain, and furthermore to probe more issues such as the underlying patterns of connectivity between different regions at rest. Studying the architecture of functional activity in the resting brain is a compelling prospect in neonatal subjects, as emphasised by the findings that dramatic increases in inter-hemispheric and long range functional connectivity are seen with fMRI in preterm infants even over the short time period that corresponds to the third trimester of gestation (Doria et al. 2010, Smyser et al. 2010). It could even be postulated that a deeper understanding of the establishment and maturation of these "resting state networks" may hold the key to finally comprehending indistinct (but nevertheless fascinating) concepts such as "consciousness" and "self-awareness" in early human life (Lagercrantz 2009, Lagercrantz & Changeux 2009). Through the integration of information acquired from both fMRI and diffusion MRI studies, it is hoped that eventually a comprehensive model of brain "connectivity" in early human life can be constructed (as is being attempted currently in a large multi-centre study of 1200 adult subjects, dubbed the "human connectome project") (van Essen et al. 2011, van Essen & Ugurbil 2012). While such a major undertaking represents a truly daunting prospect, it would indisputably be a valuable future resource for both developmental neuroscience and clinical medicine alike.

An important consideration with respect to the information derived from BOLD fMRI is that it represents an indirect measure of neural activity over a relatively large "population" of neurons. To resolve this potential limitation, an essential but highly complex challenge in the coming years will be to successfully integrate information gained through multiple different neuroimaging modalities; each of which individually have long provided meaningful but limited information, but collectively

may hold the potential to providing a true “model” of brain function. As both measure temporal changes in the local haemodynamic response to neural activity, the highly complimentary nature of NIRS and BOLD fMRI is relatively easy to see (Huppert et al. 2006, Lloyd-Fox et al. 2010). No less important, but conceptually far more complex to do, will be amalgamating the findings of electrophysiological studies which are on a markedly different temporal and spatial scale to that of BOLD fMRI. While great advances have been described in the creation of algorithms which can provide accurate source localisation in EEG and MEG studies (He & Liu 2008, Brookes et al. 2012), an obstacle particular to neonatal subjects may arise due to the structurally immature (and physically smaller) brain. While these challenges may appear immense, the prospect of integrating such complex but complimentary information to provide a full model of functional brain activity from the cellular to system wide level is not only exciting for neuroscience, but is also likely to be integral to further advances in experimental and translational medicine.

Ultimately, it is hoped that the knowledge gained through the more widespread application of BOLD fMRI, will provide a much needed new perspective on the mechanisms of perinatal brain injury. The importance of this challenge is increasing, with the incidence of preterm birth continuing to rise in the developed world, with the survivors still found to have a markedly increased risk of developing later adverse neurodevelopmental outcome (Hintz et al. 2005b, Allen 2008, Ment et al. 2009, Volpe 2009b, Johnson & Marlow 2011). Although there have been encouraging decreases in the incidence of the severe brain lesions typically associated with prematurity, recent studies have identified a worrying trend towards an increased risk of learning, behavioural, and psychiatric disabilities in adulthood (Johnson & Marlow 2011, van Haastert et al. 2011, Nosarti et al. 2012, Sugiura et al. 2012). By way of the highly detailed and quantitative information it provides, and its non-invasive nature, MRI is ideal for studying the underlying mechanisms of preterm brain injury. In addition to providing a potentially powerful new way with which to learn about the underlying pathophysiology of perinatal brain injury, fMRI techniques may also represent a promising new biomarker for

predicting outcome and monitoring the effects of novel interventional therapies. Unfortunately, due to the time constraints of the thesis data collection period it was not possible to either collect neurodevelopmental follow-up data from the subjects in the studies, or attempt to correlate the findings of the functional data with eventual clinical outcome. However, such processes will be vital to know if the techniques can be utilised as biomarkers, and to put the findings in context.

In summary, the work described in this thesis has demonstrated that fMRI can be successfully applied to study brain activity in the newborn brain, and furthermore is capable of characterising key aspects of brain development. It is hoped that the findings of this thesis will provide a foundation on which further studies can be carried out; and that fMRI may make it possible to definitively answer fundamental questions about the establishment of functional brain activity, connectivity, and anatomy in the developing human brain. Furthemore, fMRI may be capable of providing much needed novel diagnostic and prognostic information, and ultimately may prove to be a valuable tool in clinical neurology of the newborn.

THESIS REFERENCES

Adibelli ZH, Songu M, Adibelli H, 2011. Paranasal sinus development in children: a magnetic resonance imaging analysis. American Journal of Rhinology & Allergy; 25(1): 30-5.

Aguirre GK, Zarahn E, D'Esposito M, 1998a. The inferential impact of global signal covariates in functional neuroimaging analyses. Neuroimage; 8(3): 302-6.

Aguirre GK, Zarahn E, D'Esposito M, 1998b. The variability of human, BOLD hemodynamic responses. Neuroimage; 8(4): 360-9.

Ajayi-Obe M, Saeed N, Cowan FM et al, 2000. Reduced development of cerebral cortex in extremely preterm infants. Lancet; 356(9236): 1162-3.

Aljabar P, Bhatia KK, Murgasova M et al, 2008. Assessment of brain growth in early childhood using deformation-based morphometry. Neuroimage; 39(1): 348-58.

Aljabar P, Wolz R, Srinivasan L et al, 2011. A combined manifold learning analysis of shape and appearance to characterize neonatal brain development. IEEE Transactions on Medical Imaging; 30(12): 2072-86.

Allen MC, 2002. Preterm outcomes research: a critical component of neonatal intensive care. Mental Retardation and Developmental Disabilities Research Reviews; 8(4): 221-33.

Allen MC, 2008. Neurodevelopmental outcomes of preterm infants. Current Opinion in Neurology; 21: 123-8.

Allison JD, Meador KJ, Loring DWm et al, 2000. Functional MRI cerebral activation and deactivation during finger movement, Neurology; 54(1): 135-42.

Altman DI, Powers WJ, Perlman JM et al, 1988. Cerebral blood flow requirement for brain viability in newborn infants is lower than in adults. Annals of Neurology; 24(2): 218-26.

Altman NR, Bernal B, 2001. Brain activation in sedated children: auditory and visual functional MR imaging. Radiology; 221(1): 56-63.

Amaro E, Barker G, 2006. Study design in fMRI: basic principles. Brain and Cognition; 60(3): 220-32.

Amato M, Fauchere JC, Hermann U Jr, 1988. Coagulation abnormalities in low birth weight infants with peri-intraventricular hemorrhage. Neuropediatrics; 19(3): 154-7.

Ambalavanan N, Carlo WA, 2006. Ventilatory strategies in the prevention and management of bronchopulmonary dysplasia. Seminars in Perinatology; 30(4): 192-9.

Amemiya S, Kunimatsu A, Saito N, Ohtomo K, 2012. Impaired hemodynamic response in the ischemic brain assessed with BOLD fMRI. Neuroimage; 61(3): 579-90.

Ancel PY, Livinec F, Larroque B et al, 2006. Cerebral Palsy among very preterm children in relation to gestational age and neonatal ultrasound abnormalities: the EPIPAGE cohort study. Pediatrics; 117(3): 828-35.

Anderson AW, Marois R, Colson ER et al, 2001. Neonatal auditory activation detected by functional magnetic resonance imaging. Magnetic Resonance Imaging; 19(1): 1-5.

Anjari M, Srinivasan L, Allsop JM et al, 2007. Diffusion tensor imaging with tract-based spatial statistics reveals local white matter abnormalities in preterm infants. Neuroimage; 35(3): 1021-7.

Anjari M, Counsell SJ, Srinivasan L et al, 2009. The association of lung disease with cerebral white matter abnormalities in preterm infants. Pediatrics; 124(1): 268-76.

Aoyama S, Toshima T, Saito Y et al, 2010. Maternal breast milk odour induces frontal lobe activation in neonates: a NIRS study. Early Human Development; 86(9): 541-5.

Aronica E, Iver A, Zurolo E, Gorter JA, 2011. Ontogenic modifications of neuronal excitability during brain maturation: Developmental changes of neurotransmitter receptors. Epilepsia; 52(s8): 3-5.

Armstrong D, Norman MG, 1974. Periventricular leucomalacia in neonates: complications and sequelae. Archives of Disease in Childhood; 49: 367-77.

Armstrong E, Schleicher A, Omran et al, 1995. The ontogeny of human gyrification. Cerebral Cortex; 5(1): 56-63.

Ashburner J, 2012. SPM: a history. Neuroimage; 62(2): 791-80.

Assaf M, Jagannathan K, Calhoun VD et al, 2010. Abnormal functional connectivity of default mode sub-networks in autism spectrum disorder patients. Neuroimage; 53(1): 247-56.

Attwell D, Iadecola C, 2002. The neural basis of functional brain imaging signals. Trends in Neuroscience; 25(12): 621-5.

Attwell D, Gibb A, 2005. Neuroenergetics and the kinetic design of excitatory synapses. Nature Reviews Neuroscience; 6: 841-9.

Attwell D, Buchan AM, Charpak S, Lauritzen M et al, 2010. Glial and neuronal control of brain blood flow. Nature; 468: 232-43.

Avlonitou E, Balatsouras DG, Margaritis E et al, 2011. Use of chloral hydrate as a sedative for auditory brainstem response testing in a pediatric population. International Journal of Pediatric Otorhinolaryngology; 75(6): 760-3.

Ball G, Counsell SJ, Anjari M et al, 2010. An optimized tract-based spatial statistics protocol for neonates: applications to prematurity and chronic lung disease. Neuroimage; 53(1): 94-102.

Ball G, Boardman JP, Rueckert D et al, 2011. The effect of preterm birth on thalamic and cortical development. Cerebral Cortex; 22(5): 1016-24.

Bandettini PA, Wong EC, Hinks RS et al, 1992. Time course EPI of human brain function during task activation. Magnetic Resonance in Medicine; 25(2): 390-7.

Bandettini PA, Jesmanowicz A, Wong EC, Hyde JS, 1993. Processing strategies for time-course data sets in functional MRI of the human brain. Magnetic Resonance in Medicine; 30: 161-73.

Bandettini PA, Wong EC, Jesmanowicz A et al, 1994. Spin-echo and gradient-echo EPI of human brain activation using BOLD contrast: a comparative study at 1.5T. NMR in Biomedicine; 7(1-2): 12-20.

Bandettini PA, Cox RW, 2000. Event-related fMRI contrast when using constant interstimulus interval: theory and experiment. Magnetic Resonance in Medicine; 43: 540-8.

Bandettini PA, 2001. Selection of the optimal pulse sequence for functional MRI. (*Chapter 6*) In: Jezzard P, Matthews PM, Smith SM (eds), 2001. Functional MRI an introduction to methods. Oxford University Press; New York, USA.

Banker BQ, Larroche JL, 1962. Periventricular leukomalacia in infancy: a form of neonatal anoxic encephalopathy. Archives of Neurology; 7: 386-410.

Barkovich AJ, 1998. MR of the normal neonatal brain: assessment of deep structures. American Journal of Neuroradiology; 19: 1397-403.

Bassi L, Ricci D, Volzone A et al, 2008. Probabilistic diffusion tractography of the optic radiations and visual function in preterm infants at term equivalent age. Brain; 131(pt2): 573-82.

Bassi L, Chew A, Merchant N et al, 2011. Diffusion tensor imaging in preterm infants with punctuate white matter lesions. Pediatric Research; 69(6): 561-9.

Basu A, Graziadio S, Smith M et al, 2010. Developmental plasticity connects visual cortex to motorneurons after stroke. Annals of Neurology; 67(1): 132-6.

Battin MR, Maalouf EF, Counsell SJ et al, 1998. Magnetic resonance imaging of the brain in very preterm infants: visualization of the germinal matrix, early myelination, and cortical folding. Pediatrics; 101(6): 957-62.

Battin MR, Rutherford MA, 2002. Magnetic resonance imaging of the brain in preterm infants: 24 weeks' gestation to term (*chapter 3*). In: Rutherford MA, 2002-12. MRI of the Neonatal Brain. http://www.mrineonatalbrain.com/

Bax M, 1964. Terminology and classification of cerebral palsy. Developmental Medicine and Child Neurology; 6: 295-7.

Bax M, Goldstein M, Rosenbaum P et al. 2005. Proposed definition and classification of cerebral palsy, April 2005. Developmental Medicine and Child Neurology; 47: 571-6.

Beaino G, Khoshnood B, Kaminski M et al, 2010. Predictors of cerebral palsy in very preterm infants: the EPIPAGE prospective population-based cohort study. Developmental Medicine and Child Neurology; 52(6): e119-25.

Beckmann CF, Jenkinson M, Smith SM, 2003. General multilevel linear modeling for group analysis in fMRI. Neuroimage; 20: 1052-63.

Beckmann CF, Smith SM, 2004. Probabilistic Independent Component Analysis for Functional Magnetic Resonance Imaging. IEEE Transactions on medical imaging; 23(2): 137-52.

Beckmann CF, De Luca M, Devlin JT, Smith SM, 2005. Investigations into resting-state connectivity using independent component analysis. Philosophical Transactions of the Royal Society B: Biological Sciences; 360(1457): 1001-13.

Beckmann CF, 2012. Modeling with independent components. Neuroimage; 62(2): 891-901.

Beecham J, O-Neill T, Goodman R, 2001. Supporting young adults with hemiplegia: services and costs. Healthy and Social Care in the Community; 9(1): 51-9.

Behrens TEJ, Johansen-Berg H, Woolrich MW et al, 2003a. Non-invasive mapping of connections between human thalamus and cortex using diffusion imaging. Nature Neuroscience; 6(7): 750-7.

Behrens TEJ, Woolrich MW, Jenkinson M et al, 2003b. Characterization and propagation of uncertainty in diffusion-weighted MR imaging. Magnetic Resonance in Medicine; 50(5): 1077-88.

Behrens TEJ, Johansen Berg H, Jbabdi S, Rushworth MFS, Woolrich MW, 2007. Probabilistic diffusion tractography with multiple fibre orientations: what can we gain. Neuroimage; 34(1): 144-55.

Behzadi Y, Liu TT, 2006. Caffeine reduces the initial dip in the visual response at 3T. Neuroimage; 32: 9-15.

Belliveau JW, Kennedy DN Jr, McKinstry RC et al, 1991. Functional mapping of the human visual cortex by magnetic resonance imaging. Science; 254(5032): 716-9.

Ben-Ari Y, Gaiarsa JL, Tyzio R, Khazipov R, 2007. GABA: a pioneer transmitter that excites immature neurons and generates primitive oscillations. Physiology Reviews; 87(4): 1215-84.

Ben Bashat D, Ben Sira L, Graif M et al, 2005. Normal white matter development from infancy to adulthood: comparing diffusion tensor and high b value diffusion weighted MR images. Journal of Magnetic Resonance Imaging; 21(5): 503-11.

Bhadwaj RD, Curtis MA, Spalding KL et al, 2006. Neocortical neurogenesis in humans is restricted to development. Proceedings of the National Academy of Sciences USA; 103(33): 12564-8.

Bianciardi M, Fukunaga M, van Gelderen P, de Zwart JA, Duyn DH, 2010. Negative BOLD-fMRI signals in large cerebral veins. Journal of Cerebral Blood Flow & Metabolism; 31(2): 401-12.

Bingham PM, Churchill D, Ashikaga T, 2007. Breast milk odor via olfactometer for tube-fed, premature infants. Behavioural Research Methods; 39(3): 630-4.

Biswal B, Yetkin FZ, Haughton VM, Hyde JS, 1995. Functional connectivity in the motor cortex of resting human brain using echo-planar MRI. Magnetic Resonance In Medicine; 34(4): 537-41.

Blair E, Watson L, 2006. Epidemiology of Cerebral Palsy. Seminars in Fetal and Neonatal medicine; 11(2): 117-125.

Blasi A, Mercure E, Lloyd-Fox S et al, 2011. Early specialization for voice and emotion processing in the infant brain. Current Biology; 21:1-5.

Blauw-Hospers CH, Hadders-Algra M, 2005. A systematic review of the effects of early intervention on motor development. Developmental Medicine & Child Neurology; 37: 421-32.

Boardman JP, Counsell SJ, Rueckert D et al, 2006. Abnormal deep grey matter development following preterm birth detected using deformation-based morphometry. Neuroimage; 32: 70-8.

Boardman JP, Counsell SJ, Rueckert D et al, 2007. Early growth in brain volume is preserved in the majority of preterm infants. Annals of Neurology; 62(2): 185-92.

Boardman JP, Craven C, Valappil S et al, 2010. A common neonatal image phenotype predicts adverse neurodevelopmental outcome in children born preterm. Neuroimage; 52: 409-14.

Bonakdarpour B, Parrish TB, Thompson CK, 2007. Hemodynamic response function in patients with stroke-induced aphasia: implications for fMRI data analysis. Neuroimage; 36: 322-31.

Born AP, Miranda MJ, Rostrup E et al, 2000. Functional Magnetic Resonance imaging of the normal and abnormal visual system in early life. Neuropediatrics; 31: 24-32.

Born AP, Law I, Lund TE et al, 2002a. Cortical Deactivation induced by visual stimulation in human slow-wave sleep. Neuroimage; 17: 1325-35.

Born AP, Rostrup E, Miranda MJ et al, 2002b. Visual cortex reactivity in sedated children examined with perfusion MRI (FAIR). Magnetic Resonance Imaging; 20(2): 199-205.

Born P, Rostrup E, Leth H et al, 1996. Change of visually induced cortical activation patterns during development. Lancet; 347(9000): 543.

Born P, Leth H, Miranda MJ et al, 1998. Visual activation in infants and young children studied by functional magnetic resonance imaging. Pediatric Research; 44(4): 578-83.

Bourgeois JP, Jastreboff P, Rakic P, 1989. Synaptogenesis in the visual cortex of normal and preterm monkeys: evidence for intrinsic regulation of synaptic overproduction. Proceedings of the National Academy of Sciences USA; 86: 4297-301.

Boynton GM, Engel SA, Glover GH, Heeger DJ, 1996. Linear systems analysis of functional magnetic resonance imaging in human V1. The Journal of Neuroscience; 16(13): 4207-21.

Brammer MJ, 2001. Head motion and its correction. (*Chapter 13*) In: Jezzard P, Matthews PM, Smith SM (eds), 2001. Functional MRI an introduction to methods. Oxford University Press; New York, USA.

Brenner S, Sejnowski TJ, 2011. Understanding the Human Brain. Science; 334(4): 567.

Brett M, Johnsrude IS, Owen AM, 2002. The problem of functional localization in the human brain. Nature Review Neuroscience; 3: 243-9.

Briggs SW, Galanopoulou AS, 2011. Altered GABA signalling in early life epilepsies. Neural Plasticity; 2011: 527605.

Broitman E, Ambalavan N, Higgins RD, et al, 2007. Clinical data predict neurodevelopmental outcome better than head ultrasound in extremely low birth weight infants. Journal of Pediatrics; 151: 500-5.

Brookes MJ, Woolrich MW, Barnes GR, 2012. Measuring functional connectivity in MEG: a multivariate approach insensitive to linear source leakage. Neuroimage; (*epub ahead of print; PMID: 22484306*).

Broser P, Vargha-Khadem F, Clark CA, 2011. Robust subdivision of the thalamus in children based on probability distribution functions calculated from probabilistic tractography. Neuroimage; 57(2): 403-15.

Brouwer A, Groenendaal F, van Haastert IL et al, 2008. Neurodevelopmental outcome of preterm infants with severe intraventricular hemorrhage and therapy for post-hemorrhagic ventricular dilatation. Journal of Pediatrics; 152(5): 648-54.

Buckner RL, Bandettini PA, O'Craven KM et al, 1996. Detection of cortical activation during averaged single trials of cognitive task using functional magnetic resonance imaging. Proceedings of the National Academy of Sciences USA; 93(25): 14878-83.

Buckner RL, Andrews-Hanna JR, Schacter DL, 2008. The brain's default network: anatomy, function, and relevance to disease. Annals of the New York Academy of Sciences; 1124: 1-38.

Buijs PC, Krabbe-Hartkamp MJ, Bakker CJ et al, 1998. Effect of age on cerebral blood flow: measurement with ungated two-dimensional phase-contrast MR angiography in 250 adults. Radiology; 209: 667-74.

Bullmore E, Brammer M, Williams S et al, 1996. Statistical methods of estimation and inference for functional MR image analysis. Magnetic Resonance in Medicine; 35: 261-77.

Bullmore E, Sporns O, 2012. The economy of brain network organization. Nature Reviews Neuroscience; 13: 336-49.

Buxton RB, Wong EC, Frank LR, 1998. Dynamics of blood flow and oxygenation changes during brain activation: the balloon model. Magnetic Resonance in Medicine; 39: 855-64.

Buxton RB, Uludag K, Dubowitz D, Liu TT, 2004. Modeling the hemodynamic response to brain activation. Neuroimage; 23: s220-s233.

Buxton RB, 2009. Introduction to functional magnetic resonance imaging (2nd edition). Cambridge University Press; New York, USA.

Buxton RB, 2012. Dynamic models of BOLD contrast. Neuroimage; 62(2): 953-61.

Bystron I, Blakemore C, Rakic P, 2008. Development of the human cerebral cortex: Boulder Committee revisited. Nature Reviews Neuroscience; 9: 110-22.

Cardoso MMB, Sirotin YB, Lima B, Glushenkova E, Das A, 2012. The neuroimaging signal is a linear sum of neurally distinct stimulus- and task-related components. Nature Neuroscience; 15(9): 1298-308.

Carmignoto G, Gomez-Gonzalo M, 2009. The contribution of astrocyte signaling to neurovascular coupling. Brain Research Reviews; 63: 138-48.

Carusone LM, Srinivasan J, Gitelman DR, 2002. Hemodynamic response changes in cerebrovascular disease: implications for functional MR Imaging. American Journal of Neuroradiology; 23: 1222-8.

Cauli B, Hamel E, 2010. Revisiting the role of neurons in neurovascular coupling. Frontiers in Neuroenergetics; 2: 1-8.

Chan KC, Xing K, Cheung MM, Zhou IY, Wu EX, 2010. Functional MRI of postnatal visual development in normal and hypoxic-ischemic-injured superior colliculi. Neuroimage 49(3): 2013-20.

Chen JJ, Pike GB, 2009a. Origins of the BOLD post-stimulus undershoot. Neuroimage; 46: 559-68.

Chen J, Pike GB, 2009b. BOLD-specific cerebral blood volume and blood flow changes during neuronal activation in humans. NMR in Biomedicine; 22: 1054-1062.

Chen J, Pike GB, 2010a. Global cerebral oxidative metabolism during hypercapnia and hypocapnia in humans: implications for BOLD MRI. Journal of Cerebral Blood Flow and Metabolism; 30(6): 1094-9.

Chen J, Pike GB, 2010b. MRI measurement of the BOLD-specific flow-volume relationship during hypercapnia and hypocapnia in humans. Neuroimage; 53(2): 383-91.

Chen Y, Parrish TB, 2009. Caffeine dose effect on activation-induced BOLD and CBF responses. Neuroimage; 46(3): 577-83.

Cheong JL, Thompson DK, Wang HX et al, 2009. Abnormal white matter signal on MR imaging is related to abnormal tissue microstructure. American Journal of Neuroradiology; 30(3): 623-8.

Chi JG, Dooling EC, Gilles FH, 1977. Gyral development of the human brain. Annals of Neurology; 1: 86-93.

Chugani HT, Phelps ME, 1986. Maturational changes in cerebral function in infants determined by 18FDG positron emission tomography. Science; 231(4740): 840-3.

Civardi E, Tzialla C, Garofoli F et al, 2011. Nutritional needs of premature infants. Journal of Maternal-Fetal and Neonatal Medicine; 24(supp1): 27-9.

Clancy B, Darlington RB, Finlay BL, 2001. Translating developmental time across mammalian species. Neuroscience; 105(1): 7-17.

Cohen ER, Ugurbil K, Kim SG, 2002. Effect of basal conditions on the magnitude and dynamics of the blood oxygenation level-dependent fMRI response. Journal of Cerebral Blood Flow and Metabolism; 22(9): 1042-53.

Colonnese MT, Philips MA, Constanine-Paton M et al, 2008. Development of hemodynamic responses and functional connectivity in rat somatosensory cortex. Nature Neuroscience; 11(1): 72-9.

Constable RT, Ment LR, Vohr BR et al, 2008. Prematurely born children demonstrate white matter microstructural differences at 12 years of age, relative to term control subjects: an investigation of group and gender effects. Pediatrics; 121(2): 306-16.

Constantine-Paton M, 2008. Pioneers of cortical plasticity: six classic papers by Wiesel and Hubel. Journal of Neurophysiology; 99(6): 2741-4.

Cornette LG, Tanner SF, Ramenghi LA et al, 2002. Magnetic resonance imaging of the infant brain: anatomical characteristics and clinical significance of punctate lesions. Archives of Disease in Childhood Fetal Neonatal Edition; 86: F171-7.

Counsell SJ, Kennea NL, Herlihy AM et al, 2003. T2 relaxation values in the developing preterm brain. American Journal of Neuroradiology; 24: 1654-60.

Counsell SJ, Shen Y, Boardman JP et al, 2006. Axial and radial diffusivity in preterm infants who have diffuse white matter changes on magnetic resonance imaging at term-equivalent age. Pediatrics; 117(2): 376-86.

Counsell SJ, Dyet LE, Larkman DJ et al, 2007. Thalamo-cortical connectivity in children born preterm mapped using probabilistic magnetic resonance tractography. Neuroimage; 34: 896-904.

Counsell SJ, Edwards AD, Chew AT et al, 2008. Specific relations between neurodevelopmental abilities and white matter microstructure in children born preterm. Brain; 131(12): 3201-8.

Cowan FM, 2002. Magnetic Resonance Imaging of the normal brain: term to 2 years (*Chapter 4*). In: Rutherford MA, 2002-12. MRI of the Neonatal Brain. http://www.mrineonatalbrain.com/

Cox RW, 2012. AFNI: what a long strange trip it's been. Neuroimage; 62(2): 743-7.

Dale AM, Buckner RL, 1997. Selective averaging of rapidly presented individual trials using fMRI. Human Brain Mapping; 5: 329-40.

Dale AM, 1999. Optimal experimental design for event-related fMRI. Human Brain-Mapping; 8(2-3): 109-14.

Dechent P, Schutze G, Helms G et al, 2011. Basal cerebral blood volume during the poststimulation undershoot in BOLD MRI of the human brain. Journal of Cerebral Blood Flow and Metabolism; 31: 82-89.

de Graaf-Peters VB, Hadders-Algra M, 2006. Ontogeny of the human central nervous system: What is happening when? Early Hum Dev 82: 257-66.

Dehaene-Lambertz G, Dehaene S, Hertz-Palmer L, 2002. Functional Neuroimaging of speech perception in infants. Science; 298(5600): 2013-5.

de Kieviet JF, Zoetebier L, van Elburg RM et al, 2012. Brain development of very preterm and very low-birthweight children in childhood and adolescence. Developmental Medicine and Child Neurology; 54(4): 313-23.

Delpy DT , Cope MC, Cady EB et al, 1987. Cerebral monitoring in newborn infants by magnetic resonance and near infrared spectroscopy. Scandinavian Journal of Clinical & Laboratory Investigation Supplement; 188: 9-17.

Deng W, Pleasure J, Pleasure D, 2008. Progress in Periventricular Leukomalacia. Archives of Neurology; 65(10: 1291-5.

Deoni SC, 2010. Quantitative relaxometry of the brain. Topics in Magnetic Resonance Imaging; 21(2): 101-13.

Deoni SCL, Mercure E, Blasi A et al, 2011. Mapping infant brain myelination with Magnetic Resonance Imaging. The Journal of Neuroscience; 31(2): 784-91.

D'Esposito M, Zarahn E, Aguirre GK, Rypma B, 1999. The effect of normal aging on the coupling of neural activity to the BOLD hemodynamic response. Neuroimage; 10: 6-14.

D'Esposito M, Deouell LY, Gazzaley A, 2003. Alterations in the BOLD fMRI signal with ageing and disease: a challenge for neuroimaging. Nature Reviews Neuroscience; 4: 863-72.

Devor A, Tian P, Nishimura N et al, 2007. Suppressed neuronal activity and concurrent arteriolar vasoconstriction may explain negative blood oxygenation level-dependent signal. The Journal of Neuroscience; 27(16): 4452-9.

de Vries LS, Eken P, Pierrat V, Daniels H, Casaer P, 1992. Prediction of neurodevelopmental outcome in the preterm infants: short latency cortical somatosensory evoked potentials compared with cranial ultrasound. Archives of Disease in Childhood; 67: 1177-81.

de Vries LS, Roelants-Van Rijn AM, Rademaker KJ et al, 2001. Unilateral parenchymal haemorrhagic infarction in the preterm infant. European Journal of Pediatric Neurology; 5: 139-149.

de Vries LS, Groenendaal F, Meiners LC, 2002. Ischaemic lesions in the preterm brain. (*Chapter 8*) In: Rutherford MA, 2002-12. MRI of the Neonatal Brain. http://www.mrineonatalbrain.com/

de Vries LS, van Haastert IL, Rademaker C et al, 2004. Ultrasound abnormalities preceding cerebral palsy in high-risk preterm infants. Journal of Pediatrics; 144: 815-20.

Dhavan R, Tsai LH, Tsai LH, 2001. A decade of CDK5. Nature Reviews Molecular Cell Biology; 2: 749-59.

Donahue MJ, Near J, Blicher JU, Jezzard P, 2010. Baseline GABA concentration and fMRI response. Neuroimage; 53: 392-8.

Donaldson DL, Buckner RL, 2001. Effective paradigm design. (*Chapter 9*) In: Jezzard P, Matthews PM, Smith SM (eds), 2001. Functional MRI an introduction to methods. Oxford University Press; New York, USA.

Doria V, Beckmann CF, Arichi T et al, 2010. Emergence of resting state networks in the preterm human brain. Proceedings of the National Academy of Sciences USA; 107(46): 20015-20.

Doyle LW, 2010. Adult Outcome of Extremely Preterm Infants. Pediatrics; 126(2): 342-351.

Dubois J, Benders M, Cachia A et al, 2008. Mapping the early cortical folding process in the preterm newborn brain. Cerebral Cortex; 18(6): 1444-54.

Dudink J, Kerr JL, Paterson K, Counsell SJ, 2008. Connecting the developing preterm brain. Early Human Development; 84(12): 777-82.

Dyet LE, Kennea N, Counsell SJ et al 2006. Natural history of brain lesions in extremely preterm infants studied with serial magnetic resonance imaging from birth and neurodevelopmental assessment. Pediatrics; 118: 536-48.

Edwards AD, Wyatt JS, Richardson et al, 1988. Cotside measurement of cerebral blood flow in ill newborn infants by near infrared spectroscopy. Lancet; 2(8614): 770-1.

Edwards AD, Arthurs OJ, 2011. Paediatric MRI under sedation: is it necessary? What is the evidence for the alternatives. Pediatric Radiology; 41: 1353-64.

Eichenwald EC, Stark AR, 2008. Management and outcomes of very low birth weight. The New England Journal of Medicine; 358: 1700-11.

Elster AD, 1994. Questions and Answers in Magnetic Resonance Imaging. Mosby; St. Louis MI, USA.

Elwell CE, Cope M, Delpy DT, 1997. An analytical model for determining cerebrovascular transit time using Near Infrared Spectroscopy. Advances in Experimental Medicine and Biology; 428: 561-8.

Encha-Razavi F, Sonigo P, 2003. Features of the developing brain. Child's Nervous System; 19: 426-8.

Erberich SG, Freidlich P, Seri I et al, 2003. Functional MRI in neonates using neonatal head coil and MR compatible incubator. Neuroimage; 20(2): 683-92.

Erberich SG, Panigrahy A, Freidlich P et al, 2006. Somatosensory lateralization in the newborn brain. Neuroimage; 29(1): 155-61.

Ernst T, Henning J, 1994. Observation of a fast response in functional MR. Magnetic Resonance in Medicine; 32: 146-9.

Eroglu C, Barres BA, 2010. Regulation of synaptic connectivity by glia. Nature; 468: 223-31.

Eyre JA, 2007. Corticospinal tract development and its plasticity after perinatal injury. Neuroscience & Biobehavioural Reviews; 31(8): 1136-49.

Fair DA, Brown TT, Petersen SE, Schlagger BL, 2006. fMRI reveals novel functional neuroanatomy in a child with perinatal stroke. Neurology; 67(12): 2246-9.

Ferrari F, Todeschini A, Guidotti I et al, 2011. General movements in full-term infants with perinatal asphyxia are related to basal ganglia and thalamic lesions. Journal of Pediatrics; 158(6): 904-11.

Finger S, 2004. Paul Broca (1824-1880). Journal of neurology; 251: 769-70.

Fitzgerald M, 2005. The development of nociceptive circuits. Nature Reviews Neuroscience; 6: 507-520.

Fox PT, Raichle ME, 1986. Focal physiological uncoupling of cerebral blood flow and oxidative metabolism during somatosensory stimulation in human subjects. Proceedings of the National Academy of Sciences USA; 83(4): 1140-4.

Fox K, Wong ROL, 2005. A comparison of experience-dependent plasticity in the visual and somatosensory systems. Neuron; 48: 465-477.

Frahm J, Kruger G, Merboldt KD, Kleinschmidt A, 1996. Dynamic uncoupling and recoupling of perfusion and oxidative metabolism during focal brain activation in man. Magnetic Resonance in Medicine; 35: 143-8.

Frahm J, Baudewig J, Kallenberg K et al, 2008. The post-stimulation undershoot in BOLD fMRI of human brain is not caused by elevated cerebral blood volume. Neuroimage; 40: 473-81.

Franceschini MA, Thaker S, Themelis G et al, 2007. Assessment of infant brain development with frequency-domain near-infrared spectroscopy. Pediatric Research; 61: 546-51.

Fransson P, Skiöld BM, Horsch S et al, 2007. Resting-state networks in the infant brain. Proceedings of National Academy of Science USA; 104(39): 15531-6.

Fransson P, Skiold BM, Engstrom M et al, 2009. Spontaneous brain activity in newborn brain during natural sleep – an fMRI study in infants born at full term. Pediatric Research; 66(3): 301-5.

Fransson P, Aden U, Blennow M, Lagercrantz H, 2011. The functional architecture of the infant brain as revealed by resting-state fMRI. Cerebral Cortex; 21(1): 145-54.

Friston KJ, Jezzard P, Turner R, 1994a. Analysis of Functional MRI time-series. Human Brain Mapping; 1: 153-71.

Friston KJ, Worsley K, Frackowiak R et al, 1994b. Assessing the significance of focal activation using their spatial extent. Human Brain Mapping; 1: 214-20.

Friston KJ, Ashburner J, Firth CD et al, 1995a. Spatial registration and normalization of images. Human Brain Mapping; 2: 165-89.

Friston KJ, Frith CD, Turner R, Frackowiak RSJ, 1995b. Characterizing evoked hemodynamics with fMRI. Neuroimage; 2: 157-65.

Friston KJ, Holmes A, Worsley K et al, 1995c. Statistical parametric maps in functional imaging: a general linear approach. Human Brain Mapping; 2: 189-210.

Friston KJ, Williams S, Howard R et al, 1996. Movement-related effects in fMRI time-series. Magnetic Resonance in Medicine; 35(3): 346-55.

Friston KJ, Fletcher P, Josephs O et al, 1998a. Event-related fMRI: characterizing differential responses. Neuroimage; 7; 30-40.

Friston KJ, Josephs O, Rees G, Turner R, 1998b. Non-linear event-related responses in fMRI. Magnetic Resonance in Medicine; 39: 41-52.

Frith CD, 2007. Making up the mind. Blackwell Publishing; Malden MA, USA.

Galliard WD, Hertz-Pannier L, Mott SH et al, 2000. Functional anatomy of cognitive development: fMRI of verbal fluency in children and adults. Neurology; 54: 180-5.

Galliard WD, Grandon CB, Xu B, 2001. Developmental Aspects of Pediatric fMRI: considerations for image acquisition, analysis, and interpretation. Neuroimage; 13: 239-249.

Gao W, Zhu H, Giovanello KS et al, 2009. Evidence on the emergence of the brain's default network from 2-week-old to 2-year old healthy pediatric subjects. Proceedings of the National Academy of Sciences USA; 106(16): 6790-5.

Gao W, Gilmore JH, GiovanelloKS et al, 2011. Temporal and spatial evolution of brain network topology during the first two years of life. PLoS One; 6(9): e25278.

Gao W, Gilmore JH, Shen D et al, 2012. The synchronization within and interaction between the default and dorsal attention networks in early infancy. Cerebral Cortex; (*epub ahead of print, PMID: 22368080*)

Garey LJ, 1999. Brodmann's "localisation in the cerebral cortex". Imperial College Press; London, UK.

Garrity AG, Pearlson GD, McKiernan K et al, 2007. Aberrant "default mode" functional connectivity in schizophrenia. American Journal of Psychiatry; 164(3): 450-7.

Gassert R, Burdet E, Chinzei K, 2008. Opportunities and challenges in MR-compatible robotics: reviewing the history, mechatronic components, and future directions of this technology. IEEE Engineering in Medicine and Biology Magazine; 27(3): 15-22.

Geng X, Gouttard S, Sharma A et al, 2012. Quantitative tract-based white matter development from birth to age 2 years. Neuroimage; 61: 542-57.

Genovese CR, Lazar NA, Nichols TE, 2002. Thresholding of statistical maps in functional neuroimaging using the false discovery rate. Neuroimage; 15(4): 870-8.

George SR, Taylor MJ, 1991. Somatosensory evoked potentials in neonates and infants: developmental and normative data. Electroencephalography and clinical Neurophysiology; 80: 94-102.

Gibson NA, Graham M, Levene MI, 1992. Somatosensory evoked potentials and outcome in perinatal asphyxia. Archives of disease in Childhood; 67: 393-8.

Gilles FH, 2001. Telencephalic angiogenesis: a review. Developmental Medicine and Child Neurology; 86: 3-5.

Gilmore EC, Herrup K, 2001. Neocortical cell migration: GABAergic neurons and cells in layers I and VI move in a cycline-dependent kinase 5-independent manner. Journal of Neuroscience; 21(24): 9690-700.

Giminez C, Junque A, Narberhaus A et al, 2006. White matter volume and concentration reductions in adolescents with history of very preterm birth: a voxel-based morphometry study. Neuroimage; 32: 1485-98.

Gjedde A, 2001. Brain energy metabolism and the physiological basis of the haemodynamic response. (*Chapter 2*) In: Jezzard P, Matthews PM, Smith SM (eds), 2001. Functional MRI an introduction to methods. Oxford University Press; New York, USA.

Glover GH, 1999. Deconvolution of impulse response in event-related BOLD fMRI. Neuroimage; 9: 416-29.

Goebel R, 2012. BrainVoyager – Past, present, future. Neuroimage; 62(2): 748-56.

Greisen G, 1986. Cerebral blood flow in preterm infants during the first few weeks of life. Acta Paediatrica Scandinavia; 75(1): 43-51.

Griffeth VE, Buxton RB, 2011. A theoretical framework for estimating cerebral oxygen metabolism changes using the calibrated-BOLD method: modeling the effects of blood volume distribution, hematocrit, oxygen extraction fraction. And tissue signal properties on the BOLD signal. Neuroimage; 58: 198-212.

Groenendaal F, Termote JU, van der Heide-Jalving M et al, 2010. Complications affecting preterm neonates from 1991 to 2006: what have we gained? Acta Paediatrica; 99(3): 354-8.

Groppo M, Ricci D, Bassi L et al, 2012. Development of the optic radiations and visual function after premature birth. Cortex: (*epub ahead of print, PMID: 22482694*).

Grubb RL Jr, Raichle ME, Eichling JO, Ter-Pogossian MM, 1974. The effects of changes in PaCO2 on cerebral blood volume, blood flow, and vascular mean transit time. Stroke; 5(5): 630-9.

Gu H, Stein EA, Yang Y, 2005. Nonlinear responses of cerebral blood volume, blood flow and blood oxygenation during visual stimulation. Magnetic Resonance Imaging; 23(9): 921-8.

Guzzetta A, Staudt M, Petacchi E et al, 2007. Brain representation of active and passive hand movements in children. Pediatric Research; 61(4): 485-90.

Habas PA, Scott JA, Roosta A et al, 2012. Early folding patterns and asymmetries of the normal human brain detected from in utero MRI. Cerebral Cortex; 22(1): 13-25.

Hack M. Adult outcomes of preterm children, 2009. Journal of Developmental and Behavioural Pediatrics; 30(5): 460-70.

Hadders-Algra M, Groothuis AMC, 1999. Quality of general movements in infancy is related to the development of neurological dysfunction, attention deficit hyperactivity disorder and aggressive behavior. Developmental Medicine and Child Neurology; 41: 381-91.

Hadders-Algra M, 2004. General movements: a window for early identification of children at high risk for developmental disorders. Journal of Pediatrics; 145: S12-18.

Hadders-Algra M, 2011. Challenges and limitations in early intervention. Developmental Medicine and Child Neurology; 53(s4): 52-55.

Hagmann CF, de Vita E, Bainbridge A et al, 2009. T2 at MR imaging is an objective quantitative measure of cerebral white matter signal intensity abnormality in preterm infants at term-equivalent age. Radiology; 252(1): 209-17.

Hajnal JV, Myers R, Oatridge A et al, 1994. Artifacts due to stimulus-correlated motion in functional images of the brain. Magnetic Resonance Imaging in Medicine; 31: 283-91.

Hamandi K, Laufs H, Nöth U et al, 2008. BOLD and perfusion changes during epileptic generalised spike wave activity. Neuroimage; 39(2): 608-18.

Hamrick SEG, Miller SP, Leonard C et al, 2004. Trends in severe brain injury and neurodevelopmental outcome in premature newborn infants: the role of cystic periventricular leukomalacia. The Journal of Pediatrics; 145(4): 593-9.

Handwerker DA, Ollinger JM, D'Esposito M, 2004. Variation of BOLD hemodynamic responses across subjects and brain regions and their effects on statistical analyses. Neuroimage; 21: 1639-1651.

Handwerker DA, Gonzalez-Castillo J, D'Esposito M, Bandettini PA, 2012. The continuing challenge of understanding and modeling hemodynamic variation in fMRI. Neuroimage; 62(2): 1017-23.

Harmer J, Sanchez-Panchuelo RM, Bowtell R, Francis ST, 2012. Spatial location and strength of BOLD activation in high-spatial-resolution fMRI of the motor cortex: a comparison of spin echo and gradient echo fMRI at 7T. NMR in Biomedicine; 25(5): 717-25.

Harris JJ, Reynell C, Attwell D, 2011. The physiology of developmental changes in BOLD functional imaging signals. Developmental Cognitive Neuroscience; 1: 199-216.

Hart A, Whitby E, Wilkinson S et al, 2011. Neuro-developmental outcome at 18 months in premature infants with diffuse excessive high signal intensity on MR imaging of the brain. Pediatric Radiology; 41(10): 1284-92.

Hartley C, Berthouze L, Mathieson SR et al, 2012. Long-Range temporal correlations in the EEG bursts of human preterm babies. PloS One; 7(2): e31543.

Hayasaka S, Nichols TE, 2004. Combining voxel intensity and cluster extent with permutation test framework. Neuroimage; 23(1): 54-63.

Hayes D, Meadows JT, Murphy BS et al, 2011. Pulmonary function outcomes in bronchopulmonary dysplasia through childhood and into adulthood: implications for primary care. Primary Care Respiratory Journal; 20(2): 128-33.

He B, Liu Z, 2008. Multimodal functional neuroimaging: integrating functional MRI and EEG/MEG. IEEE Reviews in Biomedical Engineering; 1: 23-40.

Heep A, Scheef L, Jankowski J et al, 2009. Functional magnetic resonance imaging of the sensorimotor system in preterm infants. Pediatrics; 123(1): 294-300.

Henson R, 2003. Analysis of fMRI timeseries. (*Chapter 10, Section 2*) In: Frackowiak RSJ, Friston KJ, Frith C et al (eds), 2003. Human Brain Function (2nd edition). Academic Press, USA.

Hillman EM, Devor A, Bouchard MB et al, 2007. Depth-resolved optical imaging and microscopy of vascular compartment dynamics during somatosensory stimulation. Neuroimage; 35(1): 89-104.

Hintz SR, Benaron DA, Siegel AM et al, 2005a. Bedside functional imaging of the premature infant brain during passive motor activation. Journal of Perinatal Medicine; 29(4): 335-43.

Hintz SR, Kendrick DE, Vohr BR et al, 2005b. Changes in Neurodevelopmental outcomes at 18 to 22 month's corrected age among infants of less than 25 weeks gestational age born in 1993-99. Pediatrics; 115(6): 1645-51.

Hirano Y, Stefanovic B, Silva AC, 2011. Spatiotemporal evolution of the functional Magnetic Resonance Imaging response to ultrashort stimuli. The Journal of Neuroscience; 31(4): 1440-7.

Hoge RD, Pike GB, 2001. Quantitative measurement using fMRI. (*Chapter 8*) In: Jezzard P, Matthews PM, Smith SM (eds), 2001. Functional MRI an introduction to methods. Oxford University Press; New York, USA.

Hoge RD, 2012. Calibrated fMRI. Neuroimage; 62(2): 930-7.

Hu X, Le TH, Ugurbil K, 1997. Evaluation of the early response in fMRI in individual subjects using short stimulus duration. Magnetic Resonance in Medicine; 37: 877-84.

Hu X, Yacoub E, 2012. The story of the initial dip in fMRI. Neuroimage; 62(2): 1103-8.

Hua J, Stevens RD, Huang AJ, et al, 2011. Physiological origin for the BOLD poststimulus undershoot in human brain: vascular compliance versus oxygen metabolism. Journal of Cerebral Blood Flow and Metabolism; 31(7): 1-13.

Huang H, Zhang J, Wakana S et al, 2006. White and gray matter development in human fetal, newborn, and pediatric brains. Neuroimage; 33(1): 27-38.

Huettel SA, Singermann JD, McCarthy G, 2001. The effects of aging upon the hemodynamic response measured by functional MRI. Neuroimage; 13: 161-75.

Huettel SA, Song AW, McCarthy G, 2004. Functional Magnetic Resonance Imaging. Sinauer Associates Inc; Sunderland MA, USA.

Huppert TJ, Hoge RD, Diamond SG et al, 2006. A temporal comparison of BOLD, ASL, and NIRS hemodynamic responses to motor stimulation in adult humans. Neuroimage; 29: 368-82.

Hűppi PS, Maier S, Peled G et al, 1998. Microstructural development of human newborns cerebral white matter assessed by diffusion tensor MRI. Pediatric Research; 44: 584-90.

Hűppi PS, Warfield S, Kikinis R et al, 1998. Quantitative magnetic resonance imaging of brain development in premature and mature newborns. Annals of Neurology; 43(2): 224-35.

Huttenlocher PR, Dabholkar AS, 1997. Regional differences in synaptogenesis in human cerebral cortex. The Journal of Comparative Neurology; 387(2): 167-78.

Inder TE, Neil J, Kroenke C et al, 2005. Investigation of cerebral development and injury in the prematurely born primate by magnetic resonance imaging and histopathology. Developmental Neuroscience; 27(2-4): 100-11.

Inder TE, Warfield SK, Wang H et al, 2005. Abnormal cerebral structure is present at term in premature infants. Pediatrics; 115(2): 286-94.

Isobe K, Kusaka T, Nagano K et al, 2001. Functional imaging of the brain in sedated newborn infants using near infrared topography during passive knee movement. Neuroscience Letters; 299: 221-4.

Jack AI, Shulman GL, Snyder AZ et al, 2006. Separate modulations of human V1 associated with spatial attention and task structure. Neuron; 51: 135-47.

Jacobs J, Hawco C, Kobayashi et al, 2008. Variability of the hemodynamic response as a function of age and frequency of epileptic discharge in children with epilepsy. Neuroimage; 40(2): 601-14.

Jasanoff, 2007. Bloodless fMRI. Trends in Neurosciences; 30(11): 603-10.

Jenkinson M, Bannister PR, Brady JM, Smith SM, 2002. Improved optimisation for the robust and accurate linear registration and motion correction of brain images. Neuroimage; 17(2): 825-41.

Jenkinson M, 2001. Registration, atlases and cortical flattening. (*Chapter 15*) In: Jezzard P, Matthews PM, Smith SM (eds), 2001. Functional MRI an introduction to methods. Oxford University Press; New York, USA.

Jenkinson M, Beckmann CF, Behrens TEJ et al, 2012. FSL. Neuroimage; 62(2): 782-90.

Jezzard P, Balaban RS, 1995. Correction for geometric distortion in echo planar images from B0 field variations. Magnetic Resonance in Medicine; 34(1): 65-73.

Jezzard P, Clare S, 1999. Sources of distortion in functional MRI data. Human Brain Mapping; 8: 80-85.

Jiang S, Xue H, Glover A et al, 2007. MRI of moving subjects using multislice snapshot images with volume reconstruction (SVR): application to fetal, neonatal, and adult brain studies. IEEE Transactions on Medical Imaging; 26(7): 967-80.

Jin T, Kim SG, 2008. Cortical layer-dependent dynamic blood oxygenation, cerebral blood flow and cerebral blood volume responses during visual stimulation. Neuroimage; 43(1): 1-9.

Joeri P, Huisman T, Loenneker T et al, 1996. Reproducibility of fMRI and effects of pentobarbital sedation in cortical activation during visual stimulation. Neuroimage; 3: 280.

Johnson BN, Sobel N, 2007. Methods for building an olfactometer with known concentration outcomes. Journal of Neuroscience Methods; 160(2): 231-45.

Johnson MH, 1990. Cortical Maturation and the development of visual attention in early infancy. Journal of Cognitive Neuroscience; 2(2): 81-95.

Johnson S, Hennessy E, Smith R et al, 2009. Academic attainment and special educational needs in extremely preterm children at 11 years of age: the EPIcure study. Archives of Disease in Childhood Fetal Neonatal Edition; 94(4): F283-9.

Johnson S, Hollis C, Kochhar P et al, 2010. Psychiatric disorders in extremely preterm children: longitudinal finding at age 11 years in the EPIcure study. Journal of the American Academy of Child and Adolescent Psychiatry; 49(5); 453-63.

Johnson S, Marlow N, 2011. Preterm Birth and Childhood Psychiatric Disorders. Pediatric Research; 69(5 pt 2): 11R-18R.

Johnston MV, 2009. Plasticity in the developing brain: implications for rehabilitation. Developmental Disabilities Research Reviews; 15(2): 94-101.

Jones T, Rabiner EA, 2012. The development, past achievements, and future directions of brain PET. Journal of Cerebral Blood Flow and Metabolism; 32: 1426-54.

Judaš M, Šimić G, Petanjek Z et al, 2011. The Zagreb collection of human brains: a unique, versatile, but underexploited resource for the neuroscience community. Annals of the New York Academy of Sciences; 1225(s1): E105-30.

Kadri H, Malwa AA, Kazah J, 2006. The incidence, timing, and predisposing factors of germinal matrix and intraventricular hemorrhage (GMH/IVH) in preterm neonates. Child's Nervous System; 22: 1086-90.

Kamei A, Houdou S, Mito T, Konomi H, Takashima S, 1992. Developmental change in type VI collagen in human cerebral vessels. Pediatric Neurology; 8(3): 183-6.

Kapellou O, Counsell SJ, Kennea N et al, 2006. Abnormal cortical development after premature birth shown by altered allometric scaling of brain growth. PLoS Med; 3(8):e265.

Karniski W, 1992a. The late somatosensory evoked potential in premature and term infants I. Principal component topography. Electroencephalography and Clinical Neurophysiology; 84(1): 32-43.

Karniski W, Wyble L, Lease L, Blair RC, 1992b. The late somatosensory evoked potential in premature and term infants II. Topography and latency development. Electroencephalography and Clinical Neurophysiology; 84(1): 44-54.

Kastrup A, Baudewig J, Schnaudigel S et al, 2008. Behavioral correlates of negative BOLD signal changes in the primary somatosensory cortex. Neuroimage; 41: 1364-71.

Kathuria S, Gregg L, Chen J, Gandhi D, 2011. Normal cerebral arterial development and variations. Seminars in Ultrasound, CT and MRI; 32(3): 242-51.

Kaur C, Ling EA, Wong WC, 1989. Development of the various glial cell types in the cerebral cortex of postnatal rats. Acta Anatomica; 136: 204-10.

Kent AL, Wright IM, Abdel-Latif ME et al, 2012. Mortality and adverse neurologic outcomes are greater in preterm male infants. Pediatrics; 129(1): 124-31.

Kesler SR, Reiss AL, Vohr B et al, 2008. Brain volume reductions within multiple cognitive systems in male preterm children at age twelve. Journal of Pediatrics; 152(4): 513-20.

Kidokoro H, Anderson PJ, Doyle LW et al, 2011. High signal intensity on T2-weighted MR imaging at term-equivalent age in preterm infants does not predict 2-year neurodevelopmental outcomes. American Journal of Neuroradiology; 32(11): 2005-10.

Kim SG, Ogawa S, 2012. Biophysical and physiological origins of blood oxygenation level-dependent fMRI signals. Journal of Cerebral Blood Flow and Metabolism; 32: 1188-206.

Kinney HC, Brody BA, Kloman AS, Gilles FH, 1988. Sequence of central nervous system myelination in human infancy. II. Patterns of myelination in autopsied infants. Journal of Neuropathology and Experimental Neuroscience; 47(3): 217-34.

Klingner CM, Hasler C, Brodoehl S, Witte OW, 2010. Dependence of the negative BOLD response on somatosensory stimulus intensity. Neuroimage; 53: 189-95.

Klingner CM, Ebenau K, Hasler C et al, 2011. Influences of negative BOLD responses in positive BOLD responses. Neuroimage; 55(4): 1709-15.

Koldewijn K, van Wassenaer A, Wolf MJ et al, 2010. A Neurobehavioual intervention and assessment program in very low birth weight infants: outcome at 24 months. Journal of Pediatrics; 156(3): 359-65.

Konishi Y, Taga G, Yamada H, Hirasawa K, 2002. Functional brain imaging using fMRI and optical topography in infancy. Sleep Medicine; 3 (supp 2): S41-3.

Kostović, Golman-Rakic P, 1983. Transient cholinesterase staining in the mediodorsal nucleus of the thalamus and its connections in the developing human and monkey brain. The Journal of Comparative Neurology; 219(4): 431-47.

Kostović I, Rakic P, 1990. Developmental history of the transient subplate zone in the visual and somatosensory cortex of the macaque monkey and human brain. Journal of Computational Neurology; 297: 441-70.

Kostović I, Judaš M, Radoš M, Hrabač P, 2002. Laminar organisation of the fetal cerebrum revealed by histochemical markers and magnetic resonance imaging. Cerebral Cortex; 12(5): 536-44.

Kostović I, Jovanov-Milošević, 2006. The development of cerebral connections during the first 20-45 weeks gestation. Seminars in Fetal and Neonatal Medicine; 11: 415-422.

Krishnan ML, Dyet LE, Boardman JP et al, 2007. Relationship between white matter apparent diffusion coefficients in preterm infants at term-equivalent age and developmental outcome at 2 years. Pediatrics; 120~(3): e604-9.

Krispin S, Nitzan E, Kalcheim C, 2010. The dorsal neural tube: a dynamic setting for cell fate decisions. Developmental Neurobiology; 70(12): 796-812.

Krűger G, Kastrup A, Glover G, 2001. Neuroimaging at 1.5 T and 3.0 T: comparison of oxygenation-sensitive Magnetic Resonance Imaging. Magnetic Resonance in Medicine; 45: 595-604.

Kruse M, Michelson SI, Meulengracht-Flachs E et al. Lifetime costs of cerebral palsy. Developmental Medicine and Child Neurology 2009; 51(8): 622-628.

Kuban KCK, Gilles FH, 1985. Human telencephalic angiogenesis. Annals of Neurology; 17: 539-48.

Kuklisova-Murgasova M, Aljabar P, Srinivasan L et al, 2011. A dynamic 4D probabilistic atlas of the developing brain. Neuroimage; 54(4): 2750-63.

Kusaka T, Isobe K, Miki T et al, 2011. Functional lateralization of sensorimotor cortex in infants measured using multichannel Near-Infrared Spectroscopy. Pediatric Research; 69(5 part 1): 430-5.

Kusters CD, Chen ML, Follett PL, Dammann O, 2009. “Intraventricular” hemorrhage and cystic periventricular leukomalacia in preterm infants: how are they related? Journal of Child Neurology; 24(9): 1158-70.

Kwong KK, Belliveau JW, Chesler DA et al, 1992. Dynamic magnetic resonance imaging of human brain activity during primary sensory stimulation. Proceedings of the National Academy of Sciences USA; 89(12): 5675-9.

Lagercrantz H, Ringstedt T, 2001. Organization of the neuronal circuits in the central nervous system during development. Acta Pædiatrica; 90: 707-15.

Lagercrantz H, 2009. The birth of consciousness. Early Human Development; 85: S57-8.

Lagercrantz H, Changeux JP, 2009. The Emergence of Human Consciousness: from fetal to neonatal life. Pediatric Research; 65(3): 255-60.

Larroque B, Marret S, Ancel PY et al, 2003. White matter damage and intraventricular hemorrhage in very preterm infants: the EPIPAGE study. Journal of Pediatrics; 143(3): 477-83.

Larroque B, Ancel PY, Marret S et al, 2008. Neurodevelopmental disabilities and special care of 5-year-old children born before 33 weeks gestation (the EPIPAGE study): a longitudinal study. The Lancet; 371:813-820.

Lauritzen M, 2005. Reading vascular changes in brain imaging: is dendritic calcium the key? Nature Reviews Neuroscience; 6: 77-85.

Lauronen L, Nevalainen P, Wikström H et al, 2006. Immaturity of somatosensory cortical processing in human newborns. Neuroimage; 33: 195-203.

Lauterbur PC, 1973. Image formation by induced local interactions: examples employing nuclear magnetic resonance. Nature; 242: 190-1.

Le Bihan D, Urayama S, Aso T et al, 2007. Direct and fast detection of neuronal activation in the human brain with diffusion MRI. Proceedings of the National Academy of Sciences, USA; 103(21): 8263-8.

Lee JH, Durand R, Grandinaru V et al, 2010. Global and local fMRI signals driven by neurons defined optogenetically by type and wiring. Nature; 465(7299): 788-92.

Lee W, Donner EJ, Nossin-Manor R et al, 2012. Visual functional magnetic resonance imaging of preterm infants. Developmental Medicine and Child Neurology; 54(8): 724-9.

Lent R, Azevedo FAC, Andrade-Moraes CH, Pinto AVO, 2011. How many neurons do you have? Some dogmas of quantitative neuroscience under revision. European Journal of Neuroscience; 35(1): 1-9.

Leppert IR, Almli CR, McKinstry RC et al, 2009. T(2) relaxometry of normal pediatric brain development. Journal of Magnetic Resonance Imaging; 29(2): 258-67.

Levene MI, de Crespigny LC, 1983. Classification of intraventricular hemorrhage. Lancet; 1(8325): 643.

Limperopoulos C, Benson CB, Bassan H et al. 2005. Cerebellar hemorrhage in the preterm infant: ultrasonographic findings and risk factors. Pediatrics; 116: 717-24.

Limperopoulos C, Soul JS, Gauvreau K et al, 2005. Late gestation cerebellar growth is rapid and impeded by premature birth. Pediatrics; 115(3): 688-95.

Limperopoulos C, du Plessis AJ, 2006. Disorders of cerebellar growth and development. Current Opinion in Pediatrics; 18(6): 621-7.

Limperopoulos C, Bassan H, Gauvreau K et al, 2007. Does cerebellar injury in premature infants contribute to the higher prevalence of long-term cognitive, learning, and behavioral disability in survivors? Pediatrics; 120(3): 584-93.

Limperopoulos C, 2010. Advanced Neuroimaging techniques: their role in the development of future fetal and neonatal neuroprotection. Seminars in Perinatology; 34(1): 93-101.

Lin W, Zhu Q, Gao W et al, 2008. Functional connectivity MR imaging reveals cortical functional connectivity in the developing brain. American Journal of Neuroradiology; 29(10): 1883-9.

Lind A, Parkkola R, Lehtonen L et al, 2011. Associations between regional brain volumes at term-equivalent age and development at 2 years of age in preterm children. Pediatric Radiology; 41(8): 953-61.

Lindauer U, Villringer A, Dirnagel U, 1993. Characterization of CBF response to somatosensory stimulation: model and influence of anesthetics. American Journal of Physiology; 264(4 Pt 2): H1223-28.

Lindquist MA, Loh JM, Atlas LY, Wager TR, 2009. Modeling the hemodynamic response function in fMRI: efficiency, bias, and mis-modeling. Neuroimage; 45: 5187-98.

Liu TT, Behzadi Y, Restom K et al, 2004. Caffeine alters the temporal dynamics of the visual BOLD response. Neuroimage; 23: 1402-1413.

Lloyd-Fox S, Blasi A, Elwell CE, 2010. Illuminating the developing brain: the past, present and future of functional near infrared spectroscopy. Neuroscience and Biobehavioural Reviews; 34(3): 269-84.

Logotheis NK, Pauls J, Auguth M et al, 2001. Neurophysiological investigation of the basis of the fMRI signal. Nature; 412: 150-7.

Logothetis NK, Pfeuffer J, 2004. On the nature of BOLD fMRI contrast mechanism. Magnetic Resonance Imaging; 22(10): 1517-1531.

Logothetis NK, 2008. What we can do and what we cannot do with fMRI. Nature; 453: 869-78.

Luján R, Shigemoto R, Lopez-Bendito G, 2005. Glutamate and GABA receptor signaling in developing brain. Neuroscience; 130(3): 567-80.

McCaslin AFH, Chen BR, Radosevich AJ, Cauli B, Hillman EMC, 2011. In vivo 3D morphology of astrocyte-vasculature interactions in the somatosensory cortex: implications for neurovascular coupling. Journal of Cerebral Blood Flow and Metabolism; 31(3): 795-806.

McClure KD, McClure SM, Richter MC, Richter W, 2005. The kinetics of the BOLD response depend on inter-stimulus time. Neuroimage; 27: 817-23.

McKeown MJ, Makeig S, Brown GG et al, 1998. Analysis of fMRI data by blind separation into independent spatial components. Human Brain Mapping; 6(3): 160-88.

McRobbie DW, Moore EA, Graves MJ, Prince MR, 2010. MRI from picture to proton (3rd ed). Cambridge University Press; New York, USA.

Maalouf EF, Duggan PJ, Rutherford MA et al, 1999, Magnetic resonance imaging of the brain in a cohort of extremely preterm infants. Journal of Pediatrics; 135: 351-7.

Maalouf EF, Counsell SJ, 2002. Imaging the preterm infant: practical issues. (*Chapter 2*) In: Rutherford MA, 2002-12. MRI of the Neonatal Brain. http://www.mrineonatalbrain.com/

Mall V, 2005. Recruitment of the sensorimotor cortex – a developmental fMRI study. Neuropediatrics; 36(6): 373-9.

Malonek D, Grinvald A, 1996. Interactions between electrical activity and cortical microcirculation revealed by imaging spectroscopy: implications for functional brain mapping. Science; 272: 551-4.

Mandeville JB, Marota JJA, Kosofsky BE et al, 1998. Dynamic functional imaging of relative cerebral blood volume during rat forepaw stimulation. Magnetic Resonance in Medicine; 29: 615-24.

Mandeville JB, Marota JJA, Ayata C et al, 1999. Evidence of a cerebrovascular post-arteriole Windkessel with delayed compliance. Journal of Cerebral Blood Flow and Metabolism; 19: 679-89.

Manent JB, Repressa A, 2007. Early paracrine actions of GABA and Glutamate modulate neuronal migration. The Neuroscientist; 13(3): 268-79.

Mangham LJ, Petrou S, Doyle LW et al, 2009. The cost of preterm birth throughout childhood in England and Wales. Pediatrics; 123: e312-27.

Mangia S, Giove F, Tkáč I et al, 2009. Metabolic and hemodynamic events after changes in neuronal activity: current hypotheses, theoretical predictions and in vivo NMR experimental findings. Journal of Cerebral Blood Flow and Metabolism; 29: 441-63.

Mansfield P, 1977. Multi-planar image formation using NMR spin echoes. Journal of Physics C: Solid State Physics; 10: L55-8.

Manto MU, Jissendi P, 2012. Cerebellum: links between development, developmental disorders and motor learning. Frontiers in Neuroanatomy; 6: 1-10.

Marcar VL, Strässle AE, Loenneker T et al, 2004. The influence of cortical maturation on the BOLD response: an fMRI study of visual cortex in children. Pediatric Research; 56(6): 967-74.

Martin E, Joeri P, Loenneker T, Ekatodramis D et al, 1999. Visual processing in infants and children studied using functional MRI. Pediatric Research; 46(2): 135-40.

Martin E, Thiel T, Joeri P et al, 2000. Effect of pentobarbital on visual processing in main. Human Brain Mapping; 10(3): 132-9.

Martin JH, 2007. Development of the corticospinal system and spinal motor circuits. (*Chapter 3*) In: Eisen AA, Shaw PJ (eds), 2007. Handbook of Clinical Neurology, Vol 82(3rd series): Motor neuron disorders and related diseases. Elsevier, Philadelphia PA, USA.

Masterton RAJ, Harvery AS, Archer JS et al, 2010. Focal epileptiform spikes do not show canonical BOLD response in patients with benign rolandic epilepsy (BECTS). Neuroimage; 51(1): 252-60.

Matsuura T, Fujita H, Kashikura K, Kanno I, 2000. Evoked local cerebral blood flow induced by somatosensory stimulation is proportional to the baseline flow. Neuroscience Research; 38(4): 341-8.

Matthews PM, 2001. An introduction to functional magnetic resonance imaging of the brain. (*Chapter 1*) In: Jezzard P, Matthews PM, Smith SM (eds), 2001. Functional MRI an introduction to methods. Oxford University Press; New York, USA.

Matthews PM, Rabiner I, Gunn R, 2011. Non-invasive imaging in experimental medicine for drug development. Current Opinions in Pharmacaology; 11(5): 501-7.

Mazziota J, Toga A, Evans A et al, 2001. A probabilistic atlas and reference system for the human brain: international consortium for brain mapping (ICBM). Philosophical Transactions of the Royal Society B: Biological Sciences; 356(1412): 1293-322.

Meek JH, Tyszczuk L, Elwell CE, Wyatt JS, 1998. Cerebral blood flow increases over the first three days of life in extremely preterm neonates. Archives of Disease in Childhood Fetal and Neonatal edition; 78(1): F33-7.

Meier P, Zierler LL, 1954. On the theory of the indicator-dilution method for measurement of blood flow and volume. Journal of Applied Physiology; 6: 731-44.

Mellon RD, Simone AF, Rappaport BA, 2007. Use of Anesthetic agents in neonates and young children. Pediatric Anesthesia 2007; 104: 509-20.

Menon RS, Goodyear BG, 2001. Spatial and temporal resolution in fMRI (*Chapter 7*) In: Jezzard P, Matthews PM, Smith SM (eds), 2001. Functional MRI an introduction to methods. Oxford University Press; New York, USA.

Ment LR, Constable RT, 2007. Injury and recovery in the developing brain: evidence from functional MRI studies of prematurely born children. Nature Clinical Practice Neurology; 3(10): 558-71.

Ment LR, Hirtz D, Hűppi PS, 2009. Imaging biomarkers of outcome in the developing preterm brain. Lancet Neurology; 8(11): 1042-55.

Merchant N, Groves A, Larkman DJ et al, 2009. A patient care system for early 3.0 Tesla magnetic resonance imaging of very low birth weight infants. Early Human Development; 95(12): 779-83.

Mercuri E, Ricci D, Pane M, Baranello G, 2005. The neurological examination of the newborn baby. Early Human Development; 81(12): 947-56.

Michaelsen K, Lohman C, 2010. Calcium dynamics at developing synapses: mechanisms and functions. European Journal of Neuroscience; 32(2): 218-23.

Miezin FM, Maccotta L, Ollinger JM et al, 2000. Characterizing the hemodynamic response: effects of presentation rate, sampling procedure, and the possibility of ordering brain activity based on relative timing. Neuroimage; 735-59.

Miller RH, 2002. Regulation of oligodendrocyte development in the vertebrate CNS. Progress in Neurobiology; 67(6): 451-67.

Miller DH, 2004. Biomarkers and surrogate outcomes in neurodegenerative disease: Lessons from multiple sclerosis. Neurotherapeutics; 1(2): 284-94.

Miranda MJ, Olofsson K, Sidaros K, 2006. Noninvasive measurements of regional perfusion in preterm and term neonates by magnetic resonance arterial spin labeling. Pediatric Research; 60(3): 359-63.

Monti MM, 2011. Statistical analysis of fMRI time-series: a critical review of the GLM approach. Frontiers in Human Neuroscience; 5(28): 1-13.

Morita T, Kochiyama T, Yamada H et al, 2000. Difference in the metabolic response to photic stimulation of the lateral geniculate nucleus and the primary visual cortex of infants: a fMRI study. Neuroscience Research; 38(1): 63-70.

Mullen KM, Vohr BR, Katz KH et al, 2011. Preterm birth results in alterations in neural connectivity at age 16 years. Neuroimage; 45(4): 2563-70.

Mumford JA, Nichols TE, 2006. Modeling and inference of multisubject fMRI data. IEEE Engineering in Medicine and Biology Magazine; 25(2): 42-51.

Mumford JA, Poldrack RA, 2007. Modeling group fMRI data. Social Cognitive and Affective Neuroscience; 2(3): 251-7.

Muramoto S, Yamada H, Sadato N et al, 2002. Age-dependent change in metabolic response to photic stimulation of the primary visual cortex in infants: functional magnetic resonance imaging study. Journal of Computer Assisted Tomography; 26(6): 894-901.

Muresan L, Renken R, Roerdink JB, Duifhuis H, 2005. Automated correction of spin-history related motion artefacts in fMRI: simulated and phantom data. IEEE Transactions in Biomedical Engineering; 52(8): 1450-60.

Murphy K, Bodurka J, Bandettini PA, 2007. How long to scan? The relationship between fMRI temporal signal to noise ratio and necessary scan duration. Neuroimage; 34: 565-74.

Muthukumaraswamy SD, Edden RAE, Jones DK et al, 2009. Resting GABA concentration predicts peak gamma frequency and fMRI amplitude in response to visual stimulation in humans. Proceedings of the National Academy of Sciences, USA; 106(20): 8356-61.

Muthukumaraswamy SD, Evans CJ, Edden RAE et al, 2012. Individual variability in the shape and amplitude of the BOLD-HRF correlates with endogenous GABAergic inhibition. Human Brain Mapping; 33(2): 455-65.

Nagasawa S, Kawanishi M, Tada Y et al, 2000. Intra-operative measurement of cortical arterial flow volumes in posterior circulation using Doppler sonography. Neurological Research; 22: 194-6.

Nagy Z, Ashburner J, Andersson J et al, 2009. Structural correlates of preterm birth in the adolescent brain. Pediatrics; 124(5): e964-72.

Neil JJ, Shiran SI, McKinstry RC et al, 1998. Normal brain in human newborns: apparent diffusion coefficient and diffusion anisotropy measured by using diffusion tensor MR imaging. Radiology; 209(1): 57-66.

Nevalainen P, Lauronen L, Sambeth A et al, 2008. Somatosensory evoked magnetic fields from the primary and secondary somatosensory cortices in healthy newborns. Neuroimage; 40(2): 738-45.

Nichols TE, Holmes AP, 2002. Nonparametric permutation tests for functional neuroimaging: a primer with examples. Human Brain Mapping; 15(1): 1-25.

Nichols TE, Hayasaka S, 2003. Controlling the familywise error rate in functional neuroimaging: a comparative review. Statistical Methods in Medical Research; 12(5): 419-46.

Nichols TE, 2012. Multiple testing corrections, nonparametric methods, and random field theory. Neuroimage; 62(2): 811-5.

Nishitani S, Miyamura T, Tagawa M et al, 2009. The calming effect of a maternal breast milk odor on the human newborn infant. Neuroscience Research; 63(1): 66-71.

Niwa T, de Vries LS, Benders MJ et al, 2011. Punctate white matter lesions in infants: new insights using susceptibility-weighted imaging. Neuroradiology; 53(9): 669-79.

Nongena P, Ederies A, Azzopardi DV, Edwards AD, 2010. Confidence in the prediction of neurodevelopmental outcome by cranial ultrasound and MRI in preterm infants. Archives of Disease in Childhood Fetal and Neonatal Edition; 95: F388-90.

Norman MG, O'Klusky JR, 1986. The Growth and development of micro-vasculature in human cerebral cortex. Journal of Neuropathology and Experimental Neurology; 45(3): 222-33.

Nosarti C, Giouroukou E, Healy E et al, 2008. Grey and white matter distribution in very preterm adolescents mediates neurodevelopmental outcome. Brain; 131(pt1): 205-17.

Nosarti C, Reichenberg A, Murray RM, et al, 2012. Preterm Birth and Psychiatric disorders in young adult life. Archives of General Psychiatry; 69(6): 610-7.

Nowakowski RS, 2006. Stable neuron numbers from cradle to grave. Proceedings of the National Academy of Sciences USA; 103(33): 12219-20.

Øberg GK, Campbell SK, Girolami GL, et al, 2012. Study protocol: an early intervention program to improve motor outcome in preterm infants: a randomized controlled trial and a qualitative study of physiotherapy performance and parental experiences. BMC pediatrics; 12: 15.

Ogawa S, Lee TM, 1990a. Magnetic resonance imaging of blood vessels at high fields: in vivo and in vitro measurements and image simulation. Magnetic Resonance in Medicine; 16(1): 9-18.

Ogawa S, Lee TM, Kay AR, Tank DW, 1990b. Brain magnetic resonance imaging with contrast dependent on blood oxygenation. Proceedings of the National Academy of Sciences USA; 87: 9868-72.

Ogawa S, Lee TM, Nayak AS, Glynn P, 1990c. Oxygenation-sensitive contrast in magnetic resonance image of rodent brain at high magnetic field. Magnetic Resonance in Medicine; 14:68-78.

Ogawa S, Tank DW, Menon R et al, 1992. Intrinsic signal changes accompanying sensory stimulation: functional brain mapping with magnetic resonance imaging. Proceedings of the National Academy of Sciences USA; 89(13): 5951-5.

Ogawa S, Menon RS, Tank DW et al, 1993. Functional brain mapping by blood oxygenation level-dependent contrast magnetic resonance imaging: a comparison of signal characteristics with a biophysical model. Biophysical Journal; 64: 803-12.

Orton J, Spittle A, Doyle L, et al, 2009. Do early intervention programmes improve cognitive and motor outcomes for preterm infants after discharge? A systematic review. Developmental Medicine Child Neurology; 51(11): 851-9.

Padget DH, 1948. The development of the cranial arteries in the human embryo. Control of Embryology Carnegie Institution for Science; 12: 205-261.

Palmer FB, 2004. Strategies for the early diagnosis of cerebral palsy. The Journal of Pediatrics; 145(2): S8-11.

Panigrahy A, Borzage M, Blumi S, 2010. Basic Principles underlying recent advances in magnetic resonance imaging of the developing brain. Seminars in Perinatology; 34(1): 3-19.

Parelkar NK, Silswal N, Jansen K et al, 2010. 2,2,2-Trichloroethanol Activates a Nonclassical Potassium Channel in Cerebrovascular Smooth Muscle and Dliates the Middle Cerebral Artery. Journal of Pharmacology and Experimental Therapeutics; 332(3): 8083-10.

Parker J, Mitchell A, Kalpakidou A et al, 2008. Cerebellar growth and behavioural & neuropsychological outcome in preterm adolescents. Brain; 131(pt5): 1334-51.

Parpura V, Heneka MT, Montana V et al, 2012. Glial cells in (patho)physiology. Journal of Neurochemistry; 1: 4-27.

Pennock J, 2001. Patient preparation, safety and hazards in imaging infants and children (*Chapter 1*). In: Rutherford MA, 2002-12. MRI of the Neonatal Brain. http://www.mrineonatalbrain.com/

Perani D, Saccuman MC, Scifo P et al, 2010. Functional specializations for music processing in the human newborn brain. Proceedings of the National Academy of Sciences USA; 107(10: 4758-63.

Perani D, Saccuman MC, Scifo P et al, 2011. Language networks at birth. Proceedings of the National Academy of Sciences USA; 108(38): 16056-61.

Perlman JM, McMenamin JB, Volpe JJ, 1983. Fluctuating cerebral blood-flow velocity in respiratory-distress syndrome. Relation to the development of intraventricular hemorrhage. New England Journal of Medicine; 309(4): 204-9.

Perthen JE, Lansing AE, Liau J et al, 2008. Caffeine-induced uncoupling of cerebral blood flow and oxygen metabolism: a calibrated BOLD fMRI study. Neuroimage; 40(1): 237-247.

Peters AM, Brookes MJ, Hoogenraad FG et al, 2007. T2* measurements in human brain at 1.5, 3 and 7T. Magnetic Resonance Imaging; 24: 748-53.

Peterson BS, Vohr B, Staib LH et al, 2000. Regional brain volume abnormalities and long-term cognitive outcome in preterm infants. Journal of the American Medical Association; 284*15): 1939-47.

Pihko E, Lauronen L, 2004. Somatosensory processing in healthy newborns. Experimental Neurology; 190 (supp1): S2-7.

Pihko E, Nevalainen P, Stephen J et al, 2009. Maturation of somatosensory cortical processing from birth to adulthood revealed by magnetoencephalography. Clinical Neurophysiology; 120: 1552-61.

Pike AA, Marlow N, 2000. The role of cortical evoked potentials in predicting neuromotor outcome in very preterm infants. Early Human Development; 57: 123-35.

Pimentel MA, Vilela P, Sousa I, Figueiredo, 2011. Localization of the hand motor area by arterial spin labeling and blood oxygen level-dependent functional magnetic resonance imaging. Human Brain Mapping; (*epub ahead of print*, PMID: 22121040).

Pineiro R, Pendlebury S, Johansen-Berg H, Matthews PM, 2002. Altered hemodynamic responses in patients after subcortical stroke measured by functional MRI. Stroke; 33: 103-9.

Platt MJ, Cans C, Johnson A et al, 2007. Trends in cerebral palsy among infants of very low birthweight (<1500g) or born prematurely (<32 weeks) in 16 European centres: a database study. The Lancet; 369: 43-50.

Poellinger A, Thomas R, Lio P et al, 2001. Activation and habituation in olfaction – an fMRI study. Neuroimage; 13: 547-60.

Poline JP, Brett M, 2012. The general linear model and fMRI: does love last forever? Neuroimage; 62(2): 871-80.

Pont-Lezica L, Béchade C, Belarif-Cantaut Y et al 2011. Physiological roles of microglia during development. Journal of Neurochemistry; 119(5): 901-8.

Popp R, Sommer M, Muller K, Hajak G, 2004. Olfactometry in fMRI studies: odor presentation using nasal continuous positive airway pressure. Acta Neurobiologiae Experimentalis; 64(2): 171-6.

Power JD, Barnes KA, Synder AZ et al, 2012. Spurious but systematic correlations in functional connectivity MRI networks arise from subject motion. Neuroimage; 59(3): 2142-54.

Prechtl HFR, Ferrari F, Cioni G, 1993. Predictive value of general movements in asphyxiated fullterm infants. Early Human Development; 35: 91-120.

Prechtl HFR, 2001. General movement assessment as a method of developmental neurology: new paradigms and their consequences. Developmental Medicine and Child Neurology; 43: 836-42.

Purves D, Augustine GJ, Fitzpatrick D et al, 2001. Neuroscience (*2nd edition*). Sinauer Associates; Sunderland MA: USA.

Radoš M, Judaš M, Kostović I, 2006. In vitro MRI of brain development. European Journal of Radiology; 57(2): 187-98.

Raichle ME, MacLeod AM, Snyder AZ et al, 2001. A default mode of brain function. Proceedings of the National Academy of Sciences USA; 98(2): 676-82.

Rakic P, 1995. A small step for the cell, a giant leap for mankind: a hypothesis of neocortical expansion during evolution. Trends in Neuroscience; 18(9): 383-8.

Rallu M, Corbin J, Fishell G, 2002. Parsing the prosencephalon. Nature Reviews Neuroscience; 3: 943-51.

Ramenghi LA, Fumagali M, Righini A et al, 2007. Magnetic resonance imaging assessment of brain maturation in preterm neonates with punctate white matter lesions. Neuroradiology; 48: 161-7.

Rathbone R, Counsell SJ, Kapellou O et al, 2011. Perinatal cortical growth and childhood neurocognitive abilities. Neurology; 77(16): 1510-7.

Raybaud C, 2010. Normal and abnormal embryology and development of the intracranial vascular system. Neurosurgical Clinics of North America; 21(3): 399-426.

Rees S, Walker D, Jennings E, 2010. Development of the somatosensory system (*chapter 9*). In: Lagercrantz H, Hanson MA, Ment LR (eds) 2010. The Newborn brain: Neuroscience and Clinical Applications (2nd edition). Cambridge University Press; Cambridge UK

Richards LJ, Planchez C, Ren T, 2004. Mechanisms regulating the development of the corpus callosum and its agenesis in mouse and human. Clinical Genetics; 66(4): 276-89.

Richter W, Richter M, 2003. The shape of the fMRI BOLD response in children and adults changes systematically with age. Neuroimage; 20(2): 1122-31.

Risser L, Plouraboué F, Cloetens P, Fonta C, 2009. A 3D-investigation shows that angiogenesis in primate cerebral cortex mainly occurs at capillary level. International Journal of Neuroscience; 27: 185-196.

Rivkin MJ, Wolraich D, Als H et al, 2004. Prolonged T2* values in newborn versus adult brain: implications for fMRI studies of newborns. Magnetic Resonance Medicine; 51(6): 1287-91.

Robertson CM, Watt MJ, Yasui Y, 2007. Changes in the prevalence of cerebral palsy for children born very prematurely within a population-based program over 30 years. JAMA; 297: 2733-40.

Roche-Labarbe N, Carp SA, Surova A et al, 2010. Noninvasive optical measures of CBV, StO(2), CBF index, and rCMRO(2) in human premature neonates' brains in the first six weeks of life. Human Brain Mapping; 31(3): 341-52.

Roche-Labarbe N, Fenoglio A, Aggarwal A et al, 2012. Near-infrared spectroscopy assessment of cerebral oxygen metabolism in the developing premature brain. Journal of Cerebral Blood Flow and Metabolism; 32(3): 481-8.

Roze E, Harris PA, Ball G et al, 2012. Tractography of the corticospinal tracts in infants with focal perinatal brain injury: comparison with normal controls and to motor development. Neuroradiology; 54(4): 507-16.

Rueckert D, Sonoda LI, Hayes C et al, 1999. Nonrigid registration using free-form deformations: application to breast MR images. IEEE Transactions in Medical Imaging; 18(8): 712-21.

Rutherford MA, Pennock JM, Counsell SJ et al, 1998. Abnormal Magnetic Resonance signal in the internal capsule predicts poor neurodevelopmental outcome in infants with hypoxic-ischaemic encephalopathy. Pediatrics; 102(2): 323-8.

Rutherford MA, 2002-12. MRI of the Neonatal Brain. *http://www. Mrineonatalbrain .com/*

Rutherford MA, Malamateniou C, Zeka J, Counsell SJ, 2004. MR imaging of the neonatal brain at 3 Tesla. European Journal of Paediatric Neurology; 8: 281-9.

Rutherford MA, Jiang S, Allsop JA et al, 2008. MR Imaging methods for assessing fetal brain development. Developmental Neurobiology; 68(6): 700-11.

Rutherford MA, Supramaniam V, Ederies A, 2010. Magnetic resonance imaging of white matter diseases of prematurity. Neuroradiology; 52(6): 505-21.

Sadler TW, 2005. Embryology of Neural tube development. American Journal of Medical Genetics Part C (Seminars in Medical Genetics) 135C: 2-8.

Sarnat HB, 2003. Functions of the corticospinal and corticobulbar tracts in the human newborn. Journal of Pediatric Neurology; 1(1): 3-8.

Satterthwaite TD, Wolf DH, Loughead J et al, 2012. Impact of in-scanner head motion on multiple measure of functional connectivity: relevance for studies of neurodevelopment in youth. Neuroimage; 60(1): 623-43.

Savic I, 2002. Imaging of brain activation by odorants in humans. Current Opinion Neurobiology; 12(4): 455-61.

Schäfer K, Blankenburg F, Kupers R et al, 2012. Negative BOLD signal changes in ipsilateral primary somatosensory cortex are associated with perfusion decreases and behavioral evidence for functional inhibition. Neuroimage; 59: 3119-27.

Schapiro MB, Schmithorst VJ, Wilke M et al, 2004. BOLD fMRI signal increases with age in selected brain regions in children. Neuroreport; 15: 2575-8.

Schellinger PD, Richter G, Kohrmann M, Dorfler A, 2007. Noninvasive angiography (magnetic resonance and computed tomography) in the diagnosis of ischemic cerebrovascular disease: Techniques and clinical applications. Cerebrovascular disease; 24(supp 1): 16-23.

Seghier ML, Lazeyras F, Zimine S et al, 2004. Combination of event-related fMRI and diffusion tensor imaging in an infant with perinatal stroke. Neuroimage; 21: 463-72.

Seghier ML, Lazeyras F, Zimine S et al, 2005. Visual recovery after perinatal stroke evidenced by functional and diffusion MRI: case report. BMC Neurology; 5: 17.

Seghier ML, Lazeyras F, Huppi PS, 2006. Functional MRI of the newborn. Seminars in Fetal & Neonatal Medicine; 11: 479-88.

Seghier ML, Hűppi PS, 2010. The role of functional magnetic resonance imaging in the study of brain development, injury, and recovery in the newborn. Seminars in Perinatology; 34: 79-86.

Serag A, Aljabar P, Ball G et al, 2012. Construction of a consistent high-definition spatio-temporal atlas of the developing brain using adaptive kernel regression. Neuroimage; 59(3): 2255-65.

Shah DK, Anderson PJ, Carlin JB et al, 2006. Reduction in cerebellar volumes in preterm infants: relationship to white matter injury and neurodevelopment at two years of age. Pediatric Research; 60(1): 97-102.

Sherman SM, 2007. The thalamus is more than just a relay. Current Opinions in Neurobiology; 17: 417-22.

Shmuel A, Yacoub E, Pfeuffer J et al, 2002. Sustained negative BOLD, blood flow and oxygen consumption response and its coupling to the positive response in the human brain. Neuron; 36(6): 1195-210.

Shmuel A, Auguth M, Oeltermann AM, Logethetis NK, 2006. Negative functional MRI response correlates with decreases in neuronal activity in monkey visual area V1. Nature Neuroscience; 9: 569-77.

Siero JCW, Petridou N, Hoogduin H et al, 2011. Cortical depth-dependent temporal dynamics of the BOLD response in the human brain. Journal of Cerebral Blood Flow and Metabolism; 10: 1999-2008.

Silk TJ, Wood AG, 2011. Lessons about neurodevelopment from anatomical magnetic resonance imaging. Journal of Developmental & Behavioural Pediatrics; 32(2): 158-68.

Silvennoinen MJ, Clingman CS, Golay X et al, 2003. Comparison of the dependence of blood R2 and R2* on oxygen saturation at 1.5 and 4.7 Tesla. Magnetic Resonance in Medicine; 49(1): 47-60.

Simpson D, 2005. Phrenology and the Neurosciences: contributions of F.J. Gall and J.G. Spurzheim. ANZ Journal of Surgery; 75(6): 475-82.

Sisson DF, Siegel J, 1989. Chloral hydrate anesthesia: EEG power spectrum analysis and effects on VEPs in the rat. Neurotoxicology and Teratology; 11(1): 51-6.

Smith AT, Singh KD, Greenlee MW, 2000. Attentional suppression of activity in the human visual cortex. Neuroreport; 11(2): 271-77.

Smith AT, Williams AL, Singh KD, 2004. Negative BOLD in the visual cortex: evidence against blood stealing. Human Brain Mapping; 21(4): 213-20.

Smith SM, 2001a. Overview of fMRI analysis. (*Chapter 11*) In: Jezzard P, Matthews PM, Smith SM (eds), 2001. Functional MRI an introduction to methods. Oxford University Press; New York, USA.

Smith SM, 2001b. Preparing fMRI data for statistical analysis. (*Chapter 12*) In: Jezzard P, Matthews PM, Smith SM (eds), 2001. Functional MRI an introduction to methods. Oxford University Press; New York, USA.

Smith SM, Jenkinson M, Woolrich MW et al, 2004. Advances in functional and structural MR image analysis and implementation as FSL. Neuroimage; 23(supp1): S208-19.

Smith SM, Jenkinson H, Johansen-Berg D et al, 2006. Tract-based spatial statistics: voxelwise analysis of multi-subject diffusion data. Neuroimage; 31(4): 1487-505.

Smith SM, Fox PT, Miller KL, 2009. Correspondence of the brain's functional architecture during activation and rest. Proceedings of the National Academy of Sciences, USA; 106(31): 13040-5.

Smith SM, Nichols TE, 2009. Threshold-free cluster enhancement: addressing problems of smoothing, threshold dependence and localization in cluster inference. Neuroimage; 44(1): 83-98.

Smith SM, 2012. The future of FMRI connectivity. Neuroimage; 62(2): 1257-66.

Smyser CD, Inder TE, Shimony JS et al, 2010. Longitudinal analysis of neural network development in preterm infants. Cerebral Cortex; 20(12): 2852-62.

Smyser CD, Snyder AZ, Neil JJ, 2011. Functional connectivity MRI in infants: exploration of the functional organization of the developing brain. Neuroimage; 56(3): 1437-52.

Sokoloff L, Reivich M, Kennedy C et al, 1977. The [14C] deoxyglucose method for the measurement of local cerebral glucose utilization: theory, procedure, and normal values in the conscious and anesthetized albino rat. Journal of Neurochemistry; 28: 897-916.

Soria-Pastor S, Padilla N, Zubiaurre-Elorza L et al, 2009. Decreased regional brain volume and cognitive impairment in preterm children at low risk. Pediatrics; 124(6): e1161-70.

Soul JS, Hammer PE, Tsuji M et al, 2007. Fluctuating pressure-passivity is common in the cerebral circulation of sick premature infants. Pediatric Research; 61: 467-73.

Sowell ER, Thompson PM, Holmes CJ et al, 1999. In vivo evidence for post-adolescent brain maturation in frontal and striatal regions. Nature Neuroscience; 2: 859-61.

Sowell ER, Peterson BS, Thompson PM et al, 2003. Mapping cortical change across the human life span. Nature Neuroscience; 6(3): 309-15.

Sowell ER, Thompson PM, Leonard CM et al, 2004. Longitudinal mapping of cortical thickness and brain growth in normal children. Journal of Neuroscience; 24(38): 8223-31.

Srinivasan L, Allsop J, Counsell SJ et al, 2006. Smaller cerebellar volumes in very preterm infants at term-equivalent age are associated with the presence of supratentorial lesions. American Journal of Neuroradiology; 27: 573-9.

Srinivasan L, Dutta R, Counsell SJ et al, 2007. Quantification of deep gray matter in preterm infants at term-equivalent age using manual volumetry of 3-Tesla magnetic resonance images. Pediatrics; 119: 759-65.

Staudt M, Lidzba K, Grodd W et al, 2002. Right-hemispheric organization of language following early left-died brain lesions: functional MRI topography. Neuroimage; 16(4): 954-67.

Staudt M, 2010. Brain Plasticity following early life brain injury: insight from neuroimaging. Seminars in Perinatology; 34(1): 87-92.

Steffener J, Tabert M, Reuben A, Stern Y, 2010. Investigating hemodynamic response variability at the group level using basis functions. Neuroimage; 49: 2113-22.

Studholme C, 2011. Mapping fetal brain development in utero using magnetic resonance imaging: the big bang of brain mapping. Annual Review of Biomedical Engineering; 13: 345-68.

Sugiura T, Goto T, Ueda et al, 2012. Periventricular Leukomalacia is decreasing in Japan. Pediatric Neurology; 47(1): 35-9.

Surman G, Hemming K, Platt MJ, 2009. Children with cerebral palsy: severity and trends over time. Paediatric and Perinatal Epidemiology; 23(6): 513-21.

Sylvester CM, Shulman GL, Jack AI, Corbetta M, 2007. Asymmetry of anticipatory activity in the visual cortex predicts the locus of attention and perception. Journal of Neuroscience; 27: 14424-33.

Takashima S, Itoh M, Oka A, 2009. A history of our understanding of cerebral vascular development and pathogenesis of perinatal brain damage over the past 30 years. Seminars in Pediatric Neurology; 16(4): 226-36.

Taoka T, Iwasaki S, Uchida H et al, 1998. Age correlation of the time lag in signal change on EPI-fMRI. Journal of Computer Assisted Tomography; 22(4): 514-7.

Tawia S, 1992. When is the capacity for sentience acquired during human fetal development? The Journal of Maternal-Fetal Medicine; 1: 153-65.

Taylor MJ, Murphy WJ, Whyte HE, 1992. Prognostic reliability of somatosensory and visual evoked potentials of asphyxiated term infants. Developmental Medicine and Child Neurology; 34: 507-15.

Taylor MJ, Boor R, Ekert PG, 1996. Preterm maturation of the somatosensory evoked potential. Electroencephalography and clinical Neurophysiology; 100: 448-52.

Thayyil S, Chandrasekaran M, Taylor A et al, 2010. Cerebral magnetic resonance biomarkers in neonatal encephalopathy: a meta-analysis. Pediatrics; 125(2): e382-95.

Thornton C, Rousset CI, Kichev A et al, 2012. Molecular mechanisms of neonatal brain injury. Neurology Research International; 2012: 506320.

Thulborn KR, Waterton JC, Mattews PM, Radda GK, 1982. Oxygenation dependence of the transverse relaxation time of water protons in whole blood at high field. Biochemica et Biophysica Acta; 714: 265-70.

Toft PB, Leth H, Lou HC et al, 1995. Local vascular CO_2 reactivity in the infant brain assessed by functional MRI. Pediatric Radiology; 25: 420-4.

Tucker J, McGuire W 2004. Epidemiology of preterm birth. British Medical Journal; 329(7467): 675-8.

Tusor N, Wusthoff C, Smee N et al, 2012. Prediction of neurodevelopmental outcome after hypoxic-ischaemic encephalopathy treated with hypothermia by diffusion tensor imaging analyzed using tract-based spatial statistics. Pediatric Research; 72(1): 63-9.

Uematsu M, Takasawa M, Hosoi R, Inoue O, 2009. Uncoupling of flow and metabolism by chloral hydrate: a rat in-vivo autoradiographic study. Neuroreport; 20: 219-222.

Uludağ K, 2008. Transient and sustained BOLD responses to sustained visual stimulation. Magnetic Resonance Imaging; 26(7): 863-9.

van der Aa NE, DeBode S, van Diessen E et al, 2011a. Cortical reorganisation in a preterm born child with unilateral watershed infarction. European Journal of Paediatric Neurology; 15(6): 554-7.

van der Aa NE, Leemans A, Northington FJ et al, 2011b. Does diffusion tensor imaging-based tractography at 3 months of age contribute to the prediction of motor outcome after perinatal arterial ischemic stroke? Stroke; 42(12): 3410-4.

van der Knaap MS, Valk J, 1990. MR imaging of the various stages of normal myelination during the first year of life. Neuroradiology; 31: 459-70.

van der Knaap MS, Wezel-Meijler G, Barth PG et al, 1996. Normal gyration and sulcation in preterm and term neonates: appearance on MR images. Radiology; 200: 389-96.

van Dijk KR, Sabuncu MR, Buckner RL, 2012. The influence of head motion on intrinsic functional connectivity MRI. Neuroimage; 59(1): 431-8.

van Essen DC, 1997. A tension-based theory of morphogenesis and compact wiring in the central nervous system. Nature; 385: 313-8.

van Essen DC, Ugurbil K, Auerbach E et al, 2012. The human connectome project: a data acquisition perspective. Neuroimage; 62(4): 2222-31.

van Essen DC, Ugurbil K, 2012. The future of the human connectome. Neuroimage; 62(2): 1299-1310.

van Haastert IC, Groenendaal F, Uiterwaal CS et al, 2011. Decreasing incidence and severity of cerebral palsy in prematurely born children. Journal of Pediatrics; 159(1): 86-91.

Vanhatalo S, Palva JM, Andersson S et al, 2005. Slow endogenous activity transients and developmental expression of K^+ Cl^- cotransporter 2 in the immature human cortex. European Journal of Neuroscience; 22: 2799-804.

Vanhatalo S, Lauronen L, 2006. Neonatal SEP - Back to bedside with basic science. Seminars in Fetal and Neonatal Medicine; 11: 464-470.

Vanhatalo S, Jousmäki V, Andersson S, Metsäranta M, 2009. An easy and practical method for routine, bedside testing of somatosensory systems in extremely low birth weight infants. Pediatric Research; 66(6): 710-3.

van Kooij BJ, Benders MJ, Anbeek P et al, 2012. Cerebellar volume and proton magnetic resonance spectroscopy at term, and neurodevelopment at 2 years of age in preterm infants. Developmental Medicine and Child Neurology; 54(3): 260-6.

van Kooij BJ, deVries LS, Ball G et al, 2012. Neonatal tract-based spatial statistics findings and outcome in preterm infants. American Journal of Neuroradiology; 33(1): 188-94.

van Zijl PCM, Hua J, Lu H, 2012. The BOLD post-stimulus undershoot, one of the most debated issues in fMRI. Neuroimage; 62(2): 1092-102.

Varela M, Groves AM, Arichi T, Hajnal JV, 2012. Mean cerebral blood flow measurements using phase contrast MRI in the first year of life. NMR in Biomedicine; 25(9): 1063-72.

Vartanian G, Corfas G, Li Y et al, 1994. A role for acetylcholine receptor-inducing protein ARIA in oligodendrocyte development. Proceedings of the National Academy of Sciences USA; 91: 11626-30.

Verney C, 1999. Distribution of the Catecholaminergic neurons in the central nervous system of human embryos and fetuses. Microscopy research and technique; 46: 24-47.

Verney C, Lebrand C, Gaspar P, 2002. Changing distribution of monoaminergic markers in the developing human cerebral cortex with special emphasis on the serotonin transporter. Anatomical Record; 267: 87-93.

Verney C, 2003. Phenotypic expression of monoamines and GABA in the early development of human telencephalon, transient or not transient. Journal of Chemical Neuroanatomy; 26; 283-92.

Vernooij MW, van der Lugt A, Ikrm MA, et al 2007. Total cerebral blood flow and total brain perfusion in the general population: The Rotterdam Scan Study. Journal of Cerebral Blood Flow and Metabolism; 28: 412-9.

Volpe JJ, 2008. Neurology of the Newborn (5th edition). Saunders Elsevier; Philadelphia PA, USA.

Volpe JJ, 2009a. The Encephalopathy of prematurity – brain injury and impaired brain development inextricably intertwined. Seminars in Pediatric Neurology; 16:167-78.

Volpe JJ, 2009b. Brain injury in premature infants: a complex amalgam of destructive and developmental disturbances. Lancet Neurology; 8: 110-24.

Volpe JJ, Kinney HC, Jensen FE, Rosenberg PA, 2011. The developing oligodenderocyste: key cellular target in brain injury in the premature infant. International Journal of Developmental Neuroscience; 29(4): 423-40.

Volpe P, Campobasso G, De Robertis V, Rembouskos G, 2009. Disorders of prosencephalic development. Prenatal diagnosis; 29: 340-54.

Wang Q, Webber RM, Stanley GB, 2010. Thalamic synchrony and the adaptive gating of information flow to cortex. Nature Neuroscience; 13(12): 1534-43.

Weidenheim KM, Bodhireddy SR, Rashbaum WK et al, 1996. Temporal and spatial expression of major myelin proteins in the human fetal spinal cord during the second trimester. Journal of Neuropathology & Experimental Neurology; 55: 734-45.

Westbrook C, Roth C, 2005. MRI in Practice (3rd edition). Blackwell Publishing; Oxford, UK.

Westlye LT, Walhovd KB, Dale AM et al, 2010. Differentiating maturational and aging-related changes of the cerebral cortex by use of thickness and signal intensity. Neuroimage; 52(1): 172-85.

White T, Su S, Schmidt M et al, 2010. The development of gyrification in childhood and adolescence. Brain and Cognition; 72(1): 36-45.

Williams LA, Gelman N, Picot PA et al, 2005. Neonatal brain: regional variability of in vivo MR imaging relaxation rate at 3.0T – initial experience. Radiology; 235(2): 595-603.

Wimberger DM, Roberts TP, Barkovich AJ et al, 1995. Identification of ”premyelination” by diffusion-weighted MRI. Journal of Computer Assisted Tomography; 19: 28-33.

Wood E, 2006. The Child with Cerebral Palsy: Diagnosis and Beyond. Seminars in Pediatric Neurology; 13: 286-96.

Woolrich MW, Ripley BD, Brady M, Smith SM, 2001. Temporal autocorrelation in univariate linear modelling of fMRI data. Neuroimage; 14: 1370-86.

Woolrich MW, Behrens TE, Smith SM, 2004. Constrained linear basis sets for HRF modelling using Variational Bayes. Neuroimage; 21(4): 1748-61.

Worsley KJ, Friston KJ, 1995. Analysis of fMRI time-series revisited—again. Neuroimage; 2(3): 173-81.

Wyatt JS, Cope M, Delpy DT et al, 1990. Quantification of cerebral blood flow volume in human infants by near-infrared spectroscopy. Journal of Applied Physiology; 68(3): 1086-91.

Wylie GR, Genova H, DeLuca J et al, 2012. Functional magnetic resonance imaging movers and shakers: does subject-movement cause sampling bias? Human Brain Mapping; (*in press, PMID: 22847906*).

Xue H, Srinivasan L, Jiang S et al, 2007. Automatic segmentation and reconstruction of the cortex from neonatal MRI. Neuroimage; 38(3): 461-77.

Yacoub E, Hu X, 2001. Detection of the early decrease in fMRI signal in the motor area. Magnetic Resonance in Medicine; 45(2): 184-90.

Yamada H, Sadato N, Konishi Y et al, 1997. A rapid brain metabolic change in infants detected by fMRI. Neuroreport; 8(17): 3775-8.

Yamada H, Sadato N, Konishi Y et al, 2000. A milestone for normal development of the infantile brain detected by functional MRI. Neurology; 55(2): 218-23.

Yeşilyurt B, Uğurbil K, Uludağ K, 2008. Dynamics and nonlinearities of the BOLD response at very short stimulus durations. Magnetic Resonance Imaging; 26: 853-62.

Zacharia A, Ziminie S, Lovblad KO et al, 2006. Early assessment of brain maturation by MR imaging segmentation in neonates and premature infants. American Journal of Neuroradiology; 27(5): 972-7.

Zhang K, Sejnowski TJ, 2000. A universal scaling law between gray matter and white matter of the cerebral cortex. Proceedings of the National Academy of Sciences USA; 97(10): 5621-6.

Zhang Y, Brady M, Smith S, 2001. Segmentation of brain MR images through a hidden Markov random field model and the expectation-maximization algorithm. IEEE Transactions in Medical Imaging; 20(1): 45-57.

Zhang L, Thomas KM, Davidson MC et al, 2005. MR quantification of volume and diffusion changes in the developing brain. American Journal of Neuroradiology; 26: 45-9.

Appendix A: Balloon manufacturing process

Reproduced from the MSc report "Design of a small robotic proprioceptive stimulator for premature babies" by Amélie Moraux (supervisor Dr Etienne Burdet): Human Robotics Group, Department of Bioengineering, Imperial College London; 2008.

The first step in the manufacturing of the balloon is to create the clay pattern that will be coated with liquid latex. To do so, modelling clay should be inserted between the two parts of the plastic mould in order to be shaped to the balloon size. As this clay cast will have to be immersed into a cup of liquid latex it needs a support to be hold. The technique can be to enter a screw holding a wooden stick at the bottom of the clay cast (while it is still inside the plastic mould). When the clay cast is immersed into latex, it is hold by the wooden stick which is lying on the edge of the cup. Once shaped and fixed to the wooden stick, the clay should be removed from the mould, to be left drying overnight.

The parameters for the latex application are:

-Dip quickly the cast several times into latex to prevent any bubbles forming on the surface of the latex and then leave the cast to immerse for 12 minutes.

-Remove and leave to dry for at least 4 hours.

-Sew the nylon cloth on the cast following the instructions given below.

-Apply a first coating of liquid latex onto the nylon cloth (once on the balloon) with a brush so that the nylon is filled with liquid latex and then immerse into liquid latex for another 12 minutes.

-Remove and leave to dry overnight.

-The following day, the clay should be broken and removed from the latex. To do so, protect the latex surface with a piece of cloth and hammer the balloon. The clay should easily break inside the latex balloon so that it can be pulled out through the neck.

The manufacturing of a new balloon takes 3 days in overall.

To attach the balloon to the pipe, use melt silicon glue and apply it at the interface between the pipe and the balloon neck. Ensure that no air can pass through the junction and leave to cool down. In order to ease this process, the balloon can be hold to the pipe using a hose clip that should be removed after the glue is cold and strong.

Sewing technique

1. The balloon after the first coating of latex should look like in this picture.

2. A paper or preferably cardboard template has to be shaped in order to ease the cut of the nylon cloth. The size of the cardboard template is explained below.

3. Two pieces of nylon cloth have to be cut to match the size of the cardboard template. These pieces will be placed in front and back of the balloon.

4. Once the nylon cloth is cut, it will have to be sewed on the side. To facilitate this process, it is advised to hold the two pieces of cloth together with safety pins to prevent them from sliding on one another.

5. The two pieces of cloth must then be sewed together on each side on half the height of the cloths. It is advised to use the backstitch for this sewing as it is very strong. The threads should not be cut but left hanging in prevision of the end of the stitching.

6. To close the top of a cloth in a node, the technique used was to make a long running stitch 2mm from the top, going along the circle outline made by the pieces of cloth together. The thread should then be pulled, leading to the closing of the cloth.

7. The node needs to be secured by having the thread go through the node several times. The thread can then be cut after being securely held.

8. The nylon cloth should then look like this.

9. It has to be put in place in top of the first layer of latex. The cloth should be pulled downwards so that the cloth is as close to the nylon as possible.

10. The sewing on the sides of the balloon can then go. The sewing line should be as close as possible from the cast.

11. When sewing the second side, it is advised to slightly pull on the nylon cloth so that it is sewed strained without any fold.

12. The balloon should then look more or less like this.

13. The extra cloth on the side of the balloon can then be cut with caution so that the sewing is not damaged.

14. The balloon must then be immersed into latex for the second coating.

Size of the cloth

The size of the pieces of cloth used should be designed according to the size of the "clay balloon"

For example for balloons made with the 3D template, the height of the balloon is 35mm and the diameter is 8mm. The height of the cloth used should be 5mm bigger than the size of the balloon i.e. 40 mm. The width of the cloth depends on the perimeter of the balloon at maximum diameter i.e. 8mm. The perimeter is then 50mm which means that each piece of cloth should be 25mm wide. The user has to add the width of cloth necessary for the sewing which should roughly be around 2mm on each side. These measurements greatly depend on the user because the way the nylon is cut and sewed, slightly influences the size of the cloth needed.

Advice:

-The nylon cloth should not be pulled to hard when sewed or placed on the balloon cast as it will reduce the amplitude of inflation of the balloon once finished.

-Before immersing the balloon 'with cloth' into the latex for the second time, it is advised to first brush some liquid latex on the nylon so that all the nylon pores are filled

Appendix B: Shell script written for creating peristimulus data

```
#!/bin/bash

#script for creating hrf timeseries from event-related data, put in .feat directory
#timings of stimulation: volumes 4,86,168,250,332,414,496,578,660,742,824,906
#please make sure these timings are correct and alter script appropriately if
necessary
#baseline calculated from first 2 seconds of each peristimulus block

mkdir hrf_timeseries_nb
cd hrf_timeseries_nb
echo "calculating baseline";
	for f in ../filtered_func_data.nii.gz;
		do fslroi $f baseline01 0 4;
		fslroi $f baseline02 82 4;
		fslroi $f baseline03 164 4;
		fslroi $f baseline04 246 4;
		fslroi $f baseline05 328 4;
		fslroi $f baseline06 410 4;
		fslroi $f baseline07 492 4;
		fslroi $f baseline08 574 4;
		fslroi $f baseline09 656 4;
		fslroi $f baseline10 738 4;
		fslroi $f baseline11 820 4;
		fslroi $f baseline12 902 4;
		fslmerge -t baseline_all baseline01 baseline02 baseline03 baseline04
baseline05 baseline06 baseline07 baseline08 baseline09 baseline10 baseline11
baseline12;
		fslmaths baseline_all -Tmean Baseline_image
		rm baseline*
	done

	for	b in Baseline_image.nii.gz
	do
		echo "creating peristimulus image and sampled hrf text file";
		fslmaths $f -sub $b -mul 100 -div $b estpc_image.nii.gz;
		fslroi estpc_image volume01 4 82;
		fslroi estpc_image volume02 86 82;
		fslroi estpc_image volume03 168 82;
		fslroi estpc_image volume04 250 82;
		fslroi estpc_image volume05 332 82;
		fslroi estpc_image volume06 414 82;
		fslroi estpc_image volume07 496 82;
		fslroi estpc_image volume08 578 82;
		fslroi estpc_image volume09 660 82;
		fslroi estpc_image volume10 742 82;
		fslroi estpc_image volume11 824 82;
		fslroi estpc_image volume12 906 82;
		fslmaths volume01.nii.gz -add volume02.nii.gz -add volume03.nii.gz -
add volume04.nii.gz -add  volume05.nii.gz -add volume06.nii.gz -add volume07.nii.gz
-add volume08.nii.gz -add volume09.nii.gz -add volume10.nii.gz -add volume11.nii.gz
-add volume12.nii.gz -div 12 estpc_psimage.nii.gz
		rm volume*;
	done

	for s in ../stats/pe1.nii.gz; do
		p="$(grep "/PPheights" ../design.con | awk '{print $2 }')";
		echo "P-P height: $p";
		fslmaths $s -mul $p -mul 100 -div Baseline_image pc_image;
	done
```